# Untersuchung zur Zellulären Pharmakologie von peptidischen und nichtpeptidischen Wirkstoffmolekülen

## Investigation of the Cellular Pharmacology of Peptidic and Non-Peptidic Compounds

DISSERTATION

der Fakultät für Chemie und Pharmazie
der Eberhard Karls Universität Tübingen

zur Erlangung des Grades eines Doktors
der Naturwissenschaften

2010

vorgelegt von

IVO ROBERT RUTTEKOLK

Tag der mündlichen Prüfung          18.12.2009

Dekan:                              Prof. Dr. Lars Wesemann
1. Berichterstatter:               Prof. Dr. Roland Brock
2. Berichterstatter:               Prof. Dr. Stefan Laufer

Meiner Familie

Die vorliegende Arbeit wurde unter Anleitung von

Prof. Dr. Stefan Laufer

und unter Betreuung von Prof. Dr. Roland Brock

in der Zeit von März 2006 bis November 2009 am Institut für Pharmazeutische Chemie und am Interfakultären Institut für Zellbiologie an der Eberhard Karls Universität Tübingen und in der Afdeling Biochemie am Nijmegen Centre for Molecular Life Sciences (NCMLS) an der Radboud Universiteit Nijmegen (Nimwegen, Niederlande) durchgeführt.

# Danksagung

Peter van Gaalen danke ich für die Hilfestellung bei den ESI-MS-Messungen, Michiel van Dommelen für die Wartung und Reparatur der Mikroskope.

Meinen Eltern Petra und Frank Ruttekolk und meinen Großeltern Helga und Karl Lueg möchte ich danken, dass sie mir ein Studium in Tübingen ermöglicht haben. An dieser Stelle bin ich auch dem kostengünstigen deutschen Bildungssystem dankbar.

Ganz besonders möchte ich zuletzt meiner geliebten Frau Philine Ruttekolk danken für ihre immerwährende moralische Unterstützung, ihr Verständnis für meine Arbeit und dafür, dass sie es geduldig ertragen hat, mich über zwei Jahre lang in 600 km Entfernung zu wissen.

Allen hier nicht wörtlich genannten Kolleginnen und Kollegen gilt ebenfalls mein Dank für das angenehme Arbeitsklima, ebenso den zahlreichen "unsichtbaren" Unterstützern und Unterstützerinnen, wie den Reinigungskräften, den HauspostmitarbeiterInnen und den MitarbeiterInnen in Verwaltung und Spüldienst.

# Table of contents

# List of abbreviations

For amino acids the *IUPAC* nomenclature was applied (IUPAC, 1984).

| | |
|---|---|
| Å | ångström, $10^{-10}$ m |
| ABL1 | Abelson kinase 1 |
| Ac | acetyl moiety |
| ACN | acetonitrile |
| Ahx | 6-aminohexanoic acyl spacer |
| AOBS | acusto-optical beam splitter |
| APD | avalanche photo diode |
| ATP | adenosine triphosphate |
| BCS | Biopharmaceutics Classification System |
| Boc | *tert.*-butyloxycarbonyl |
| bp | base pairs |
| BP | band pass filter |
| BS | beam splitter |
| BSA | bovine serum albumin |
| CD | circular dichhroism |
| CPP | cell-penetrating peptide |
| DCM | dichloromethane |
| Dde | 1-(4,4-dimethyl-2,6-dioxocyclohexylidene)ethyl |
| DHFR | dihydrofolate reductase |
| DIC | N,N'-diisopropylcarbodiimide |
| DIPEA | N,N'-diisopropylethylamine |
| DMF | N,N'-dimethylformamide |
| DMEM | Dulbecco's Modified Eagle's Medium |
| DMSO | dimethyl sulfoxide |
| DNA | deoxyribonucleic acid |
| DPC | dodecylphosphocholine |
| DPMC | 1,2-dimyristoyl-sn-glycero-3-phosphocholin |
| DPMg | 1,2-dimyristoyl-sn-glycero-3-phosphoglycerol |
| EC50 | concentration that leads to half-maximal effect |
| EDT | ethanedithiol |
| EDTA | ethylenediaminetetraacetic acid |

| | |
|---|---|
| ESI-MS | electrospray ionisation mass spectrometry |
| EtOH | ethanol |
| eq | equivalent |
| FCCS | fluorescence cross-correlation spectroscopy |
| FCS | fluorescence correlation spectroscopy |
| Fluo | 5(6)-carboxyfluorescein |
| Fmoc | N-(9-fluorenyl)methoxycarbonyl |
| FPLC | fast protein liquid chromatography |
| fpm | fluorescence per molecule |
| FRET | fluorescence resonance energy transfer |
| GFP | green fluorescence protein |
| HBS | HEPES-buffered saline |
| HEPES | N-(2-hydroxyethyl)piperazine-N'-(2-ethansulfonic acid) |
| HIV-1 | human immunodifiency virus-1 |
| hLF | human lactoferrin |
| HOBt | 1-hydroxybenzotriazole |
| HPLC | high-performance liquid chromatography |
| HS | heparin sulfate |
| HSPG | heparin sulphate proteoglycan |
| IC50 | concentration that leads to half-maximal inhibition |
| IUB | International Union of Biochemistry |
| Kd | dissociation constant |
| $K_i$ | inhibitor constant |
| $K_m$ | Michaelis-Menten constant |
| LP | long pass filter |
| LPS | lipopolysaccharide |
| LSM | laser scanning microscopy |
| logP value | logarithmic octanol/water partition coefficient |
| MALDI | matrix-assisted laser desorption ionisation |
| MeOH | methanol |
| MS | mass spectrometry |
| MTX | methotrexate |
| Mw | molecular weight |
| m/z | mass/charge ratio |
| N | particle number |
| NMR | nuclear magnetic resonance |
| PAGE | polyacrylamide gel electrophoresis |

| | |
|---|---|
| PB | protein-binding |
| PBS | phosphate-buffered saline |
| PCR | polymerase chain reaction |
| PD | Parke-Davis compound PD173956 |
| PEG | polyethylene glycol |
| pH | *potentia hydrogenii* = $-\log[H^+]$ |
| PMT | photomultiplier tubes |
| PTD | protein transduction domain |
| PSA | Polar Surface Area |
| Pur | purvalanol B |
| RhG | Rhodamine Green |
| rLF | rat lactoferrin |
| RIfs | reflectrometric interference spectroscopy |
| RPMI | Roswell Park Memorial Institute |
| S | structure parameter |
| SAR | structure-activity relationship |
| S0387 | 2-(4-acetanilino-1,3-butadienyl)-3,3dimethyl-1-(4-sulfobutyl)-indolinum salt |
| SPR | surface plasmon resonance |
| $t_{1/2}$ | biological half-life |
| $\tau_D$ | diffusion time |
| tBu | *tert.*-butyl |
| TCEP | Tris(2-carboxyethyl)phosphine hydrochloride |
| TIS | triisopropylsilane |
| TFA | trifluoroacetic acid |
| TOF | time of flight |
| Tris | tris(hydroxymethyl)aminomethane |
| Trt | trityl |
| UV | ultraviolet |

# Preface - Cellular Pharmacology

For more than 100 years, trials in "systemic" or "clinical" pharmacology have been revealing the behavior of drug-like molecules in organisms. In this context pharmacology is divided in pharmacodynamics and pharmacokinetics. Whereas pharmacodynamics deal with the impact of a drug or a combination of those on organisms, pharmacokinetics in turn describe the impact of an organism and its metabolic systems on the fate of the drug compound. Moreover, in the last decades many biophysical and bioanalytical techniques were developed and established to display the exact binding properties of defined binding partners, an area of activity that is often named "molecular pharmacology". Especially high-throughput screening approaches play a key role in today's drug discovery. In cell culture-based approaches mostly the impact of a molecule on a single response that can be easily read out is displayed. Between systemic and molecular pharmacology there is still a large gap and the behavior of a molecule in its cellular and subcellular context is misleadingly assumed to be rather simple: the compound penetrates the plasma membrane, binds to its dedicated target structure and thereby executes its mode of action. In reality, the processes are highly complex and there is still an unmet need to untangle the network of a compound's behavior in its physiological context. In future drug discovery many questions that deal with cellular pharmacology will certainly play a crucial role: How does a certain molecule enter the cell? Can this be influenced by combinations of drugs or by formulations? Where is the molecule located intracellularly? What is its binding profile like in its native environment? Does it diffuse freely or is it bound to membranes, proteins or other high-molecular weight structures? What is the unbound concentration in the direct environment of the target structure? How fast is a molecule degraded, exported or transported within or out of the cell? This thesis addresses some of the most relevant questions concerning "cellular pharmacology". In one chapter the modular assembly of peptides conjugated to a chemically inert polymeric backbone and the impact of a backbone on the activity of the peptides as well as the import efficiency of the conjugates is investigated. These results should support the untangling of signal transduction networks. A second chapter concentrates on the effect of polymer-conjugation on the peptide stability, a third one on the residence time of peptides and conjugates within cells and therefore the time in which these can influence signal transduction networks. A forth chapter focuses on the tertiary structure-based mode of action of a cell-penetrating peptide derived from the human milk protein human lactoferrin and its ability to facilitate the uptake of a cargo. And, finally, one chapter focuses on the intracellular binding profile of small molecule anti-cancer drugs.
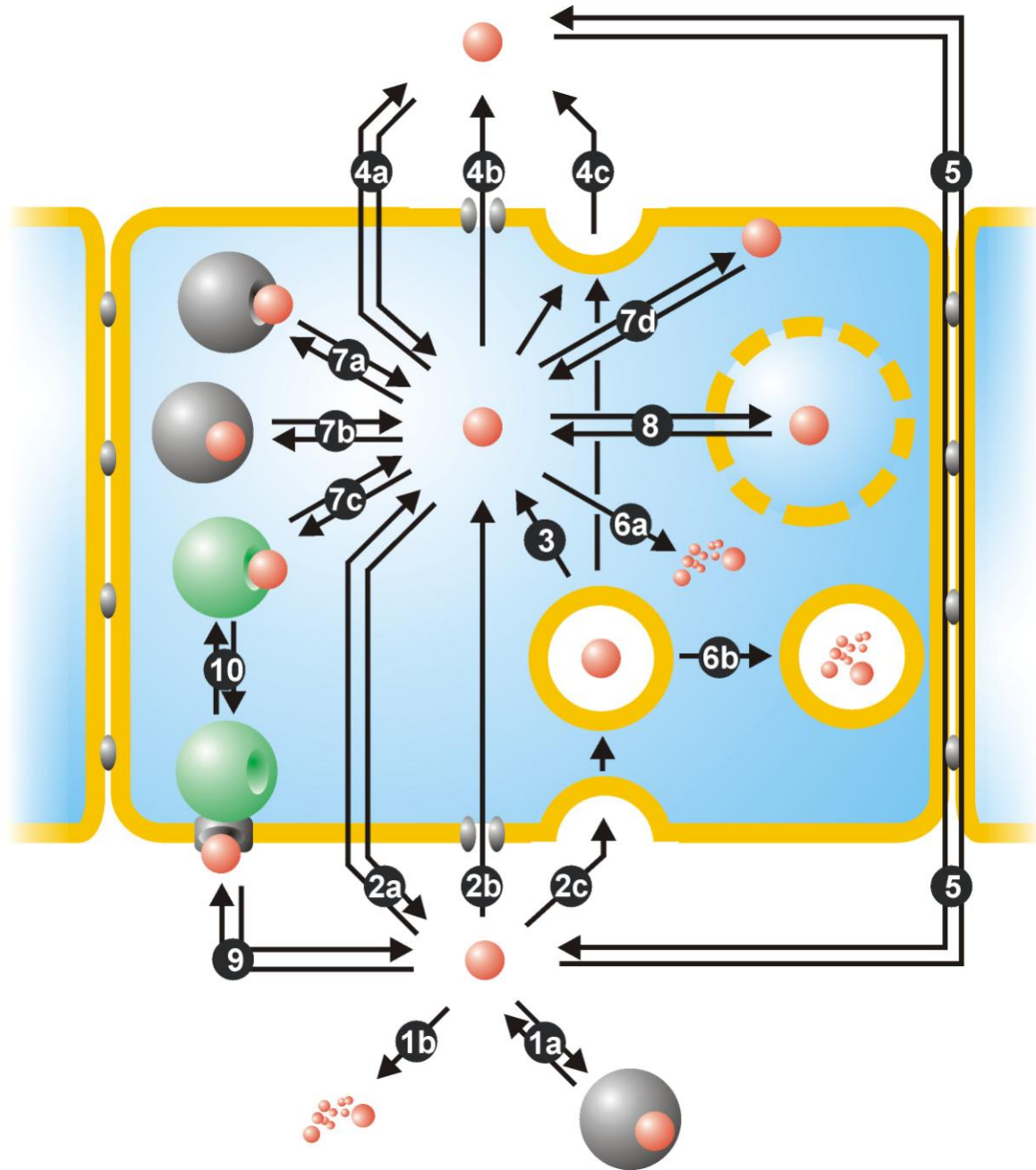
**Fig. 0.1. Challenges of cellular pharmacology – a complex network of reversible and irreversible processes.** (1a-b) extracellular behavior of compound, (1a) interaction with serum proteins, (1b) degradation; (2a-c) cellular import, (2a) direct and passive membrane penetration, (2b) active/passive transport, (2c) endocytosis; (3) endosomal escape; (4a-c) cellular export, (4a) direct and passive penetration, (4b) active export via transporters, (4c) exocytosis; (5) paracellular transport; (6a-b) intracellular degradation or metabolism, (6a) cytosolic degradation, (6b) endosomal degradation; (7a-d) intracellular binding properties, (7a) binding to specific off-target binding sites, (7b) unspecific binding to proteins, (7c) binding to the target protein(s), (7d) interaction with/insertion into the membrane; (8) intracellular transport (directed motion/ undirected diffusion); (9) binding activity to extracellular receptors; (10) indirect influence on intracellular signal transduction processes by binding to cofactors and other binding partners

## Contents of this thesis

The content of this thesis had been adopted from five manuscripts:

1.　"HPMA as a scaffold for the modular assembly of functional peptide polymers by native chemical ligation"
Bioconjugate Chemistry (2008), 19, 2081-2087
I.R. Ruttekolk, F. Duchardt, R. Fischer, K.-H. Wiesmüller, J. Rademann, R. Brock

2.　"Coupling to polymeric scaffolds stabilizes biofunctional peptides for intracellular applications"
I.R. Ruttekolk*, M. Richter*, A. Chakrabarti, F. Duchardt, H. Glauner, R. Brock, J. Rademann, *to be submitted* [*: shared first authorship]

3.　"Short intracellular residence times limit the applicability of bioactive peptides in cells"
*to be submitted*

4.　"A cell-penetrating peptide derived from human lactoferrin with conformation-dependent uptake efficiency"
F. Duchardt*, I.R. Ruttekolk*, W. Verdurmen, H. Lortat-Jacob, J. Bürck, H. Hufnagel, R. Fischer, M. van den Heuvel, D.W.P.M. Löwik, G.W. Vuister, A. Ulrich, M. Waard, R. Brock, *submitted* [*: shared first authorship]

5.　"Simultaneous detection of intracellular target and off-target binding of small molecule cancer drugs at nanomolar concentrations"
H. Glauner*, I.R. Ruttekolk*, K. Hansen, B. Steemers, Y. Chung, F. Becker, S. Hannus, R. Brock, *submitted* [*: shared first authorship]

# 1. Introduction

# 1.1. Pharmacokinetics on the cellular level

### 1.1.1. Cellular ADME kinetics - "ALL LIFE IS MOVEMENT" (Leonardo Da Vinci)

**ADME kinetics** on the cellular level deal with the absorption of molecules into the cell, the distribution within the cell and its compartments, the enzyme-mediated metabolism and finally the elimination of molecules or their metabolic products out of the cells.

Uptake into the cell can be facilitated via numerous ways such as endocytosis (Conner and Schmid, 2003) followed by endosomal escape, via active transport by ATP-driven transporters (Pedersen, 2007), via passive diffusion through channels or by direct penetration though the membrane. The distribution and localization of a molecule inside the cell can also be controlled by active transport mechanisms, by diffusion, by its physicochemical properties such as its size, shape, hydrophobicity or charge or by its pharmacodynamic binding profile. Hydrophobicity significantly influences the subcellular localization (Verma *et al.*, 2008). In fact, the distribution can have a considerable impact on the intracellular local concentration. Furthermore, certain intracellular locations can prevent the compound from degradation or in turn accelerate these processes.
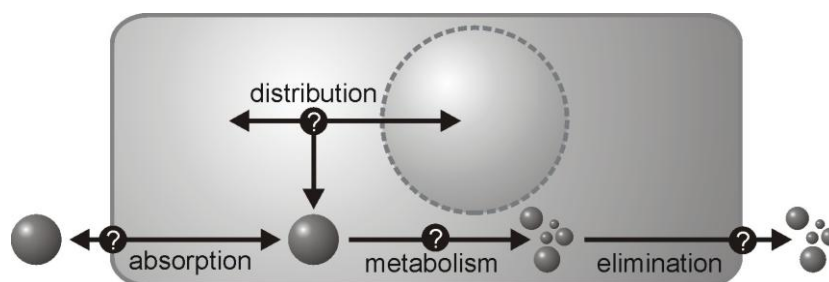


**Fig. 1.1. The four phases of ADME kinetics on the cellular level.**

Regarding metabolic processes Phase I and Phase II are distinguished (Oesch *et al.*, 2007; Huang *et al.*, 2009; Testa and Kramer, 2009). The **Phase I metabolism** is characterized by cleavage (catalyzed by proteases, protease complexes, esterases, epoxyd hydrolases, etc.), by oxidation (catalyzed by the cytochrome P450 (CYP) superfamily, peroxidases, dehydrogenases, monooxygenases, monoamine oxidases, etc.) or by reduction (catalyzed by reductases or a consequence of the reductive cytoplasm). In this thesis, especially proteases and phosphatases play a key role. The **Phase II metabolism** is characterized by the conjugation of other molecules to the compound (catalyzed by gluthathion-S-

transferases, UDP-glucoronsyltransferases, acetyltransferases, sulfotransferases, kinases, etc.). Mostly, these processes inactivate the pharmaceutical active molecule, but in some cases a **prodrug** has to be metabolized to become active, the molecule cannot be entirely inactivated or changes its target spectrum (Rautio *et al.*, 2008). In this case the product of the metabolic processes is named **active metabolite** (Testa, 2009; Testa and Kramer, 2009). The elimination of the therapeutic molecule is facilitated by passive diffusion through the cell membrane, via passive channels or via active transport by ATP-driven transporters (Multidrug Resistance Proteins (MDRs), Multidrug Resistance-Related Proteins (MRPs), etc.).

## 1.1.2. Cellular pharmacokinetic parameters

The usage of pharmacokinetic parameters allows the description of the molecule's properties regarding its behavior in organisms, tissues and cells.

In terms of cells **the biological half-life $t_{1/2}$** describes the time in which half of the **initial concentration $c_0$** of the observed molecule has either left the cell, actively or passively, or is metabolized. But, as uptake into the cell is a time-dependent process and the uptake and elimination kinetics temporally overlap, the initial concentration can only be estimated. The kinetics of the **concentration $c$** rather follow a Bateman Equation (see below). Instead of an initial concentration the integral of the concentration curve is given as the **area under the curve $AUC$**.

The **protein-binding coefficient $PB$** describes the fraction of molecules that is bound to proteins and is therefore subducted from the free concentration. In systemic pharmacokinetics the $PB$ value describes the fraction of molecules in blood serum that is protein-bound, mostly to albumins. For cellular pharmacokinetics it is defined here as the description of the total protein binding capacity to extra- and intracellular proteins.

The $PB$ value is mostly related to the hydrophobicity of a molecule, which is quantified by the logarithmic octanol/water partition coefficient, the **logP value**.

Additionally, the hydrophobicity has a direct impact on the uptake mechanism. Whereas hydrophilic molecules have to be taken up via transporters or channels, hydrophobic molecules can also enter the cell by direct penetration of the cell membrane. Highly hydrophobic molecules, in contrast, tend to accumulate in membrane bilayers. Alternatively, the hydrophobicity of a pharmaceutical molecule can be describe by means of the computer-based approach of calculating the **Polar Surface Area ($PSA$)**. Here, the area, given in $Å^2$, that is covered by polar heteroatoms, is calculated (Ertl *et al.*, 2000), the smaller the $PSA$ the

more likely is the molecule cell-permeable.The *logP value* and the *PSA* can be calculated via open source programms such as. *molinspiration* (http://www.molinspiration.com/cgi-bin/properties) (Ertl *et al.,* 2000). The fraction of compound that is absorbed by a cell can also be classified by the **resorbance factor *f***. In general, therapeutic molecules are often described by the **Biopharmaceutics Classification System (*BCS*)**. Here, the molecules are classified by their ability to penetrate cell membranes and by their solubility in an aqueous environment. The molecules are allocated in four *BCS* classes that can be specified by their physicochemical properties (van de Waterbeemd, 1998).

**Tab. 1.1. The Biopharmaceutics Classification System (*BCS*):**

| Class I | Class II |
|---|---|
| high permeability high solubility | high permeability low solubility |
| **Class III** | **Class IV** |
| low permeability high solubility | low permeability low solubility |

Whereas Class I molecules show an unproblematic behavior as they can easily enter cells and are well-soluble in biological matrices, Class II molecules require special treatment regarding to their pharmaceutical formulation to enhance their solubility in biological systems and Class III and Class IV molecules have to be modified by means of conjugation to other molecules, capping of respective active groups or non-covalent formulation to enhance their permeability.

Other parameters that are regularly used in systemic pharmacokinetics as the **volume of distribution *$V_D$*** and the **bioavailability *F*** are less important on the level of single cells and are not described here further. In summary, the pharmacokinetics-related usability of a drug candidate can be predicted due to its physicochemical properties. One of the first computer-based approaches with an wide applicability was proposed by Christopher A. Lipinski (*Pfizer Inc.*) (Lipinski *et al.*, 2001). As an alternative, Arup K. Ghose (*Amgen Inc.*) published a frequently cited approach (Ghose *et al.*, 1999).

**Tab. 1.2. Physicochemical requirements on a therapeutic molecule**

| | Lipinski et al. | Ghose et al. |
|---|---|---|
| hydrogen bond donors | < 5 | |
| hydrogen bond acceptors | < 10 | |
| molecular weight | < 500 | 160 to 480 |
| logarithmic octanol/water partition coefficient | < 5 | -0.4 to 5.6 |
| molar refractivity | | 40 to 130 |
| heavy atoms | | 20 to 70 |

Both approaches bear several significant drawbacks. On the one hand, the presence of cellular transporters and channels, that can also facilitate the efficient uptake of hydrophilic or

high-molecular weight compounds, is totally ignored. On the other hand, the possibility of chemical modifications and pharmaceutical formulations of compounds possessing promising pharmacodynamic properties is not taken into consideration. Experimental and predicted pharmacokinetic data and parameters can be found in open source domains such as *DrugBank* (University of Alberta, Alberta, Canada, http://www.drugbank.ca/) or *PubChem* (National Center for Biotechnology Information (NCBI), Bethesda, USA, http://pubchem.ncbi.nlm.nih.gov/). Some well-accepted and orally administered drugs such as methotrexate (*logP* -1.8, value based on the *PubChem data base*) or peptide- and protein-based drugs such as vancomycin (*logP* -2.6) would not be classified as useful compounds according to the above-mentioned computer-based approaches. Nevertheless, the computer-based approaches are a valuable tool to save costs and time as they allow a pre-selection of possible lead structures without experimental effort.

The **cellular uptake efficiency *J*** of a drug can be characterized by the drug transported per unit of time and per membrane surface area. It is dependent on the **permeability coefficient *P***, and the concentration gradient between the **concentration in the donor compartment $c_D$** and the **concentration in the receiver compartment $c_R$** (Goldberg and Gomez-Orellana, 2003).

$$J = P * (c_D - c_R) \tag{1.1}$$

## 1.1.3. Description of cellular pharmacokinetic processes

Dynamic processes such as the degradation or the metabolism of a molecule are described by exponential functions of differing orders. The order depends on the number of rate-limiting steps. In pharmacokinetic systems mostly kinetics of the first order are employed as here solely the concentration of the drug-like molecule is rate-limiting. Therefore, the reaction rate *v* over the time *t* is dependent on the substrate concentration [*S*] and the rate constant *k*.

$$v = -\frac{dS}{dt} = k \cdot [S] \tag{1.2}$$

integrated

$$[S] = [S]_0 \cdot e^{kt} \tag{1.3}$$

Enzyme activity is quantified by the **Michaelis-Menten Equation** (Michaelis and Menten, 1913). In general, Michaelis-Menten kinetics are based on the theory that the formation of the high-energetic enzyme-substrate complex *ES* is not the rate-limiting reaction, but rather

the subsequent quasi-irreversible generation of the product $P$. Thus, the concentration of [$ES$] is not changing within a short time interval and Michelis-Menten kinetics are based on a steady-state approximation.

$$E + S \underset{k_1'}{\overset{k_1}{\rightleftharpoons}} \quad ES \quad \overset{k_2}{\longrightarrow} \quad E + P \tag{1.4}$$
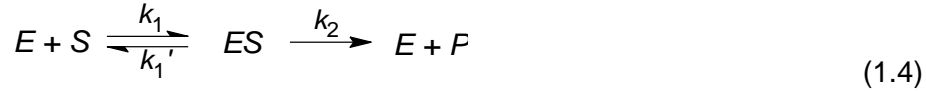
In Michaelis-Menten kinetics the formation of the product [$P$] and the decrease of the substrate concentration [$S$] are solely limited by the rate constant of the second reaction step $k_2$. The maximal turnover rate $v_{max}$ of substrate, also named molecular activity or $k_{cat}$, is given by the *IUB*-conform unit kat (katal: 1 mol/s) or the more widely used unit U (international unit: 1 μmol/min) (Liebecq, 1992). The concentration [$S$] that is required to achieve a reaction rate of 1/2 $v_{max}$ is represented by the Michaelis-Menten constant $K_m$.

$$v = \frac{v_{\max} \cdot [S]}{K_m + [S]} \tag{1.5}$$

If the concentration of the substrate clearly exceeds the capacity of the metabolic system the kinetics are only dependent on the rate constant $k$ and follow a linear kinetic profile. Alcohol for instance is regularly metabolized linearly and only below a very low concentration the kinetic follows the first order. If two limited compounds, e.g. a coenzyme and a pharmaceutical compound, react with each other at the enzymatic reaction site the kinetics follow a second order.

Processes that consider the absorption, distribution, metabolism and elimination, all ADME parameters, are described by the **Bateman Equation**.

$$[S] = [S]_0 \cdot \frac{k_a}{k_e - k_a}(e^{-k_a t} - e^{-k_e t}) \tag{1.6}$$

Absorption and distribution kinetics are described by the rate constant $k_a$, whereas metabolism and elimination are depicted by $k_e$. The applied dose is represented by $[S]_0$.

Although most drugs of current therapies target extracellular targets such as receptors (45 %) or ion channels (5 %) or represent hormones (11 %) (Drews, 2000), they are still preferably developed to overcome the intestinal barrier in order to enable oral applicability. Therefore, also the for these the capacity to cross membranes and pharmacokinetics in the intestinal endothelium are highly important.

## 1.1.4. Enhancement of cellular and tissue uptake

Molecules can be taken up into cells via direct penetration of the membranes, endocytosis, transporters or via paracellular transport. As mentioned above the chemical properties of a molecule determine its pharmaceutical properties. For drugs of a molecular weight Mw of less than 500-700 the cellular uptake efficiency is independent on the molecular weight. In contrast, for drugs beyond Mw 700 the uptake efficiency decreases considerably with an increasing molecular weight (Donovan *et al.*, 1990a; Donovan *et al.*, 1990b).

The attachment of lipophilic moieties or the employment of the *Eligen* system (Malkov *et al.*, 2005) increase the permeability by the enhancement of lipophilicity and lead to a direct penetration of the membrane.

In order to exploit efficient transport processes, the drug molecules can be conjugated to molecular structures that interact with membrane transporters such as glucose (Rouquayrol *et al.*, 2002), bile acids (Swaan *et al.*, 1997) or di- or tripeptides (Nielsen *et al.*, 2001).

Receptor-mediated endocytosis can be induced by conjugation of vitamin $B_{12}$ (Russell-Jones *et al.*, 1995) or an Fc fragment (Spiekermann *et al.*, 2002).

Finally, the rate of paracellular transport can be enhanced by means of tight junction modifications. These occur upon the employment of nitric-oxid donors (Yamamoto *et al.*, 2001), zonula occludence toxin (Fasano and Uzzau, 1997), Pz-peptides (Yen and Lee, 1995) and chitosans (Thanou *et al.*, 2001).

## 1.1.5. Uptake of peptides

According to the rules of Lipinski and Ghose charged high-molecular weight molecules such as proteins, peptides, polynucleic acids, peptidoids etc. cannot cross the cell membrane as many of the hydrophobic, small molecule drugs can. Notwithstanding, nature has created backdoors to overcome this barrier. Numerous peptide-like toxins that are found in poisonous mushrooms (e.g. phalloidin, $\alpha$-amanitine) and plants (e.g. ricin) or are secreted by bacteria (e.g. cholera toxin) can enter the cytosol effectively, mostly via endocytotic pathways and subsequent endosomal escape.

It was demonstrated that oligo-amino acid sequences, such as poly-L-lysine can facilitate the uptake of proteins (Ryser *et al.*, 1978; Shen and Ryser, 1978) and small drugs such as methotrexate (Ryser and Shen, 1978).

In the 1990ies nontoxic peptide sequences that could overcome the plasma membrane were found in proteins such as a peptide derived from the third helix of the antennapedia

homeodomain from *drosophila melanogaster* (Derossi *et al.*, 1994), that is also named penetratin (Pen/Antp), or the Tat peptide that was derived from the *human immunodeficiency virus-1* (*HIV-1*) (Vives *et al.*, 1997). It was recognized that these peptides comprised of numerous arginine residues. Therefore, synthetic polyarginine peptides were employed to facilitate uptake (Mitchell *et al.*, 2000; Wender *et al.*, 2000). Here, the efficiency of the polyarginine peptides depended on the number of arginines, and thus the valency of guanidinium groups, plays a crucial role (Kawamura *et al.*, 2006). Interestingly, these peptides, mostly named cell-penetrating peptides (CPPs) in Europe and protein transduction domains (PTDs) in the United States, are able to facilitate the uptake of a large variety of conjugated substances (Langel, 2002). CPPs can be employed in order to generate cell-permeable conjugates of peptides (Choi *et al.*, 2003; Rohrbach *et al.*, 2005), proteins (Fawell *et al.*, 1994; Nagahara *et al.*, 1998), peptide nucleic acids (PNAs) (Oehlke *et al.*, 2004; Turner *et al.*, 2005; Wolf *et al.*, 2006), nanoparticles (Lewin *et al.*, 2000), quantum dots (Santra *et al.*, 2005a; Santra *et al.*, 2005b), organometallic bioconjugates (Noor *et al.*, 2009) and polymer-conjugated drugs (Nori *et al.*, 2003). The cargo, even if it is a small molecule, can have a significant impact on the intracellular localization of the conjugate (Fischer *et al.*, 2002). Most studies dealing with CPPs have been conducted in mammalian cells. Nevertheless, it has been demonstrated that polyarginines can also enter protoplasts, thus, plant cells lacking cell walls via a comparable mechanism. (Unnamalai *et al.*, 2004; Chang *et al.*, 2005; Chugh and Eudes, 2007; Chugh and Eudes, 2008). Polyarginine peptides can even enter plant cells bearing a cell wall, although a considerable fraction of the cationic CPP is localized in the highly negatively charged cell wall (Mizuno *et al.*, 2009).

For the cellular attachment of cationic CPPs the heparan sulphate proteoglycans at the cell surface are considered an important structure (Fuchs and Raines, 2004). Structure-based studies show that peptides likely change their conformation upon interaction with phospholipid vesicles (Magzoub *et al.*, 2001) and that the mode of membrane interaction is different for cationic and amphiphilic sequences (Zhang and Smith, 2005). Especially at lower concentrations clathrin-mediated endocytotic uptake plays a key role for cationic CPPs as was shown by means of the employment of variant specific endocytosis inhibitors (Fotin-Mleczek *et al.*, 2005a). But still, the endosomal escape mechanism required to mediate entry into the cytoplasm is not fully understood yet (Fischer *et al.*, 2005). On the other hand, the employment of a splice correction assay (El-Andaloussi *et al.*, 2006) could clearly demonstrate that CPP-cargo conjugates that are taken up by endocytosis are released from the endosomes effectively enough to allow the cargo to display its action in the cytosol (Lundin *et al.*, 2008). In this context, it could be shown that the transmembrane pH gradient is required for efficient membrane permeation (Magzoub *et al.*, 2005).

Endocytosis can lead to receptor internalizate and as a consequence change the response of a cell to external stimuli. For instance, cationic CPPs can trigger the internalization of the tumor necrosis factor (TNF) receptor (Fotin-Mleczek *et al.*, 2005b). In addition to endocytosis, CPPs can enter the cell via a second mechanism independent of endocytosis. This rapid uptake mechanism is found especially at higher concentrations (Duchardt *et al.*, 2007), whereas membrane integrity is entirely maintained. D-peptides show differing rates of rapid uptake (Tunnemann *et al.*, 2008). Recently, it was demonstrated that certain peptides can also facilitate the cellular export of a cargo (Dupont *et al.*, 2007).

Independent of the uptake mechanism, proteolytic degradation of CPPs is one of the limiting factors of their application (Fischer *et al.*, 2004). Additionally, in *in vivo* applications immunogetity is always a prominent concern. For that reason, peptides of human origin such as a human calcitonin-derived peptide (Schmidt *et al.*, 1998) or peptides derived from human signal transduction proteins (Rojas *et al.*, 1998) are of interest.



**hydrophobic**

**HIV-gp41 fusion sequence**
GALFLGFLGAAGSTMGA

**Kaposi FGF signal sequence**
AAVALLPAVLLALLAP

**human integrin β3-signal sequence**
VTVLALGALAGVGVG

**cationic**

**poly-arginine peptides**

**nuclear localisation sequences**
VQRKRQKLMP
PKKKRKV
ERKKRRRE

**HIV Tat-1-derived**
YGRKKRRQRRR

**SynB1**
RGGRLSYSRRRFSTSTGRA

**antimicrobial**

**Buforin**
GIGKFLHSAKKFGKAFVGEIMNS

**Magainin**
TRSSRAGLQFPVGRVHRLLRK

**proline-rich**

**proline-rich dendrimers**

**N-terminal repetitive domain of maize gamma-zein**
(VxLPPPP)$_n$ [x: H,R or K]

**peptides that facilitate cellular uptake**

**tertiary structure dependent**

**lactoferrin-derived peptides**
KCFQWQRNMRKVRGPPVSCIKR

**amphiphatic**

**penetratin**
RQIKIWFQNRRMKWKK

**W/R penetratin**
RRWRRWWWRRWWRRWRR

**model peptide**
KLALKLALKALKAALKLA

**chimeric**

**Transportan**
GWTLNSAGYLLGKINLKALAALAKKIL

**Chariot**
KETWWETWWTEWSQPKKKRKV

**MPG**
GALFLGFLGAAGSTMGAWSQPKKKRKVC

**loligomers**

**various sources**

**PreS2-TLM**
PLSSIFSRIGDG

**calcitonin-derived peptide**
LGTYTQDFNKFHTFPQTAIGVGAP

**Fig. 1.2. The CPP family.** Adopted and updated from R. Fischer (Fischer *et al.*, 2005).

## 1.1.6. Endocytotic uptake of small molecules

Recent studies suggest that also small molecules are taken up by endocytotic processes to a larger extend than expected before. Reduction of the endocytotic rates in malignant cancer cells can lead to drug resistance (Chauhan *et al.*, 2003). Recent studies indicate that polynuclear alkylamine platinum(II) complexes are beside other paths taken up by endocytosis (Chauhan *et al.*, 2003). As a high rate of macropinocytosis is mostly related to changes in the intracellular signal transduction of the respective cells (Amyere *et al.*, 2002) it can very likely function as an indicator for motile and metastatic cancer cells. The alkylamine platinum(II) complexes molecules show higher specificity to cancer cells than other platinum complexes (Kapp *et al.*, 2006).

## 1.1.7. The lactoferrin-derived cell-penetrating peptide

One CPP of human origin is the human lactoferrin derived peptide. The 80 kDa human lactoferrin protein is an iron-binding glycoprotein of 703 amino acids (Metz-Boutigue *et al.*, 1984). It is found in considerable concentrations in human milk (15 % of the total protein content) and in lower concentrations in tears, nasal fluids, saliva, pancreatic, gastrointestinal and reproductive tissue secretions and in blood plasma (Levay and Viljoen, 1995). Here, it acts as an antimicrobial, antifungal and antiviral protein and, therefore, plays an important role in the innate immune defense (Legrand *et al.*, 2008) by depletion of iron (Ward and Conneely, 2004) and through direct interaction with bacterial components (Valenti and Antonini, 2005).

Oral uptake leads to a pepsin-mediated cleavage of the highly positively charged N-terminal domain off the rest of the protein, which is then degraded. The released peptide comprises 49 amino acids, named lactoferricin (Bellamy *et al.*, 1992), that carries potent antimicrobial activity (Gifford *et al.*, 2005). In aqueous environment it comprises a "nascent helix" and a loop structure that is stabilized by two disulfide bonds. The helical structure is stable in the full-length protein and can be also stabilized by membrane-mimetic solvents (Hunter *et al.*, 2005). The structure of lactoferricin reveals hydrophobic and positively charged sections comparable to those found in numerous peptides that display antimicrobial activity (De and Contreras, 2005; Toke, 2005).

It was demonstrated that antimicrobial peptides with these characteristics are taken up into mammalian cells (Takeshima *et al.*, 2003) and that, the other way round, many CPPs show antimicrobial activities (Nekhotiaeva *et al.*, 2004). It could be proven that a lactoferrin-derived

peptide can also act as a CPP (Brock *et al.*, 2007). A cell-penetrating peptide was derived from the N-terminal domain of human lactoferrin, corresponding to amino acid residues 38-59.



**Fig. 1.3. Structure of lactoferrin.** The structure of full-length lactoferrin (Anderson *et al.*, 1990) bears the lactoferrin-derived cell-penetrating peptide as a disulfide bond-stabilized loop on its surface (the CPP sequence is highlighted in yellow) (A). Whereas the 3D structure of lactoferricin is only partly helical in aqueous buffers (B), it is stabilized in a membrane-mimicking solvent (Hunter *et al.*, 2005) (C) (the CPP sequence is highlighted in yellow).

An analogous peptide sequence is found in all known lactoferrin sequences of different species. The sequences differ considerably, whereas the pontentially structure-determining residues are highly conserved. The sequence of all known species begins with lysine and cysteine, followed by a presumed $\alpha$-helical sequence of 8-11 residues which contains a methionine residue in all species except the pig and is able to bind lipopolysaccharides, a presumed turn region with at least one proline residue and a short presumed $\beta$-sheet region with a second cysteine.

**Tab. 1.3. Sequence comparison of lactoferrin peptides of different species.**

| sequence | origin (common name) | origin (Latin name) | amino acids | position |
|---|---|---|---|---|
| **KCFQWQRNMR-KVRGPPVSCIKR** | Human | Homo sapiens | 709 | 38-59 |
| **KCFRWQRNMR-RVRGPPVSCIKR** | Chimpanzee | *Pan trolodytes* | 711 | 38-59 |
| **KCSQWQRNLR-RVRGPPVSCIKR** | *Short-tailed Opossum* | *Macaca cyclopis* | 710 | 37-58 |
| **KCAQWQRRMK-KVRGPSVTCVKK** | Dromedary | *Camelus dromedarius* | 708 | 37-57 |
| **KCAKFQRNMK-KVRGPSVSCIKR** | Horse | *Equus caballus* | 698 | 37-56 |
| **KCYQWQRRMR-KLGAPSITCVRR** | Goat | *Carpa hircus* | 708 | 37-58 |
| **KCYQWQRRMR-KLGAPSITCVRR** | Sheep | *Ovis aries* | 708 | 37-58 |
| **KCHRWQWRMK-KLGAPSITCVRR** | Water buffalo | *Babalus babalus* | 708 | 37-38 |
| **KCRRWQWRMK-KLGAPSITCVRR** | Bovine | *Bos taurus* | 708 | 37-38 |
| **KCRRWQWRMK-KLGAPSITCVRR** | Wild Yak | *Bos grunniens* | 708 | 37-58 |
| **KCRQWQSKIR-RTN-P-IFCIRR** | Pig | *Sus scorfa* | 704 | 37-56 |
| **KCLRWQNEMR-KVGGPPLSCVKK** | Mouse | *Mus musculus* | 707 | 36-56 |
| **KCFMWQ-EMCNKAGVPKLRCARK** | Rat | *Rattus norvegicus* | 709 | 38-57 |
| **KCXXWQXXM1-12X2P2-2C211** | consensus sequence | | | |

Highly conserved residues are displayed in blue, residues identical to those in the human peptide in red, residues similar to those in the human peptide regarding their physicochemical properties are bold. In the consensus sequence "1" represents a positively charged amino acid residue, "2" a hydrophobic one and "X" an arbitrary one. Between the two cysteine residues a disulfide bound in formed. According to Chou-Fasman calculations the conservation of the residues corresponds to a highly conserved secondary structure.
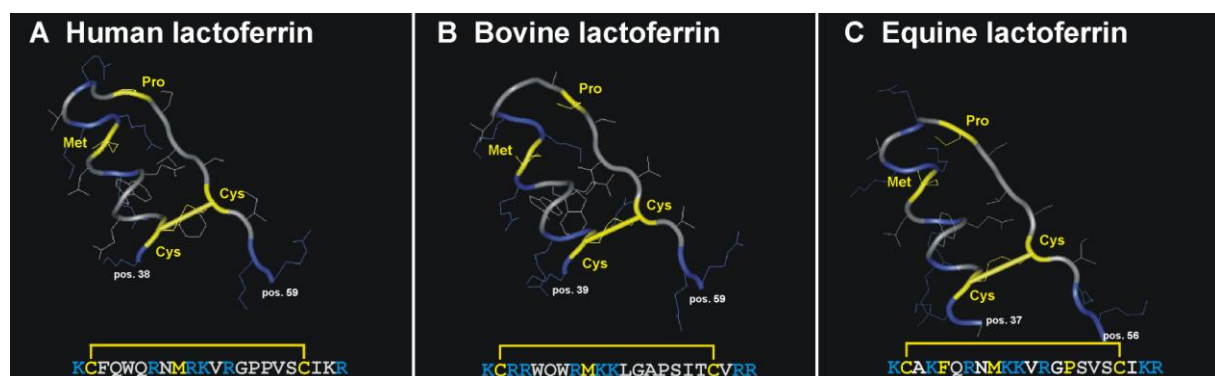


**Fig. 1.4. Structure comparison of different species.** Although the sequences are considerably different in different species, the tertiary structures in the crystal structures of the full-length proteins are highly conserved for the structures corresponding to (A) the hLF peptide. The structure of (B) the bovine and (C) the equine lactoferrin are depicted.

## 1.1.8. Conjugation of therapeutic molecules to polymeric backbones

Pharmacokinetic properties of therapeutic molecules can be altered by the conjugation to polymeric molecules (Duncan, 2003). For numerous drugs the conjugation to polymeric backbones has some explicit advantages such as improved and elongated blood circulation and therefore slower release kinetics (Seymour *et al.*, 1990), decreased toxicity of many of the conjugated drugs such as doxorubicin (Duncan *et al.*, 1998) and improved solubility of Class II and Class IV drugs such as doxorubicin and paclitaxel. In today's drug discovery many drugs are conjugated to polyethylene glycol (PEG) (Harris and Chess, 2003), especially orally delivered macromolecules often require polymer-conjugation (Goldberg and Gomez-Orellana, 2003). As tumour vessels bear a higher permeability for high-molecular weight molecules and many malignant tumour cells bear an increased macropinocytosis rate (Amyere *et al.*, 2002) the polymer-conjugation of small molecule drugs accomplishes a certain selectivity for tumour tissues and cells by size-exclusion effects (Seymour *et al.*, 1995). The co-functionalization with different molecules, such as cell-penetrating peptides and small molecules (Nori *et al.*, 2003) is possible and upon higher moiety loadings multivalency effects are observable (Mammen *et al.*, 1998).

Today, polymer-conjugated drugs are widely used in clinical trials, particularly in the field of anticancer drugs (Vicent and Duncan, 2006). SMANCS (*Zinostatin stimalamer*) represents the first protein-polymer conjugate that was brought to the market (Maeda, 2001). Proteins and peptides are regularly conjugated to polyethylene glycol (PEG) in order to prevent the molecules from degradation in the blood stream (Lee *et al.*, 1999; Veronese, 2001; Esposito *et al.*, 2003). One of the most common polymer backbone for small molecules represents HPMA (Poly[N-(2-hydroxypropyl)methacrylamide]) copolymers (Kopecek and Bazilova, 1973). HPMA is widely used in numerous applications, mostly in cancer treatment (Kopecek *et al.*, 2000) such as carriers for anti-angiogenesis drugs (Satchi-Fainaro *et al.*, 2004). It could be demonstrated that polymeric backbones can be targeted to special cell types via antibodies (Kovar *et al.*, 2002). In this thesis the advantages of the polymer-conjugation in cellular applications of peptides are combined with those of the CPPs.

# 1.2. Cellular pharmacodynamics

## 1.2.1. The molecular binding - "CORPORA NON AGUNT NISI FIXATA"

("Compounds do not act if they are not bound.", Paul Ehrlich)

The first methodical pharmacodynamic studies were performed by the German scientist Paul Ehrlich and his co-workers in the end of the 19th century. On the basis of the previous findings that certain dyes were able to stain cellular structures selectively, his group developed the **"magic bullet" concept**. This theory explains that a toxic molecule, that binds selectively to its target structure(s), is able to eliminate harmful cells in order to cure patients. Today, this theory is still the basis of all chemotherapies. After a methodological lead identification and optimization process the outcome of his studies was the anti-syphilic agent Salvarsan (arsphenamine). Furthermore, Ehrlich conceived - contemporary with John Langley - the **receptor theory** stating that a therapeutic molecule, named **ligand**, has to bind to at least one certain target structure, named **receptor**, to show any activity. Consequently, the term for their interaction is **ligand-receptor interaction**. This is the case for chemotherapeutical as well as palliative drugs. Hence, the binding and its **specificity** is the molecular basis of all pharmacodynamic theories.

A binding process can only occur if two molecules interact at their **binding sites** by means of physicochemical processes. First, they require a reasonable spatial compatibility. Here, small molecules offer infinit rotational degrees of freedom. High-molecular weight molecules, such as proteins, are often able to a adjust their binding site slightly by **induced fit**. Most ligand-receptor interactions are non-covalent and are based on ionic, polar, hydrophobic and van der Waals interactions and interactions of aromatic $\pi$-oritals. Additionally, the hydrogen bond has an outstanding importance in biological and biopharmaceutical systems. Most interactions are reversible, therefore, competable and dynamic (Gohlke and Klebe, 2002).

The molecular binding can be described from different points of view. In total, it is classified thermodynamically. Here, the **Gibbs free energy G** must decrease in the total system while a binding occurs. The changes of $G$ during the binding process are related to the **changes in the enthalpy $\Delta H$** and **changes of the entropy $\Delta S$**.

$$\Delta G = \Delta H - T\Delta S \qquad (1.7)$$

An interaction in an aqueous environment as it is observed in this thesis requires the dissolution of the hydrate sphere of the binding partners (with $\Delta S > 0$ and $\Delta H < 0$) and the non-covalent attachment of the ligand to the receptor (with $\Delta S < 0$ and $\Delta H > 0$).

## 1.2.2. Polyvalency effects influence the molecular binding

In a polyvalent system the total change of the Gibbs free energy *G* is given by

$$\Delta G_{total} = \sum_{N} \Delta G_{N,mono} RT \ln(\beta_N) \qquad (1.8)$$

Here, $\beta$ is the enhancement factor for each single binding due to polyvalency effects (Mammen *et al.*, 1998). Normally, $\beta$ is rather positive which results in an exponentially increasing binding affinity of polyvalent systems. This is of particular interest in this thesis as polyarginines bear polyvalent guanidinium groups and multivalent peptide-polymer conjugates represent typical polyvalent systems.

In contact with lipid bilayers, polyvalently positively charged polymers can change the local lipid composition by lateral lipid segregation (Yaroslavov *et al.*, 2009).

The theory of multivalency can also be adopted to other ligand-receptor models such as the binding of a small molecule drug to its receptor. Whereas few hydrogen and ionic bonds lead to a weak binding, a higher number can lead to extremely high affinities as it is observed for the methotrexate-dihydrofolate interaction that is used as a model system in this thesis. Then the changes in the Gibbs enthalpy of a single interaction $\Delta G_n$ are summed up (Gohlke and Klebe, 2002). The same can be applied to protein-protein interactions (Reichmann *et al.*, 2007).

$$\Delta G_{total} = \sum_{1}^{n} \Delta G_n \qquad (1.9)$$

The effective valency of a polyvalent molecule is often determined by the steric properties of the molecule itself or the monomers it consists of. Some proteins have more than one binding site for a certain ligand. Streptavidin for instance bears four binding sites for biotin, many viruses have a well-defined topology resulting in a rather well-defined valency. The same is true for binding groups that are conjugated to a polymeric backbone in a site-specific manner.

If, however, an artificial polymer is synthesized randomly by the polymerisation of a mixture of two or more different monomers of which only one can bind to the ligand or if ligand-binding molecules are conjugated to a polymeric backbone in a non site-specific manner the average ratio of binding groups per molecule can be often determined experimentally. In the real situation there is a large statistic variety of ratios of both molecules. In this case the

distribution of molecules with different valencies can be assessed by means of a **Poisson distribution**

$$P_\lambda = \frac{\lambda^k}{k!} e^{-\lambda} \hspace{6cm} (1.10)$$

Here, the **valency distribution $P_\lambda$** and thus the fraction of a certain species of the polyvalent molecules with the **valencies $k$** is described by the **average ratio of ligand-binding groups per molecule** $\lambda$.
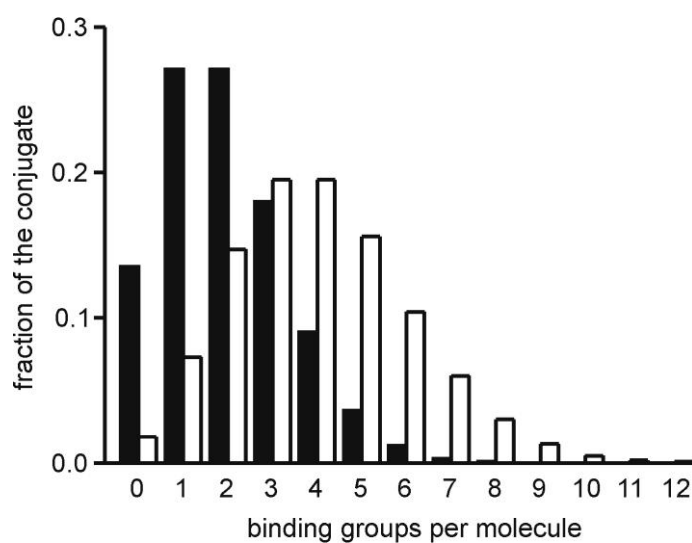


**Fig 1.5. The distribution of conjugates with different valencies in a mixture of statistically distributed polymers.** The black bars represent a conjugate with the average loading ratio of 2, the white bars represent a conjugate with the average loading ratio of 4.

The Poisson distribution obviously loses its validity if cooperative effects occur in the synthesis procedure.

## 1.2.3. The binding of small molecules to protein targets

The structure of a small therapeutic molecule can be divided in subareas. Whereas the subarea named pharmacophore is required for the specific ligand-receptor interaction, additional binding groups facilitate improved binding activity and specificity to the target. Often, one or more sites of the molecule are freely modifiable, but affect its pharmacokinetic properties. In these positions the drug can be conjugated to other molecules such as fluorophores. Within this thesis this was the case for the attachment of a linker and the fluorophore Cy5 to methotrexate and Parke-Davis compound.

The drug can compete with other molecules such as endogenous compounds for one particular binding site. Moreover, the drug molecule can also bind to other endogenous high-molecular weight targets, therefore **side targets**, which often decreases its specificity. For these reasons, it is of utmost importance to classify the **pharmacodynamic binding profile**, thus, the endogenous binding partners of the pharmaceutical molecule and the affinity of the respective ligand-receptor interactions.

Additionally, the range of efficacy of a drug can also be based on pharmacokinetics such as an explicitly high uptake rate in certain tissues or cells, as it is found for many polymeric drugs (Duncan, 2003), or it can be related to a differing metabolism in a certain cell type, that leads to variations in the molecular environment (Herman *et al.*, 2005).

Today, it is assumed that the human organism comprises between 5000 and 10000 potential drug targets (Drews, 2000) of which currently only approximately 500 are targeted by small molecule drugs (Drews and Ryser, 1997; Imming *et al.*, 2006). Hence, there is still an unmet need for the exploitation of novel drugable targets.
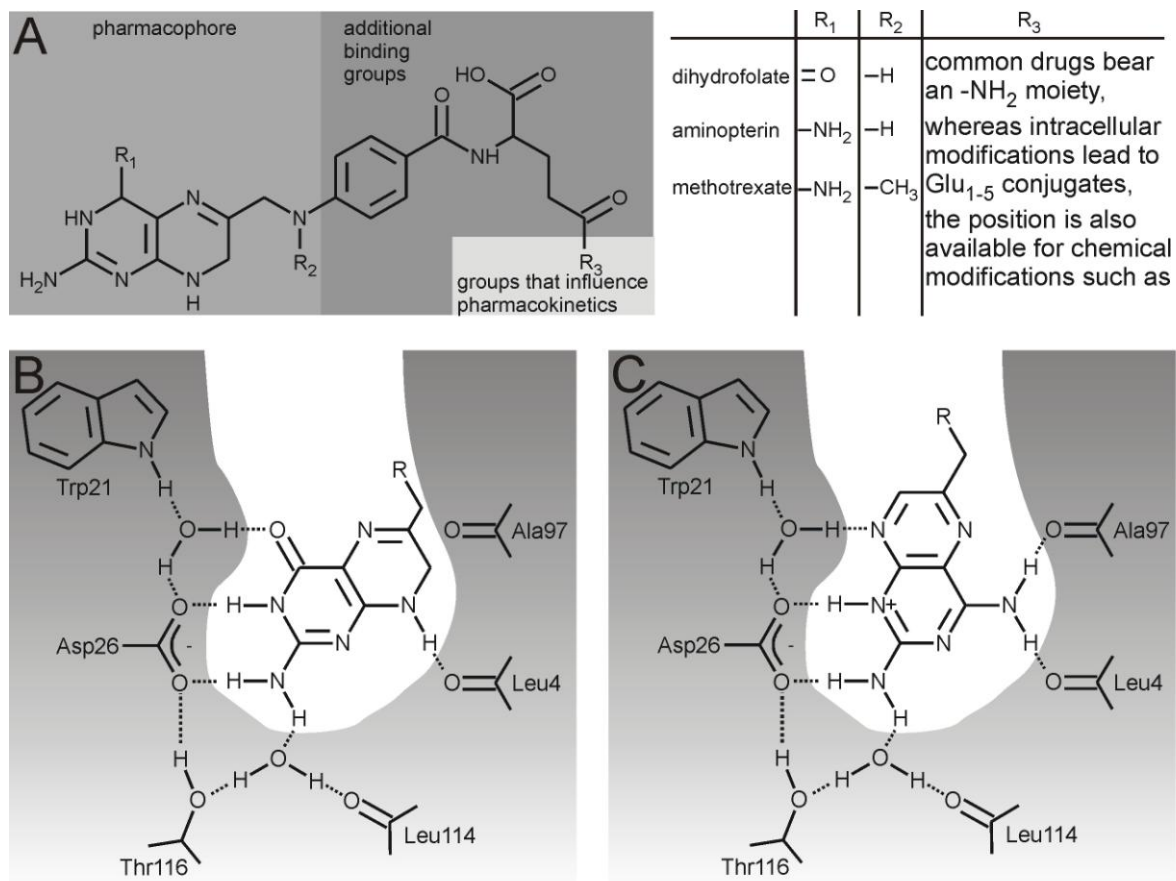
**Fig. 1.6. Structural requirements of the ligand-receptor interaction of dihydrofolate and its competitors with the dihydrofolate reductase binding site.** (A) The molecule can be divided in subareas: the pharmacophore, additional binding groups and a freely modifiable subarea. (B) The dihydrofolate pharmacophore interacts in a highly specific manner and binds non-covalently in its binding pocket in the dihydrofolate reductase. (C) Methotrexate binds to the same site, but the molecule is thereby slightly rotated and binding strengthened due to an additional hydrogen bond. The images were adopted from published data (Kubinyi, 1994; Steinhilber/Schubert-Zsilavecz/Roth, 2005).

## 1.2.4. Cellular pharmacodynamic parameters

The affinity of the interaction of a small molecule to a protein is typically described as the ratio between the concentrations of the unbound binding partners, therefore, the small molecule ligand $[L]_{free}$ and the unbound protein $[P]_{free}$ devided by the concentration of their complex $[PL]_{complex}$. It is quantified as the **equilibrium dissociation constant Kd**.

$$Kd = \frac{[L]_{free} \cdot [P]_{free}}{[PL]_{complexed}}$$
(1.11)

The inverse of the *Kd* value is named the **equilibrium association constant Ka**. The *Kd* value can also be also described thermodynamically by:

$$Kd = e^{-\frac{\Delta G}{RT}}$$
(1.12)

The parameter *R* is the gas constant, 8.31 JK$^{-1}$mol$^{-1}$. The third possibility to express the *Kd* is to describe it kinetically as a function of the **rate constant of the association $k_{on}$** and of the **rate constant of the dissociation $k_{off}$**.

$$Kd = \frac{k_{on}}{k_{off}}$$
(1.13)

Kinetics and thermodynamics are combined here. This is highly relevant as this relationship shows that a high affinity can also be based on kinetics if the association is particularly fast and/or the dissociation is particularly slow. The logarithm of the equilibrium constant $K_S$, that describes the degree of proton dissociation and association to a substance *S*, respectively, is for acidic compounds given by the **Henderson-Hasselbalch Equation**

$$pK_S = pH - \log \frac{[S^-]}{[SH]}$$
(1.14)

and for basic compounds as

$$pK_S = pH - \log \frac{[S]}{[S^+]}$$
(1.15)

By means of inductive, tautomeric and mesomeric effects the charge can be distributed over larger areas of the molecule.The above-mentioned relationships have a crucial impact on the binding properties, but also on pharmacokinetic parameters such as hydrophobicity, cell permeability and intracellular localization. For instance, a substance that is dissolved in blood or an respective buffer at pH 7.4 and is taken up via endocytosis may change its properties completely due to lysosomal acidification to approximately pH 5. In the cytosol, with a pH value of approximately 7.2, the proton concentration is therefore nearly 160-fold lower. There is evidence that this plays a key role in the endosomal escape of arginine-rich peptides (Fischer *et al.*, 2004), but was not quantified for many drugs so far.

At a given total target protein concentration and a total small molecule concentration and known *Kd* the fraction of the bound receptor molecules, the **occupancy**, can be easily calculated by

$$PL_{complexed} = \frac{100\% \cdot [L]}{K_D + [L]}$$

(1.16)

If a certain concentration of a competitive inhibitor *[I]* with an **inhibitor constant $K_i$** is added to the ligand-receptor equilibrium, the fraction of complex between the ligand and the protein diminishes.

$$[PL]_{complexed} = \frac{100\% \cdot [L]}{\left(1 + \frac{[I]}{K_i}\right) K_D + [L]}$$

(1.17)

In general, the concentration that is required in order to reach the half-maximal effect is given as *EC50*. For enzymatic inhibition the concentration of the half-maximal inhibition, the *IC50*, is given. The results of binding experiments are plotted as **dose-response curves**. Here, the respective *EC50* can be directly quantified. The biological activity or effect at a certain ligand-inhibitor-receptor equilibrium is named **potency**. If the receptor concentration is also known, the *Kd* can be easily calculated.
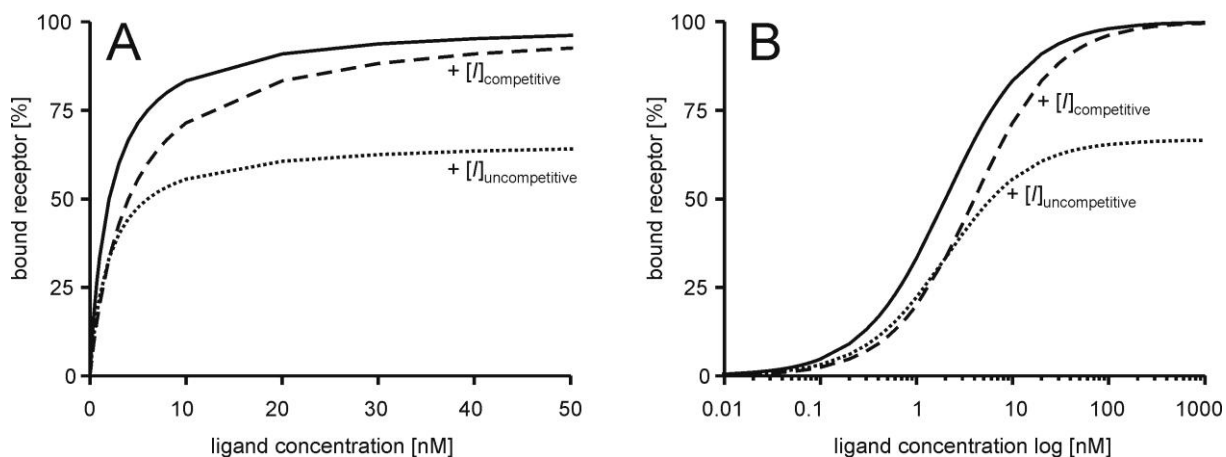
**Fig. 1.7. Dose-response curves of a theoretical experiment.** The calculations assume a ligand-receptor interaction with an *EC50* of 2 nM and are shown as (A) a linear and as (B) a logarithmic plot. The data without an inhibitor show the half-maximal binding at 2 nM, which exactly represents the *EC50*. If a competitive inhibitor is added (dashed lines), the curve is shifted to larger ligand concentrations, whereas an uncompetitive inhibitor (dotted lines) leads to lower levels of bound receptor.

The above-mentioned dose-response curves can be fitted by the formula

$$effect = bottom + \frac{top - bottom}{1 + \left(\dfrac{c}{EC50}\right)^{hillslope}} \qquad (1.18)$$

Here, the hill slope reflects the steepness of the curve. According to the **Cheng-Prusoff Equation** the *IC50* value is not only proportional to the inhibitor constant $K_i$ of the compound, but also reciprocally proportional to the concentration of a second ligand [*L*] divided by the $K_m$ value of *L* (Cheng and Prusoff, 1973). This is of particular interest in experiments dealing with kinase inhibitors as in this particular case considerable impurities with other kinases and especially the competition with endogenous ATP plays a crucial role.

$$K_i = \frac{IC50}{1 + \dfrac{[L]}{K_m}} \qquad (1.19)$$

## 1.2.5. Special concerns regarding protein kinase inhibitors

The formation of phosphate esters is naturally catalyzed by kinases and plays a key role in cellular homeostasis and intracellular signal transduction. Protein kinases control the cell cycle (Butt *et al.*, 2008), intercellular attachment, interaction with extracellular matrices, angiogenesis (Roodhart *et al.*, 2008), apoptosis (So *et al.*, 2007; Strasser *et al.*, 2009), inflammation (Wagner and Laufer, 2006) and other intracellular signalling cascades, they control the excretion of hormones, interleukines and other factors that allow intercellular communication. Great efforts were made to untangle the highly complex signal transduction networks of kinases (Stoevesandt and Taussig, 2007). A divergent balance of stimuli can lead to differing effects of the same signal transduction network and thus to different effects of certain small molecule inhibitors (Kohler *et al.*, 2008). More than 500 putative protein kinase genes have been identified, constituting about 1.7 % of all human genes (Manning *et al.*, 2002). Many of the phosphorylated sequences are recognized by phosphorylation-dependend binding motifs such as Src homology 2 (SH2), phosphotyrosine binding (PTB), BRCA1 C-terminal (BRCT) and 14-3-3 domains. More than 175 kinases and their substrate specificities and over 100 phosphorylation-dependent binding domains of all kind were collected in an atlas in the data bank *NetPhorest* (*http://netphorest.info*) (Miller *et al.*, 2008). Recently, the structure and function of numerous protein phosphotyrosine containing proteins and their binding partners was elucidated further (Barr *et al.*, 2009).

As protein kinases are involved in numerous serious diseases with a large market potential such as cancer, up to 30 % of all drug-discovery programs in the pharmaceutical industry deal with kinase inhibitors and numerous drug kinase inhibitors are in clinical trials or are on the market (Knight and Shokat, 2005).
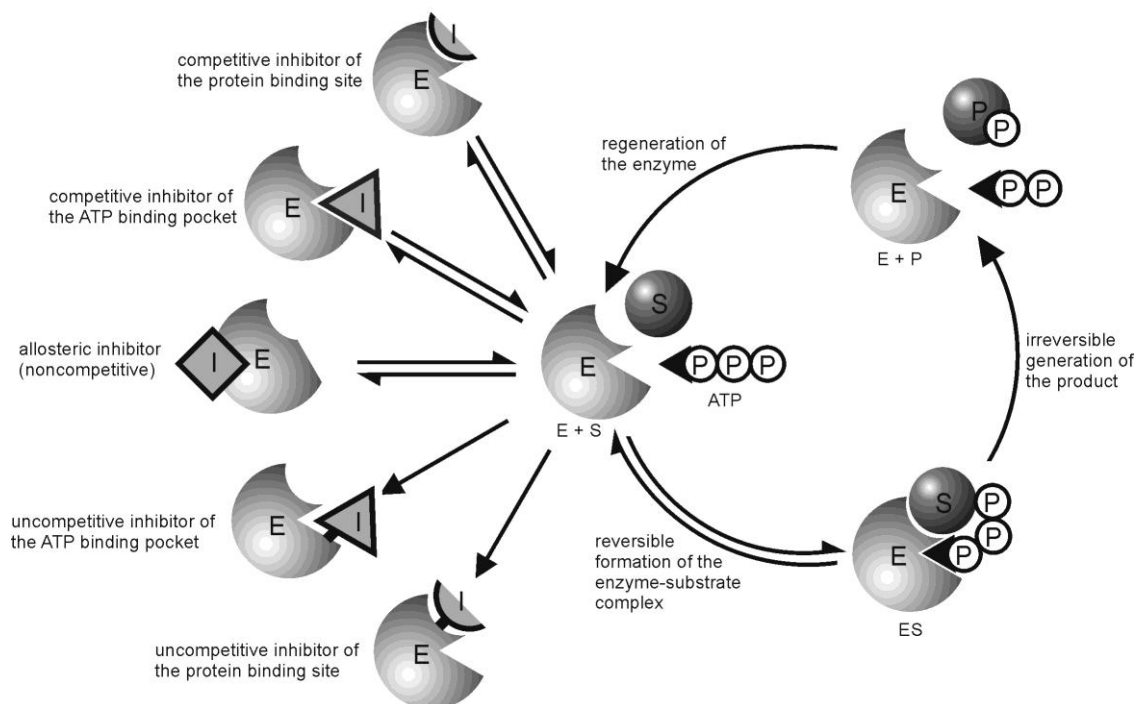
**Scheme. 1.8. Protein kinase inhibitors.** Most commercial kinase inhibitors (*I*) compete reversibly for the ATP binding pocket.

The vast majority of synthetic small molecule protein kinase inhibitors binds to the ATP binding pocket and competes with endogenous ATP. Here, the Michaelis-Menten constant $K_M$ for ATP in various kinases differs over three orders of magnitudes (Knight and Shokat, 2005). Thus, the ATP concentration employed in an *in vitro* assay certainly is a critical issue as well as the concentrations of cofactors such as magnesium ions (Chrisman *et al.*, 1984). Due to the similarity of the ATP binding sites in various kinases and other ATP-consuming enzymes many kinase inhibitors bear a rather promiscuous target profile (Capdeville *et al.*, 2002). Entirely specific effective kinase inhibitors were not developed yet.

For this reason, inhibitors that facilitate the disruption of protein-protein interactions with a *Kd* in the nanomolar range would be of great interest (Berg, 2008). Although protein-protein interactions are examined by means of numerous approaches that combine bioinformatics and peptide-based experimental techniques such as protein epitope mimetic (Robinson *et al.*, 2008), the physicochemical mechanisms of protein-protein interactions are still not entirely understood (Reichmann *et al.*, 2007).

In summary, the screening and *in vitro* testing of kinase inhibitors is still a delicate issue and is hampered by the imperfection of the implemented screening techniques.

## 1.2.6. Screening and lead optimization of kinase inhibitors

In a first step, the modern drug discovery strategies require the identification of hit structures that are subsequently altered and optimized regarding their pharmacodynamic and pharmacokinetic properties and are finally pharmaceutically formulated and tested in preclinical and clinical phases. Lead structures can be of natural origins or be the outcome of high-throughput screening processes in which libraries of more or less randomly or rationally synthesized compounds are tested.

The libraries used for primary screens regularly comprise more than $10^5$ compounds, the ones utilized for secondary screens approximately $10^3$ compounds. The compounds are tested in protein binding assays, kinetic studies and cell culture tests. Approximately 10 promising candidate structures are selected as lead structures, optimized further and tested in preclinical studies. Only few compounds, if any, reach the phase I-IV clinical studies (Nolan, 2007).

Traditionally, kinase inhibiting compounds are tested in protein activity assays by means of radioactivly labeled $\gamma^{32}$P-ATP (Witt and Roskoski, Jr., 1975; Casnellie, 1991). This test method is relatively slow, requires considerable care of the experimenters and is nowadays often displaced by other techniques (Lehel *et al.*, 1997). Colorimetric assays have gained an increasing importance in high-throughput screening (Chapman and Wong, 2002). These assays and the $\gamma^{32}$P-ATP-based assays mentioned above are based on highly purified kinases that often tend to precipitate.

One of the most important assays for the screening of drug-target interactions in today's drug discovery programs is the fluorescence depolarisation assay (van de Ven *et al.*, 1984; Seethala and Menzel, 1997). Typically, a small molecule ligand is conjugated to spacers and fluorophores and is mixed with the purified high-molecular weight protein binding partner. The labelled small molecule ligand is competed with various amounts of different unlabeled compounds. Polarized light is irradiated into a sample and the excites molecules emit light. The rate-dependent loss of linear polarization is measured. As it is dependent on the rotation of the molecules and small molecules rotate faster and therefore show a higher rate of depolarization, the binding equilibria can be calculated. The advantages of the fluorescence depolarization assay are that the protein consumption is rather low and that the test is extremely fast and allows high-throughput screening of whole libraries of millions of substances in a respectively short period of time. The major drawback is that the technique is not very precise and that binding to side targets and unspecific binding is not distinguishable. Each fluorescently labeled molecule that binds to any high-molecular weight binding partner shows binding activity whether it binds to its specific binding site or just adsorbs

unspecifically. In order to perform accurate measurements the technique requires highly purified kinases.

A relatively modern approach is the use of *Kinobeads* (*Cellzome AG*). Here, small molecule ligands were conjugated to microspheres and the kinase binding partners are fished out of a solution, that can represent or imitate the physiological environment. By means of competition experiments this assay allows the generation of quantitative data regarding the target profile of drugs (Bantscheff *et al.*, 2007). This technique is useful for the description of target profiles of molecules by means of competition assays.

For lead optimization procedures optical biosensors have an increasing importance (Cooper, 2002). Especially the techniques that are based on surface plasmon resonance (SPR) are able to display the kinetics and dynamics of molecular binding processes (Flanagan and Pantell, 1984). Many commercially available SPR-based tools are on the market (e.g. *Affinity sensors*, *Biacore*, etc.). The technique is based on changes of the refractive index of a layer due to binding of one binding partner and allows the calculation of Kd values based on measurements of the on and off rates. A similar technique is represented by reflectrometric interference spectroscopy (RIfs) (Piehler *et al.*, 1996). Here, the changes in the thickness of a layer are detected. Both techniques are highly dynamic, work with label-free ligands and receptors and give information about the ligand-receptor binding process and several samples can be read-out in parallel, but have the considerable drawback that the specificity of the binding is not displayed, purified receptor molecules are required and the receptor or the ligand have to be immobilized in a way that maintain activity.

Furthermore, structure-related techniques such as the nuclear magnetic resonance (NMR) spectroscopy have an increasing importance concerning lead optimization processes (Pellecchia *et al.*, 2002).

In summary, it is obvious that there is still an unmet need for development of technologies that facilitate *in vitro* measurements of compound-target interactions in a physiological context and that do therefore not require purified enzymes and that are able to distinguish between specific on-target, off-target and unspecific binding. Next to others, this challenge is addressed in this thesis.

# 1.3. Techniques

## 1.3.1. Confocal laser scanning microscopy

Confocal laser scanning microscopy (LSM) represents an optical technique that allows the pixel-wise scanning of a precisely defined optical plane.

Referring to the microscopic system used in this thesis, one or two laser beams are reflected by a semi-transparent filter (an acusto-optical beam splitter (AOBS)) and are focused into the specimen by an immersion objective with a high numerical aperture *NA*. The latter is required to achieve an efficient collection of the fluorescent light out of a small detection volume (Abbe, 1873). The parameter *n* describes the refractive index of the immersion medium between the lens and the specimen and *sin θ* represents the half-angle of the light cone that can enter the lens.

$$NA = n \cdot \sin \theta \qquad\qquad (1.20)$$

The numerical aperture limits the maximal resolution *d* of all common light microscopes. The theoretically maximum of the resolution of a classical microscope is also limited by the wavelength *λ* of the used light. The shorter the wavelength, the higher is the achievable resolution. This drawback in resolution has recently been overcome by the Stimulated Emission Depletion (*STED*) technique (Westphal and Hell, 2005; Kastrup *et al.*, 2005), but is not yet wide-spread, has no application in this thesis and is therefore not discussed further.

The light that has entered the sample excites the fluorophores, which emit light that is partly collected by the objective, bundled and conducted back via the same optics. The bathochrome shifted emission light can now pass the AOBS and by means of a convex lens the detection volume is imaged into a pinhole. The pinhole allows the restriction of the size of the detection volume to a sub-femtoliter volume. The light that passes the pinhole is split spectrally by means of a prism. Then, the light of a certain wavelength interval is collected by independent photomultiplyer tubes (PMTs). The image is generated by a computer-assisted method via the scanning of several thousands of pixels. Additionally, the microscope also allows the generation of a quasi-three-dimensional image by scanning numerous optical slices in different heights.

.
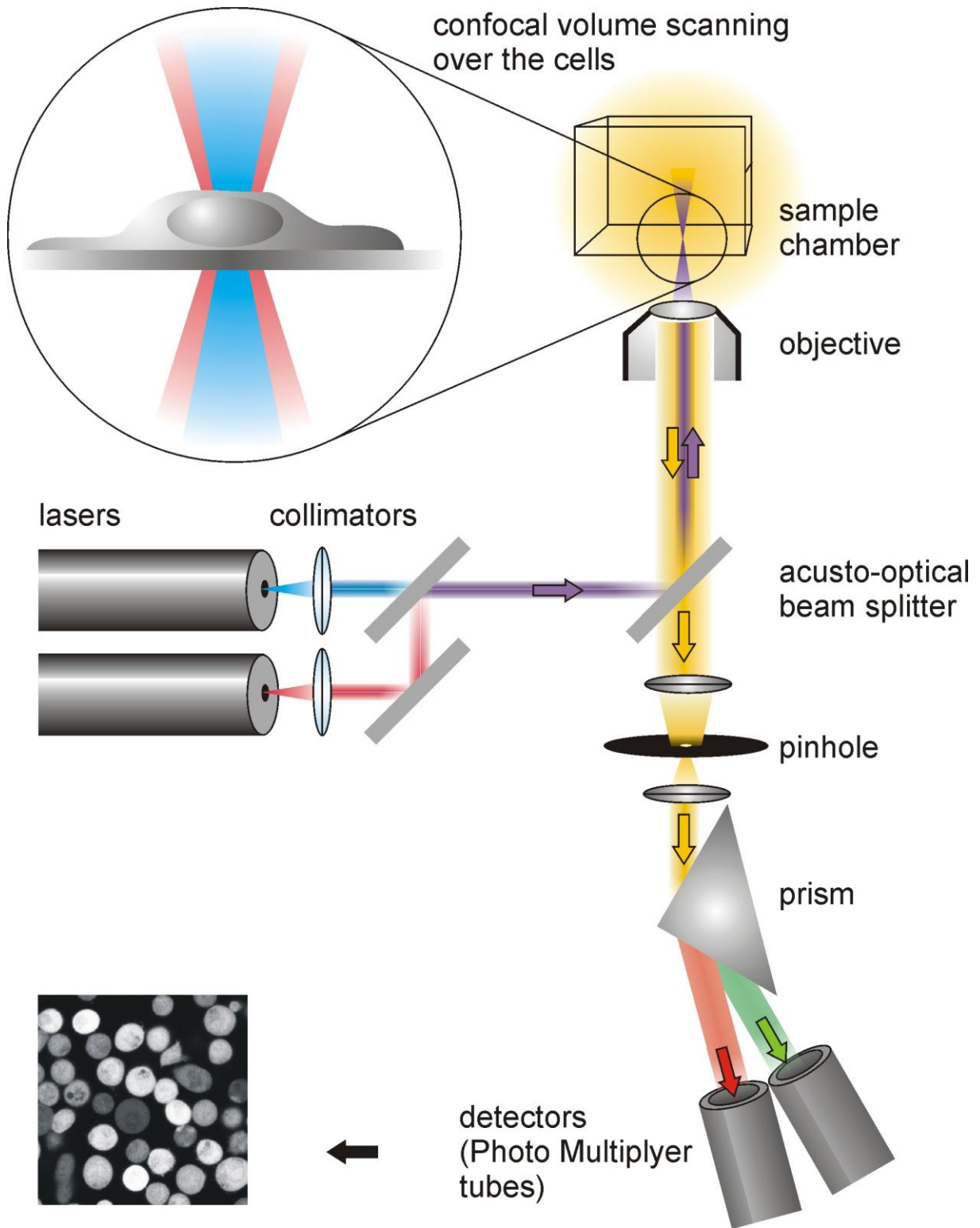
**Fig. 1.9. Optical path of a laser scanning microscope based on *Leica* technique.**

## 1.3.2. Fluorescence correlation spectroscopy

"NAM CORPUS NULLUM NISI IN TEMPORE MOUERI AUDIO. [... ] CUM ENIM MOVETUR CORPUS TEMPORE METIOR QUAMDIU MOVEATUR EX QUO MOVERI INCIPIT DONEC DESINAT." ("For I hear that no body is moved but in time. […] For when a body is moved, I by time measure how long it may be moving from the time in which it began to be moved till it left off." (Augustinus, 398))

Fluorescence correlation spectroscopy (FCS) first presented by Elson and Webb in the 1970s (Elson and Webb, 1975) was later developed further as a microscopy-based technique that allows the determination of the diffusion velocity of single molecules in solution and the exact quantification of fluorophore concentrations in a sub-nanomolar range (Rigler *et al.*, 1993). Comparable to the confocal laser scanning microscope, a laser beam is focussed into the sample via a beam splitter, in the case of the mostly employed *Leica SP5* system an acusto-optical beam splitter (AOBS), and an immersion objective with a high numerical aperture. The light that is emitted by the excited fluorophores is partly collected by the objective, bundled and conducted back via the same optics. Due to its bathochrome shift the light can now pass the AOBS and by means of a convex lens the detected sample volume is imaged into a pinhole. The latter allows the restriction of the size of the detection volume to a volume in the sub-femtoliter range. The light that passes the pinhole is detected by an avalanche photo diode (APD). Here, the photons per second are counted. A computer-assisted process generates a time-resolved fluorescence fluctuation profile and calculates an autocorrelation function. By fitting the autocrorrelation function the number of molecules $N$ that dwell averagely in the detection volume and their diffusion time $\tau_D$, thus the average residence time of the fluorophore in the detection volume, can be determined. From these values the fluorophore concentration can be calculated and the molecular weight can be assessed based on knowledge of the physical characteristics of the solvent, the influence of the measurement temperature and the shape and the density of the differing molecule. Additionally, FCS provides information about the photophysical properties of the observed molecule itself, such as its triplet time $\tau_{tr}$ and its triplet amplitude $G_{tr}$, thus, the fraction of molecules that dwell in the triplet state. Therefore, FCS is a highly valuable tool in biochemistry and can also be applied on the cellular level (Brock *et al.*, 1999; Kim *et al.*, 2007; Bacia *et al.*, 2006). An extension of the technique is the use of two fluorophores enabling fluorescence cross-correlation spectroscopy (FCCS) (Schwille *et al.*, 1997). The sample is hereby excited with the light of two laser lines, and the fluorescence is split spectrally by a beam splitter and detected by two independent APDs. This technique reveals all the information given by single-color FCS and, additionally, information on the fraction of

molecules that diffuse conjointly. It is regularly used to quantify degradation processes of dual-labeled molecules and to quantify ligand-target interactions (Weidemann *et al.*, 2002).
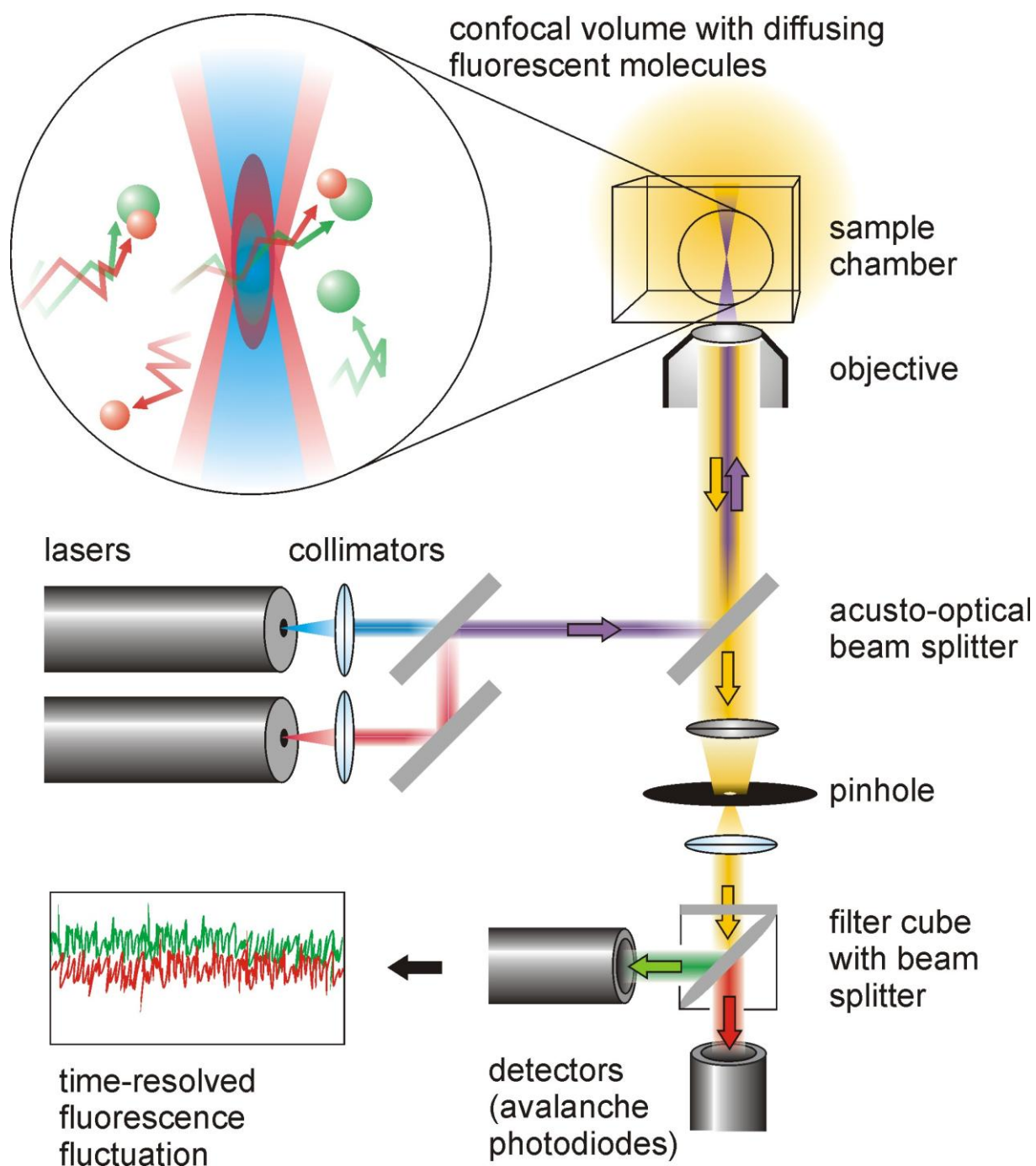


**Fig. 1.10. Mode of the operation of an FCCS apparatus based on *Leica* technique.**

The size of the detection volume is defined by the confocal optics, by the pinhole and by the wavelength-dependent diffraction of the light. The larger the wavelength $\lambda$, the weaker is the diffraction of the laser light at a given diffractive index of the lens and the larger are the dimensions of the detection volume. Thus, a light beam with a short wavelength in the green

part of the spectrum $\lambda_g$ leads to a smaller detection volume than one in the red part of the spectrum $\lambda_r$. The theoretical overlap of the two channels *CC* can be maximally

$$CC = \frac{\lambda_g^3 \cdot \lambda_r^3}{\lambda_g^3}$$

(1.21)

This value also represents the maximal fraction of cross-correlating particles, referred to the green channel. The spatial intensity profile of the excitation light is displayed by the point spread function (*PSF($\bar{r}$)*) divided by the excitation intensity $I_0$, the emission profile is expressed by the collection efficiency function (*CEF($\bar{r}$*). The spatial profile of the detection volume *W($\bar{r}$)* is therefore given by

$$W(\bar{r}) = \frac{PSF(\bar{r})}{I_0} CEF(\bar{r})$$

(1.22)

In a first approximation *W($\bar{r}$)* can also be represented by a Gaussian Distribution (Weidemann *et al.*, 2002) and is describable as an ellipsoid with the effective volume $V_{eff}$. The three-dimensional extensions are defined by the spatial positions *x, y* and *z* the lateral radius $\omega_{xy}$ and the axial radius $\omega_z$.

$$W(\bar{r}) = e^{-2\frac{x^2+y^2}{\omega_{xy}^2}} \cdot e^{-\frac{z^2}{\omega_z^2}}$$

(1.23)

$$V_{eff} = \frac{4}{3}\pi\omega_{xy}^2\omega_z$$

(1.24)

The structure parameter *S* is hereby defined as the ratio of $\omega_z$ and $\omega_{xy}$ and should be >1.

$$S = \frac{\omega_z}{\omega_{xy}}$$

(1.25)

The fluorescence occurring from the detection volume $V_{eff}$ is detected over time and the generated fluctuation profile is analyzed by means of a computer-based method. Here, the fluorescence count rate *F*, which is recorded over the entire measurement period, is averaged out.

$$\langle F \rangle = \frac{1}{T} \int_0^T F(t)dt \tag{1.26}$$

Then, the positive and negative deviation of the detected fluorescence count rate $\delta F$ from the respective average $\langle F \rangle$ is recorded for multiple time points $t$ and time intervals $\tau$. These calculations lead to the autocorrelation function $G(\tau)$

$$\delta F(t) = \int_V W(\bar{r}) \cdot \delta(\eta c(\bar{r}, t))dV \tag{1.27}$$

$$G(\tau) = \frac{\langle \delta F(t) \cdot \delta F(t + \tau) \rangle}{\langle F \rangle^2} \tag{1.28}$$

The effective number of particles that on average dwell in the detection volume $N_{eff}$ is calculated by

$$N_{eff} = \frac{1}{G(0)} \tag{1.29}$$

The triplet state is described by the triplet time $\tau_T$ and the triplet amplitude $T$

$$G(\tau) = 1 + \frac{T}{1-T} \cdot e^{\frac{\tau}{\tau_T}} \tag{1.30}$$

Thus, the entire curve can be fitted by the term

$$G(\tau) = \left(1 + \frac{T}{1-T} \cdot e^{\frac{\tau}{\tau_T}}\right) \cdot \frac{1}{N_{eff}} \cdot \frac{1}{1 + \frac{\tau}{\tau_D}} \cdot \frac{1}{\sqrt{1 + \frac{\tau}{S^2 \tau_D}}} \tag{1.31}$$

All models described here base on the assumption that all observed particles bear the same molecular brightness. This was also the case in this thesis. Otherwise, in multicomponent mixtures, the molecular brightness has to be corrected as the contribution of a certain species to the total autocorrelation function depents on its molecular brightness by the power of two (Weidemann *et al.*, 2002).
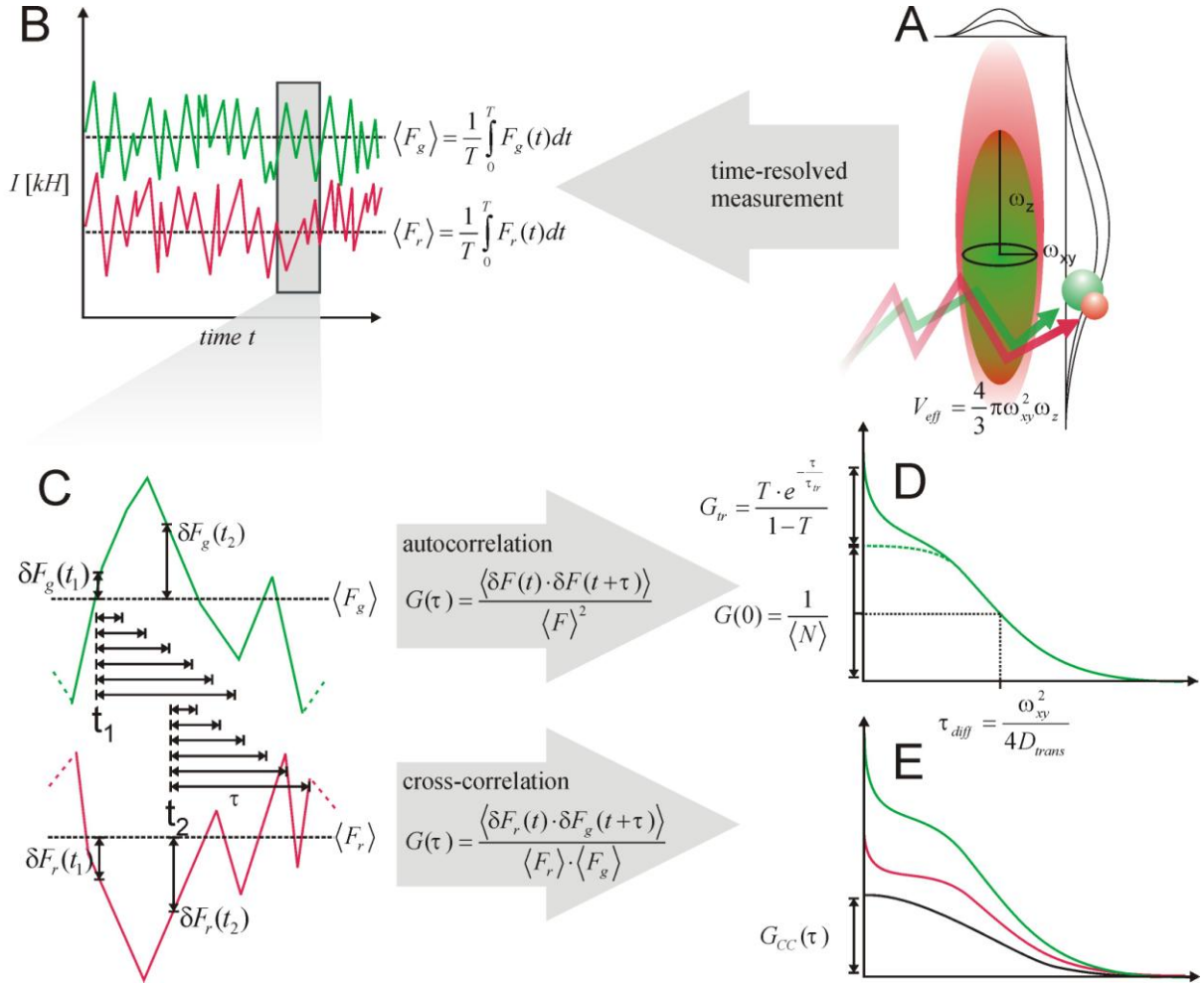
**Fig. 1.11. Generation of data from FCCS experiments.** (A) The intensity profile of the detection volume determined by means of the confocal optics represents a three-dimensional Gaussian Distribution. (B) The time-resolved fluorescence fluctuations of both channels are detected. (C) Based on these data the curves are correlated with themselves (FCS) and with each other (FCCS), respectively, which leads to (D) autocorrelation and (E) cross-correlation curves.

For dual-color FCCS the fluctuations of the detected fluorescence count rates of the green detection channel $\delta F_g$ and the red channel $\delta F_r$ from the respective averages $<F_g>$ and $<F_r>$ are correlated with each other and lead to the cross-correlation function $G_{CC}(\tau)$.

$$G_{CC}(\tau) = \frac{\left\langle \delta F_g(t) \cdot \delta F_r(t+\tau) \right\rangle}{\left\langle F_r \right\rangle \cdot \left\langle F_g \right\rangle} \tag{1.32}$$

Potential effects such as quenching and cross-talk have to be carefully considered and, if necessary, be mathematically corrected (Weidemann *et al.*, 2002; Földes-Papp, 2005). In

this thesis these obstacles were circumvented by the careful choice of spectrally and spatially well-separated fluorophores.

In order to obtain an accurate quantification of the particle number $N$ in the lower concentration ranges it is essential to take the fluorescence background as well as scattered light into consideration. Here, the signal-to-noise ratio can be relatively small and, hence, the measured particle number $N_{measured}$ is typically overestimated whereas the fluorescence per molecule $fpm$ is underestimated. Thus, the background intensity $I_{background}$, determined by the measurement of the sample buffer without the respective fluorophore, has to be subtracted from the total intensity $I_{total}$, measured in each of the corresponding fluorophore-containing samples. For an autocorrelation function $G(0)$ the corrected number of particles $N_{corrected}$ can be calculated according to the formula (Koppel, 1974) :

$$G(0) = 1 + \frac{1}{N_{measured}} = 1 + \frac{\left(1 - \frac{I_{background}}{I_{total}}\right)^2}{N_{corrected}} \tag{1.33}$$

$$N_{corrected} = N_{measured} \cdot \left(1 - \frac{I_{background}}{I_{total}}\right)^2 \tag{1.34}$$

Additionally, the fluorescence per molecule $fpm$ can be calculated, what represents an important control, as at a certain laser power the $fpm$ should not be affected by the fluorophore concentration:

$$fpm = \frac{(I_{total} - I_{background})}{N_{corrected}} \tag{1.35}$$

According to this technique the measurement of low intracellular concentrations in facilitated in the presence of background (Brock *et al.*, 1998).

In order to determine the precise concentration of the measured fluorophores the exact volume of the detection volume $V_{eff}$ has to be determined. The size of the detection volume can be determined in different ways. The first method is to measure a sample with a known concentration $c$ and, subsequently, calculate the volume by (Buschmann *et al.*, 2007)

$$V_{eff} = \frac{1}{G_0 \cdot N_A \cdot c} \tag{1.36}$$

$N_A$ represents the Avogadro number, therefore $6.022*10^{23}$ mol$^{-1}$. The major drawback is the fact that the exact adjustment of fluorophore concentrations in the lower nanomolar range is a highly critical issue.

The second possibility is to measure the diffusion time $\tau_D$ and the structure parameter $S$ in order to calculate the lateral extension of the diffusion volume $\omega_{xy}$. This approach requires knowledge about the diffusion constant $D$ of the respective fluorophore.

$$\omega_{xy}^2 = 4D\tau_D \tag{1.37}$$

Assuming that the shape of the detection volume is elliptic and the intensity profile follows a Gaussian Distribution, the effective volume $V_{eff}$ is

$$V_{eff} = \frac{4}{3}\pi\omega_{xy}^3 S \tag{1.38}$$

The effective concentration $c_{eff}$ of fluorophores can be easily calculated by the effectively measured number of measured particles $N_{eff}$ by

$$c_{eff} = \frac{N_{eff}}{V_{eff} \cdot N_A} \tag{1.39}$$

Information of protein interactions can also be gained by a novel technique named cross correlation raster image spectroscopy method (Digman *et al.*, 2009) which is based on the rapid generation of confocal images and displays the cross-correlation in each pixel of the microscopic image.

# 2. HPMA as a Scaffold for the Modular Assembly of Functional Peptide Polymers by Native Chemical Ligation

This chapter is based on a publication in Bioconjugate Chemistry in 2008. The author of this thesis contributed Fig. 2.1-2.6 The caspase assay depicted in Fig. 2.7 was kindly provided by Dr. Falk Duchardt.

## 2.1. Summary

Synthetic peptides are valuable tools in fundamental and applied biomedical research. On one hand, these molecules provide highly efficient access to competitive inhibitors of molecular interactions and enzyme substrates by rational design. On the other hand, peptides may serve as powerful vectors to mediate cellular uptake of molecules that otherwise enter cells only poorly. The coupling of both such functionalities provides access to molecules interfering with molecular processes inside the cell. However, the combination of several functionalities on one synthetic peptide may be compromised by problems associated with the synthesis of long peptides. Native chemical ligation enables the chemoselective coupling of fully deprotected functional building blocks. However, peptide thioesters are still not accessible by standard solid phase peptide synthesis. Here, we demonstrate the cofunctionalization of a thioester-activated N-hydroxypropyl methacrylate (HPMA) copolymer (28,500 Da) with the cell-penetrating peptide (CPP) nonaarginine and a bioactive peptide as independent building blocks by native chemical ligation. Nonaarginine was employed as a cell-penetrating peptide (CPP), a fluorescein-labeled analog of a pro-apoptotic peptide as a biofunctional cargo. Incorporation of the fluorescein label enabled the highly sensitive quantification of the coupling stoichiometry by fluorescence correlation spectroscopy (FCS) using 0.4 pmol/ 12 ng of labeled construct. A construct only bearing the functional cargo-peptide required cellular import by electroporation in order to show activity. In contrast, a construct combining all functionalities was active upon incubation of cells, validating the modular nature of the approach.

## 2.2. Introduction

Peptides provide a rich source of bioactive molecules and numerous peptides and analogs are now used as drugs (Hruby and Balse, 2000; Bray, 2003; Leader et al., 2008). In fundamental biological and biomedical research, peptides have become a highly valuable tool for defining the principles of molecular recognition (Cooper and Waters, 2005).

However, given the poor capacity of peptides to enter cells, most applications of bioactive peptides have focused either on extracellular targets, recombinant proteins or cell lysates. In order to mediate cellular entry, over the past years, conjugation with cell-penetrating peptides has received increasing attention. Cell-penetrating peptides are a diverse class of peptides of 8 to 30 amino acids in length that promote the cellular uptake of the cargo molecules they are connected to (Fischer *et al.*, 2005). In our hands, nonaarginine has proven to be a CPP of choice (Wender *et al.*, 2000). This CPP is very well tolerated by cells, has high import efficiency and moreover, truncated sequences also show high activity as a CPP, rendering purification less problematic (Mitchell *et al.*, 2000).

For the cellular import of peptides, in most cases, the conjugation with the CPP occurs by N-terminal elongation during solid-phase peptide synthesis. However, especially for longer peptides, purity and post synthesis work-up may become limiting factors. Moreover, in order to streamline the process from in vitro to intracellular testing, one may want to render a peptide, that has shown activity in an in vitro assay, competent for cell entry without the need for de novo synthesis of a cell-penetrating analog.

Native chemical ligation (NCL) has proven to be a potent technique for the efficient and chemoselective coupling of fully deprotected peptides (Dawson *et al.*, 1994; Tam *et al.*, 2001). In its original form, a peptide, bearing an N-terminal cysteine residue forms an amide bond with another peptide, carrying a C-terminal thioester-activated amino acid. In spites of its success in the synthesis of longer polypeptides the lack of protocols to generate the required C-terminal thioesters by standard solid-phase peptide chemistry is still a limiting factor for its broader application.

As an alternative approach to overcome these limitations, we here describe the modular coupling of cysteine-bearing unprotected peptides to thioester-activated hydroxypropyl methacrylamide copolymer (HPMA). The HPMA serves as a linear scaffold to which the functional peptides are linked. HPMA has been demonstrated to be biocompatible and has therefore been used as a drug carrier in numerous applications (Duncan, 2003; Kopecek and Bazilova, 1973; Kopecek *et al.*, 2000). Furthermore, conjugation with the Tat-derived CPP (Schwarze *et al.*, 1999) has been shown to facilitate the uptake of HPMA-doxorubicin conjugates (Nori *et al.*, 2003).

The pro-apoptotic peptide AVPIAQK (Fotin-Mleczek *et al.*, 2005b; Fulda *et al.*, 2002a) served as a bioactive cargo. This peptide corresponds to the seven N-terminal amino acids of the Smac (second mitochondria-derived activator of caspase) protein (Wu *et al.*, 2000). Smac is a pro-apoptotic protein, that, following an apoptotic stimulus, is released from mitochondria and inhibits the anti-apoptotic action of IAPs (inhibitors of apoptosis proteins) (Du *et al.*, 2000). Introduction of this peptide into cells specifically enhances the controlled cell death, i. e. apoptosis, in cells exposed to ligands of death receptors such as the Tumor Necrosis Factor-receptor or Fas (Fulda *et al.*, 2002a). This peptide exerts this activity only when introduced into the cytoplasm. We had shown for this peptide previously, that measurement of cell viability provides a reliable read-out for comparing import efficiencies of different delivery strategies (Fotin-Mleczek *et al.*, 2005b).

With respect to the quantification of coupled peptides per polymer, three options were considered. The first option had been the implementation into the synthesis protocol by photometric determination of a leaving group that is released upon coupling of a bioactive moiety (Searle *et al.*, 2001). The second option is based on the degradation of an aliquot of the conjugate post synthesis and quantification of a suitable degradation product of the bioactive moiety (Ding *et al.*, 2006). Finally, the third option is based on the spectroscopic quantification of a functional group per unit weight of polymer. Using a fluorescently labeled conjugate of the bioactive moiety we chose options two and three. Confocal fluorescence-correlation spectroscopy (FCS) was employed as the analytical method to follow the release of a degradation product according to option two (Rigler *et al.*, 1993). This technique provides information on the average number and size of fluorescently labeled molecules diffusing through a confocal detection volume. FCS works at concentrations of probe molecules in the lower nanomolar to subnanomolar range and in microliter volumes, therefore reducing sample consumption to a minimum.

Our results show that the functionalization of HPMA via NCL occurs with uniform yields. By addressing the activity and cellular uptake of HMPA conjugated either to the AVPIAQK peptide or R9 alone or a combination of both peptides it is established that all three molecular entities act as functionally independent building blocks.

## 2.3. Experimental Procedures

## 2.3.1. Reagents

The preactivated hydroxypropyl methacrylamide copolymer N-methacryloylglycylglycine p-nitrophenyl ester (poly(HPMA-co-methacrylate-Gly-Gly-p-nitrophenyl ester)) was supplied by Polymer Laboratories (Shropshire, Great Britain). It has a linear structure, an average molecular weight (MW) of 28.5 kDa (MW/Mn: 1.32) and a total nitrophenol content of 8.28 mol%. Based on the specifications provided by the manufacturer we estimated 12.5 reactive groups per molecule. Rink amide resin was from Rapp Polymers (Tübingen, Germany). Fmoc amino acids were purchased from Novabiochem (Läufelingen, Switzerland) and Senn Chemicals (Dielsdorf, Switzerland). The other chemicals for synthesis were supplied by Fluka (Deisenhofen, Germany), PD-10 columns by GE Healthcare (Uppsala, Sweden) and Sephacryl S-200 HR gel from Pharmacia Biotech (Uppsala, Sweden). Cell culture media were purchased from PAN biotech (Aidenbach, Germany). The agonistic anti-Fas-antibody was supplied by Biomol (Hamburg, Germany), cycloheximide by SIGMA (Steinheim, Germany) and Alexa647-labeled Annexin V by Invitrogen (Karlsruhe, Germany).

## 2.3.2. Peptide synthesis

Peptides were synthesized by automated solid-phase peptide synthesis using Fmoc/tBu chemistry. Fluorescein-labeled peptides were synthesized on Nα-carboxyfluorescein-labeled lysyl-Rink amide resin ((Fluo(Trt))-Lys-Rink), unlabeled peptides on Rink amide resin (Fischer *et al.*, 2003). Purity was determined by analytical RP-HPLC (Nucleosil 100, 250 × 2 mm, C18 column, 5 $\mu$m particle diameter; Grom, Herrenberg, Germany), identity was validated via MALDI-TOF-mass spectrometry. For the R9-amide analog CYRRRRRRRRR the tyrosine residue was included to enable detection at 280 nm. Concentrations were determined by UV/Vis spectroscopy of peptides and conjugates diluted 1000fold in Tris/HCl buffer pH 8.8 assuming an extinction coefficient for fluorescein $E_{492}$= 78,000 l/(mol×cm).

## 2.3.3. Synthesis of the peptide with a lysine-coupled cysteine residue

Ala-Val-Pro-Ile-Ala-Gln(Trt)-Lys(Boc)-Lys(Dde)-Lys(Boc)-Leu-Lys(Boc)-εLys(Fluo) (15 μmol) was synthesized on (Fluo(Trt))-Lys-Rink amide resin. The peptide was N-terminally protected by reaction with boc-anhydride (32.7 mg, 150 μmol) in dimethylformamide (DMF)(1 mL) containing N,N-diisopropylethylamine (DIPEA) (29.8 μL, 180 μmol) for 24 h at 20 °C. After cleavage of the Dde-protecting group by hydrazine hydrate (2% v/v in DMF, 2 × 1 mL, 5 min, 20 °C) the ε-amino group was conjugated with Fmoc-Cys(Trt)-OH (87.9 mg, 150 μmol) using 1-hydroxybenzotriazole (20.3 mg, 150 μmol) and diisopropylcarbodiimide (23.5 μL, 150 μmol) in DMF (1 mL, 24 h, 20 °C). Following removal of the Fmoc-protecting group by piperidine (20% v/v in DMF), the peptide was cleaved off the resin and side chains deprotected using a mixture of 92.5% TFA, 2.5% triisopropylsilane, 2.5% 1,2-ethanedithiol and 2.5% $H_2O$ (v/v/v), precipitated in cold diethylether (4 °C) and spun down (4000 rpm, 5 min). The precipitate was washed with cold diethylether twice. Then the precipitate was dissolved in a mixture of acetonitrile/water (4 mL, 1:1, v/v) and lyophilized.
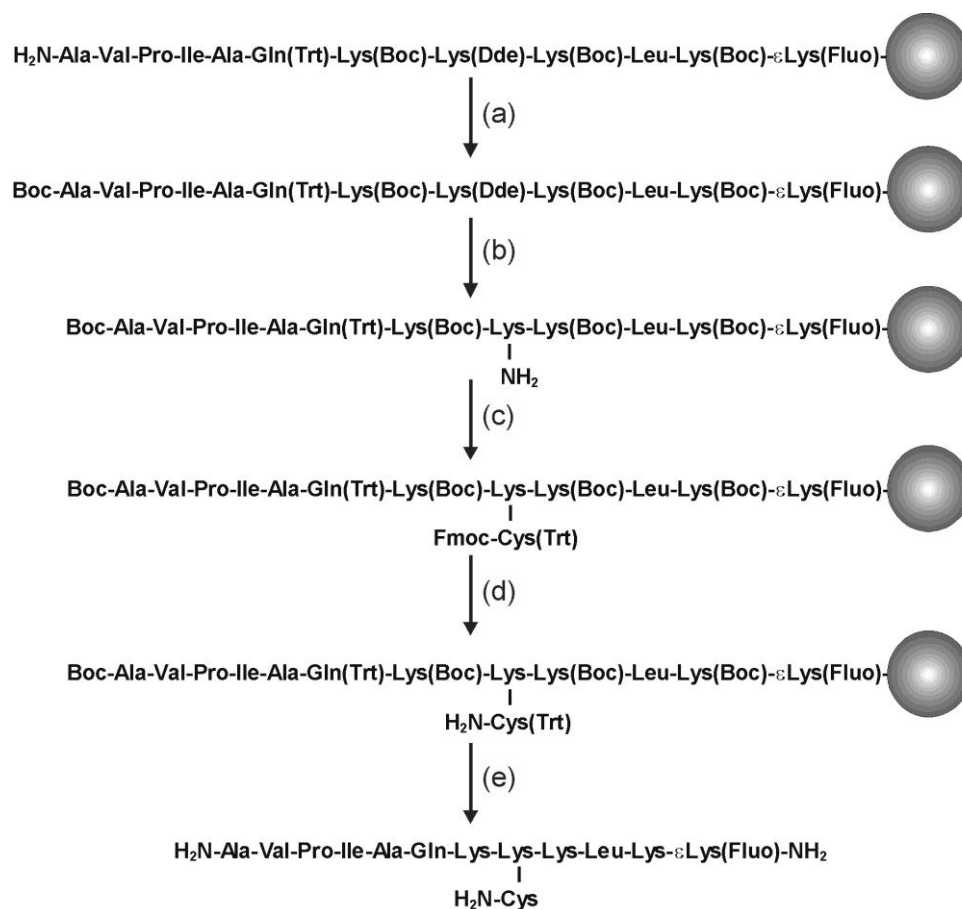


**Scheme. 2.1.** Synthesis of the proapoptotic peptide with a cysteine residue coupled to a lysine side chain

## 2.3.4. Synthesis of HPMA-peptide conjugates

Poly(HPMA-co-methacrylate-Gly-Gly-p-nitrophenylester) (4 mg) was dissolved in anhydrous DMSO (200 $\mu$L), and benzylmercaptan (50 $\mu$L) was added. After 15 min, peptide was dissolved in this solution (4.4 to 11.2 mM corresponding to an 8 to 20-fold excess over polymer and 0.64 to 1.60 excess over reactive groups, respectively) and incubated for 30 min at 20 °C. After addition of thiophenol (50 $\mu$L) and incubation for 16 h at 20 °C, phosphate buffer (100 mM), guanidiniumchloride (6 M), pH 7.5 (200 $\mu$L), was added and the mixture incubated for 72 h at 20 °C. Finally, the reaction mixture was diluted with PBS (700 $\mu$L) and purified twice with a PD-10 column followed by lyophilisation. The formation of a conjugate was validated using analytical gel filtration chromatography (ÄKTA-explorer Fast-Protein-Liquid-Chromatography (FPLC)-station; flow: 0.25 mL/min, 4 °C; Sephacryl S-200 HR-column, 150 × 10 mm). Absorption was detected at 215 nm (peptide bonds), 280 nm (aromatics) and 492 nm (fluorescein).
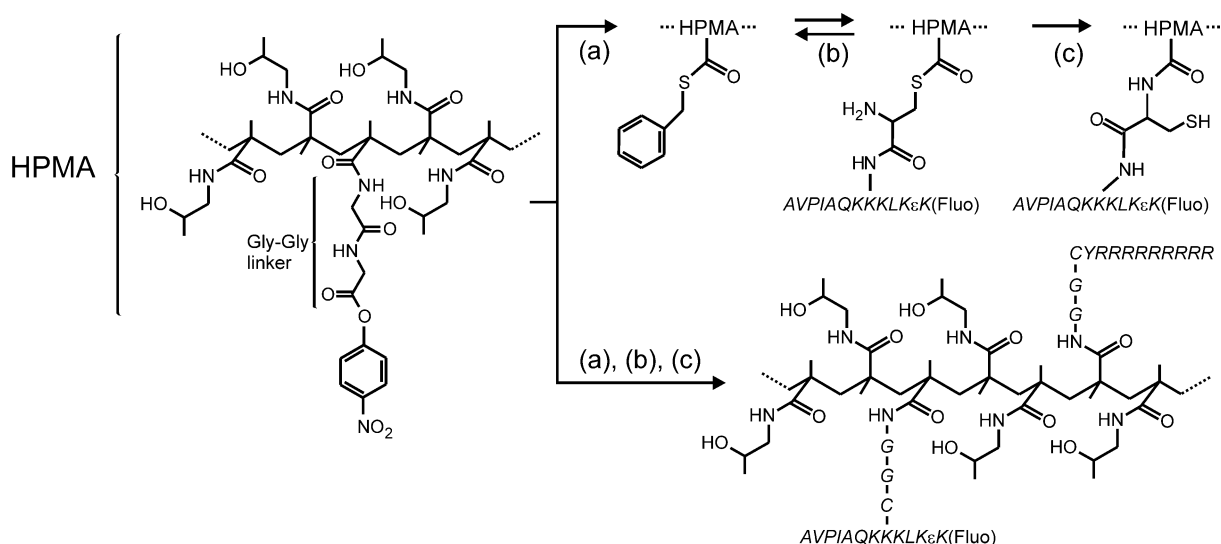


**Scheme 2.2.** Coupling of the AVPIAQK analog to a preactivated HPMA (Poly(hydroxypropyl methacrylamide)-co-(methacryloyl-Gly-Gly-nitrophenyl ester)). (a) DMSO (anhydrous), benzylmercaptane; (b) DMSO (anhydrous), thiophenol; (c) DMSO, thiophenol, phosphate buffer (100 mM), guanidiniumchloride (6 M, pH 7.5). Amino acids are printed as single letter code in italics.

## 2.3.5. Microscopy

HeLa cells were incubated with HPMA($H_2N$-AVPIAQKK(C)KLK$\varepsilon$K(Fluo)-$NH_2$)$_n$(CYR$_9$-$NH_2$)$_m$ denoted as AVPIAQK-HPMA-R9 and HPMA($H_2N$-AVPIAQKK(C)KLK$\varepsilon$K(Fluo)-$NH_2$)$_n$ denoted as AVPIAQK-HPMA (each 20 $\mu$M with respect to the AVPIAQK peptide) in RPMI medium (45 min, 37 °C) and afterwards analyzed by confocal laser scanning microscopy using an LSM 510 confocal microscope (Carl Zeiss, Göttingen) equipped with a Plan-Apochromat 63x N.A. 1.4 Oil DIC objective.

## 2.3.6. Determination of stoichiometry by FCS

Autocorrelation measurements were performed in a 384-well plate (175 $\mu$m, low-base design, MMI, Eching, Germany) using a ConfoCor 2 fluorescence correlation spectroscope equipped with a C-Apochromat 40x N.A. 1.2 water immersion lens (Carl Zeiss, Jena, Germany) and a TCS SP5 fluorescence correlation spectroscope equipped with an HCX PL APO 63x N.A. 1.2 water immersion lens (Leica Microsystems, Mannheim, Germany). A solution of 25 nM peptide-HPMA was incubated in PBS-buffer containing 30 U/ml proteinase K for 1.5 h at RT. During this incubation autocorrelation measurements were performed in regular intervals until the diffusional autocorrelation time and the amplitude of the autocorrelation function had reached a minimum. After digestion the number of particles and the fpm of intact and completely digested samples were compared. The ratio of the number of particles after and before digestions represents the stoichiometry of peptides per polymer.

## 2.3.7. Bioactivity of electroporated conjugates

HeLa cells were detached by trypsination. Cells ($4*10^5$ cells in 200 $\mu$L serum-containing medium) were electroporated with the indicated peptides or conjugates in a 4 mm-cuvette (peqlab Biotechnologie GmbH, Germany) using a 12.5 ms, 350 mV, 1700 $\mu$F pulse (Fischer, Germany). After incubation for 10 min on ice the cells were washed by centrifugation, transferred to a 96-well microtiter plate ($2*10^4$ cells per well) and incubated in 200 $\mu$L serum-containing RPMI medium with anti-Fas antibody (100 ng/mL, human activating mouse IgM, clone CH11) and CHX (2 $\mu$g/mL) for 20 h at 37 °C and 5% $CO_2$. Dead cells were removed by washing twice with PBS, whereas the attached cells were stained with crystal violet (100 $\mu$L,

0.5% w/v crystal violet, 20% methanol v/v, 80% PBS) (15 min, 20 °C). After removal of excess dye by washing with cold water, the intracellular dye was resolved in 100 $\mu$L methanol and the absorption at 550 nm was determined.


## 2.3.8. Caspase-3 activity assay

HeLa cells were incubated with medium containing constructs for 30 min at 37 °C. After one washing step cells were treated as indicated with agonistic Fas antibody (100 ng/mL) and CHX (2 $\mu$g/mL) for the induction of apoptosis followed by incubation for a further 3 h. Cells were harvested by scraping, washed with ice-cold PBS and lysed in lysis buffer (1% Triton, 150 mM NaCl, pH 7.7, supplemented with protease inhibitor cocktail tablets (Roche Diagnostics, Mannheim, Germany) for 30 min on ice. The protein content in lysates was determined using a commercially available Bradford protein assay kit (Bio Rad Laboratories, München, Germany). Equivalents of 30 $\mu$g protein for each sample were diluted in caspase activity buffer (20 mM HEPES, 10 mM dithiothreitrol, 10% glycerol, 100 mM NaCl, pH 7.5). Fluorogenic caspase-3 substrate (Ac-DEVD-AMC, Calbiochem, Bad Soden, Germany) was added to the samples to a final concentration of 2 $\mu$M. The efficiency of the substrate cleavage by active caspase-3 was analyzed immediately after substrate addition and after 3 h incubation at 37°C using a luminescence spectrometer LS50B (PerkinElmer, Norwalk, CT, USA).

## 2.4. Results

## 2.4.1. Synthesis and analytical characterization of HPMA conjugates

In order to ensure a broad applicability of a polymer-based approach, robust synthesis procedures as well as reliable analytical methods to determine coupling efficiencies are required. To validate our protocol, a series of coupling reactions with structurally different peptides was performed and, for selected peptides, also repeated several times. As a bioactive peptide, the pro-apoptotic AVPIAQK peptide was selected. This peptide requires a free N-terminus for biological activity. Therefore, in this case, the cysteine residue required for NCL was introduced via coupling to a lysine side chain (Scheme 2.1).

A protease-releasable fluorescent reporter group was introduced by C-terminal elongation with the tripeptide Lys-Leu-Lys, followed by a fluorescein-labeled lysine residue (Fischer *et al.*, 2003). The HPMA was obtained as a preactivated hydroxypropyl methacrylamide copolymer poly(HPMA-co-methacrylate-Gly-Gly-p-nitrophenyl ester) (linear structure, average MW 28.5 kDa, total nitrophenol content 8.28 mol%) with about 12.5 reactive groups per molecule. The active ester was first transesterified to a benzylmercaptyl-thiol ester in water-free DMSO, as we were concerned that due to its high reactivity the nitrophenylester moiety would engage in reactions with nucleophilic functional groups other than the sulfhydryl group of the N-terminal cysteine residue. Next, the polymer was incubated with peptide in water-free DMSO. After 16 h aqueous buffer was added. The products were purified by gel filtration chromatography (Fig. 2.1). The chemoselectivity of this modified one-pot ligation protocol was validated in an independent experiment using control peptides with and without an N-terminal cysteine residue (Fig. 2.2).
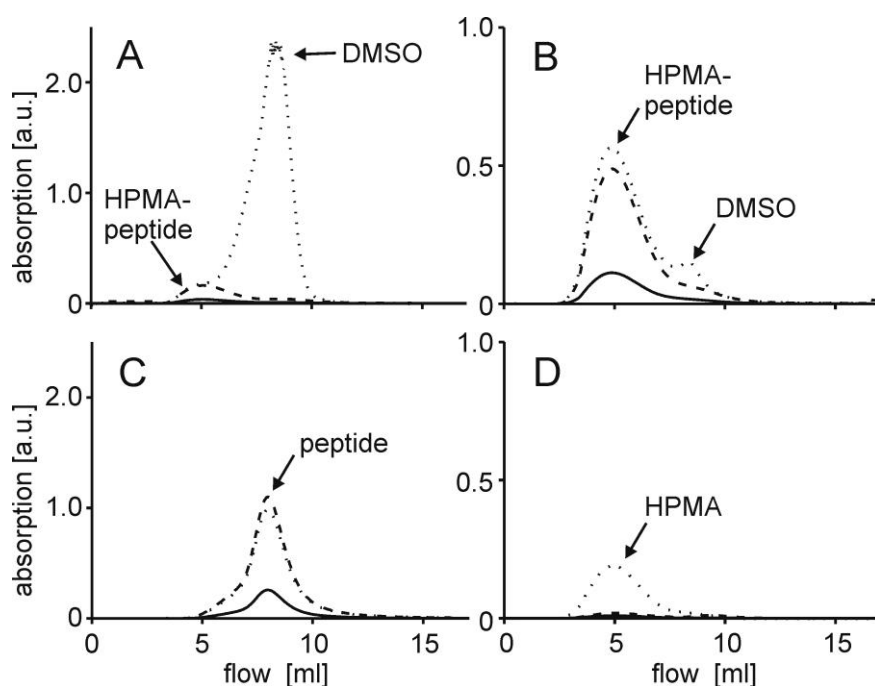
**Fig. 2.1.** Analytical gel filtration chromatography of the HPMA(H$_2$N-AVPIAQKK(C)KLKεK(Fluo)-NH$_2$) conjugate: (A) crude reaction mixture, (B) after purification with a desalting column, (C) unbound peptide H$_2$N-AVPIAQKK(C)KLKεK(Fluo)-NH$_2$, and (D) free HPMA. Chromatograms were recorded at 215 nm (dotted lines), 280 nm (solid lines) and 492 nm (dashed lines).
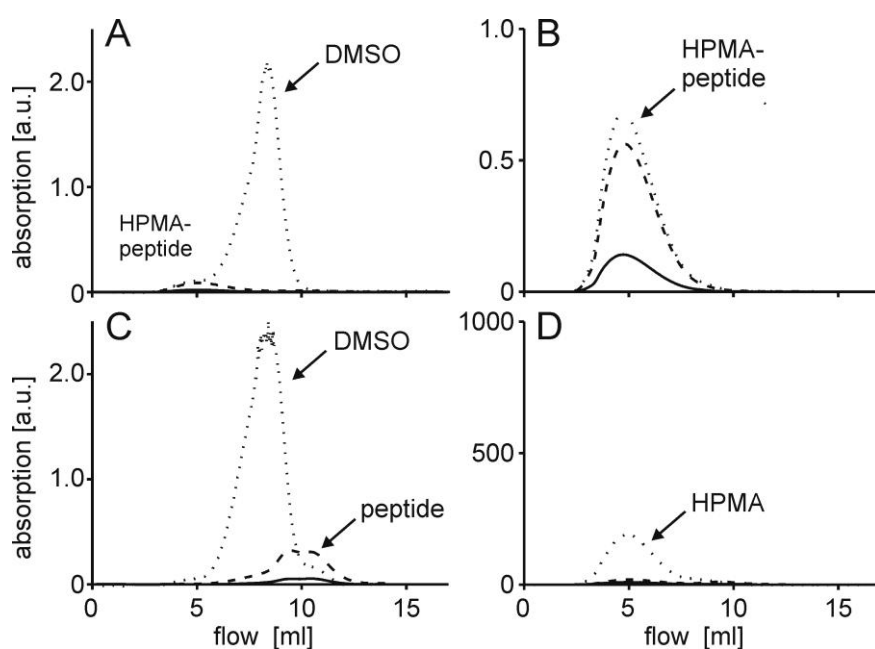


**Fig. 2.2.** Chemoselectivity of the modified NCL protocol. (A,B) Analytical gel filtration chromatography of the HPMA thioester after reaction with the peptide H$_2$N-CKLKεK(Fluo)-NH$_2$ before (A) and after (B) removal of DMSO with a desalting column. (C, D) Analytical gel filtration chromatography after incubation of the HPMA thioester with the peptide H$_2$N-AKLKεK(Fluo)-NH$_2$ before (C) and after (D) purification with a desalting column (dotted line: absorption at 215 nm, solid line: absorption at 280 nm, dashed line: absorption at 492 nm).
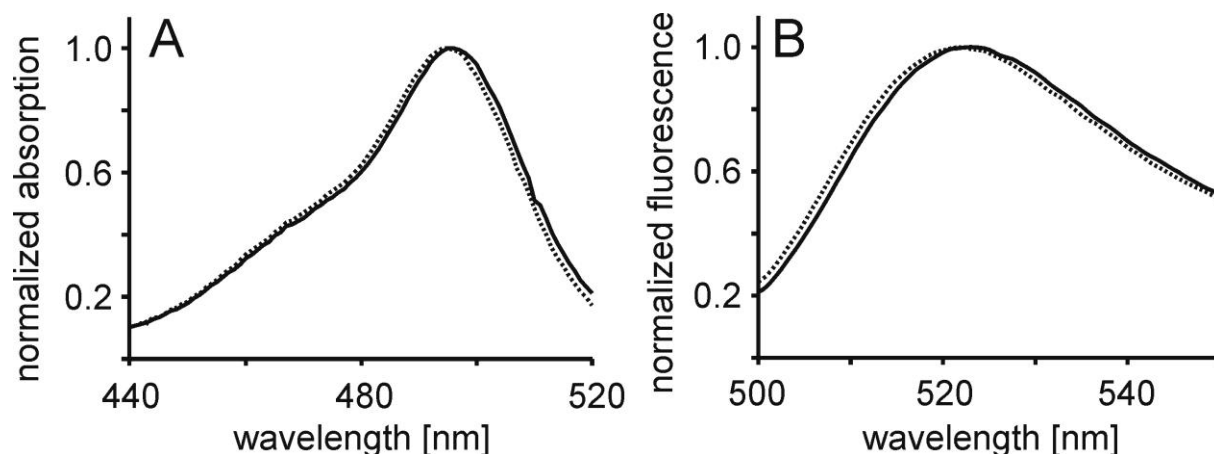
**Fig. 2.3.** Characterization of photophysical shifts occurring upon HPMA conjugation of peptides. (A) Normalized absorbance and (B) fluorescence emission spectra of the free, fluorescein-labeled AVPIAQK analog (dashed line) and the HPMA-AVPIAQK conjugate (solid line). The conjugate and the free peptide were dissolved in Tris/HCl pH 8.8 to a concentration of 2.0 $\mu$M with respect to the fluorescein moiety.

For the determination of loading efficiency two independent approaches were evaluated. First, the absorption per weight was measured for a defined amount of polymer. Second, the number of fluorescent particles before and after digestion of peptide-coupled HPMA with 30 U/ml proteinase K (Fig. 2.4) was determined by fluorescence correlation spectroscopy. Due to the nanomolar sensitivity and microliter measurement volumes of FCS only 0.4 pmol, corresponding to 12 ng of the labeled construct was required for one measurement. Digestion led to a decrease of the amplitude of the autocorrelation function (Fig. 2.4.A), corresponding to an increase in the number of fluorescent particles. The completeness of the reaction was confirmed by following the reaction over time. The stoichiometry of peptide loading was derived by calculating the number of particles before and after digestion (Table 1). The release of the fluorescent reporter group from the scaffold was also reflected by the shift in the diffusional autocorrelation time from approximately 100 $\mu$s to 35 $\mu$s (Fig. 2.4.B).

The results obtained by FCS corresponded very well to those obtained by the absorption-per-weight-based methods. A slightly lower loading efficiency was obtained by the latter. This may be due to the presence of counterions in the polymer-preparation, leading to an overestimate of the amount of material. Due to the fact that the FCS-based method is not affected by salt that compromises a correct determination of weight and requires much smaller amounts, we judge this method superior.

**Tab. 2.1.** Summary of coupling reactions. For the bifunctional conjugates, information on coupling efficiency was obtained for the fluorescein-labeled analog only.

| conjugate | fold excess | excess over reactive group | fluo-analog per polymer | reactive groups coupled to fluo-analog | rfpm[1] | used in figure |
|---|---|---|---|---|---|---|
| AVPIAQK(Fluo) - HPMA-YR9[3] | 4:4:1 | 0.64 | 1.3 | 10% | 1.1 | |
| AVPIAQK(Fluo) - HPMA-R9[3] | 10:10:1 | 1.6 | 3.4 | 27% | 1.0 | 2, 4B, 5 |
| AVPIAQK(Fluo) - HPMA[3] | 20:1 | 1.6 | 4.6[2] | 33% | | 4C |
| AVPIAQK(Fluo) - HPMA[3] | 10:1 | 0.8 | 3.3 | 26% | 1.0 | 3, 5 |
| KQAIPVA(Fluo) - HPMA[4] | 20:1 | 1.6 | 4.4[2] | 33% | | 3 |
| AVPIAQK(Fluo) - HPMA[3] | 20:1 | 1.6 | 4.1(3.4[2]) | 33% | 1.1 | 2 |
| HPMA-R9(Fluo)[5] | 10:1 | 0.8 | 2.7 | 22% | 0.8 | 4A |
| AVPIAQK(Fluo) - HPMA-R9(Fluo)[3] | 10:10:1 | 1.6 | 3.5 | 28% | 0.9 | |
| Cys(Fluo)-HPMA-R9 | 10:10:1 | 1.6 | 2.3 | 18% | 1.1 | |

[1]the relative fluorescence per molecule (rfpm) was determined by dividing the fluorescence per molecule for the conjugate as determined by FCS through the one of the released peptide.
[2]loading efficiency determined by measuring the absorption per unit weight of peptide-coupled polymer
[3]AVPIAQK(Fluo) relates to Ala-Val-Pro-Ile-Ala-Gln-Lys-Lys(Cys)-Lys-Leu-Lys-εLys(Fluo) (see experimental procedures)
[4]KQAIPVA(Fluo) relates to Lys-Gln-Ala-Ile-Pro-Val-Ala-Lys(Cys)-Lys-Leu-Lys-εLys(Fluo) (see experimental procedures)
[5]R9(Fluo) relates to Cys-Arg-εLys(Fluo)

For the coupling efficiency, there was a positive correlation between the ratio of peptide in the coupling reaction over reactive groups (Fig. 2.4.C).

Typically, with a molar excess of 10 with respect to the polymer, corresponding to 0.8 peptides per reactive group, about 3 peptides were coupled per polymer. Interestingly, in the tested concentration ranges, addition of a non-fluorescent peptide did not affect the coupling efficiency of the fluorescently labeled peptide (Fig. 2.4.D).

This observation indicates that at these concentrations, peptides did not compete for reactive groups. Also, for R9, the AVPIAQK peptide and a fluorescein-labeled cysteinyl-$\tilde{\varepsilon}$lysyl moiety, similar coupling yields were obtained. This result indicates the suitability of the coupling protocol for the testing of larger collections of structurally diverse peptides, without the need for the optimization of coupling conditions for each individual case.
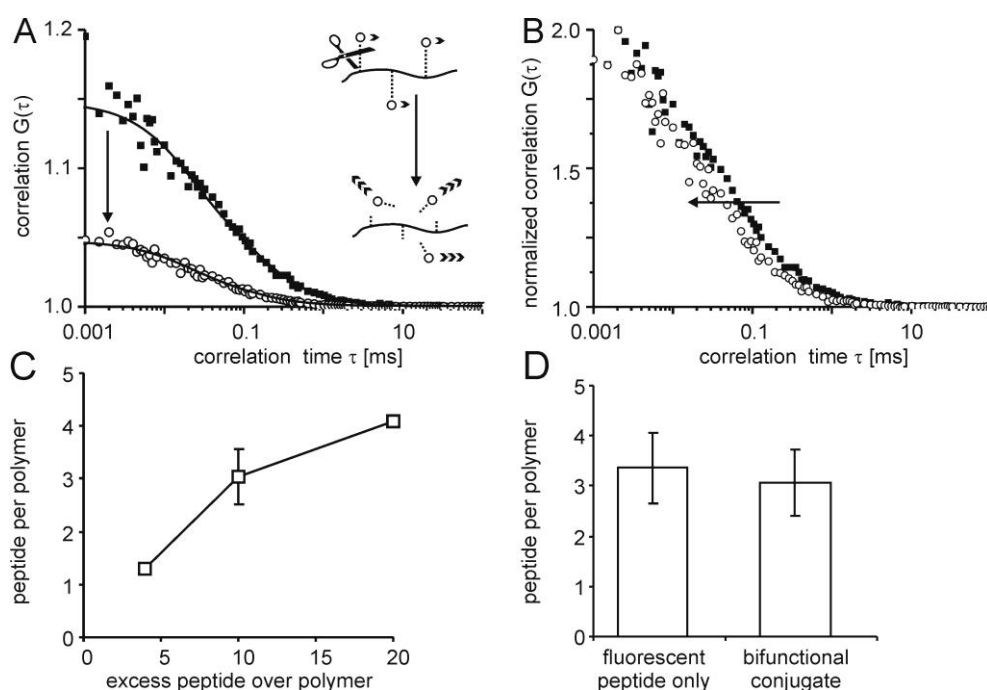


**Fig. 2.4.** Quantification of peptide loading per polymer by fluorescence correlation spectroscopy (FCS). One aliquot of the HPMA-peptide conjugate AVPIAQK-HPMA-R9 was digested by addition of proteinase K (30 U/mL) to the polymer conjugate solution (10 $\mu$M). After incubation for 1.5 h at 37°C the solution was diluted in PBS (500-fold) and transferred to a 384-well plate. A reference aliquot was prepared in the same way in the absence of proteinase K. (A) Autocorrelation functions for the digested sample (open circles) and the undigested control (filled squares), (B) superposition of the autocorrelation functions normalized to an amplitude of 1 to better visualize the shift towards shorter diffusional autocorrelation times. (C) Positive correlation of peptides coupled per polymer and the excess of peptide over polymer in the coupling reaction. Values were taken from table 1. The excess relates to the excess of the fluorescently labeled analog. (D) The coupling efficiency was independent from the presence of a second peptide. The conjugates for which the coupling efficiency was only determined by absorption-per-weight are not included in this graph.

Moreover, by dividing the total fluorescence through the average number of molecules, information on the average fluorescence per molecule (fpm) was obtained. In principle, for polymers carrying several fluorescently labeled particles, the fpm should be a function of the stoichiometry of loading. However, due to self-quenching, the fpm can also be lower than expected (Chen and Knutson, 1988). The fpm for the HPMA conjugates relative to the one of the free peptide was around 1, independent of the coupling efficiency. This result confirms the presence of fluorescence quenching. The molecular brightness of the polymers therefore does not provide information on the coupling efficiency.

We relate to quenching as a reduction of fluorescence per particle due to the spatial proximity of several fluorophores, not to the complete extinction of fluorescence for those polymers carrying more than one fluorophore. One could argue that for particles carrying several fluorophores, fluorescence is quenched completely and these conjugates could not be detected. Then, for the undigested sample, only those conjugates carrying one fluorophore could be detected. Upon digestion, fluorescent groups would be cleaved off polymers carrying several fluorophores, resulting in their dequenching. As a consequence, the number of particles per polymer would be overestimated.

However, in our view, the very good agreement of the determination of coupling efficiency based on absorbance-per-weight and the FCS-based method argue against a total quenching of fluorescence for polymers carrying several fluorescein moieties. Assuming a Poissonian distribution of coupling efficiency, then at an average coupling ratio of 3 about 15 % of the conjugates carry only 1 fluorophore. 80 % of the peptides would be coupled to polymers carrying two or more fluorophores. If all these moieties would only become visible after release from the polymer, then a coupling efficiency of 6-7 would be derived.

## 2.4.2. Coupling to HPMA preserves the activity of the AVPIAQK peptide

Next, we intended to establish that conjugation of the peptide to the polymer does not compromise its biological activity. Previously, for the AVPIAQK-peptide we had employed electroporation as a means for CPP-independent cytoplasmic delivery (Fotin-Mleczek *et al.*, 2005b). The free and the HPMA-coupled peptide as well as their counterparts with the reverse sequence were loaded into HeLa cells by electroporation. The AVPIAQK-peptide does not induce apoptosis by itself. Instead it increases cell death in the presence of an apoptosis-inducing stimulus, as for example an agonistic anti-Fas antibody. Stimulation with anti-Fas alone, reduced cell viability by 64 % (Fig. 2.5). With the AVPIAQK peptide at a concentration of 20 $\mu$M, cell viability was reduced by a further 8 %. In comparison, the

HPMA-conjugated AVPIAQK peptide at a concentration of 20 $\mu$M (related to the fluorescein moiety, i. e. AVPIAQK peptide) reduced the viability by a further 29 %. This difference in activity indicates that conjugation to the HPMA strongly promotes the activity of the peptide, possibly by protection from proteolytic degradation. The reverse sequences had no effect on cell viability. For the HPMA constructs electroporated in the absence of an apoptotic stimulus viability was also fully maintained, demonstrating the biocompatibility of the HPMA scaffold.
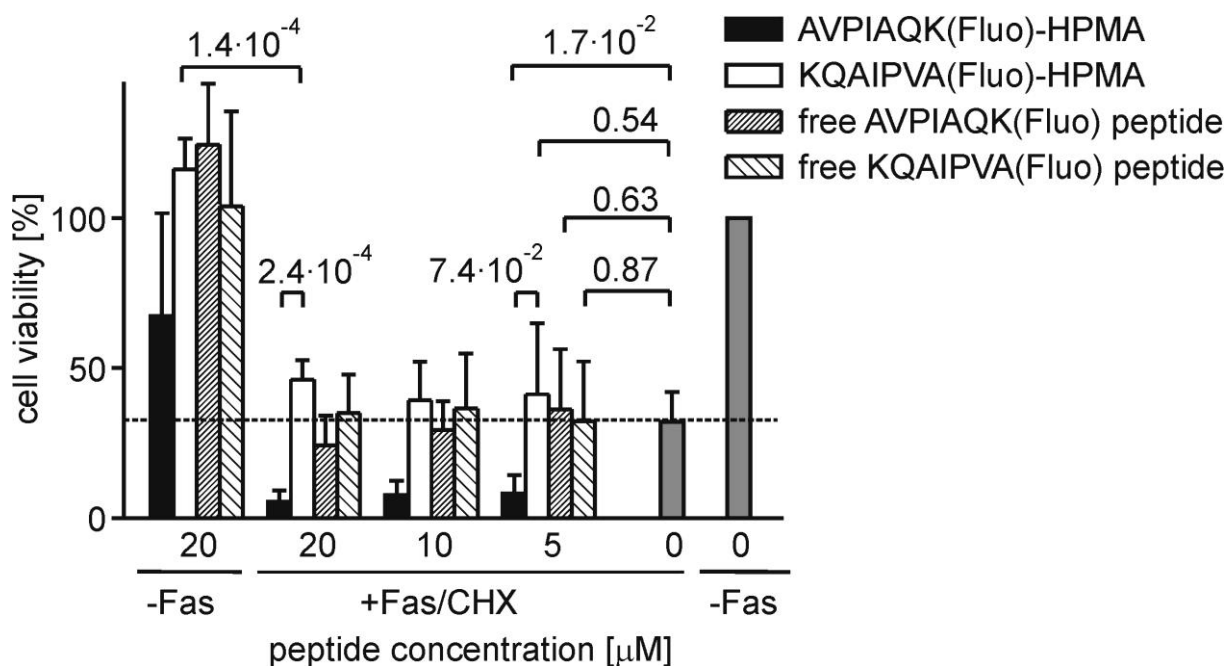


**Fig. 2.5.** Enhancement of apoptosis induction by electroporated HPMA-conjugates. The concentration was adjusted with respect to the fluorescent moiety. In this case, peptide loading was determined by absorption per weight (Tab. 2.1). Cell viability was determined by crystal violet staining. AVPIAQK(Fluo) relates to Ala-Val-Pro-Ile-Ala-Gln-Lys-Lys(Cys)-Lys-Leu-Lys-$\varepsilon$Lys(Fluo) (see experimental procedures); KQAIPVA(Fluo) relates to Lys-Gln-Ala-Ile-Pro-Val-Ala-Lys(Cys)-Lys-Leu-Lys-$\varepsilon$Lys(Fluo) (see experimental procedures). The statistical significance was determined by a two-tailed unpaired Student's T-test.

## 2.4.3. Cellular uptake and bioactivity of bifunctional conjugates

Having established, that the HPMA is inert with respect to cell entry and that the HPMA-conjugated AVPIAQK-peptide fully maintains activity, we next co-functionalized the HPMA with the AVPIAQK-peptide and nonaarginine to obtain conjugates competent for cell entry. Both, the HPMA conjugate functionalized with R9 only as well as the one cofunctionalized with R9 and the AVPIAQK peptide efficiently entered cells (Fig. 2.6).

In contrast to what we typically observe for free R9, a large part of the fluorescence was localized close to the plasma membrane. In addition, there was homogenous intracellular fluorescence. Inside the nucleus, the nucleoli were visible; an observation that we and others have made for cell-penetrating conjugates before (Duchardt *et al.*, 2007). For the bifunctional HPMA construct only the AVPIAQK-moiety was fluorescently labeled. The intracellular fluorescence therefore provided direct evidence for the cofunctionalization of the HPMA scaffold with the nonaarginine.
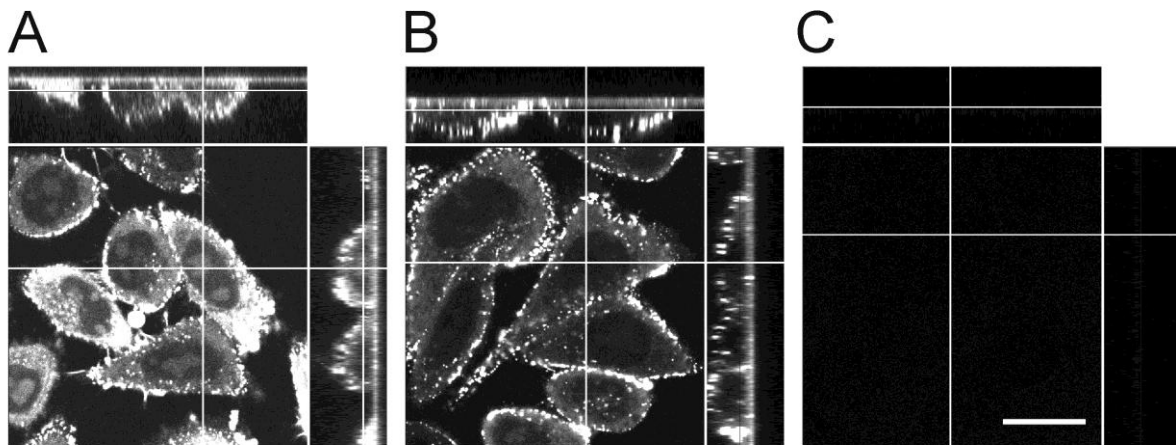


**Fig. 2.6.** Cellular uptake and subcellular distribution of HPMA-peptide-conjugates. Confocal microscopy of cells incubated (A) with HPMA-R9, (B) the bifunctional AVPIAQK-HPMA-R9 conjugate and (C) a conjugate bearing the functional peptide only (AVPIAQK-HPMA)(20 $\mu$M). One confocal slice as well as orthogonal sections along the indicated lines are shown. Cells were incubated with the respective conjugate at a concentration of 20 $\mu$M with respect to the fluorescent moiety for 45 min at 37 °C. The bar denotes 20 $\mu$m.

Finally, we assessed, whether the bifunctional HPMA-conjugate would also combine both biological functions, namely, cell entry and apoptosis enhancement. To fully establish that the conjugates acted by enhancement of apoptosis and to exclude that a reduction of cell viability was due to general cell toxic effects, we determined the activity of the executioner caspase 3 in cell lysates as an apoptosis-specific read-out.

Neither of the constructs led to an increase of caspase 3 activity beyond the about 2-fold increase in activity observed for control cells incubated in the absence of stimulus and conjugate (Fig. 2.7).

The apoptotic stimulus increased the caspase 3 activity 3.5 fold. For the conjugate bearing the AVPIAQK moiety alone, no further increase was observed, consistent with the inability of this molecule to enter the cells. In contrast, the bifunctional conjugate increased the caspase 3 activity by up to 8-fold in a concentration-dependent manner. Some increase in activity to

5.3-fold was also observed for the conjugate bearing the nonaarginine moiety, only. This activity may be due to a higher sensitivity of the apoptosis-induced cells to the import of a polycation (Law *et al.*, 2006). In the absence of the proapoptotic stimulus there was no cytotoxic activity for neither of the constructs. This result, in conjunction with the absence of activity for the electroporated reverse KQAIPVA(Fluo)-HPMA conjugate validate the biocompatibility of the conjugates.
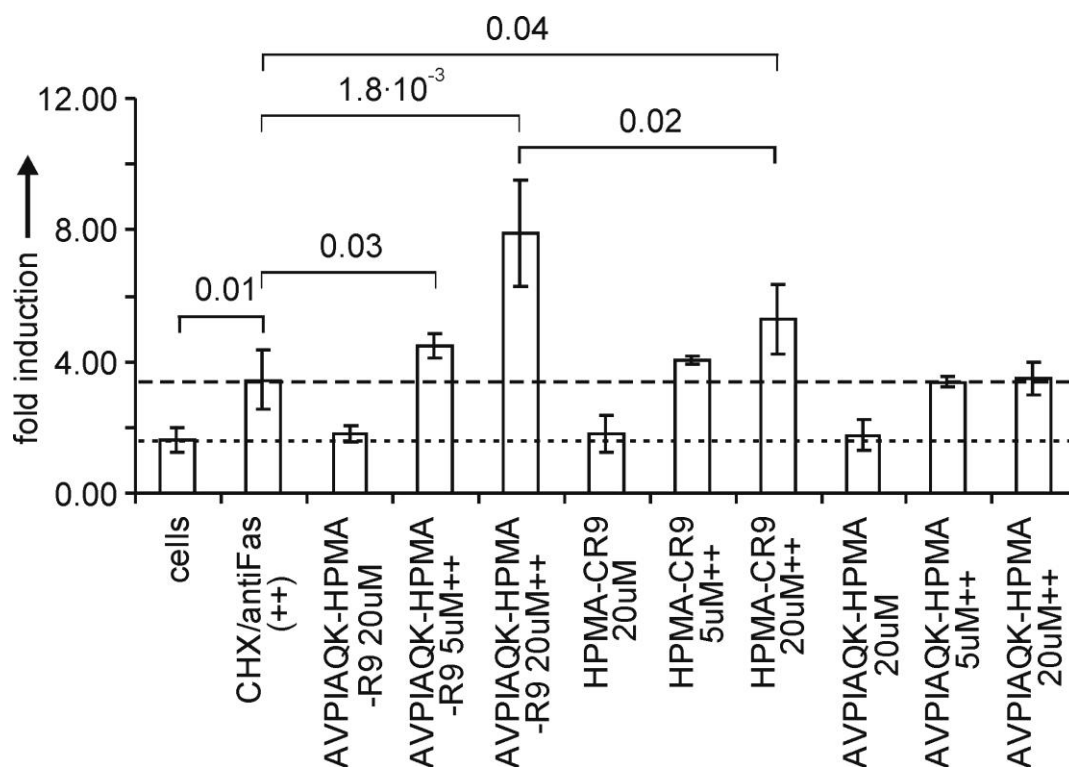


**Fig. 2.7.** Bioactivity of HPMA-conjugates. HeLa-cells were incubated with different concentrations of the counjugates for 30 min at 37°C. Afterwards the cells were washed and apoptosis was induced by stimulation with an agonistic anti-Fas antibody (100 ng/mL) and cycloheximide (CHX, 2 $\mu$g/mL).For measurements of the caspase-3 activity cells were harvested after 3 h after induction of apoptosis. The figure shows averages and standard deviations of two independent cell stimulations, that were analyzed twice/three times by a colorimetric caspase assay. The biological activity is expressed as fold-induction of caspase 3 activity in relation to lysates of untreated cells obtained at t=0. The results of the individual assays were normalized based on the accumulated absorbance of all samples. The pointed line indicates the increase of caspase 3 activity during the 3 h incubation period of the assay in the absence of an apoptotic stimulus. The dashed line indicates the Fas stimulus-dependent increase in caspase activity, ++ the presence of the apoptotic stimulus. Concentrations were derived from the absorption of fluorescein. The statistical significance was determined by a two-tailed unpaired Student's T-test.

At present the molecular basis for the different subcellular localization of the HPMA conjugates in comparison to free CPPs is not understood. To this point, we have not resolved, whether this distribution is a consequence of a poor induction of endocytosis and therefore increased association with the plasma membrane or of differential vesicular trafficking of HPMA-loaded vesicles. For free cell-penetrating peptides, sequestration within the endolysosomal compartment is also a major limitation for bioactivity (Fotin-Mleczek *et al.*, 2005b). Typically, these vesicles are distributed throughout the cell (Duchardt *et al.*, 2007). More importantly with respect to their application, the localization close to the plasma membrane is not associated with the induction of membrane damage as validated by the biocompatibility of the conjugates in the absence of an apoptotic stimulus.

## 2.5. Conclusions

In summary, our results show that the HPMA-based strategy provides a convenient access to cell-penetrating bioactive peptides. Peptides mediating cell entry and bioactivity are coupled as fully unprotected building blocks to the preactivated HPMA polymers by native chemical ligation. Due to the modular nature of the approach, shorter peptides may be employed which facilitates the synthesis of cell-penetrating conjugates especially for longer bioactive peptides. Therefore, the modular nature of the approach represents a considerable short-cut for testing the activity of peptides inside a cell. The assessment of bioactivity and uptake for the individual conjugates confirmed that the functionality of the three molecular elements, i. e. scaffold, bioactive peptide and CPP, combine independently in a modular fashion.

The coupling reaction proceeded with little day-to-day variation. Our results indicate that the coupling efficiency correlates positively with the excess of peptide over functional groups. In further studies it will therefore be highly interesting to systematically assess the effect of variations of either the number of bioactive peptides or the CPP with respect to bioactivity, uptake and trafficking. Also the incorporation of peptides known to promote endosomal release as a further element will be a promising option to explore for increasing bioactivity (Wadia *et al.*, 2004). These advancements will strongly promote the development and application of functional peptides in fundamental and applied biomedical research (Vicent and Duncan, 2006).

# 3. Coupling to polymeric scaffolds stabilizes biofunctional peptides for intracellular applications

The author of this thesis synthesized the HPMA conjugates used in this study and contributed the Fig.3.2-3.6 The caspase assay depicted in Fig. 3.1. was kindly conducted by Dr. Falk Duchardt. Moreover, Dr. Falk Duchardt contributed the apoptosis assay depicted in Fig. 3.7.

## 3.1. Summary

Peptides and proteins are rapidly gaining significance as drugs and as bioactive molecules in biomedical research. However, nearly all of these peptide-based approaches relate to extracellular applications. In contrast, the intracellular applicability is still seriously limited by the poor intracellular half-life of peptides. Stabilization by incorporation of modified amino acid residues or backbone modifications requires extensive revalidation of structure-activity relationships. Therefore, stabilization of an unmodified peptide would be highly advantageous. For extracellular applications, conjugation to polymers is a strategy for increasing stability and decreasing elimination. We have shown recently, that conjugation of peptides to a thioester-activated N-hydroxypropyl methacrylamide (HPMA) copolymer (28.5 kDa) via native chemical ligation provides polymer-coupled peptides in a simple one-pot synthesis. Here we demonstrate for an apoptosis-inducing peptide, introduced into Jurkat T cell leukemia cells by electroporation, that coupling to the polymer greatly increases the intracellular biological activity per peptide moiety. The molecular basis of this finding was elucidated in detail. Electroporation efficiency was lower for HPMA-conjugates, while the cellular residence time of fluorescence was the same. However, HPMA conjugation strongly increased the half life of the peptides in crude cell lysates, revealing proteolytic protection as the basis for higher activity. A bifunctional conjugate containing the cell-penetrating peptide nonaarginine for mediating cellular entry, induced apoptosis in a concentration-dependent manner. In summary, these results do not only present a generalization of the potential of the HPMA-based conjugation strategy, they also provide a mechanism for the increase in activity.

## 3.2. Introduction

The chemical nature of peptides provides a nearly infinite diversity in structure, accessible by highly robust and parallel synthesis protocols (Rademann and Jung G, 2000). Therefore peptides provide a highly valuable repertoire of molecular interactors, both in basic and applied biomedical research (Cooper and Waters, 2005). In the past years, numerous peptides have been admitted as drugs (Hruby and Balse, 2000; Bray, 2003; Leader *et al.*, 2008). Nevertheless, the intracellular applicability of peptides is still limited. One major drawback of short peptides is their short cytoplasmatic half-life. Major efforts have been invested into increasing the stability of peptides. The incorporation of non-native amino acids such as D-amino acids (Chorev *et al.*, 1979) beta-amino acids (Frackenpohl *et al.*, 2001; Griffith, 1986) in the peptide sequence or backbone modifications such as N-methylation (Gordon et al., 2001) have been presented as possible solutions. However, these approaches do not only render the synthesis more time consuming and expensive, they also require a careful revalidation of the structure-activity relationship of the molecule (Ruijtenbeek *et al.*, 2001).

An alternative approach that is well established in order to extend the plasma half-life of small molecule drugs in the blood stream and to prevent liver accumulation is the conjugation of the drugs to high-molecular weight polymers (Duncan, 2003; Vicent and Duncan, 2006). In this context the hydroxypropyl methacrylamide copolymer (HPMA) is widely used (Kopecek and Bazilova, 1973; Kopecek *et al.*, 2000; Malugin *et al.*, 2004; Satchi-Fainaro *et al.*, 2004).

In a previous study, we have shown that coupling of peptides containing an N-terminal cysteine residue to thioester-preactivated HPMA polymers provides a convenient and robust access to polymer-coupled peptides via native chemical ligation (Dawson *et al.*, 1994; Ruttekolk *et al.*, 2008; Tam *et al.*, 2001). Conjugates containing an apoptosis-enhancing peptide, loaded into cells by electroporation had a greatly increased biological activity in comparison to the free peptide. Correspondingly, bifunctional conjugates containing the apoptosis-enhancing peptide and nonaarginine as a cell-penetrating peptide (CPP) (Mitchell *et al.,* 2000; Wender *et al.*, 2000) showed a higher biological activity than the bioactive peptide extended by the CPP.

Differences in import efficiency, retention time inside the cell and stabilization from proteolytic break-down were considered as the basis for this observation. However, the structure of the bioactive peptide compromised a determination of the molecular basis of this observation. The peptide required free and unmodified seven N-terminal amino acids for bioactivity and could therefore only be linked to the polymer via a cysteine residue coupled to a C-terminal lysine side chain. Therefore, it was impossible to assess proteolytic cleavage of the polymer-

coupled peptide. Ideally, a peptide used for the analysis of proteolytic stability should be coupled to the polymer via its N-terminus and carry a fluorescent reporter group at its C-terminus.

Here, we therefore selected a Bid-derived BID-BH3 peptide as a model peptide (Cory *et al.*, 2003; Kuwana *et al.*, 2002; Willis and Adams, 2005). This peptide has a length of 22 amino acids and does not require a free amino terminus for biological stability. Coupling to the polymer occurred straight-forward via an N-terminal cysteine residue. A fluorescein label was attached to a C-terminal lysine residue. Therefore, in contrast to our previous choice, this peptide was ideally suited to detect proteolytic cleavage off the polymer and release of C-terminal low molecular weight fluorescein-labeled fragments. The BID-BH3 peptide can directly induce apoptosis by interacting with the multidomain proapoptotic BCL-1 family protein BAX. BAX forms homo-oligomers at the mitochondrial membrane and triggers the release of cytochrome c and other proapoptotic factors (Kuwana *et al.*, 2002; Walensky *et al.*, 2006). The free peptide was N-terminally capped by labeling with fluorescein and C-terminally blocked by amidation.

In order to eliminate the complex CPP-mediated import kinetics, involving endosomal release (Fotin-Mleczek *et al.*, 2005a), the free peptides and the conjugates were introduced into the cell via electroporation and the bioactivity of both was investigated. Again the polymer-coupled peptide exhibited a greatly increased activity.

The import efficiency and intracellular distribution were analyzed by confocal laser scanning microscopy and flow cytometry. The intracellular retention was addressed by time-lapse microscopy in combination with quantitative image analysis. Finally, the proteolytic stability was compared by incubation of conjugate and peptide with crude cell lysate. The latter measurement was performed by fluorescence correlation spectroscopy (FCS)(Rigler *et al.*, 1993). This fluorescence-based analytical technique provides information about the average number and size of fluorescently labeled molecules that diffuse through a sub-femtoliter confocal detection volume. Less than one pmol referring to few ng of the labeled construct were required per measurement. For the HPMA conjugate the import efficiency was reduced while the intracellular retention of fluorescence was the same as for the free peptide. In contrast, the stability against cytosolic proteases was tremendously increased. Finally, we demonstrated that a bifunctional HPMA conjugate, containing nonaarginine as a cell-penetrating peptide next to the functional BID-BH3 peptide induced apoptosis in a concentration dependent manner. Together, the results demonstrate a generalization of our HPMA-based approach and provide a mechanistic basis for the capacity of this approach.

## 3.3. Experimental Procedures

## 3.3.1. Reagents

Preactivated hydroxypropyl methacrylamide copolymer N-methacrylateglycylglycine p-nitrophenyl ester (poly-(HPMA-co-methacrylate-Gly-Gly-p-nitrophenyl ester)) with an average molecular weight (MW) of 28.5 kDa (Mw/Mn: 1.32) and a total nitrophenol content of 8.28 mol % was purchased from Polymer Laboratories (Shropshire, Great Britain). On the basis of the specifications provided by the manufacturer, 12.5 reactive groups were estimated per molecule. Peptides were purchased from EMC microcollections (Tübingen, Germany). The other chemicals for synthesis were supplied by Fluka (Deisenhofen, Germany), PD-10 columns by GE Healthcare (Uppsala, Sweden). Cell culture media were purchased from PAN biotech (Aidenbach, Germany). The electroporation kit Cell Line Nucleofector Kit V was provided by AMAXA (Cologne, Germany). Alexa647-labeled annexin-V was supplied by Invitrogen (Karlsruhe, Germany).

## 3.3.2. Peptide synthesis

Peptides were synthesized by automated solid-phase peptide synthesis using Fmoc/tBu chemistry. Fluorescein-labeled peptides with a C-terminal fluorophore were synthesized on preloaded carboxyfluorescein-labeled lysyl-Rink amide resin ((Fluo(Trt))-Lys-Rink) (Fischer *et al.*, 2003), unlabeled peptides on Rink amide resin. N-terminal labeling proceeded as described previously (Fischer *et al.*, 2003). The peptides were purified by preparative RP-HPLC (Grom-SIL 120 ODS-4 HE, 125× 20 mm, C18 column, 5 µm particle diameter; Grom, Herrenberg, Germany). Purity was determined by analytical RP-HPLC (Grom-SIL 120 ODS-4 HE, 100 × 2 mm, C18 column, 5 µm particle diameter; Grom), identity was validated via electrospray mass spectrometry with a LCQ Advantage Max mass spectrometer (Thermo Fisher Scientific, Waltham, USA). Concentrations were determined by UV/Vis spectroscopy of peptides and conjugates diluted 1000-fold in Tris/HCl buffer pH 8.8 assuming an extinction coefficient for fluorescein $E_{492} = 78\ 000$ L/(mol × cm).

## 3.3.3. Synthesis of HPMA-peptide conjugates

Poly(HPMA-comethacrylate-Gly-Gly-p-nitrophenylester) (4 mg) was dissolved in anhydrous benzylmercaptan (50 µL) and anhydrous DMSO (200 µL). After 15 min, peptide was dissolved in this solution (5.6 mM corresponding to a 10-fold excess over polymer and 0.8 excess over reactive groups, respectively) and incubated for 30 min at 20 °C. After addition of thiophenol (50 µL) and incubation for 16 h at 20 °C, phosphate buffer (100 mM) and guanidinium chloride (6 M), pH 7.5 (200 µL), were added and the mixture was incubated for 72 h at 20 °C. Finally, the reaction mixture was diluted with PBS (700 µL) and purified twice with a PD-10 column followed by lyophilization. Absorption was detected at 215 nm (peptide bonds), 280 nm (aromatics), and 492 nm (fluorescein). For the bifunctional conjugates either BID-BH3, or mutBID-BH3, or and C-$\varepsilon$K(Fluo)-NH$_2$ and nonaarginine were conjugated to the HPMA polymer in a ratio of 10:10:1 (cargo:nonaarginine:HPMA).
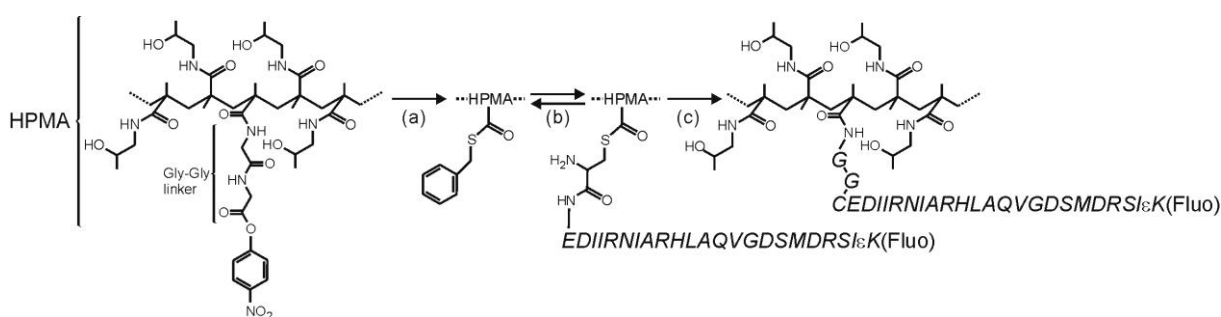


**Scheme 3.1.** Synthesis of a HPMA-BID-BH3 conjugate. (a) DMSO (anhydrous), benzylmercaptane; (b) DMSO (anhydrous), thiophenol; (c) DMSO, thiophenol, phosphate buffer (100 mM), guanidiniumchloride (6 M, pH 7.5). Amino acids are represented in single letter code and printed in italics.

## 3.3.4. Determination of stoichiometry by FCS

The determination of stoichiometry proceeded as described previously (Ruttekolk *et al.*, 2008) using fluorescence correlation spectrosopy (FCS). FCS measurements were performed in 384-well plates (175 µm, low-base design, MMI, Eching, Germany). A solution of 25 nM peptide-HPMA was incubated in PBS-buffer containing 40 U/mL proteinase K for 1.5 h at RT. During this incubation, autocorrelation measurements using a TCS SP5 fluorescence correlation spectroscope equipped with an HCX PL APO 63× N.A. 1.2 water immersion lens (Leica Microsystems, Mannheim, Germany) were performed in regular

intervals until the diffusional autocorrelation time and the amplitude of the autocorrelation function had reached a minimum. After digestion, the number of particles and the fluorescence per molecule (fpm), calculated by dividing the total background-corrected fluorescence by the number of molecules, of intact and completely digested samples were compared. The ratio of the number of particles after and before digestions represents the stoichiometry of peptides per polymer.

**Tab. 3.1. Summary of Peptides and HPMA Conjugates.**

| name | conjugate | fold excess | fluo-analog per polymer[1] | reactive groups coupled to fluo-analog | Rfpm[2] |
|---|---|---|---|---|---|
| BID-BH3 | Fluo-EDIIRNIARHLAQVGDSMDRSI | / | / | / | / |
| mBID-BH3 | Fluo-EDIIRNIARH<u>A</u>AQVG<u>A</u>S<u>A</u>DRSI[3] | / | / | / | / |
| HPMA-BID-BH3 | HPMA-CEDIIRNIARHLAQVGDSMDRSI(Fluo) | 10:1 | 1.8 | 14% | 1.2 |
| HPMA-mBID-BH3 | HPMA-CEDIIRNIARH<u>A</u>AQVG<u>A</u>S<u>A</u>DRSI(Fluo)[3] | 10:1 | 2.1 | 17% | 1.0 |
| R9-HPMA-BID-BH3 | R9-HPMA-CEDIIRNIARHLAQVGDSMDRSI(Fluo) | 10:10:1 | 2.4 | 19% | 1.2 |
| R9-HPMA-mBID-BH3 | R9-HPMA-CEDIIRNIARH<u>A</u>AQVG<u>A</u>S<u>A</u>DRSI(Fluo)[3] | 10:10:1 | 2.8 | 22% | 1.1 |
| R9-HPMA-C | R9-HPMA-C(Fluo)[2] | 10:10:1 | 2.3 | 18% | 0.9 |

[1]The loading refers to the fluorescein moieties per polymer.
[2]the relative fluorescence per molecule (rfpm) was determined by dividing the fluorescence per molecule for the conjugate as determined by FCS through the one of the released peptide.
[3]The mutated amino acid residues are underlined.

## 3.3.5. Electroporation

$10^6$ Jurkat E6.1 cells were resuspended in 100 μL Nucleofector Solution V (Lonza Cologne, Cologne, Germany) and the respective peptide or HPMA conjugate was added into the electroporation cuvette (Lonza Cologne) in the desired concentration. Electroporation was performed in a Nucleofector (Lonza Cologne) using the electroporation method X-001 according to the recommendations of the manufacturer. Subsequently, 900 μL RPMI medium were added carefully and the cells were incubated for 5 min at RT. Subsequently, the cell suspension was washed in medium by centrifugation.

## 3.3.6. Bioactivity of conjugates

For the testing of the activity of electroporated conjugates, the electroporated cells were washed, transferred to a 24-well tissue culture plate with flat bottom (Sarstedt, Nümbrecht, Germany) and incubated for 20 h in RPMI medium. Subsequently, the cells were washed in cold PBS and incubated in 100 μL annexin-binding buffer (10 mM HEPES, 140 mM NaCl and 2.5 mM $CaCl_2$, pH 7.4) containing 5 μL annexin-V Alexa Fluor 647 for 15 min on ice. 400 μL annexin-binding buffer were added and the samples were analyzed by flow cytometry with a FACSCalibur System (BD Biosciences, San Jose, USA).

For determination of apoptosis induction by cell-penetrating conjugates Jurkat cells were incubated either with BID-BH3-HPMA-R9, mutBID-BH3-HPMA-R9 or Lys(Fluo)-HPMA-R9. Concentrations were adjusted based on the fluorescein absorption of the cargo moieties. Following incubation with the conjugates for 10 h at 37 °C the cells were washed with PBS by centrifugation and stained with Alexa647-labeled annexin V. Dead cells were quantified by flow cytometry. An aliquot of the annexin-labeled cells was resuspended in DMEM-medium containing 10 % FCS and examined by confocal laser scanning microscopy. For microscopy, here an LSM510 confocal microscope (Carl Zeiss, Jena, Germany) was used. For the double detection of fluorescein-labeled peptide conjugates and Alexa647-labeled annexin V the 488 nm line of an argon ion laser and the light of a 633 nm helium-neon laser were directed into the sample with an HFT UV/488/633 beam splitter and fluorescence was detected using an HFT 545 beam splitter in combination with a BP 505-530 band pass filter for fluorescein detection and an LP 650 long pass filter for Alexa647 detection.

## 3.3.7. Analysis of peptide release

$5 \times 10^5$ electroporated Jurkat E6.1 cells were incubated in 200 $\mu$L phenol red-free RPMI medium for 10 min at 37 °C until they had settled on the bottom of a 8-well chambered coverglass (Nunc, Rochester, USA). Subsequently, the cells were analyzed by confocal laser scanning microscopy using a Leica SP5 confocal microscope equipped with an HCX PL APO 63× N.A. 1.2 water immersion lens (Leica Microsystems, Mannheim, Germany). The cells were incubated at 37°C and 5 % $CO_2$ in an cell culture incubator and in certain time intervals confocal images were taken by laser scanning microscopy. The microscopy stage was housed in an incubator box maintained at 37°C.

## 3.3.8. Image analysis

For intracellular quantification of fluorescence, the confocal microscopy images were imported into the program ImageJ 1.41. The images were smoothed with a low pass filter and converted into a black and white mask with a threshold that was adjusted to include all cells. Adjacent cells were separated with a watershed operation. This binary mask was used for segmentation of the original image. The program automatically quantified the mean fluorescence intensity of the cells.

## 3.3.9. Proteolytic stability in cell lysate

For preparation of cell lysate $4 \times 10^6$ HeLa cells were harvested by treatment with trypsin and EDTA and washed with medium and PBS. The cells were resuspended in 1 mL PBS containing 1 % (v/v) Triton-X-100 and lysed for 45 min on ice. Subsequently, the cell membranes were removed by centrifugation (20,000 g for 20 min at 4°C). The supernatant was split into two aliquots of 500 $\mu$L, each, into which either 2 $\mu$M HPMA-BID-BH3 conjugate or BID-BH3 peptide were added. The concentration of the cell suspension was adjusted so that the degradation of the peptide and conjugate could be followed over several hours. The samples were incubated at 37°C. At the indicated times samples of 5 $\mu$L were taken, mixed with 95 $\mu$L protease inhibitor cocktail (Complete, Roche Diagnostics, Mannheim, Germany) and frozen. Finally, the frozen samples were thawn, 1000 $\mu$L Tris buffer (100 mM Tris-HCl, pH 8.8) were added and aliquots of 50 $\mu$L were transferred into a 384-well plate (175 µm, low-base design, MMI). Autocorrelation measurements were performed using a TCS SP5

fluorescence correlation spectroscope equipped with an HCX PL APO 63× N.A. 1.2 water immersion lens. The fractions of intact and degraded polymer or peptide were derived from two-component fits to the autocorrelation function. The diffusional autocorrelation times for the high molecular weight component were fixed to values determined for the intact conjugate or peptide. The diffusional autocorrelation time for the low molecular weight component was fixed to the one of a fully degraded sample. After 24 h a high concentration of 40 U/mL proteinase K (2 U in 50 µL) was added in order to validate the general sensitivity of the conjugates to protease degradation.

## 3.4. Results

## 3.4.1. Synthesis and analytical characterization of HPMA conjugates

Following our previously published procedure (Ruttekolk *et al.*, 2008), the BID-BH3 peptide, containing an uncapped N-terminal cysteine residue was coupled to an active ester-preactivated HPMA polymer by native chemical ligation. For the determination of loading efficiency the number of fluorescent particles before and after digestion of the HPMA-peptide conjugate with 40 U/mL proteinase K (2 U in 50 µL) was determined by fluorescence correlation spectroscopy. Digestion led to a decrease of the amplitude of the autocorrelation function, corresponding to an increase in the number of fluorescent particles. The release of the fluorescent reporter group from the scaffold was also reflected by the shift in the diffusional autocorrelation. The completeness of the reaction was confirmed by observing the reaction over time. The stoichiometry of peptide loading was derived from calculating the number of particles before and after digestion. On average each polymer carried two peptides (Tab. 3.1.). Assuming a Poissonian distribution of coupling efficiency, at an average coupling ratio of 2 about 27 % of the conjugates carried only 1 peptide, 59 % of the polymers carried two or more peptides and 14 % of the polymers had remained unfunctionalized. Fluorescence correlation spectroscopy also revealed the molecular brightness per molecule (fpm – fluorescence per molecule), calculated by dividing the total background-corrected fluorescence of a sample by the number of molecules. As before, even though the polymer on average carried two fluorophores per molecules, the molecular brightness was the same for the polymers and for the free peptide (Tab. 3.1.). This observation is very likely due to quenching of fluorescence.

## 3.4.2. Bioactivity of electroporated conjugates

Cellular import of functional conjugates lacking a cell-penetrating moiety was chosen to elucidate whether coupling to the polymer affected the activity per peptide. For the cellular import, electroporation was chosen. In electroporation cells are briefly exposed to a strong electric field that transiently introduces pores into the plasma membrane (Gehl, 2003). Electroporation is a powerful method to introduce molecules directly into the cytoplasm of cells. For our analyses of intracellular activity, electroporation therefore circumvented the complications of endosomal uptake, breakdown and release associated with CPP-mediated cellular import (Fischer *et al.*, 2005; Fotin-Mleczek *et al.*, 2005a). After washing by centrifugation the cells were incubated for 20 h to allow the induction of apoptosis. Quantification of apoptotic cells occurred by incubation with annexin-V Alexa Fluor 647 using flow cytometry. Annexin-V binds to the phospholipid phosphatidylserine on the cell surface, which is externalized to the outer leaflet of the plasma membrane during apoptosis. Only the HPMA-BID-BH3 conjugate showed activity in a concentration dependent manner (Fig. 3.1). As the indicated concentrations represent peptide concentrations, this result demonstrates that the specific activity of the peptides was increased considerably due to the conjugation of the peptides to polymers.

We therefore aimed to resolve the molecular basis of the different activities. Next to a mere difference in electroporation efficiency of the polymer and the free peptide, differences in intracellular residence time or stabilization from proteolytic breakdown were considered.
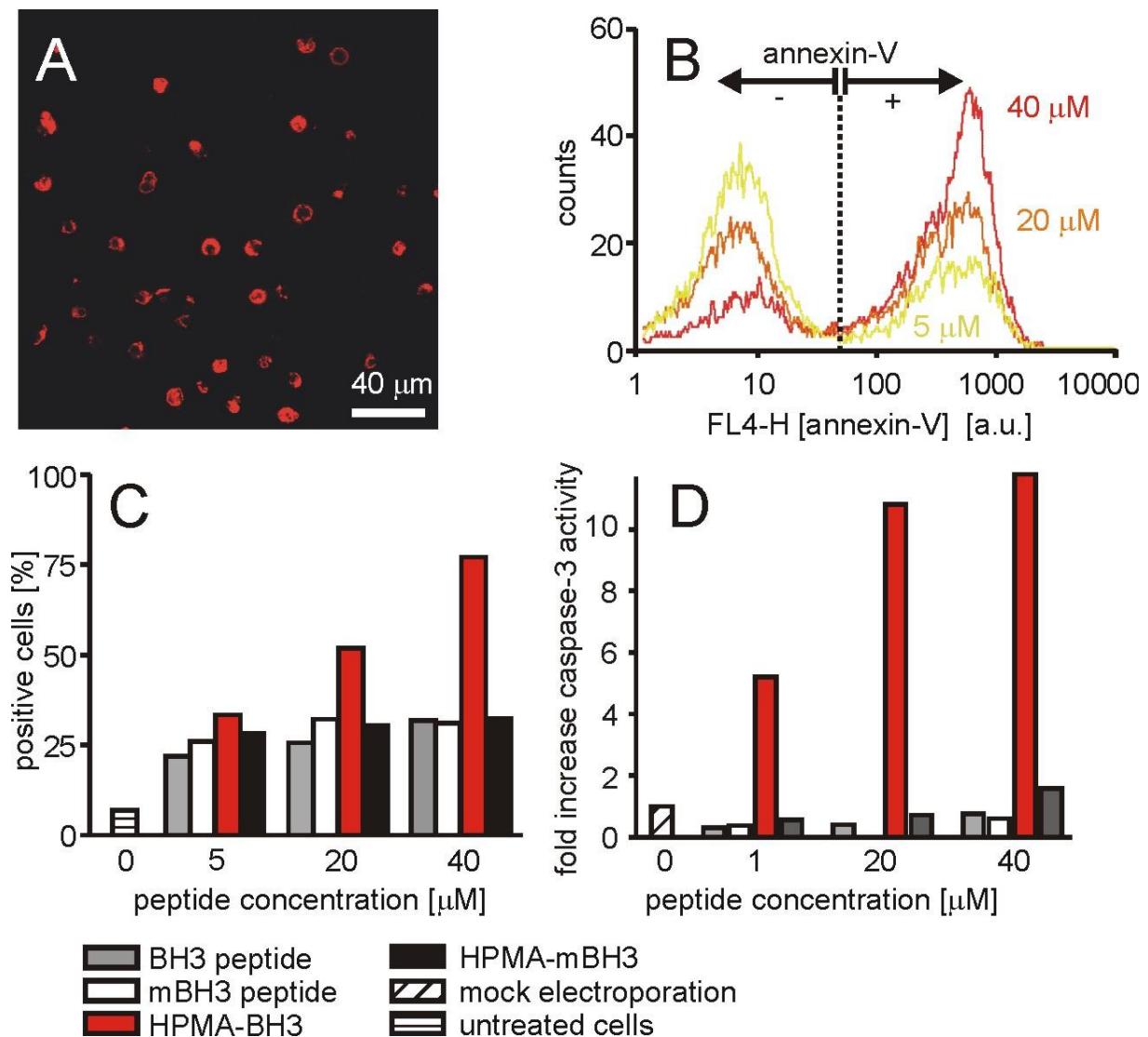
**Fig. 3.1.** Apoptosis induction by HPMA conjugates and free peptides. Jurkat cells were electroporated with the free apoptosis-inducing BID-BH3 peptide, the mutated mBID-BH3 peptide or the respective polymer-conjugated peptides HPMA-BID-BH3 and HPMA-mBID-BH3 in the indicated concentrations. (A-C) The cells were washed and incubated in FCS-containing medium for 20 h. Subsequently, cells were stained with Alexa 647-labeled annexin-V. (A) Microscopy image of annexin-V-stained cells, electroporated with 40 μM HPMA-BID-BH3, 20 h after incubation. (B) Flow cytometry histograms of Jurkat cells electroporated with various concentrations of HPMA-BID-BH3 and stained for phosphatidylserine exposure with Alexa 647-labeled annexin-V. (C) Fraction of annexin-V-positive Jurkat cells upon electroporation of peptides and HPMA conjugates. (D) Jurkat cells were electroporated with peptides and HPMA conjugates and after incubation for 6 h in FCS-containing medium the caspase-3 activity was determined. The figures show the results of representative experiments. The concentrations relate to the number of bioactive peptides.

## 3.4.3. Quantification of electroporation efficiency

In a first step, we compared the electroporation efficiency of the conjugates and the free peptides. To this end, 30 $\mu$M of the BID-BH3 peptide and the HPMA-BID-BH3 conjugate were electroporated into Jurkat E6.1 cells. The intracellular fluorescence was quantified by flow cytometry and observed by confocal laser scanning microscopy 1 h after electroporation. All electroporated cells were positive for fluorescence. The cellular fluorescence of the peptide was approximately 4-fold higher than that of the HPMA conjugate (Fig. 3.2). Considering that (i) both the peptide and the conjugate had the same molecular brightness and (ii) that the polymer carried on average two peptides per polymer, this finding indicated that in case of the free peptide about twice as many peptides were inside the cells than in the case of the polymer-coupled peptides.
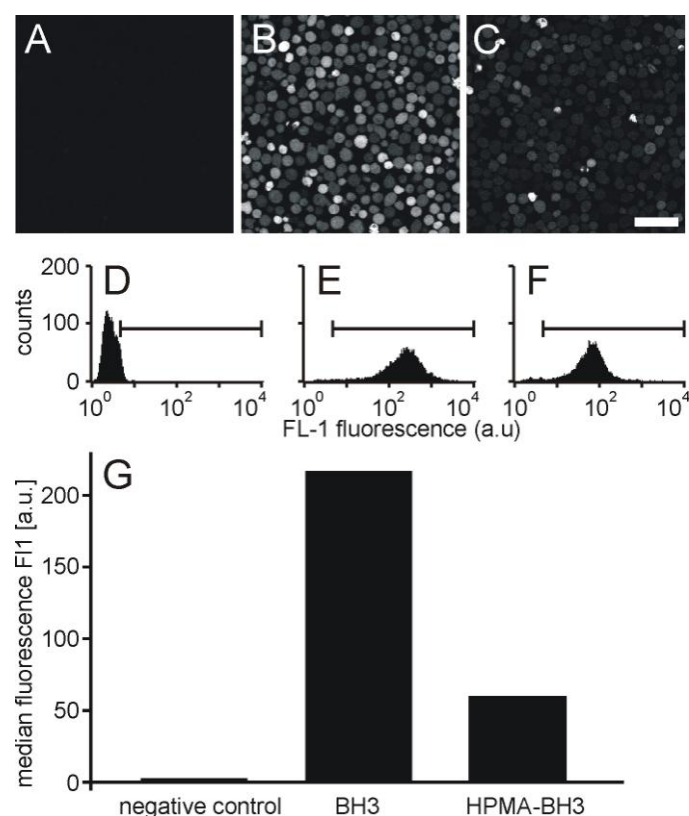


**Fig. 3.2.** Electroporation efficiency of peptides and conjugates. Jurkat E6.1 cells were electroporated with (A) medium 30 $\mu$M of (B) BID-BH3 peptide or (C) HPMA-BID-BH3. The concentration of conjugate related to the number of peptide moieties. Subsequently, the living cells were washed with medium and observed by (A-C) confocal laser scanning microscopy 1 h after electroporation. The scale bar in the microscopy images represents 50 $\mu$m; (D-E) corresponding flow cytometry histograms and (G) medians of intracellular fluorescein intensities.

## 3.4.4. Determination of intracellular retention

The induction of apoptosis was determined 20 h after electroporation. We therefore reasoned that the higher biological activity could be explained by a longer residence time of the higher molecular weight conjugates. For a comparison of residence times, Jurkat E6.1 cells were electroporated with 30 $\mu$M solutions of the peptides and conjugates. The cells were washed and observed by confocal laser scanning microscopy over time in a chase experiment (Fig. 3.3). Subsequently, the images were analyzed by digital image analysis and the average brightness of the cells was calculated (Fig. 3.4). The fluorescence residence time of the unbound BID-BH3 peptide had a half life of 5.8 ± 1.8 h, the one for the free mBID-BH3 peptide 5.0 ± 1.1 h, the HPMA-BID-BH3 conjugate 10.6 ± 7.4 h and the HPMA-mBID-BH3 conjugate 4.4 ± 1.7 h. In contrast, the free fluorescein molecules had an intracellular half-life of less than 0.5 h. For the HPMA-conjugates larger errors were found repeatedly due to the lower intensity of cellular fluorescence that also precluded an observation over longer times. The intracellular distribution did not change significantly over time (Fig. 3.5). In all cases, fluorescence remained homogenuously distributed inside the cytoplasm demonstrating that no sequestration into intracellular structures occurred. These results clearly indicate that the intracellular residence time is not a relevant factor to explain the increased activity of HPMA-conjugated peptides.
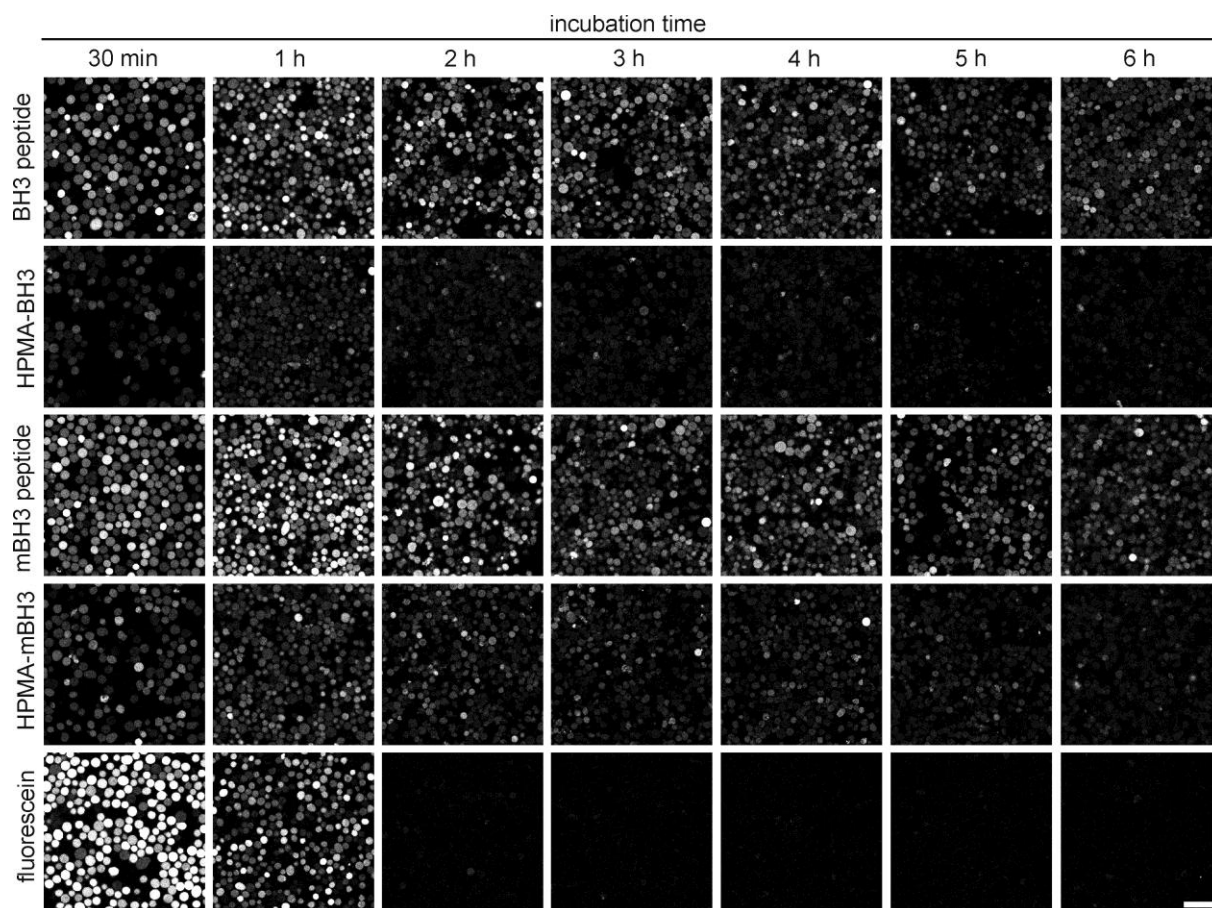
**Fig. 3.3.** Release of cellular fluorescence after electroporation of peptides and HPMA conjugates**.** Jurkat E6.1 cells were electroporated with 30 $\mu$M of peptides and HPMA conjugates or fluorescein. The concentration of conjugate related to the number of peptide moieties. Subsequently, the cells were washed twice with medium, seeded into an 8-well chambered coverglass and incubated at 37°C. In certain time intervals confocal images were taken by laser scanning microscopy. The scale bar represents 50 $\mu$m.
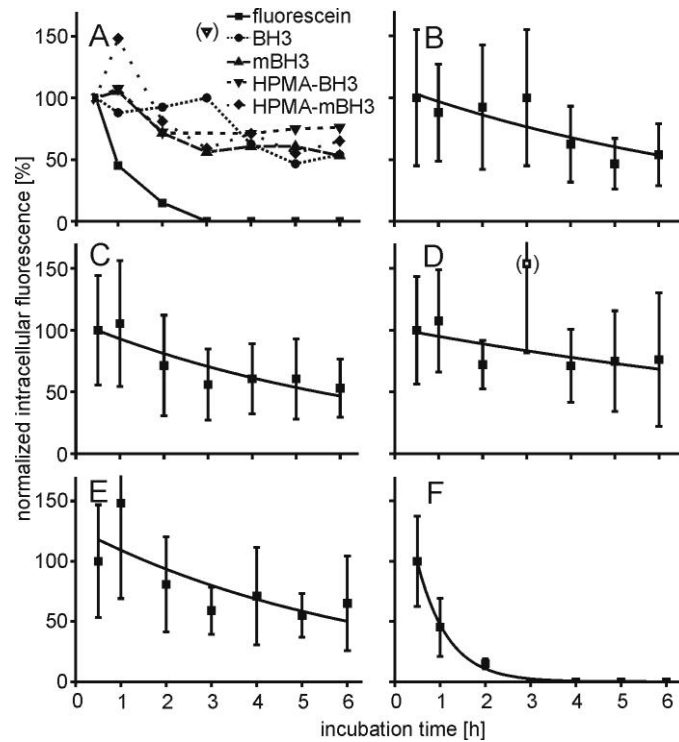
**Fig. 3.4.** Analysis of release kinetics. The confocal images generated by laser scanning microscopy (Fig. 3.3) were analyzed by quantitative image analysis via ImageJ. (A) Superposition of all curves (the intensity at the beginning of the experiment was set to 100 %), (B) BID-BH3 peptide, (C) mBID-BH3 peptide, (D) HPMA-BID-BH3 conjugate, (E) HPMA-mBID-BH3 conjugate and (F) fluorescein. The data were fitted with a first order exponential decay.
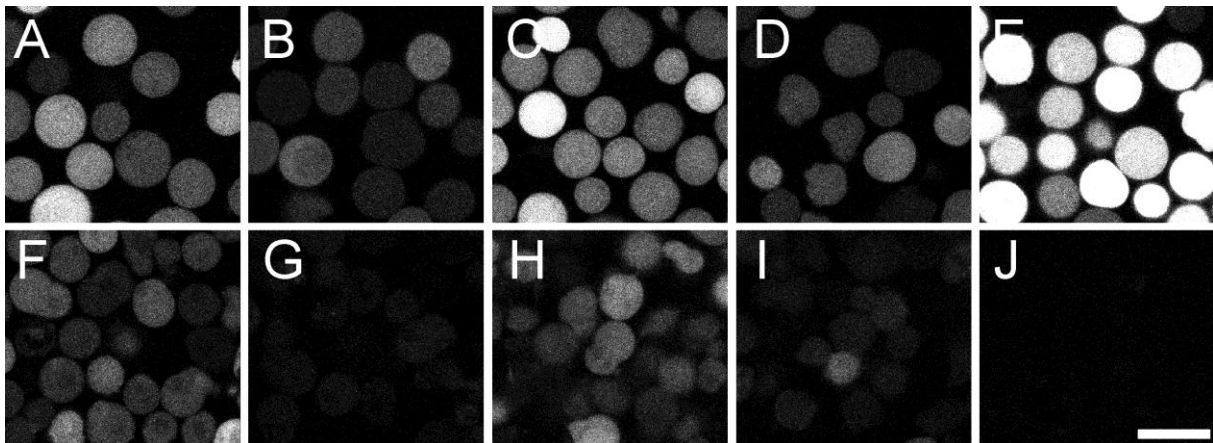


**Fig. 3.5.** Intracellular distribution of fluorescence at different time points after electroporation. Jurkat E6.1 cells electroporated with (A) the BID-BH3 peptide, (B) the HPMA-BID-BH3 conjugate, (C) the mBID-BH3 peptide, (D) the HPMA-mBID-BH3 conjugate and (F) fluorescein were observed (A-E) 30 min after electroporation and (F-J) 6h after electroporation. The scale bar represents 20 μm.

## 3.4.5. Peptide stability

Having excluded differences in loading and retention as the source for the increased biological activity, we therefore addressed the sensitivity to proteolytic breakdown of the free peptide and the HPMA-conjugated peptide. It has been shown that terminal capping (Brinckerhoff et al., 1999) as well as linking of peptides to dendrimers (Bracci et al., 2003) increases the resistance towards serum proteases. HPMA-BID-BH3 conjugate and BID-BH3 peptide were incubated with crude HeLa cell lysate as a source of proteolytic activity. The concentration of the lysate was adjusted so that the degradation of peptide and conjugate could be followed over several hours. The samples were incubated at 37 °C for 24 h. At certain times aliquots were extracted. Degradation was detected by fluorescence correlation spectroscopy. In a representative experiment the autocorrelation time $\tau_D$ for the intact HPMA-BID-BH3 conjugate was 80.9 $\mu$s, for the undigested BID-BH3 peptide 50.4 $\mu$s and for the digested samples 30.6 $\mu$s. By fixing these values, the fractions of intact and degraded polymer/peptide were derived from two component fits to the autocorrelation functions. With the selected concentration of cell lysate, the HPMA-BID-BH3 conjugate showed a half-life of 51.7 ± 12.6 h whereas the unbound BID-BH3 peptide showed a half-life of only 1.8 ± 0.2 h (Fig. 3.6). The complete degradation of both, peptide and conjugate upon conjugation with proteinase K confirmed that both molecules could be in principle digested by proteases. The results revealed that the HPMA conjugate stabilizes the peptide from being proteolytically digested in cell lysate. Given the very similar loading efficiencies and comparable intracellular retention times, protection from proteolytic breakdown should therefore be the explanation for the higher biological activity.
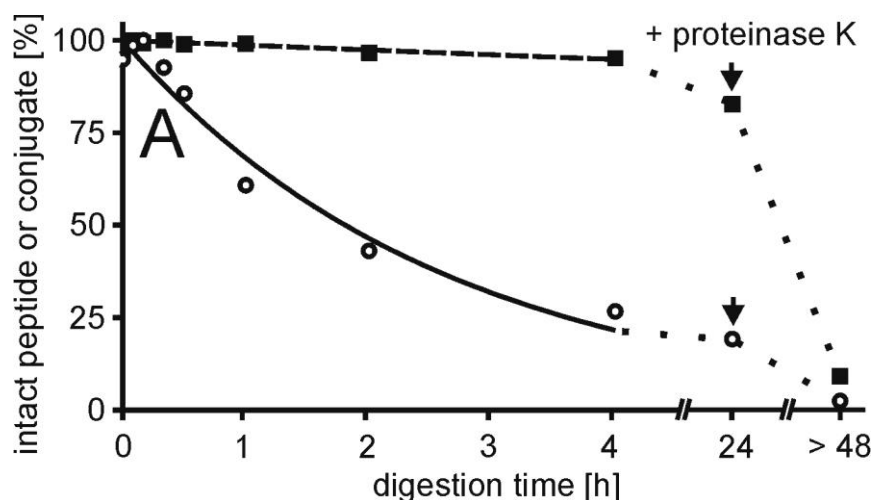
**Fig. 3.6.** Proteolytic stability of HPMA-BID-BH3 and the free BID-BH3 peptide in crude HeLa cell lysate. Cell lysate was generated by lysis of HeLa cells in Triton-X-100. The cell lysate was mixed with 2 $\mu$M HPMA-BID-BH3 conjugate and BID-BH3 peptide and the samples were incubated at 37°C. The concentration is related to the number of peptide moieties. After certain time points samples were extracted and frozen. After 24 h proteinase K was added to the samples in order to confirm the general sensitivity to proteases. The fractions of intact peptide (blank circles) and conjugate (filled squares) were determined by fluorescence correlation spectrosopy and derived from two-component fits of the autocorrelation functions. Half-lifes were derived from first-order exponential fits. The figure shows the results of a representative experiment.


## 3.4.6. Biological activity of a bifunctional cell-penetrating conjugate


Finally, we addressed whether for the BID-BH3 peptide as well, cofunctionalization of the HPMA polymer with a cell-penetrating moiety would yield a bioactive conjugate that would induce apoptosis by CPP-mediated cell entry.

The bifunctional BID-BH3-HPMA-R9 conjugate was also conveniently obtained following the standard synthesis protocol. The conjugate effectively induced apoptosis in Jurkat cells in a concentration-dependent manner, while the mutated peptide or a cell-penetrating conjugate cofunctionalized with a cell-penetrating moiety only did not (Fig. 3.7).
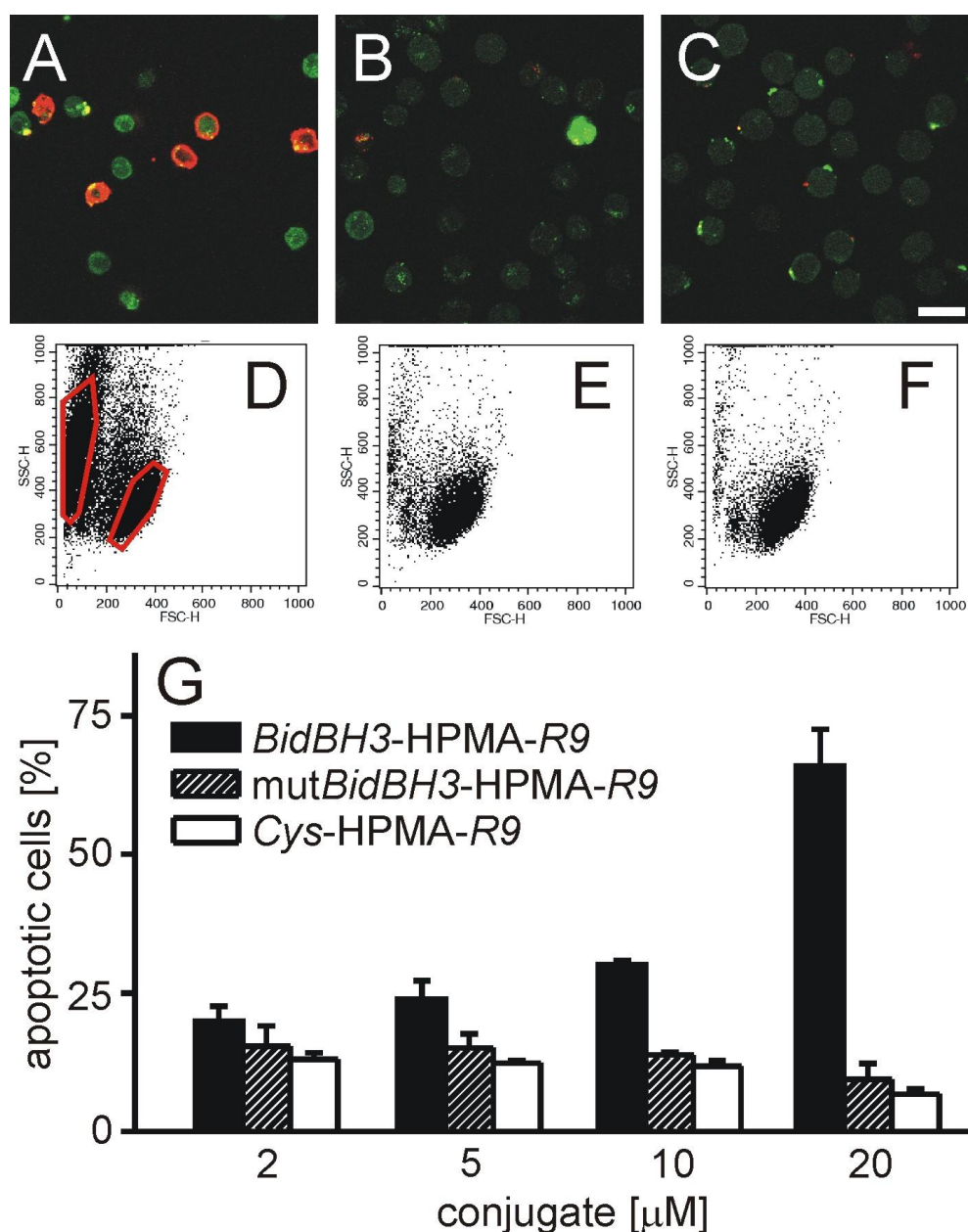
**Fig. 3.7**. Apoptosis induction by BID-BH3-HPMA-R9. (A-C) Confocal microscopy of Jurkat cells incubated with (A) BID-BH3-HPMA-R9 (20 μM), (B) mutBID-BH3-HPMA-R9 (20 μM), and (C) Lys(Fluo)-HPMA-R9 (20 μM) for 10 h at 37 °C. The exposure of phosphatidylserine on the cell surface was detected by Alexa 647-labeled annexin V (red). Fluorescein-labeled conjugates are represented in green. The bar denotes 20 μm. (D-G) Determination of cell death by flow cytometry for cells incubated with HPMA conjugates. (D-F) Flow cytometry scatter diagrams of forward versus sideward scatter for (D) BID-BH3-HPMA-R9 (20 μM), (E) mutBID-BH3-HPMA-R9 (20 μM), and (F) Lys(Fluo)-HPMA-R9 (20 μM). Jurkat cells were incubated with conjugates for 10 h at 37 °C. (G) Titration of cells with HPMA conjugates and quantification of cell death. Cell populations were gated based on forward and sideward scatter (D-F), and the fraction of dead cells determined from the ratio of events in both gates (red). Signals of dead cells are located in the left gate. Concentrations of the polymer conjugates in the medium were adjusted to the same concentration with respect to the functional peptide.

## 3.5. Conclusions

Our previous analyses had shown that coupling of peptides to an HPMA polymer by native chemical ligation yielded bioactive conjugates by a modular design (Ruttekolk *et al.*, 2008). These initial analyses had already indicated that the polymer-coupled peptides had a higher activity per peptide moiety. Differences in cellular loading efficiency, in retention inside the cell as well as in peptide stability were considered as the molecular basis for this observation. However, the bioactive peptide, derived from the proapoptotic protein Smac (Fulda *et al.*, 2002b), that we had selected was not accessible to an elucidation of these questions. For this peptide a free amino terminus was required for activity. Therefore, coupling to the polymer occurred via a cysteine residue coupled to a lysine side chain at the C-terminus of the peptide. Here, we selected an apoptosis-inducing peptide derived from the proapoptotic Bid protein that could be coupled to the polymer via the N-terminus in a straight-forward manner. Using this peptide we demonstrate an increase in the activity per peptide moiety that is very likely due to a protection from proteolytic degradation. Given the faster degradation of the free peptide one could also expect a faster release of degradation products from the cells. However, cellular retention times were the same for free peptides and for conjugates. We explain this observation by the generation of fragments that are still efficiently retained within the cells.

For a bifunctional conjugate that also carried a cell-penetrating moiety, we could also further demonstrate the general applicability of the modular approach. The synthesis was carried out by a modified native chemical ligation protocol as described before. Coupling efficiencies for this longer peptide were in the same range as those reported before, confirming the general usefulness and robustness of this synthesis procedure.

For the HPMA-conjugated peptide the activity was increased considerably per peptide moiety. In fact the free peptide did not show any activity. Previously, a conjugate of this peptide to the CPP d-octaarginine had shown apoptosis inducing activity in a number of cancer cells (Goldsmith *et al.*, 2006). However, the activity of a particular peptide inside the cell as well as sensitivity to apoptosis induction may vary largely between cell lines. The conjugate bearing the mutated peptide in which three of the residues required for activity where exchanged against alanine residues did also not show any activity. This finding confirmed that phosphatidylserine exposure was not due to electroporation or to a toxic effect by the polymer itself.

Finally, the HPMA-based strategy also prooved its potential as a modular synthesis approach for the combination of different functionalities. Synthesis of a single 29 amino acid peptide containing the BID-BH3 domain and the nonaarginine CPP is a major challenge and we

repeatedly obtained this peptide only with low purities and yields. Fusion of peptide fragments by native chemical ligation requires synthesis of a C-terminal thioester, which is also not straight forward in Fmoc peptide chemistry. Separate synthesis of the functional BID-BH3 peptide and the CPP and incorporation into the polymer therefore constitutes a major synthetic advantage.

In summary, our results show that the HPMA-based strategy provides a suitable way to increase the functionality of peptides with respect to intracellular applications in fundamental and applied biomedical research.

# 4. Short intracellular residence times limit the applicability of bioactive peptides in cells

The author of this thesis contributed all figures except Fig. 1 which was contributed by Heike Glauner.

## 4.1. Summary

Protein-protein interactions mediated by peptide motifs and protein binding domains play a crucial role in intracellular signal transduction (Pawson and Nash, 2003; Liu *et al.*, 2006; Miller *et al.*, 2008). It was previously demonstrated in cell-free systems that these interactions can be easily and highly selectively inhibited by inhibitory peptides (Pawson and Nash, 2003; Stoevesandt *et al.*, 2005b). On the other hand, the action of inhibitory peptides in living cells is highly complicate. Whereas the poor cellular uptake of peptides was extensively investigated and this drawback was finally overcome by electroporation (Knight and Scrutton, 1986), cell-penetrating peptides (Langel, 2002) and other strategies, the intracellular behavior of peptides is still not fully understood. Especially the intracellular residence time is important to achieve an adequate duration of bioactivity. In this study, we focus on the fate of fluorescently labeled peptides electroporated into living Jurkat E6.1 T cell leukemia cells. The cells were observed by confocal microscopy over time and the total intracellular fluorescence and the peptide localization was determined by digital image processing. It could be shown that the electroporation efficiency is not dependent on the physicochemical properties of the peptides. Nevertheless, the peptides had significantly different intracellular residence times with half-lifes between approximately 1 h up to more than 10 h. Interestingly, negatively charged phosphotyrosine-containing peptides showed a longer intracellular residence time than neutral or positively charged proline-rich peptides. In order to answer the question if these findings are related to the physicochemical properties only or to the proteolytic stability, we employed retro-inverso D-peptides (Chorev *et al.*, 1979), thus peptides with identical physicochemical characteristics and high proteolytic stability. These peptides were retained in cells with a much lower half life. The degradation kinetics were determined in lysate of the T cell lymphoma cells and determined by autocorrelation measurements by fluorescence correlation spectroscopy (FCS). Indeed, the cellular residence time is highly dependent on the proteolytic stability of the peptides.

## 4.2. Introduction

Signal transduction processes play a crucial role in every cell (Pawson and Nash, 2003). Especially cell types specialized on intercellular communication such as T cells have highly complicated intracellular signal transduction networks which could, to this day, not entirely disentangled due to a considerable lack of highly specific inhibitors for protein-protein interactions (Kroczek *et al.*, 2004; Turner and Billadeau, 2002; Horejsi *et al.*, 2004). T cell signal transduction represents a good example for a network in which a major part of interactions are mediated by the interplay of linear peptide motifs such as phosphotyrosine containing or proline-rich peptides with SH2 and SH3 domains (Li, 2005; Yaffe, 2002). Indeed, several protein-protein interactions could be effectively interrupted by addition of an excess of competing phosphotyrosine and proline-rich peptides (Stoevesandt *et al.*, 2005a; Stoevesandt *et al.*, 2005b; Pawson and Nash, 2003). Nevertheless, the applicability of peptides in living cells is still hampered by their poor plasma membrane permeability and inadequate intracellular stability.

In recent years several strategies have been developed in order to overcome the cell membrane barrier: Microinjection (Celis, 1984; Brandner *et al.*, 1974; Stephens and Pepperkok, 2001; Zhang and Yu, 2008) and irradiation by near-infrared lasers (Tirlapur and Konig, 2002) enable the direct transfer of impermeable molecules into single cells. But, obviously, these two techniques are restricted to a limited number of cells. The loading of molecules into cell populations can be facilitated by ultrasound (Postema and Gilja, 2007) and by the attachment of cationic lipids (Rao and Alving, 2000; Drummond *et al.*, 1999). Additionally, cell-penetrating peptides (CPPs) represent a promising approach which was shown to facilitate the uptake of a large variety of cargo molecules (Langel, 2002; Choi *et al.*, 2003; Rohrbach *et al.*, 2005; Fawell *et al.*, 1994; Nagahara *et al.*, 1998; Oehlke *et al.*, 2004; Turner *et al.*, 2005; Lewin *et al.*, 2000; Santra *et al.*, 2005b; Noor *et al.*, 2009; Nori *et al.*, 2003; Foerg and Merkle, 2008). In fact, some peptide-CPP conjugates show considerable activity within cells such as the proapoptotic Smac peptide (Fulda *et al.*, 2002a; Fotin-Mleczek *et al.*, 2005b). Nevertheless, CPPs can have a non-negligible influence on the cells. It has been reported that arginine-rich CPPs decreased the concentration of the tumor necrosis factor (TNF) receptor on the cellular surface by co-endocytosis (Fotin-Mleczek *et al.*, 2005b). As a consequence, the cells were less sensitive to TNF stimuli. Furthermore, especially at lower concentrations CPPs are mainly taken up via endocytosis (Fischer *et al.*, 2004) and only minor fractions reach the cytosol. Information on the intracellular concentrations cannot be obtained and CPP-based uptake itself is a time-dependent process. An alternative approach to overcome the plasma membrane is the employment of

electroporation (Knight and Scrutton, 1986; Gehl, 2003). Electroporation is based on a single short high-voltage pulse or on a series of pulses that cause short-term pore formation in the plasma membrane and hereby enable the cellular entry of the molecules of interest. Thus, the cytosol can be addressed directly and moreover the technique provides a well-defined temporal starting point what is of high importance for bioactivity studies. From the 1980s onward electroporation facilitated the efficient import of DNA (Neumann *et al.*, 1982), small molecules (Melvik *et al.*, 1986) and proteins (Mir *et al.*, 1988).

The second obstacle, the poor proteolytic stability of peptides, can be overcome by the employment of retro-inverso D-peptides (Chorev *et al.*, 1979), β- peptides (Frackenpohl *et al.*, 2001) and dendrimers (Haag and Vogtle, 2004). Furthermore, peptides, proteins and other molecules of therapeutic value are regularly stabilized by conjugation to for example polyethylene glycol (PEG) (Harris and Chess, 2003). Especially orally delivered macromolecules often require covalent polymer-conjugation (Goldberg and Gomez-Orellana, 2003) or non-covalent polymer attachment (Sandanaraj *et al.*, 2005). Although in recent years notable progress in the development of strategies to overcome the plasma membrane barrier and the the poor proteolytic stability have been made, still little is known about the intracellular fate of peptides. In fact, the question how long a peptide is present in the cell of interest may clearly be highly relevant for the duration of its bioactivity.

In this study, the intracellular behaviour of ten different fluorescently labeled peptides with different physicochemical properties was observed in Jurkat E6.1 T cell leukemia cells. First, it was demonstrated that the electroporation efficiency was independent of the physicochemical properties of the peptides. For this purpose a relatively mild electroporation method based on a multi-pulse protocol was employed. Subsequently, the cells were observed by confocal microscopy over a time period of 6 h. The intracellular localization could be determined and digital image processing provided quantitative results regarding the cellular residence times of the fluorescently labeled peptide moieties. As the time of the half-maximal fluorescence signal significantly varied between the different peptides, it was addressed whether proteolytic stability was the molecular basis for this observation. For this purpose, retro-inverso D-peptides (Chorev *et al.*, 1979) were synthesized, which means that these peptides contain only D-amino acids and the amino acid sequence is reversed. On the one hand they are nearly completely protease resistant due to the changed peptide backbone, on the other hand the spatial positions of the side chain moieties are comparable with the ones of the respective L-peptide. Thus, the employment of retro-inverso D-peptides provides a strategy to compare peptides of identical physicochemical properties and comparable binding patterns.

## 4.3. Experimental procedures

### 4.3.1. Reagents

The peptides were purchased from EMC microcollections (Tübingen, Germany). Peptides were N-terminally conjugated to an aminohexanoic acid spacer (Ahx) and carboxyfluorescein to enable detection of fluorescence and prevent them from N-terminal degradation. Additionally, the peptides were protected against C-terminal degradation by means of amidation. Chemicals were obtained from Fluka (Deisenhofen, Germany). Cell culture media were purchased from PAN biotech (Aidenbach, Germany). Protease inhibitor cocktail Complete was obtained from Roche Diagnostics (Mannheim, Germany). Cell Line Nucleofector Kits V were provided by Lonza (Cologne, Germany).

### 4.3.2. Peptide Synthesis

The peptides were purified by preparative RP-HPLC (Grom-SIL 120 ODS-4 HE, 125 × 20 mm, C18 column, 5 µm particle diameter; Grom, Herrenberg, Germany). Purity was determined by analytical RP-HPLC (Grom-SIL 120 ODS-4 HE, 100 × 2 mm, C18 column, 5 µm particle diameter; Grom, Herrenberg, Germany). Identity was validated via electrospray mass spectrometry with an LCQ Advantage Max mass spectrometer (Thermo Fisher Scientific Inc., Waltham, USA). Concentrations were determined by UV/Vis spectroscopy. The peptides were diluted 1000-fold in Tris/HCl buffer pH 8.8, assuming an extinction coefficient for fluorescein $E_{492} = 75,000$ L/(mol × cm).

### 4.3.3. Electroporation

Jurkat E6.1 were cultivated in RPMI medium supplemented with 10 % fetal calf serum. In order to achieve optimal electroporation $10^6$ Jurkat E6.1 cells were resuspended in 100 µL Nucleofector Solution V and the respective peptide was added. Electroporation was performed in a Nucleofector device (Lonza, Cologne, Germany). Here, the preinstalled electroporation method "X-001" was employed. Subsequently, 900 µL RPMI medium were added carefully and the cells were incubated for 5 min at RT. Finally, the cell suspension was washed in medium by centrifugation.

## 4.3.4. Flow cytometry

$5 \times 10^5$ electroporated Jurkat E6.1 cells were washed in PBS buffer and the median fluorescein fluorescence for the viable cell fraction, determined by gating in the forward versus sideward scatter plot, was analyzed by flow cytometry with a FACSCalibur System (BD Biosciences, San Jose, USA).

## 4.3.5. Microscopy

$5 \times 10^5$ electroporated Jurkat E6.1 cells were incubated in 200 $\mu$l phenol red-free RPMI medium for 10 min at 37 °C to allow them to settle on the bottom of a 8-well chambered coverglass microscopy slide (nunc, Rochester, USA). Subsequently, the cells were analyzed by confocal laser scanning microscopy over time using a Leica SP5 confocal microscope equipped with an HCX PL APO 63 × N.A. 1.2 water immersion lens (Leica Microsystems, Mannheim, Germany).

## 4.3.6. Loss of intracellular fluorscence

Solutions containing 30 $\mu$M of peptide were electroporated into Jurkat E6.1 cells. Next, cells were washed. Over an incubation period of 6 h at 37°C in a humidified atmosphere containing 5 % $CO_2$ the cells were periodically observed by confocal microscopy. Subsequently, the acquired images were analyzed by digital image processing.

## 4.3.7. Image analysis

The generated confocal microscopy images were analyzed by digital image processing using ImageJ 1.41 (freeware, National Institute of Health (NIH), USA) and ImagePro Plus (MediaCybernetics, Bethesda, USA). The images were low pass filtered and converted into a black and white mask using a fluorescence intensity and a size threshold. A watershed operation allowed the separation of adjacent cells. Finally, a mask of the cellular cross-sections was generated and applied on the original images. The program automatically quantified the mean fluorescence intensity in the optical planes of the cells.

## 4.3.8. Investigation of the proteolytic stability of L- and D-peptides

Jurkat E6.1 cells were resuspended to a density of $10^7$ cells/ml in PBS lysis buffer containing 1 % v/v Triton-X-100 and incubated for 1 h on ice. Subsequently, the membrane debris was removed by centrifugation at 20,000 x g for 20 min at 4°C. 2 $\mu$M of the L-peptides SLP179 and LATpY132 and the respective retro-inverso peptides ri-slp179 and ri-latY132 were added to aliquots of the cell lysate. The samples were incubated at 37°C. Periodically aliquots of 5 $\mu$L were withdrawn, mixed with 95 $\mu$L protease inhibitor cocktail and frozen. After an incubation period of 2h 40 U/mL proteinase K (2 U in 50 $\mu$L) was added in order to determine the accessability to proteolysis. Subsequently, the samples were incubated at 37°C for another 32 h. Frozen samples were thawed, 900 $\mu$L Tris buffer (100 mM Tris-HCl, pH 8.8) were added and aliquots of 50 $\mu$L were transferred into a 384-well plate (175 $\mu$m, low-base design, MMI). Fluorescence autocorrelation measurements were conducted employing a Leica TCS SP5 fluorescence correlation spectroscopy unit equipped with an HCX PL APO 63 × N.A. 1.2 water immersion lens. The autocorrelation functions were analyzed by the computer program ISS Vista (ISS facilities, Champaign, USA) with two-component fits assuming a triplet fraction. The autocorrelational diffusion time $\tau_D$ for the low-molecular weight component was fixed to the one determined for the fully degraded sample and the $\tau_D$ for the high-molecular weight to values determined for the intact peptides.

## 4.4. Results

## 4.4.1. Electroporation of peptides with different physicochemical properties

Jurkat E6.1 cells were electroporated with 30 $\mu$M peptide solutions. The peptides had comparable lengths but variant physicochemical properties. The cell viability and the median fluorescein fluorescence of the cells was determined by flow cytometry. For all peptides, the cell viability decreased by approximately 20 %. All peptides were imported efficiently and to a comparable degree. In contrast, the free fluorescein dye could be imported more efficiently. In general, the physicochemical properties did not influence the uptake notably.
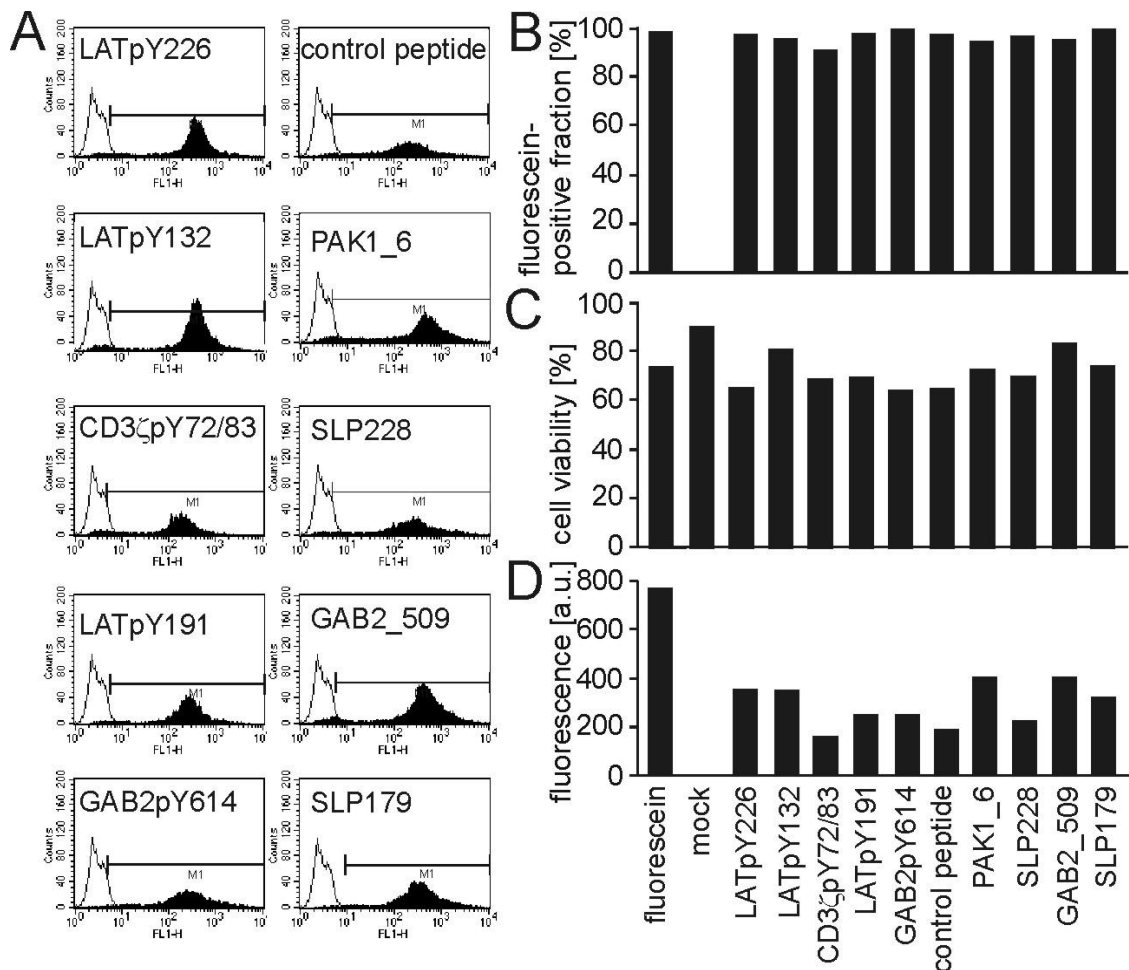


**Fig. 4.1.** Electroporation of peptides having comparable length and different physicochemical properties. Jurkat E6.1 cells were electroporated with 30 $\mu$M solutions of each peptide (table 1, A-J) or fluorescein. Subsequently, the cells were washed with medium and observed by (A) flow cytometry. The (B) fraction of fluorescein-positive cells, the (C) cell viability and (D) the median fluorescence per cell was determined.

## 4.4.2. Loss of intracellular fluorescence

Jurkat E6.1 cells were electroporated with 30 $\mu$M solutions of the peptides, washed and observed by confocal microscopy over 6 h at 37°C. Digital image analysis revealed that the negatively charged phosphotyrosine-containing peptides had a considerably longer cellular residence time than the rather positively charged proline-rich peptides. Overall, the cellular fluorescence half-lifes varied from approximately 1 h to more than 10 h. In contrast, the free fluorescein dye had a short residence time of less than 1 h, which was significantly shorter than the one for all peptides observed in this study. This indicates that the fluorescein moiety released from a fully degraded peptide would be exported efficiently. In general, the negatively charged peptides showed significantly longer cellular residence times.
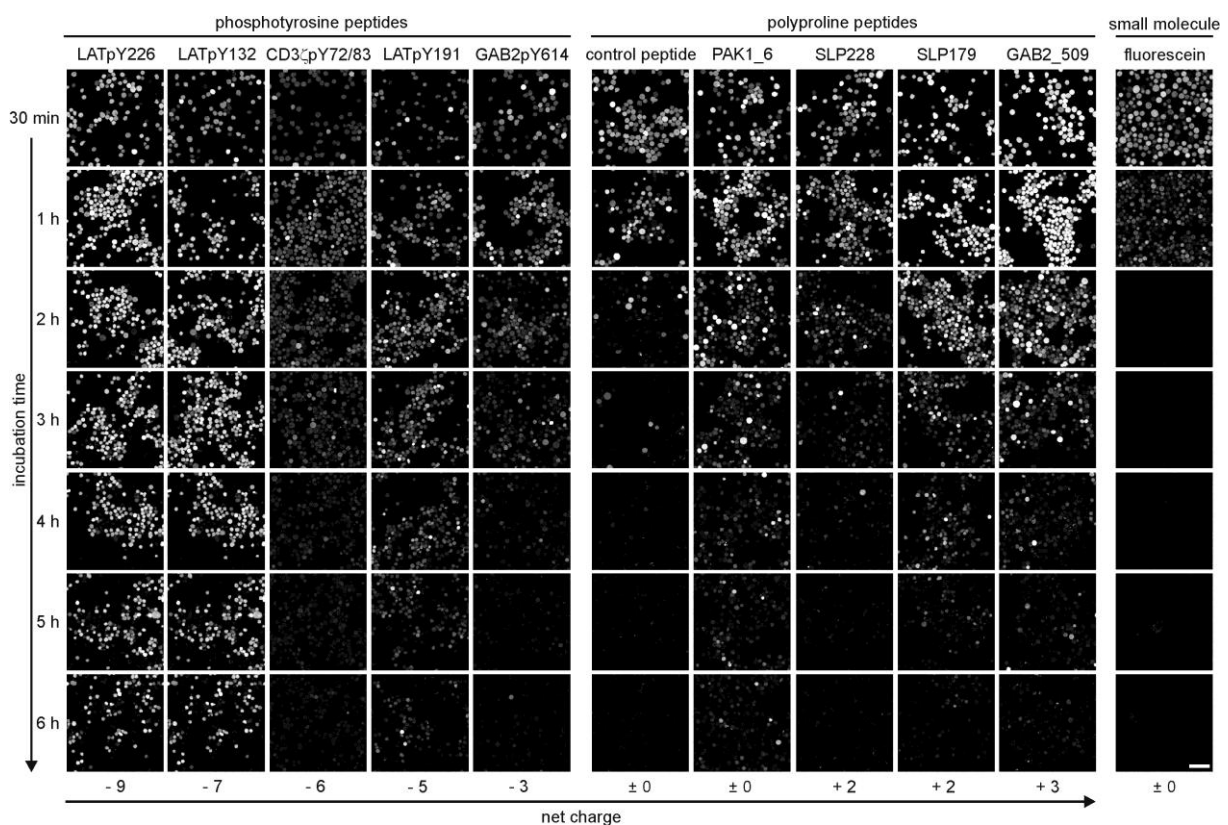


**Fig. 4.2.** Loss of fluorescence after electroporation of peptides of different physicochemical properties. Jurkat E6.1 cells were electroporated with 30 $\mu$M solutions of peptides or fluorescein. Subsequently, the cells were washed twice with medium, transferred into 8-well chambered coverglass microscopy slides and incubated at 37°C. Periodically confocal images were generated by laser scanning microscopy. The scale bar denotes 50 $\mu$m.
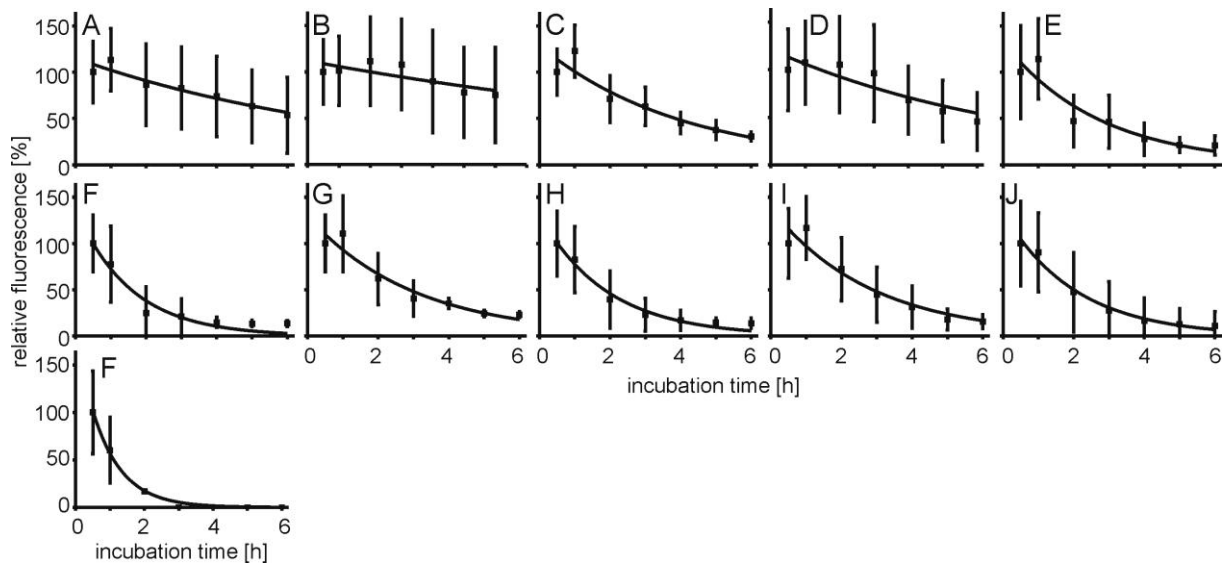
**Fig. 4.3.** Loss of cellular fluorescence for the various peptides. The peptides (table 1, A-J) (A) LATpY226, (B) LATpY132, (C) CD3ζpY72/83, (D) LATpY191, (E) GAB2pY614, (F) control peptide, (G) GAB2_509, (H) PAK1_6, (I) SLP179, (J) SLP228 and (K) fluorescein were electroporated into Jurkat E6.1 cells and the cells were incubated over time. The confocal images generated by laser scanning microscopy were analyzed by digital image analysis. The resulting values were fitted with an exponential decay of the first order depicting the fluorescence loss of the cells.
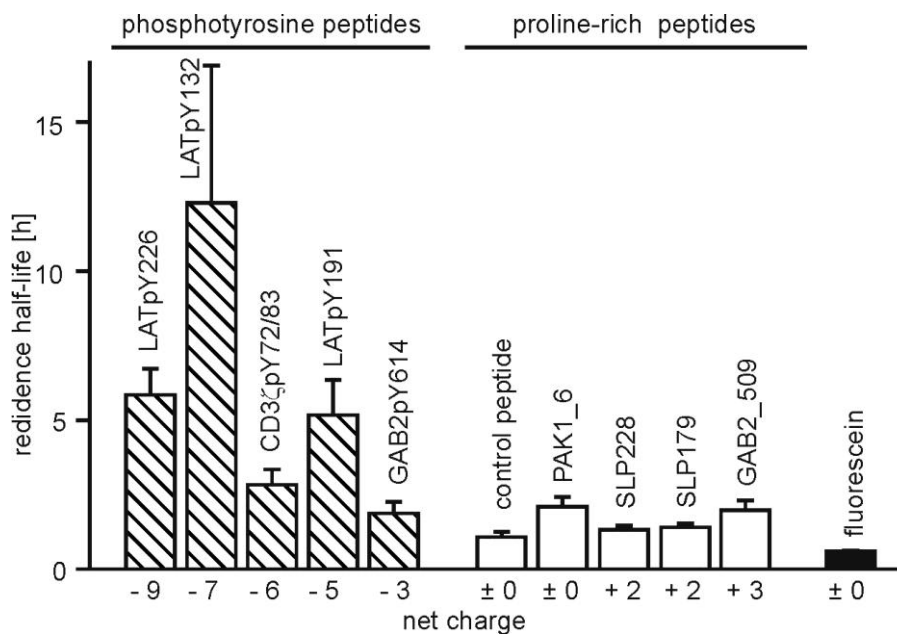


**Fig. 4.4.** Peptide residence times in dependence on the peptide net charge.

**Tab. 4.1.** Peptides and their residence times.

| name | sequence[1] | Mw [Da] | net charge | residence time [h] |
|---|---|---|---|---|
| LATpY226 | Fluo-Ahx-EVEEEGAPD(pY)ENLQELN-NH$_2$ | 2528 | - 9 | 5.8 ± 0.9 |
| LATpY132 | Fluo-Ahx-EDEDDYHNPG(pY)LVVLPDSTP-NH$_2$ | 2825 | - 7 | > 10 |
| CD3ζpY72/83 | Fluo-Ahx-NQL(pY)NELNLGRREE(pY)DV-NH$_2$ | 2868 | - 6 | 2.8 ± 0.5 |
| LATpY191 | Fluo-Ahx-EASLDGSRE(pY)VNVSQEL-NH$_2$ | 2446 | - 5 | 5.1 ± 1.2 |
| GAB2pY614 | Fluo-Ahx-KSTGSVD(pY)LALDFQPS-NH$_2$ | 2278 | - 3 | 1.9 ± 0.4 |
| control peptide | Fluo-Ahx-VKPLNEPDLPPAKIPTKPDQN-NH$_2$ | 2842 | ± 0 | 1.1 ± 0.2 |
| PAK1_6 | Fluo-Ahx-LDIQDKPPAPPMRNT-NH$_2$ | 2164 | ± 0 | 1.3 ± 0.1 |
| SLP179 | Fluo-Ahx-SGKTPQQPPVPPQRPMAAL-NH$_2$ | 2471 | + 2 | 1.7 ± 0.6 |
| SLP228 | Fluo-Ahx-AKLPAPSIDRSTKPPLDRS-NH$_2$ | 2520 | + 2 | 1.4 ± 0.1 |
| GAB2_509 | Fluo-Ahx-QPPPVNRNLKPDRKAKPTPLD-NH$_2$ | 2853 | + 3 | 2.1 ± 0.3 |
| ri- latY132 | Fluo-Ahx-ptsdplvvlygpnhyddede-NH$_2$ | 2745 | - 5 | > 10 |
| ri- slp179 | Fluo-Ahx-laamprqppvppqqptkgs-NH$_2$ | 2471 | + 2 | > 10 |
| fluorescein | | 332 | ± 0 | < 1.0 |
| 5(6)-carboxy-fluorescein | | 376 | - 1 | < 1.0 |

[1]Ahx: aminohexanoic acid, Fluo: 5(6)-carboxyfluorescein, -NH$_2$: C-terminal amidation.

## 4.4.3. Intracellular localization of peptides with different physicochemical properties

The question whether the differences in the loss of fluorescence were caused by different subcellular localization patterns was addressed by high-resolution confocal microscopy. It turned out that the peptides that possessed a shorter cellular residence time tended to be localized less homogeneously after an incubation time of 6 h at 37°C than the peptides possessing a long residence time. Nevertheless, the differences in subcellular localization cannot explain the differences in cellular residence times as no enrichment in certain compartments could be observed.
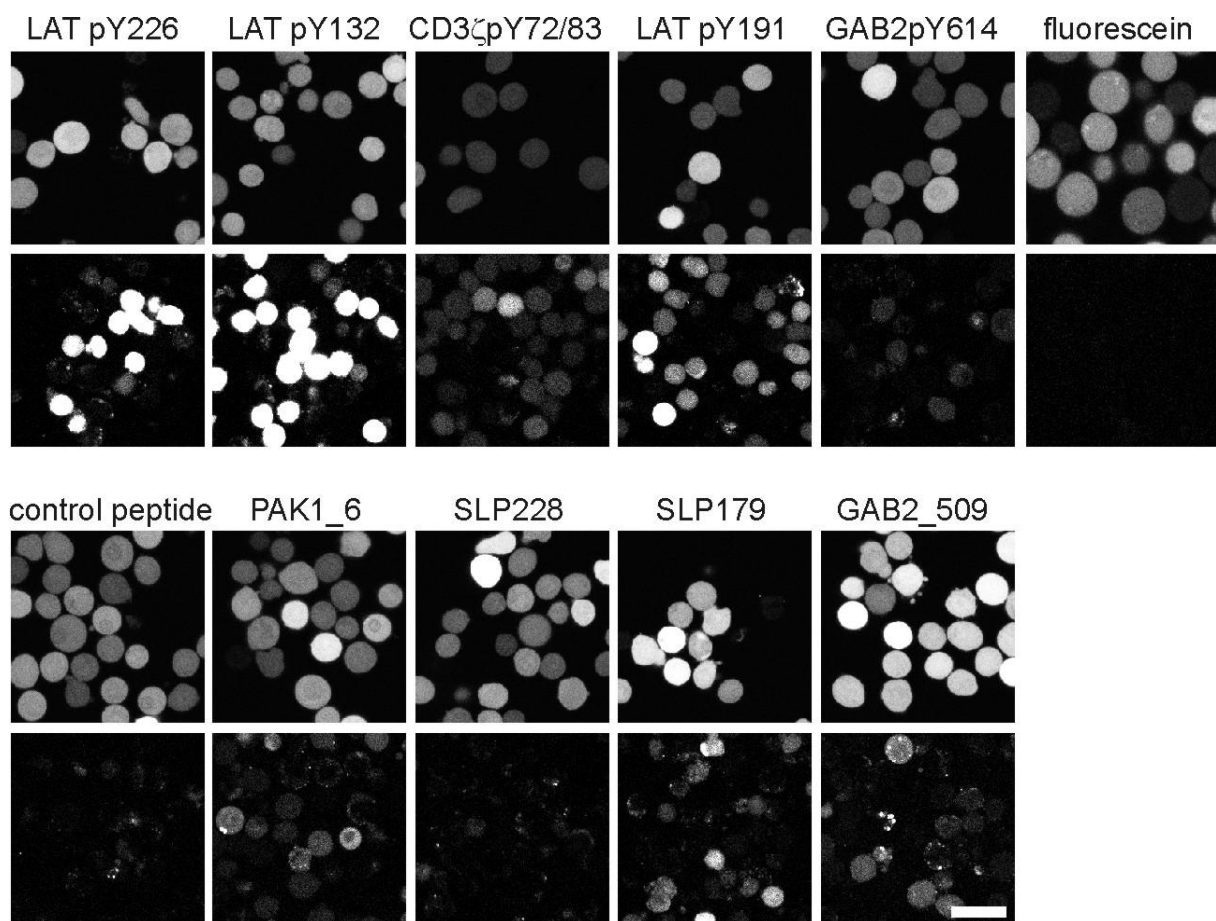
**Fig. 4.5.** Time dependence of the intracellular localization of peptides. Electroporated Jurkat E6.1 cells were observed by confocal microscopy before and after incubation for 6 h at 37°C. The brightness and contrast parameters of the images generated after 6 h were adjusted for all peptides in the same degree in order to improve the visualization of the intracellular distribution. After the incubation the peptides possessing a shorter cellular residence time were localized less homogeneously than the peptides possessing a longer residence time. The scale bar represents 20 $\mu$m.

## 4.4.4. Cellular peptide release of L- and retro-inverso D-peptides

Next, the question was, if the differences in the cellular residence time were either due to differences in the physicochemical properties of the peptides or due to differences in their proteolytic stability. In order to investigate the influence of the proteolytic stability we synthesized retro-inverso D-peptides showing extensive proteolytic stability, but the same physicochemical and binding properties as the L-peptides. In a first experiment the cellular release kinetics of L- and retro-inverso D-peptides were compared. For LatpY132 the retro-inverso peptide contained a tyrosine instead of a phosphotyrosine residue.

For this purpose 30 $\mu$M solutions of the L-amino acid peptides of LATpY132 and SLP179 and the respective retro-inverso peptides ri-latY132 and ri-slp179 were electroporated into Jurkat

E6.1 cells, the cells were washed and incubated at 37°C. Confocal images were generated over time and analyzed subsequently for cellular fluorescence.

Both retro-inverso D-peptides ri-latY132 and ri-slp179 showed very long and comparable cellular residence times >10 h. In contrast, the L-peptides showed significant differences. Whereas LATpY132 had a half maximal cellular residence time longer than 10 h, SLP179 was exported rapidly with a half-life of 1.7 ± 0.6 h. Carboxyfluorescein had a half maximal residence time < 1 h. These findings indicated that the kinetics of the cellular fluorescence loss might correlate with the proteolytic breakdown.
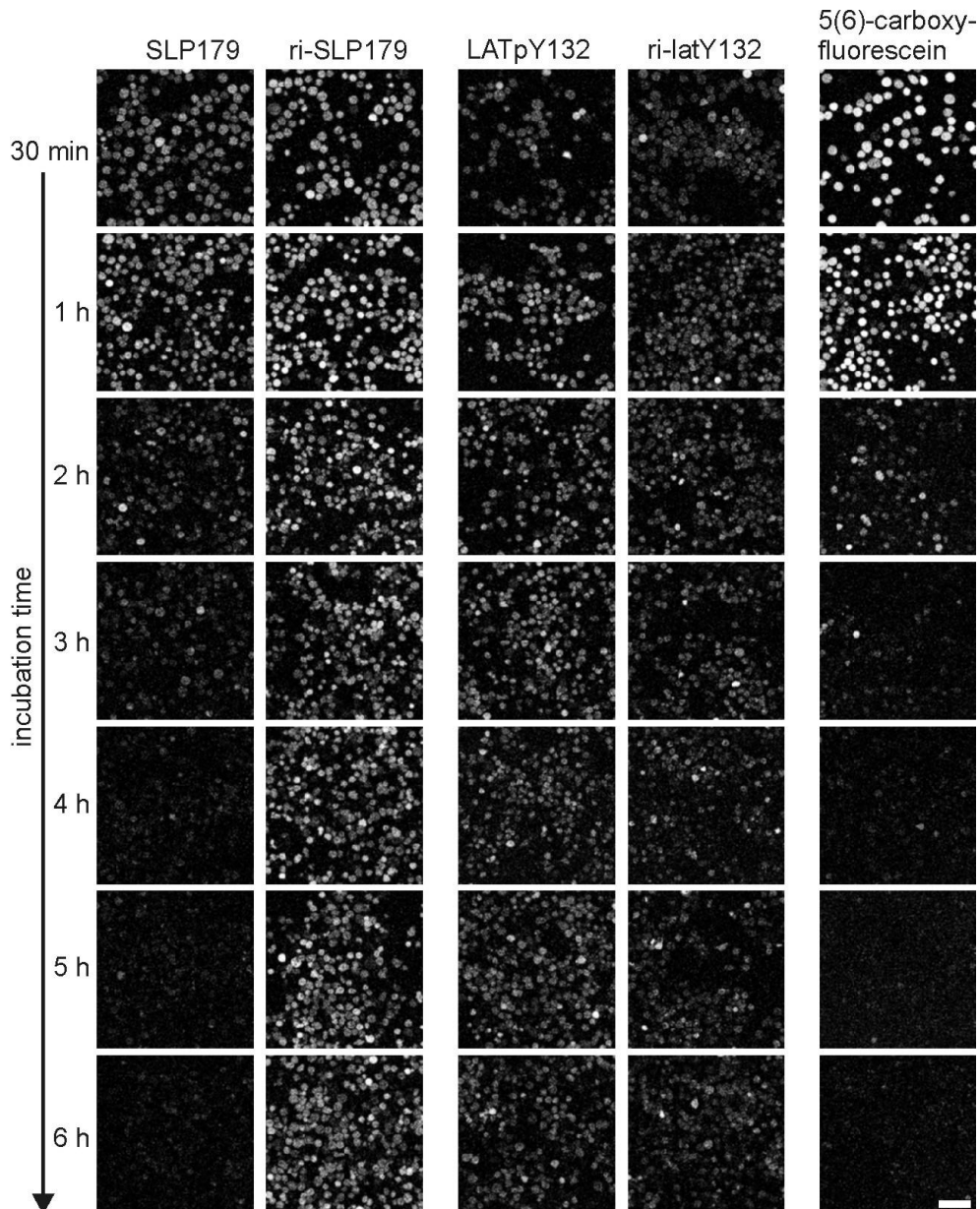


**Fig. 4.6.** Loss of fluorescence after electroporation of L- and retro-inverso D-peptides. Jurkat E6.1 cells were electroporated with peptides or 5(6)-carboxyfluorescein. The cells were washed twice with medium, seeded into 8-well chambered coverglass microscopy slides, incubated at 37°C and observed by laser scanning microscopy. The scale bar represents 50 μm.
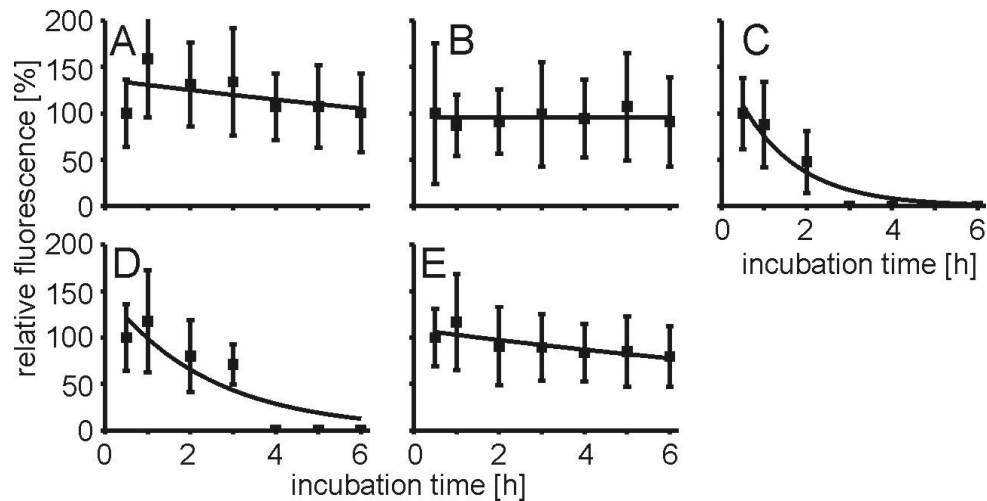
**Fig. 4.7.** Digital image analysis of the loss of fluorescence of L- and retro-inverso D-peptides. 30 µM solutions of the (A) LATp132 peptide, (B) ri-latY132 peptide, (C) 5(6)-carboxyfluorescein, (D) SLP179 peptide and (E) ri-slp179 peptide were electroporated into Jurkat E6.1 cells and the living cells were observed by confocal microscopy. Subsequently, the images were analyzed by quantitative image analysis via ImageJ. The results were fitted with an exponential decay of the first order to determine half-lifes of intracellular fluorescence.

## 4.4.5. Intracellular localization of peptides comprising L-amino acids and retro-inverso D-peptides

Next, we were interested to learn whether the increased proteolytic stability also effected the subcellular localization of retro-inverso D-peptides. Thus, the localization was investigated by high-resolution confocal microscopy. Consistent with the previous finding, it turned out that the L-amino acid peptide SLP179 that possessed the shortest cellular residence time was localized less homogeneously after an incubation time of 6 h at 37°C than the other peptides that possessed a long residence time.
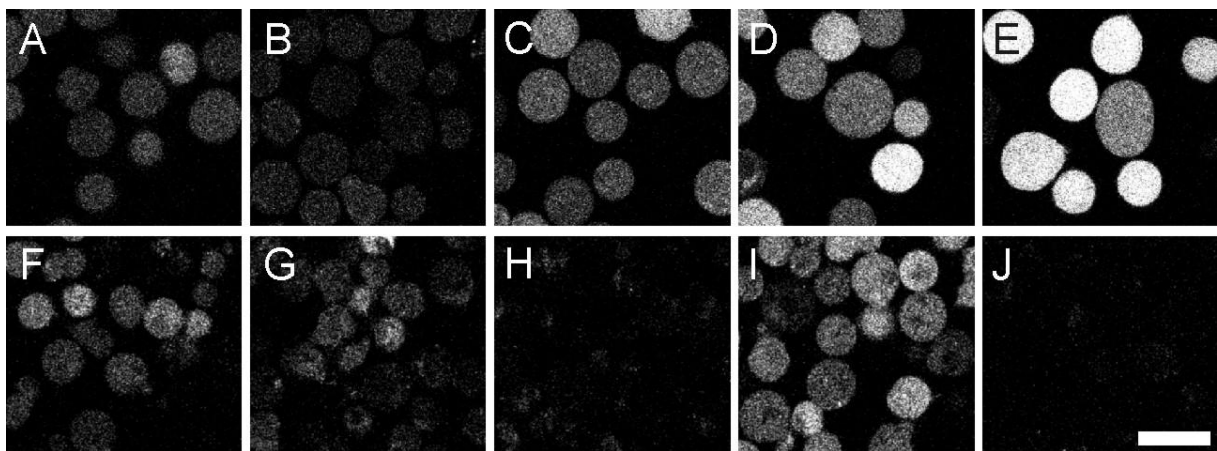


**Fig. 4.8.** The intracellular localization of L- and retro-inverso D-peptides in dependence on incubation time. Jurkat E6.1 cells were electroporated with 30 μM solutions of the peptides (A,F) LATpY132, (B,G) ri-latY132, (C,H) SLP179, (D,I) ri-slp179 and (E,J) 5(6)-carboxyfluorescein and observed by confocal microscopy (A-E) before and (F-J) after incubation of 6 h at 37°C. The brightness and contrast parameters of the images generated after 6 h were adjusted for all peptides in order to improve the visualization of the intracellular distribution. The scale bar represents 20 μm.

## 4.4.6. Long residence times correlate with high proteolytic stability

The cellular fluorescence loss was likely due to proteolytic breakdown and release of fragments. The proteolytic sensitivity was therefore determined by an incubation of the L-peptides LATpY132 and SLP179 and the retro-inverso D-peptides ri-latY132 and ri-slp179 at a concentration of 2 $\mu$M in Jurkat cell lysate. The integrity of the peptides was analyzed by fluorescence correlation spectroscopy (FCS). Whereas SLP179 had a proteolytic half-life of 0.3 ± 0.0 h, LATpY132 had longer half-life of 1.7 ± 0.4 h. In contrast, the retro-inverso peptides were not even degraded upon the addition of 40 U/ml proteinase K and subsequent incubation for another 32 h.
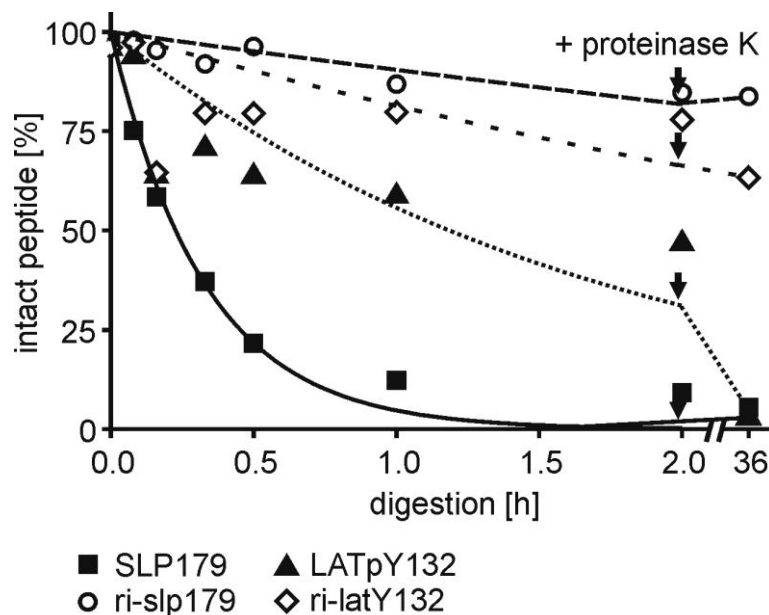


**Fig. 4.9.** Proteolytic stability of L- and retro-inverso D-peptides. Whereas the L-peptides SLP179 and LATpY132 were completely degraded in Jurkat cell lysate within a few hours, the respective retro-inverso peptides maintained integrity and could not even been degraded by 40 U/ml proteinase K (time of addition indicated by arrows) for 48 h at 37°C. Notably, the LATpY132 peptide was more stable than the SLP179 peptide.

Whereas the retro-inverso D-peptides both showed a very high and comparable proteolytic stability, the L-peptide LATpY132 showed a considerably longer half-life than SLP179. This findings correspond very well with the determined cellular residence times. These results therefore strongly indicate that higher proteolytic stability leads to extended cellular residence times.

## 4.4.7. Swelling of cells upon electroporation

In the microscopy experiments it could be observed that the cell volume increased upon electroporation. This effect was quantified with digital image processing using ImageJ. The analysis revealed that the area of the cross-section decreased by 24 % in the first 2 h after electroporation. Assuming spherical cells the cellular volume therefore decreased by approximately 50 %.
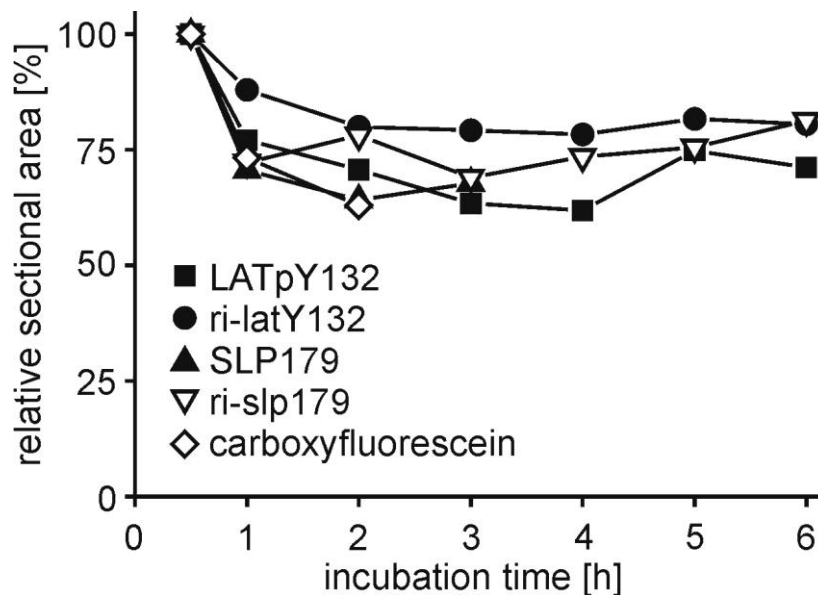


**Fig. 4.10.** Loss of cell size over time. Upon incubation the area of the cross-sections decreased by 24 % which corresponds to a volume decrease by 50 %.

This had an notable impact on the quantification of the intracellular residence time. The detected fluorescence signal occurring from the fluorescence labeled peptides detected in the first measurement after 30 min was lower than expected due to swelling and the resulting dilution effect. In fact, this effect was indeed observable. Consequently, for most peptides the cellular fluorescence intensity increased from 30 min to 2 h. Especially for molecules that have a long intracellular residence time this effect should be taken into consideration as intracellular concentrations can be easily underestimated directly after electroporation due to swollen cells that shrink over time.

## 4.5. Conclusions

Peptides are regularly used in cellular bioactivity studies and their bioactivity has been extensively elucidated. For this purpose peptides are regularly imported by means of electroporation. Nevertheless, the intracellular fate of the electroporated peptides is not fully understood yet.

In this study, fluorescently labeled peptides were electroporated into JurkatE6.1 T cell lymphoma cells and the intracellular fate of the fluorescein moiety was observed by confocal microscopy. It could be demonstrated that the electroporation efficiency was independent of the physicochemical properties of the peptides. In contrast, the observation of the cells over a time period of 6 h revealed that the cellular residence times were clearly different for the different peptides and the fluorescence half-lifes varied from approximately 1 h for a uncharged control peptide up to more than 10 h for a 7-fold negatively charged LATpY132 peptide. Interestingly, it turned out that the negatively charged phosphotyrosine peptides in general had longer residence times than the neutral or positively charged proline-rich peptides. The low-molecular weight dyes fluorescein and 5(6)-carboxyfluorescein were exported notably faster than all fluorescent peptide moieties released from the peptides employed in this study. Furthermore, we considered whether the differences in fluorescence loss were due to peptide export or due to intracellular degradation and release of fragments. In order to investigate this further, we synthesized two retro-inverso D-peptides (Chorev *et al.*, 1979). Retro-inverso D-peptides represent peptides with an reversed sequence composed of D-amino acids. Hence, they show identical physicochemical and binding properties but are proteolytically inert. As peptide sequences we chose one peptide that had a long cellular residence time, LATpY132, and SLP179 with a short residence time. Whereas the residence time of the L-peptides was in the range of few hours, both retro-inverso D-peptides ri-latY132 and ri-slp179 had a very long and comparable intracellular half-life larger than 10 h. Thus, it was very likely that proteolytic stability plays a key role in the loss in fluorescence. In order to determine the proteolytic stability of the peptides against cytosolic proteases, we generated cell lysate from the JurkatE6.1 T cell lymphoma cells in an isotonic buffer of neutral pH. The degradation was determined by fluorescence correlation spectroscopy (FCS). Rapid release strongly correlated with rapid breakdown.

In summary, we could demonstrate that the intracellular residence time is clearly dependent on the proteolytic stability and is highly sequence-specific. In cellular studies the differences in cellular residence times are an underestimated but severe challenge.

# 5. A cell-penetrating peptide derived from human lactoferrin with conformation-dependent uptake efficiency

The author of this thesis purified the peptides, contributed Fig 5.1, Fig. 5.5.A-B and conjugated hLF peptide to streptavidin (Fig. 5.8). Dr. Falk Duchardt performed the cellular experiments shown in Fig. 5.2, 5.3, 5.7.B-C and 5.8. Wouter P.R. Verdurmen performed the heparinise experiment (Fig. 5.7.A) and the comparison of hLF and rLF (Fig. 5.4). The NMR experiments were performed by Prof. Dr. Geerten W. Vuister (Fig. 5.5.C-E). the CD measurements by Dr. Jochen Bürck (Fig. 5.5.F-I) and the SPR measurements by Hugues Lortat-Jacob (Fig. 5.6).

## 5.1. Summary

The molecular events that contribute to the cellular uptake of cell-penetrating peptides (CPP) are still a matter of intense research. Here, we report on the identification and characterization of a 22 amino acid CPP derived from the human milk protein lactoferrin. The peptide exhibits a conformation-dependent uptake efficiency that is correlated with efficient binding to heparan sulfate (HS) and lipid-induced conformational changes. The peptide contains a disulfide bridge formed by terminal cysteine residues. At concentrations exceeding 10 $\mu$M, this peptide undergoes the same rapid entry into the cytoplasm that was previously described for the arginine-rich CPPs nonaarginine and the Tat peptide. Cytoplasmic entry strictly depends on the presence of the disulfide bridge. In order to better understand this conformation dependence, NMR spectroscopy was performed for the free peptide, and circular dichroism (CD) measurements were performed for the free and for the lipid-bound peptide. In solution, the peptide showed only slight differences in secondary structure, with a predominantly disordered structure both in the presence and absence of the disulfide bridge. In contrast, in complex with large unilamellar vesicles, the conformation of the oxidized and reduced forms of the peptide clearly differed. Moreover, surface plasmon resonance (SPR) experiments showed that the oxidized form binds to heparan sulfates with a considerably higher affinity compared to the reduced form. The requirement of the disulfide bond for heparan sulfate binding was further confirmed by heparin-column-based liquid chromatography. Consistently, membrane binding and cellular uptake of the peptide were reduced when heparan sulfate chains were removed.

## 5.1. Introduction

Cell-penetrating peptides (CPPs[1]) such as the antennapedia-derived penetratin (Derossi *et al.*, 1994) and the Tat peptide (Vives *et al.*, 1997) are widely used tools for the delivery of peptides, proteins and oligonucleotides into cells (Fischer *et al.*, 2001). Areas of application range from cell biology (Jarver *et al.*, 2007) to biomedical research (Langel, 2002). Most CPPs used to date are of non-human origin but the immunological relevance of these molecules is particularly important to biomedical research. Especially when conjugated to proteins and nanoparticles these molecules may give rise to an adaptive immune response. Therefore, CPPs like the human calcitonin-derived peptide (Schmidt *et al.*, 1998) and peptides corresponding to signal sequences of human proteins (Rojas *et al.*, 1998) are being considered as highly attractive import vehicles.

Human lactoferrin (hLF) is an 80 kDa iron-binding glycoprotein of 703 amino acids (Metz-Boutigue *et al.*, 1984). It constitutes about 15% of human milk protein and can also be found in low concentrations in blood plasma, tears, nasal fluids, saliva, pancreatic, gastrointestinal and reproductive tissue secretions (Levay and Viljoen, 1995). With antifungal, antimicrobial and antiviral activities, the protein plays an important role in the innate immune defense (Legrand *et al.*, 2008). In addition to iron depletion (Ward and Conneely, 2004), the protein exerts its activity through direct interaction with bacterial components (Valenti and Antonini, 2005).

The hLF N-terminal domain in particular carries potent activity against pathogens (Gifford *et al.*, 2005). In the gastrointestinal tract this domain can be cleaved through pepsin digestion resulting in the release of an antimicrobial peptide called lactoferricin (Bellamy *et al.*, 1992). Human lactoferricin comprises 49 amino acids (20 to 68 of the parent sequence) that form a loop, stabilized by two disulfide-bonds. The peptide contains sections of hydrophobic and positively charged amino acids comparable to those found in numerous peptides that display antimicrobial activity.

It has been demonstrated that antimicrobial peptides and CPPs possess concordant functional characteristics. On one hand, antimicrobial peptides are taken up into mammalian cells (Takeshima *et al.*, 2003) and on the other hand CPPs show antimicrobial activity (Nekhotiaeva *et al.*, 2004). Therefore, we considered whether a lactoferricin-derived peptide may also have the ability to act as a CPP by entering into mammalian cells.

Here, we report the characterization of a new cell-penetrating peptide derived from the N-terminal domain of human lactoferrin, corresponding to amino acid residues 38-59 (19-40 of human lactoferricin). The peptide overlaps with the lipopolysaccharide-binding region of lactoferricin (Elass-Rochard *et al.*, 1995). The peptide shows a well-defined structure-activity

relationship and enters cells efficiently. The uptake mechanism of the peptide is concentration-dependent. Above a threshold concentration rapid delivery into the cytoplasm and nucleus is observed, which has previously been described for the arginine-rich CPPs nonaarginine and the Tat-derived peptide (Duchardt *et al.*, 2007; Tunnemann *et al.*, 2006). Very remarkably, the hLF-derived peptide (hLF-peptide) contains only four arginine and two lysine residues. Instead, an intramolecular disulfide bridge is required for the efficient uptake, demonstrating that a high number of arginine residues in the peptide sequence is not a prerequisite for triggering the rapid import. Instead, for the hLF peptide efficient import is strictly conformation dependent.

A combination of surface plasmon resonance (SPR), NMR and circular dichroism experiments revealed a conformation dependence of interactions with heparan sulfate proteoglycans and demonstrated that only the cyclic form of the peptide undergoes a conformational transition when interacting with large unilamellar vesicles. Heparinase treatment of cells reduced membrane binding and uptake of the peptide, demonstrating the relevance of heparan sulfate binding for the function of the peptide as a CPP. By using a biotinylated analog of the peptide, we validated the capacity of the peptide to mediate cellular import of a protein cargo. These results illustrate that the hLF-peptide is a promising new candidate for a human CPP with a structure-activity relationship that should stimulate further research on the molecular principles that govern CPP interaction with cell membranes.

## 5.3. Experimental Procedures

## 5.3.1. Cells and Reagents

The human cervical carcinoma cell line HeLa was obtained from the American Type Culture Collection (Manassas, VA, USA). 1,4-Dithiothreitol (DTT) was from Merck (Darmstadt, Germany). 3-(4,5-dimethylthiazol-2-yl)-2,5-diphenyltetrazolium bromide (MTT), heparinases I-III, BSA and glucose were obtained from Sigma (Steinheim, Germany). Rottlerin was from Calbiochem (Bad Soden, Germany). The Zenon mouse IgG1 AlexaFluor647 labeling kit (specific for the Fc part of IgG1 antibodies) was purchased from Invitrogen (Karlsruhe, Germany). The anti-heparan sulfate (HS) VSV-tagged single chain antibody HS4C3 (van Kuppevelt *et al.*, 1998) and the mouse anti-VSV (clone P5D4) antibody were a kind gift of Dr. Toin van Kuppevelt (Dept. of Biochemistry, Radboud University Nijmegen Medical Centre, Nijmegen, The Netherlands). Tris(2-carboxyethyl)phosphine hydrochloride (TCEP·HCl) was obtained from Thermo Fisher Scientific (Bonn, Germany). The phospholipids DPC

(dodecylphosphocholine), DMPC (1,2-dimyristoyl-sn-glycero-3-phosphocholine) and DMPG (1,2-dimyristoyl-sn-glycero-3-phosphoglycerol) used for vesicle preparation were purchased from Avanti Polar Lipids (Alabaster, AL, USA). Biotin-LC-hydrazide was from Pierce (Rockford, USA). The HBS-P buffer (10 mM HEPES, 150 mM NaCl, 3 mM EDTA, 0.005 % surfactant P20, pH 7.4) was from Biacore AB (Uppsala, Sweden).

## 5.3.2. Peptide synthesis

Unlabeled hLF peptide was supplied by Thermo Fisher Scientific. The other peptides were purchased from EMC microcollections (Tübingen, Germany) and fluorescently labeled by N-terminal conjugation of 5(6)-carboxyfluorescein. The purity of all peptides was determined by analytical HPLC. The identity of the peptides was confirmed by MALDI-TOF mass spectrometry. Peptides with a purity of less than 90% were purified by preparative HPLC.

**Tab. 5.1.** Primary structures of the peptides used in this study. All peptides were synthesized as C-terminal peptide amides (-$CONH_2$). Fluo represents 5(6)-carboxyfluorescein and Ahx aminohexanoic acid.

| Peptide | Sequence |
|---|---|
| R9 | Fluo-RRRRRRRRR-$CONH_2$ |
| penetratin | Fluo-RQIKIWFQNRRMKWKK-$CONH_2$ |
| hLF peptide | Fluo-KCFQWQRNMRKVRGPPVSCIKR-$CONH_2$ |
| M1 | Fluo-KCFQWQRNMRKVRGPPVSC-$CONH_2$ |
| M2 | Fluo-KSFQWQRNMRKVRGPPVSSIKR-$CONH_2$ |
| M3 | Fluo-KCFQWQRNMRKVR-$CONH_2$ |
| M4 | Fluo-FQWQRNMRKVRGPPVS-$CONH_2$ |
| M5 | Fluo-QRNMRKVRGPPVSCIKR-$CONH_2$ |
| M6 | Fluo-QRNMRKVR-$CONH_2$ |
| biotinylated hLF peptide | Biotin-Ahx-KCFQWQRNMRKVRGPPVSCIKR-$CONH_2$ |

## 5.3.3. Peptide modification

For intramolecular disulfide bond formation, peptides were oxidized by introducing pure oxygen into the peptide solution followed by an incubation at 37°C for 2 h. For reduction of the disulfide bond 10 mM DTT was added and the peptide solution was then incubated for 2 h at 37°C. Biotinylated hLF peptides (200 μM) were bound to Streptavidin-AlexaFluor488 conjugates (50 μM) (Invitrogen) by incubation at 4°C for 12 h in PBS. For the analysis of cellular uptake the solution was diluted 1:10 with medium.

## 5.3.4. Flow cytometry

HeLa cells were incubated with medium containing peptides at the indicated concentrations for 45 min at 37°C. After incubation, cells were washed with medium, detached by trypsinization for 5 min, suspended in PBS and measured immediately by flow cytometry (BD FACSCalibur System, Becton Dickinson, Heidelberg, Germany). In each case, the fluorescence of 10,000 viable cells was acquired. Viable cells were gated based on sideward and forward scatter.

## 5.3.5. Confocal laser scanning microscopy

Confocal laser scanning microscopy was performed on an inverted LSM510 laser scanning microscope (Carl Zeiss, Göttingen, Germany) using a Plan-Apochromat 63 x 1.4 N.A. Oil DIC lens and a TCS SP5 confocal laser scanning microscope (Leica Microsystems, Mannheim, Germany) equipped with an HCX PL APO 63 x N.A. 1.2 water immersion lens. All measurements of peptide uptake were performed with living cells.

## 5.3.6. Incubation with inhibitor

Cells were treated with rottlerin (20 μM) for 30 min at 37°C. Then, the medium was removed and medium containing peptide as well as the inhibitor was added. After 30 min incubation at 37°C cells were washed twice with medium and analyzed by confocal laser scanning microscopy or flow cytometry.

## 5.3.7. Immunofluorescence

HeLa cells were seeded at a density of 1.5 x $10^4$/well in 8-well chambered covered glasses and cultivated to 75 % confluency, after which they were incubated with medium containing 33 mIU/ml of heparinases I, 8 mIU/ml of heparinase II and 5 mIU/ml of heparinase III for 1 h at 37°C. Then the cells were washed with ice-cold HBS/BSA/glucose (10 mM HEPES, 135 mM NaCl, 5 mM KCl, 1 mM $MgCl_2$, 1.8 mM $CaCl_2$, pH 7.4 containing 0.1 % (w/v) BSA and 5 mM glucose) and incubated with the anti-HS antibody HS4C3 on ice. After 1.5 h of incubation cells were washed with ice-cold HBS/BSA/glucose. To visualize bound antibodies the cells were incubated for 1 h with an anti-VSV antibody (P5D4)/Zenon Alexa Fluor 647 conjugate on ice. The antibody staining was analyzed by confocal laser scanning microscopy.

## 5.3.8. MTT assay

HeLa cells were seeded in 96-well microtiter plates (1.5 x $10^4$/well) and cultivated over night. The next day, cells were incubated with peptides for 6 h or 24 h at 37°C. Cell viability was measured using the colorimetric MTT dye. Cells were incubated with MTT at a concentration of 1 mg/ml for 4 h. The formazan product was solubilized with SDS (10% (w/v) in 10 mM HCl). Cell viability was determined by measuring the absorbance of each sample relative to a control not treated with peptide at 570 nm using a microplate reader (Molecular Devices SpectraMax 340, GMI, USA).

## 5.3.9. Preparation of CD samples

The hLF peptide was dissolved in phosphate buffer to a concentration of 0.1 mM. Reduction of the disulfide bonds was obtained by the addition of a 30-fold molar excess of TCEP and a subsequent incubation for 2 h at 37°C. Oxidation of the hLF-peptide was obtained by purging of pure oxygen for 15 min and a subsequent incubation for 2 h at 37°C. The DMPC and DMPG lipids were dissolved in 50 % chloroform / 50 % methanol (v/v) in order to prepare lipid stock solutions. Aliquots of these stock solutions were mixed to obtain the DMPC:DMPG mixture (molar ratio 3:1). Subsequently, the organic solvents were removed under a gentle stream of nitrogen followed by overnight vacuum evaporation to remove the residual solvent from the respective DMPC or DMPC/DMPG lipid films that had been formed in the vial. The

lipid layers were dispersed by the addition of phosphate buffer, vigorous vortexing (10 x 1 min) and homogenization by ten freeze-thaw cycles. Finally, large unilamellar vesicles (LUVs) were prepared by means of 11 extrusion cycles using an Avanti mini extruder equipped with a 100 nm polycarbonate filter. Here, the temperature was maintained above 40°C by thermostatting the extruder block at 50°C.

For preparation of the final CD samples aliquots of the oxidized and reduced hLF peptide solutions were added to aliquots of the respective buffers, micellar solutions or lipid dispersions. The final peptide concentration in all samples was 17.5 µM, the SDS and DPC concentration in the micellar solutions 10 mM (peptide-to-detergent ratio 1:570) and the lipid concentration in the vesicle dispersions 1.45 mM (peptide-to-lipid ratio 1:80).

## 5.3.10. CD and UV spectroscopy

CD spectra of the reduced and oxidized hLF peptide in phosphate buffer and in membrane-mimicking environments such as 50 % TFE / 50 % phosphate buffer solution, SDS and DPC micellar solution and in DMPC or DMPG/DMPC vesicle dispersions were recorded on a J-815 spectropolarimeter (JASCO, Groß-Umstadt, Germany) equipped with 1 mm-Suprasil quartz glass cells (Hellma, Müllheim, Germany). The samples were measured at a scan-rate of 10 nm x min$^{-1}$ and a 1 nm bandwidth in 0.1 nm intervals between 260 and 185 nm at 20°C for the buffer and micellar solutions and at 30°C for the vesicle suspensions, i.e. above the phase transition temperature of the lipids contained in the vesicle suspensions. Three repeat scans were averaged for each sample. CD spectra were smoothened by the adaptive smoothing of the Jasco Spectra Analysis software and the secondary structure was analyzed by the CONTINLL program with the implemented ridge regression algorithm (Provencher and Glockner, 1981; van, I *et al.*, 1990) that is provided by the DICHROWEB server (Lobley *et al.*, 2002; Whitmore and Wallace, 2004). The quality of the fit between experimental and back-calculated spectrum corresponding to the derived secondary structure element fractions was assessed from the normalized root mean square deviation (NRMSD), with a value < 0.1 considered as a good fit (Whitmore and Wallace, 2004). For calculation of the mean residue ellipticities used for the secondary structure estimation, the results were normalized to the UV absorbance at 280 nm assuming a molar extinction coefficient of 5625 l x mol$^{-1}$ x cm$^{-1}$ for the protein with oxidized Cys residues and 5500 l x mol$^{-1}$ x cm$^{-1}$ for reduced Cys residues (Pace *et al.*, 1995). The absorption spectrum in the range of the aromatic bands due to tryptophan (and cystine for the oxidized peptide) was recorded in the range from 240–340 nm using a quartz glass half-micro-cuvette with 1 cm optical path length

(Hellma, Müllheim, Germany). For correction of the scattering, the baseline of a log absorbance against log wavelength from the non-absorbing region between 310 and 340 nm was extrapolated towards lower wavelengths and subtracted from the measured spectrum to get the final spectrum (Kelly *et al.*, 2005).

## 5.3.11. NMR

All NMR samples were prepared using a Shigemi NMR tube dissolving 0.83 mg of hLF in 300 $\mu$L 95:5 (v:v) $H_2O$ buffer/$D_2O$. Two-dimensional ROESY and NOESY experiments employing a WATERGATE solvent suppression scheme were performed at 10°C or 20°C on a Varian Inova 600 MHz spectrometer equipped with a 5 mm triple-resonance three-axis gradient probe using a 200 ms ROE or NOE mixing period. The spectra were recorded as 2048 x 512 hypercomplex points with 9009.1 x 8000 Hz spectral widths for the F2 and F1 dimensions, respectively. Spectra were transformed using the nmrPipe processing package.

## 5.3.12. Surface plasmon resonance binding experiments

The surface plasmon resonance experiments were conducted as described previously (Ram *et al.*, 2008). The reducing ends of 6 kDa HS were biotinylated by preactivated biotin-LC-hydrazide (Pierce). The biotinylation procedure was verified by streptavidin-peroxidase labeling after blotting of the material onto zetaprobe membrane. CM4 flow cell Biacore sensorchips were activated with 50 $\mu$L of 0.2 M N-ethyl-N'-(diethylaminopropyl)-carbodiimide and 0.05 M N-hydroxysuccinimide before injection of 50 $\mu$L of streptavidin (0.2 mg/ml in 10 mM acetate buffer, pH 4.2). The remaining activated groups were blocked with 50 $\mu$L ethanolamine 1 M, pH 8.5. Typically, this procedure permitted the coupling of approximately 3.000–3.500 resonance units (RU) of streptavidin. Subsequently, the biotinylated HS (10 $\mu$g/ml) molecules were immobilized by injection over a one-surface flow cell leading to an immobilization level of approximately 50 RU. The flow cells were then conditioned with several injections of 2 M NaCl. Untreated one-flow cells served as negative control. Binding assays were conducted with different concentrations of oxidized and reduced hLF in HBS-P and at 25°C and a flow rate of 20 $\mu$L/min. Regeneration of the sensorchip surface was achieved by a 5 min pulse of 2 M NaCl in HBS-P buffer.

## 5.4. Results

## 5.4.1. Cellular uptake of the human lactoferrin-derived peptide

For the use of peptides in biomedicine there are grave concerns of potential immunogenicity. This is especially the case, when peptides are conjugated to larger molecular weight proteins. Given recent observations that certain antimicrobial peptides may act as cell-penetrating peptides, we selected a peptide corresponding to amino acids 38 to 59 from human lactoferrin as a potential candidate for a new CPP derived from a human protein. This peptide was shown previously to possess antimicrobial activity (Groenink *et al.*, 1999). The peptide comprises an exposed loop of the lactoferrin protein that is terminally flanked by cysteine residues. These cysteine residues form a disulfide bridge, both in the protein and in lactoferricin, a naturally occurring degradation product of lactoferrin. In our peptide, at the N-terminal side of the first cysteine residue, a lysine residue of the lactoferrin sequence was preserved. Similarly, a lysine and an arginine residue from the lactoferrin sequence were included at the C-terminus of the second cysteine residue. Given the requirement for positive charge to promote cellular uptake, we reasoned that these three residues should promote the function of the peptide as a CPP.

The peptide was synthesized as a peptide amide labeled with carboxyfluorescein at its N-terminus. In order to apply stringent criteria for classifying this peptide as a potential new CPP, uptake was compared with the uptake of fluorescein-labeled analogs of the well-established CPPs penetratin and R9. Hela cells were incubated with these peptides at concentrations ranging from 5 to 20 $\mu$M and uptake quantified in living cells by flow cytometry. Trypsinization of cells, required to detach the cells from the tissue culture plate prior to flow cytometry, was used to remove peptides merely adsorbed to the outer plasma membrane.
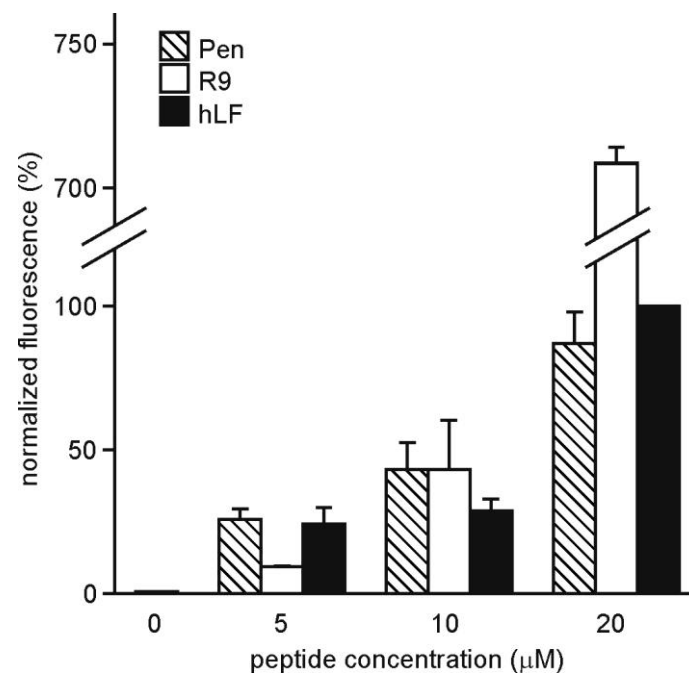
**Fig. 5.1.** Concentration dependence of uptake. HeLa-cells were incubated with increasing concentrations of the indicated peptides for 45 min. Afterwards the cells were washed with cold PBS and harvested with trypsin/EDTA. Uptake into cells was analyzed by flow cytometry. Independent experiments were normalized to the median fluorescence for 20 $\mu$M hLF.
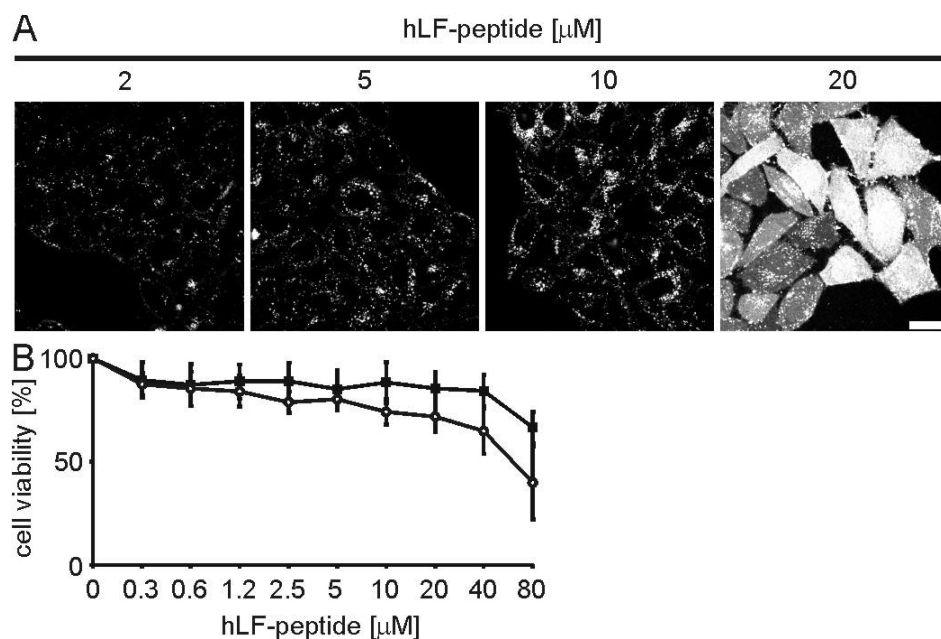


**Fig. 5.2.** Concentration-dependent phenotypes for the cellular uptake of the hLF peptide and toxicity. (A) HeLa cells were incubated for 30 min with different concentrations of the peptide. After two washing steps the cellular peptide uptake was analyzed by confocal laser scanning microscopy. The scale bar indicates 20 $\mu$m. (B) HeLa cells were incubated with increasing concentrations of the hLF peptide for 6 h (squares) or 24 h (circles) and subsequently cell viability was determined using the MTT assay.

All three peptides were taken up in a concentration-dependent manner and no saturation of uptake was observed (Fig. 5.1). For penetratin, the cellular import was proportional to the concentration of peptide present in the medium. R9 uptake increased strongly at 20 $\mu$M which very likely reflects the efficient cytoplasmic uptake via localized areas of the plasma membrane that we have called nucleation zones (NZ) (Duchardt *et al.*, 2007). Uptake of the hLF peptide also showed a clear concentration dependence. From 10 to 20 $\mu$M, the relative increase in uptake was notably stronger than from 5 to 10 $\mu$M.

## 5.4.2. Intracellular distribution of the hLF peptide

Given our recent observation of a rapid cytoplasmic delivery of certain CPPs at higher concentrations, we were particularly interested to investigate the concentration dependence of the intracellular distribution of the hLF-peptide. The intracellular localization of the peptide in living cells was investigated by confocal microscopy. For concentrations up to 10 $\mu$M the peptide was predominantly localized in vesicles (Fig. 5.2.A). In contrast, at a concentration of 20 $\mu$M, next to a vesicular staining, nearly all cells showed a homogeneous cytoplasmic and nuclear peptide distribution. This concentration dependence of the intracellular distribution very much ressembled our former observation for the R9 and Tat peptides (Duchardt *et al.*, 2007) of a cytoplasmic entry via NZ. In order to further establish that entry of the hLF-peptide occurred via the same process, we followed the uptake by time-lapse confocal fluorescence microscopy. This experiment confirmed the induction of NZ as the basis for rapid entry (not shown). We previously showed that for arginine-rich peptides this rapid entry is neither associated with membrane damage nor with cytotoxicity. To exclude also for the hLF-peptide that the cytoplasmic delivery results in cell death HeLa cells were incubated with peptide for 6 h and 24 h and cell viability was assessed by the MTT assay. After 6 h of incubation the cells were viable at peptide concentrations up to 40 $\mu$M, whereas viability was reduced by 25 % for cells incubated for 24 h at a peptide concentration of 10 $\mu$M.

## 5.4.3. Structure-activity relationship of the hLF-peptide for efficient uptake

After testing the uptake properties and intracellular distribution, we were interested in defining the structure-activity-relationship of the hLF peptide for efficient cellular uptake. With 22 amino acids, the hLF peptide is a CPP of intermediate length. Four of the seven cationic amino acids and the aromatic amino acids are localized in the sequence nested between the cysteine residues. Positively charged and aromatic residues are typically associated with CPP activity. In the full-length protein, the cysteine residues form a disulfide bridge that constrains the domain into a loop conformation (Peterson *et al.*, 2000).

First, we wondered whether a shorter peptide would also show efficient import (Table 1). Removal of the three C-terminal residues following the cysteine residue was tolerated (5.3.A). In contrast, as soon as a cysteine residue was omitted, import efficiency was reduced dramatically. This result suggested a structural requirement for the formation of the disulfide bridge for obtaining efficient import. We therefore also tested a peptide, in which the cysteine residues were exchanged for serine residues. Again import of the resulting analog was reduced drastically. This finding further demonstrates that efficient uptake can be attributed to the capacity of the cysteines to form a disulfide bridge. Formation of the disulfide bridge was analytically confirmed by mass spectrometry (see below). We validated the result by confocal microscopy comparing the uptake of hLF and the C/S hLF mutant (M2) (Fig. 5.3.B). For the mutant peptide the intracellular distribution was strictly vesicular. Also at higher concentrations, the cytoplasmic import could not be observed, demonstrating that this import is a function of the disulfide bridge. To test whether the number of positive charges of the side chains was involved or whether additional sequence-specific elements were involved in the uptake, the uptake of hLF was compared with a rat-derived lactoferrin peptide containing 6 positively charged amino acids, versus 7 for the hLF peptide. The rLF also contains a disulfide bridge. The uptake efficiency was greatly reduced for rLF compared to hLF (Fig. 5.4), suggesting that the specific sequence of hLF is important for uptake.
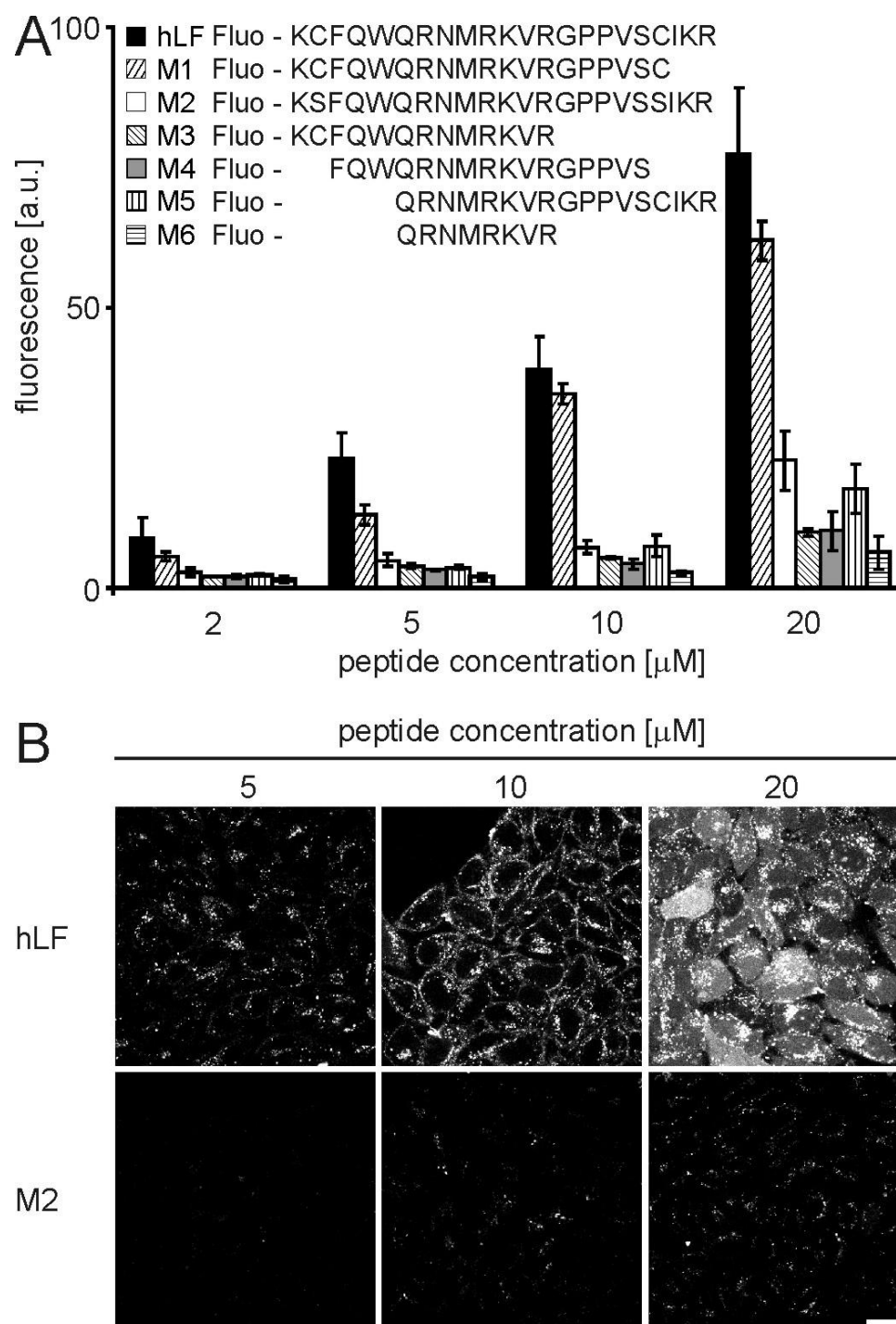
**Fig. 5.3.** Structure-activity relationship of hLF. (A) HeLa-cells were incubated with increasing concentrations of the indicated peptides for 30 min. Afterwards the cells were washed and harvested with trypsin/EDTA. Uptake into cells was quantitated by flow cytometry. (B) HeLa-cells were incubated with increasing concentrations of the indicated peptides for 30 min, washed and analyzed by confocal laser scanning microscopy. The scale bars indicate 20 μm.
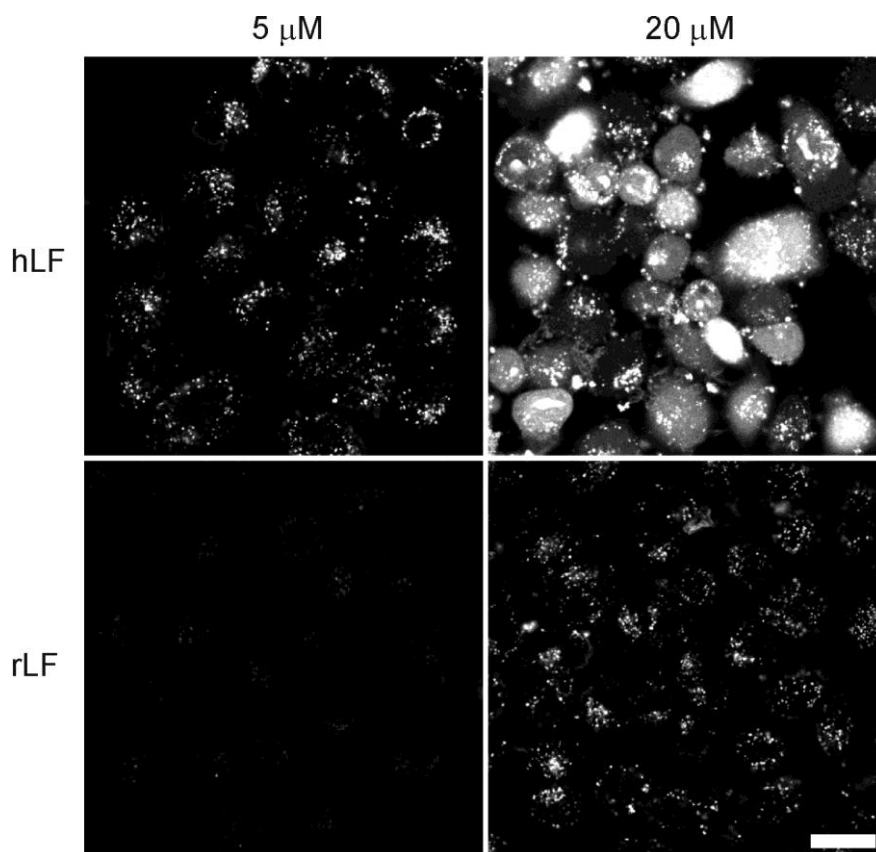
**Fig. 5.4.** Comparison of the uptake of human (h) and rat (r)-derived LF peptides. HeLa cells were incubated with 5 and 20 μM hLF or rLF for 60 min at 37°C in RPMI supplemented with 10% fetal calf serum. Cells were washed twice and imaged immediately using confocal microscopy. The scale bar indicates 20 μm.

## 5.4.4. Structural analyses

The cellular uptake experiments provided strong functional evidence for the requirement of cyclization for the efficient cellular import of the hLF-peptide. Therefore, we next addressed explicitly the structure of the peptide and how this structure depended on the presence of the disulfide bridge. The hLF-peptide comprises the loop and one disulfide bridge of human lactoferricin which at pH 4 forms a nascent helix (Hunter *et al.*, 2005). Formation of the disulfide bridge upon oxidation was confirmed by mass spectrometry (Fig. 5.5.A-B).

First, we addressed conformational differences of the reduced and oxidized, cyclic form of the peptide using NMR. The spectra showed relatively broad and ill-defined peaks and only limited ROE cross peak patterns. In particular, no amide-amide ROE or NOE cross-peaks indicative of helix formation were observed and amide-$H^\alpha$ cross-peaks in the fingerprint region did not identify significantly down-field shifted $H^\alpha$ resonances indicative of extended conformation, expected for the N-terminal residues of the peptide (Fig. 5.5.C). The absence

or presence of the disulfide bridge did not result in major changes in the NMR spectral appearance. Lowering the temperature to 10°C did also not result in a substantial improvement of the spectrum. In contrast to the NOE spectra recorded previously for the longer lactoferricin peptide (Hunter *et al.*, 2005), the ROESY spectra recorded on the hLF discriminate cross-peaks resulting from the ROE with those originating from chemical exchange on the basis of their sign. Interestingly, clear exchange cross-peaks were observed in the aromatic/amide region as well as in the aliphatic region of the spectrum (Fig. 5.5.D-E). Dissolving the peptide in the solvent mixture $H_2O:CD_3OD:CDCl_3$ (1:4:4, w/w/w) as previously employed (Hunter *et al.*, 2005), did not radically change the spectral appearance, although an increase in spectral dispersion was observed and weak, upfield shifted $H^\alpha$ resonances as well as downfield shifted methyl resonances suggested the formation of an extended structure (not shown). However, relatively broad lines were again observed in conjunction with a lack of cross-peaks in the fingerprint region and amide region. It is noteworthy that under all conditions the single, easily identifiable Trp42 (peptide: Trp5) sidechain N1-proton shows as much as four different resonances of varying intensities. Overall, the NMR data suggest a potentially oligomeric, (partially) folded state, subject to conformational exchange.

Having failed to observe an oxidation-dependent conformational difference in an aqueous buffer, we next employed CD spectroscopy for obtaining information about the secondary structure in membrane mimicking environments and in buffers containing micelles or vesicles. Consistent with the NMR analysis, in aqueous buffer, reduction of the disulfide bridge by incubation with DTT had no effect on the shape of the CD spectrum in a temperature range of 5°C to 20°C (not shown). The CD spectra could not be described by a linear combination of CD spectra for classical secondary structure elements, i.e. $\alpha$-helix, $\beta$-sheet and random coil. However, the spectrum was also distinct from the one to be expected for purely random coil. Addition of 50 % TFE led to the formation of an $\alpha$-helix in the reduced and oxidized states of the peptide.

In contrast, both forms showed different spectra in solutions containing detergent or lipid. SDS increased the $\beta$-sheet content in the reduced form, only, DPC increased the content in the reduced and in the oxidized form. In contrast, for DMPC and DMPC/DMPG, the $\beta$-sheet content increased only for the oxidized form, with DMPC/DMPG inducing the most pronounced changes (Fig. 5.5.F-I). The latter results demonstrate that oxidation affects the capacity of the peptide to undergo conformational changes.
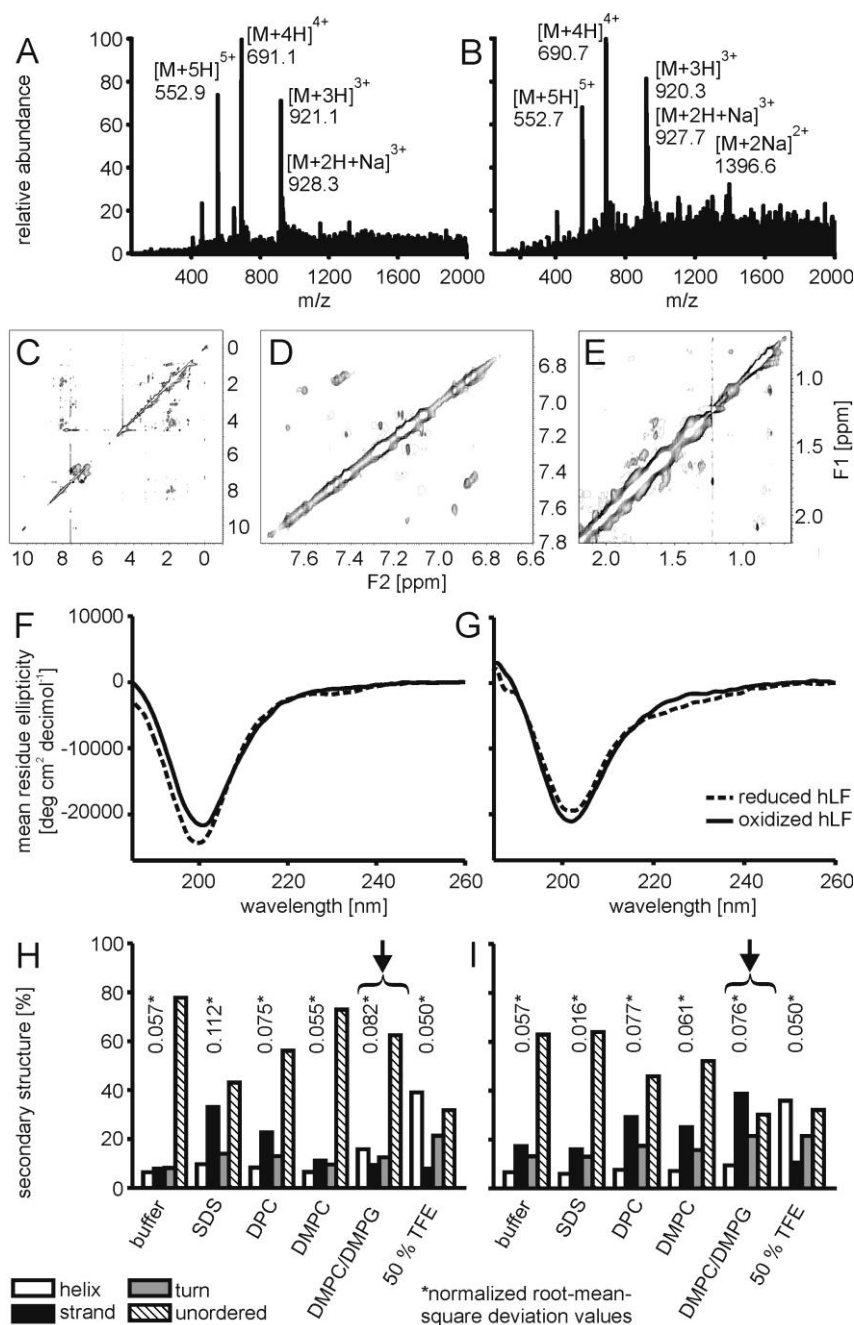
**Fig. 5.5.** Structural analyses at micellar membranes. (A, B) Electro spray mass spectrometry spectra depict the multiple-charged species of the reduced (A) and oxidized (B) form of the hLF peptide identifying a m/z shift of +2 Da upon reduction of the peptide. (C) NOESY spectrum of 1 mM hLF in H$_2$O solution. Up-field (D) and aliphatic (E) regions of the ROESY spectrum of hLF in H$_2$O solution. Cross-peaks with negative intensity (corresponding to ROE peaks) are shown as single contours, whereas cross peaks with positive sign (corresponding to the diagonal and exchange peaks) are shown with multiple, exponentially spaced contours. (F, G) CD spectroscopy in an aqueous phosphate buffer (F) and phosphate buffer containing DMPC/DMPG 3:1 vesicles (G). (H,I) Data analysis via the CONTINLL algorithm of the reduced peptide (H) and the oxidized hLF peptide (I). Especially at the surface of DMPC/DMPG 3:1 vesicles (highlighted by the arrows) β-strand formation was induced for the oxidized form of the peptide.

## 5.4.5. Binding of the hLF peptide and hLF C/S to heparan sulfate proteoglycans

Heparan sulfate proteoglycans (HSPGs) have been reported to contribute to the uptake of several CPPs (Poon and Gariepy, 2007; Tyagi *et al.*, 2001). Therefore, these sugars could also contribute to the dependence of uptake on the presence of the disulfide bridge. The difference between the oxidized and reduced hLF was observed using a SPR based binding assay, a more physiologically relevant system in which low amount of HS is coupled through its reducing end to a sensorchip, thus better representing HSPG presentation at the cell surface. Injection of reduced hLF over this surface, in the 250 – 3000 nM range, gave binding curves plateauing at 25 to 75 resonance units (RU), while the oxidized form of the peptide gave binding curves plateauing at 48 to 156 RU (Fig. 5.6). From the binding curves of the oxidized peptide a Kd value of 2 $\mu$M was obtained. In a similar set of experiments in which binding of the fluorescein-labeled hLF was compared to binding of the fluorescein-labeled C/S mutant, a Kd value of 10 $\mu$M was obtained for the wild-type hLF while no binding could be detected for the mutant peptide (not shown). These results validate the specificity of binding of the hLF peptide for HS. The residual binding obtained for the reduced peptide may be due to incomplete reduction.
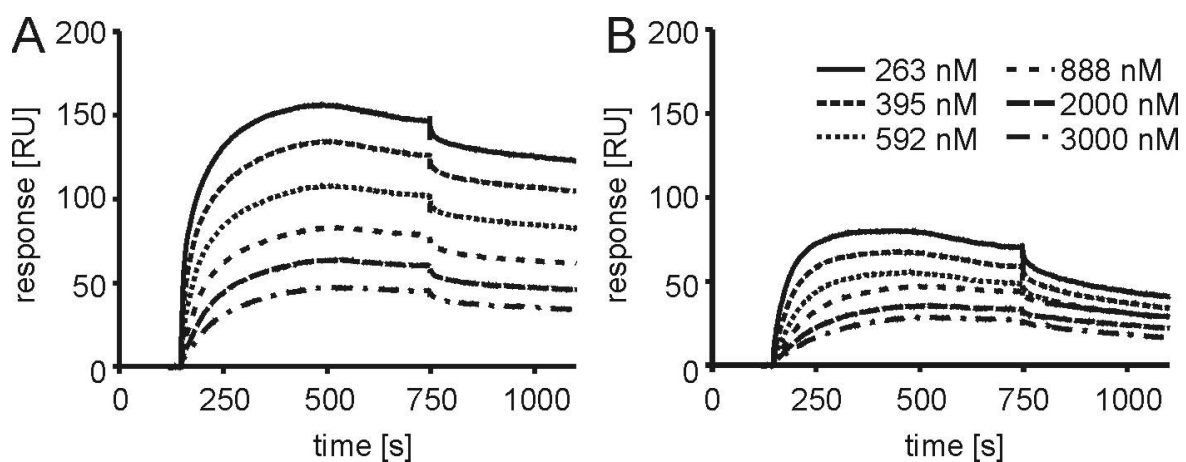


**Fig. 5.6.** Affinity measurements of (A) oxidized and (B) reduced hLF for HS-coated surfaces using SPR.

## 5.4.6. HSPG-dependence and rottlerin sensitivity of the uptake

Having observed a strong conformational dependence of the binding of the hLF-peptide to HS using biochemical assays, we next addressed the relevance of this interaction for the binding to cells. Removal of HS chains after a one-hour treatment with heparinases I-III nearly abolished the binding of the hLF peptide to the cell surface and reduced the number and intensity of vesicles (Fig. 5.7.A).

Furthermore we tested the effect of rottlerin on the cytoplasmic uptake of the oxidized hLF-peptide. Rottlerin has been described originally as a PKC inhibitor with strongest activity towards the PKC-$\delta$ isoform (Gschwendt *et al.*, 1994). However, the specificity was questioned later (Davies *et al.*, 2000). Previously, we showed that this drug acts as an effective inhibitor of cellular peptide uptake via nucleation zones (Duchardt *et al.*, 2007). Cells were preincubated with rottlerin and peptide uptake was analyzed by flow-cytometry and fluorescence microscopy (Fig. 5.7.B-C). At low peptide concentrations, at which only vesicular uptake occurred, rottlerin reduced uptake only weakly. At peptide concentrations at which uptake via NZ occurred, peptide uptake was inhibited by up to 50 %. Confocal microscopy confirmed that rottlerin only inhibits the efficient cytoplasmic peptide uptake. The concentration-dependent increase in cell-associated fluorescence observed in the presence of rottlerin (Fig. 5.7.B) may therefore be attributed to the vesicular peptide uptake which is not affected by rottlerin.
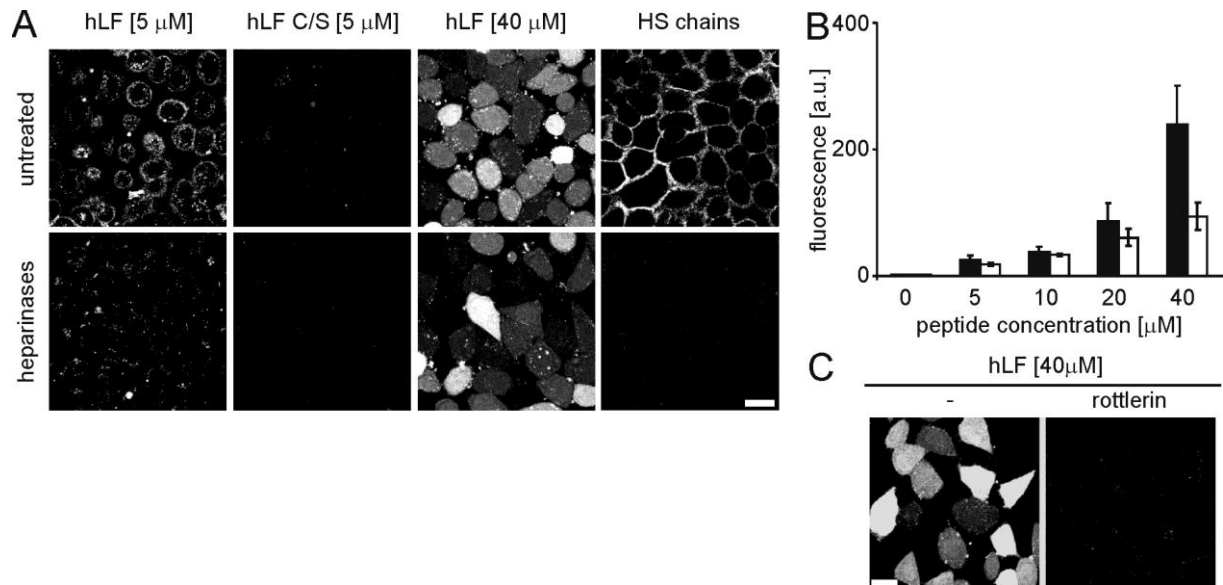
**Fig. 5.7.** Cytoplasmic import of hLF is HS proteoglycan-dependent and negatively affected by rottlerin. (A) HeLa cells were treated for 1 h with heparinases I, II and III (33, 8 and 5 mIU/ml, respectively) or remained untreated. Subsequently, the cells were washed and incubated with different concentrations of the hLF peptide. Images were taken after 30 min of peptide incubation. Removal of HS chains from the cell surface was confirmed by immunofluorescence staining of treated and untreated cells. (B, C) HeLa cells were treated with 20 μM rottlerin for 30 min or remained untreated. After one washing step the cells were incubated with different concentrations of hLF in the presence (white bars) or absence of rottlerin (black bars). After 30 min of incubation the cells were analyzed by flow cytometry or confocal laser scanning microscopy. The scale bars indicates 20 μm.

## 5.4.7. hLF-mediated import of protein cargos

The ability to mediate cellular uptake of a diverse set of cargos is an important characteristic for a CPP to be valuable for applications in biological and biomedical research. As such, the fluorophore could already be considered a cargo since it may affect the cellular trafficking of a CPP (Dupont *et al.*, 2007). Therefore, our data suggest that lactoferrin is well suited for the efficient cellular import of small molecules that otherwise cross the plasma membrane only poorly. In addition, we tested whether the hLF peptide was able to mediate import of a large molecular weight protein cargo. For these complexes, potential immunogenicity of the CPP is an important concern. Therefore, using a human protein-derived peptide is of particular importance. To this end, a biotinylated hLF was synthesized and coupled to Alexa488-labeled streptavidin in a molar ratio of 4:1 (peptide:streptavidin). Import of these conjugates into HeLa cells was visualized by confocal fluorescence microscopy (Fig. 5.8). Streptavidin-Alexa488 was internalized into vesicular compartments, in accordance with observations for high molecular weight complexes of other CPPs (Tunnemann *et al.*, 2006). This uptake occurred only when the protein was conjugated to biotinylated hLF peptide. Neither the protein alone nor the protein in the presence of non-biotinylated hLF peptide was taken up.
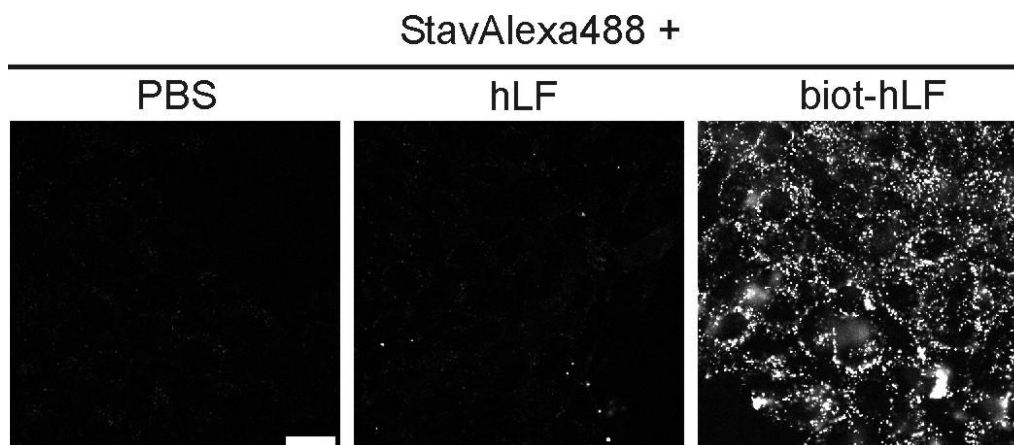


**Fig. 5.8.** Biotinylated hLF peptide efficiently transports streptavidin-Alexa488 into cells. HeLa cells were incubated for 30 min with 5 μM of the biotinylated hLF-streptavidin-Alexa488 complex. After two washing steps the cellular uptake was analyzed by confocal laser scanning microscopy. Coincubation of streptavidin with PBS and non-biotinylated hLF peptide served as controls. The scale bar indicates 20 μm.

## 5.5. Conclusions

The results shown in this chapter present a new cell-penetrating peptide corresponding to amino acids 38 to 59 of human lactoferrin (amino acids 19-40 of human lactoferricin). With 22 amino acids, the hLF peptide is a CPP of intermediate length. Nevertheless, repeated batches of peptide obtained by solid-phase peptide synthesis following standard procedures showed typical purities of the N-terminally labeled peptide of about 80 %.

In contrast to shorter ones, oligoarginine peptides of more than eight amino acids in length, enter cells more efficiently and show a concentration-dependent uptake mechanism into the cytoplasm (Kosuge *et al.*, 2008). Even though the hLF peptide contains less arginine residues compared to the Tat peptide or R9, a concentration-dependent uptake mechanism was also observed. At concentrations above 10 μM, the peptide rapidly enters the cytoplasm. The sensitivity of this uptake to rottlerin treatment of cells suggests that this mechanism is the same that was observed for R9 and the Tat-peptide. Thus far, the rottlerin-sensitive uptake mechanism was only observed for arginine-rich CPPs. Our observations on the conformation-dependent uptake of the hLF-peptide suggest that the particular structure of this peptide may functionally replace a high arginine content for this mechanism of cell entry.

The sequence nested within the two cysteine residues is reminiscent of cationic amphipathic CPPs such as penetratin. However, removal of the disulfide bridge, either by reduction of cysteine residues (not shown) or by replacement by serine residues strongly reduced the capacity of the peptide to enter cells. To our knowledge, this is the first report of a cell-penetrating peptide that requires a cyclic structure for its activity. However, numerous antimicrobial peptides have been investigated to this aim, though with differing results, such as gramicidin S (Wadhwani *et al.*, 2006), (protegrin-1 (Buffy *et al.*, 2003), (RTD-1 (Selsted, 2004), renatuerin-1 (Sonnevend *et al.*, 2004), bactenecin (Wu and Hancock, 1999) and tachyplesin-1 (Matsuzaki *et al.*, 1997; Ramamoorthy *et al.*, 2006; Doherty *et al.*, 2008). In the latter case, aggregation was found to be the de-activating factor, which is being prevented by proper cyclization.

The dependence of the efficient import on a disulfide bridge is not predicted by our current knowledge on CPPs. A prediction identified the central QWQRNMRKVR motif as essential for the CPP activity (Hällbrink *et al.*, 2005). The terminal residues in the cysteine-containing wild-type peptide as well as the serine-containing mutant analog were not predicted to influence the uptake significantly (M. Hällbrink, personal communication). This consideration indicates that for the hLF peptide, a simple examination of the primary structure fails to predict the structural determinants required for efficient cell entry of the peptide.

In the crystal structure of human lactoferrin (Sun *et al.*, 1999), the residues corresponding to hLF are part of an $\alpha-\beta-\alpha$ motif that is stabilized by the formation of a disulfide bridge between $Cys^{39}$ and $Cys^{56}$ (positions 2 and 19 in the peptide) and hydrophobic interactions that involve $Trp^{42}$ andVal$^{54}$ (positions 5 and 17 in the peptide) and $Met^{46}$ and $Pro^{52}$ (positions 9 and 15 in the peptide). For the human lactoferricin peptide NMR data indicate that the amino acid residues corresponding to the hLF peptide adopt a 'nascent' helical structure in aqueous solutions and a conformation resembling the crystal structure in membrane-mimicking solvent. Our data clearly show the necessity of the presence of the $Cys^{39}$-$Cys^{56}$ (peptide: 2, 19) disulfide bridge for efficient import. However, in solution, neither CD nor NMR spectra were significantly affected by disulfide formation. Whereas the CD data indicate a non-random coil conformation of hLF, the NMR data also point to conformational exchange. It is tempting to speculate that $Trp^{42}$ (position 5 in the peptide) is a crucial factor affecting the NMR spectra because of its essential structural role and the putative large changes in shielding effects it could exert. Other dynamic effects such as dimer formation could similarly affect the NMR spectra and such a phenomenon was postulated for the longer human lactoferricin peptide in aqueous solvent (Hunter *et al.*, 2005).

Therefore, CD spectra were also recorded in the presence of phospholipid micelles in order to get further insights into the structural impact of lipid surfaces on the peptide. Here, the oxidized peptide showed a clear preference for $\beta$-strand formation, whereas the reduced peptide presented no defined secondary structure. Interestingly, the differences in secondary structure formation of the oxidized and reduced hLF peptide were most pronounced in the presence of DMPC/DMPG vesicles, which ensure strong electrostatic attraction of the peptide and are also a good mimic of the cellular membrane environment.

Additionally, the interaction with heparan sulfate chains was investigated by means of fast protein liquid chromatography, surface plasmon resonance and in cellular assays. SPR experiments showed that the interaction with HS is enhanced significantly upon oxidation of the peptide. Cellular assays show the physiological relevance of the different HS-peptide interactions. In cell experiments we made an interesting additional observation concerning the involvement of HSPG in NZ-dependent cytoplasmic uptake. Consistent with our previous results, heparinase treatment over 6 h abolished the rapid cytoplasmic uptake of hLF (not shown). In contrast, short-term treatment over only 1 h had no significant effect on NZ-dependent import. However, membrane binding of hLF at lower peptide concentrations was strongly reduced. We therefore conclude that the previously observed effect of long-term heparinase treatment on NZ-dependent uptake is due to perturbations of membrane protein organization or molecular events involved in this cytoplasmic uptake.

Given that the cell uptake experiments did not show any concentration dependent saturation, the lactoferrin-derived CPP exhibited one of the most prominent characteristics for the

uptake of CPPs. For the full length lactoferrin protein, cellular uptake has been described for various cellular systems. While it has been observed that the polycationic nature of the N-terminus confers by itself an interaction with sugars on the cell surface, cellular uptake and the biological effects of lactoferrin have been attributed to the binding to one of the several receptors identified for this protein (Suzuki *et al.*, 2005). In contrast to our peptide, binding to these receptors was therefore saturable. Very remarkably, for binding to the lymphocyte lactoferrin receptor and the platelet lactoferrin receptor, evidence for an involvement of the loop domain corresponding to the lactoferrin-derived CPP was obtained (Legrand *et al.*, 1992; Leveugle *et al.*, 1993). Competition experiments with our peptide for binding of lactoferrin may thus help to better define ligand binding domains for other types of lactoferrin receptors.

In summary, the results show that the hLF peptide is a new CPP with highly interesting structural and functional characteristics. With respect to the mechanism of import, we expect that further analyses of the structure-activity relationship will yield new insights into the molecular determinants of the cell surface that mediate the molecular interaction and induce the efficient cellular import via nucleation zones. Furthermore, it will be interesting to compare analogous peptides derived from lactoferrin of different species. In the past, the antimicrobial characteristics of bovine lactoferrin-derived peptides have been compared in detail to the ones of their human counterparts (Gifford *et al.*, 2005). Due to its human origin the hLF peptide is expected to be non-immunogenic. For this reason, this molecule is a candidate as a vector for biomedical applications, especially for the import of high molecular weight complexes.

# 6. Analysis of the intracellular pharmacokinetics and pharmacodynamics of small molecule anti-cancer drugs

The FCS measurements described in this chapter were performed by Heike Glauner and Ben Steemers. The author of this thesis performed the analysis of the data, developed, synthesized and tested the doubly-labeled FCCS standard (Fig. 6.1.B) and labeled the compound MTX-Cy5. Dr. Frank Becker, Dr. Stefan Hannus and Kerrin Hansen provided the transfected Hek293 cells, the DNA vectors and the labeled compounds PD-Cy5 and Pur-Cy5. Heike Glauner established a HeLa-TRex cell line expressing DHFR-GFP. Yi-Da Chung determined the size of the exact detection volume by microbeads and performed the gel electrophoresis depicted in Fig. 6.1.A.

## 6.1. Summary

In drug development there is great awareness that *in vitro* assays that determine activities of drug candidates with isolated targets, have only limited predictive value for activities in cellular assays. Poor membrane permeability and off-target binding are major reasons for lack of activity. However, possibilities to directly analyze these processes on a subcellular level are still very limited. To this end, the well-established dihydrofolate reductase inhibitor methotrexate and the kinase inhibitors Parke-Davis compound PD173956 and purvanolol B were conjugated via polyethyleneglycol linkers with the indocyanine fluorophore Cy5. Labeling did not affect the activity of these drugs towards their targets. The cellular uptake and subcellular distribution of these compounds in single human cancer cells was investigated by confocal laser scanning microscopy. In addition, molecular interactions inside the cell with the respective target proteins were investigated in the nanomolar range by fluorescence cross-correlation spectroscopy (FCCS) using cells stably transfected with green-fluorescent protein fusion proteins of the dihydrofolate reductase (DHFR-GFP) and Abelson kinase 1 (ABL1-GFP). Large differences in the interaction patterns were found for the investigated drugs. For methotrexate-Cy5 drug target interactions could be detected and dissociation constants determined. In contrast, PD-Cy5 strongly interacted with intracellular high-molecular weight structures. In summary, FCCS provides a powerful means to assess subcellular pharmacokinetics and -dynamics of drug candidates at nanomolar concentrations.

## 6.2. Introduction

In drug development, assays that determine the activity of a drug in intact cells are gaining significance (Perlman *et al.*, 2004; Korn and Krausz, 2007; Lang *et al.*, 2006). While providing less detailed information on the interaction of a drug candidate towards a specific molecular target, the results of such assays intrinsically provide information on off-target effects and cytotoxicity. In addition, many compounds fail to show any biological effect, even if biological activity was detected towards an isolated target molecule in an *in vitro* screen.

For compounds that exert their activity inside the cell such failure is typically attributed to poor cellular uptake. However, this assumption rather reflects a lack of knowledge of the intracellular pharmacology of a drug, rather than being based on direct evidence. This deficit is due to an absence of methods describing the interaction patterns of compounds on the subcellular level. Next to the failure to cross the plasma membrane, absence of activity may also be due to interactions with membranes, sequestration in vesicular compartments, binding to DNA in the cell nucleus and binding to cytoskeletal structures and other proteins. For example, numerous cationic amphiphilic drugs are enriched in the lysosomal compartment (Bareford and Swaan, 2007; Almela *et al.*, 2009). Great efforts have been invested to optimize the route of cellular uptake of small molecule drugs. On the one hand prodrug strategies are widely employed (Rautio *et al.*, 2008) to improve the uptake efficiency, on the other hand small molecule drugs can be conjugated to peptidic vectors (Fischer *et al.*, 2001) or high-molecular weight structures (Omelyanenko *et al.*, 1998; Duncan, 2003) in order to modify the uptake kinetics. Moreover, the subcellular localization of a drug can vary for different cell types and differences in the applied dose (Stumpf *et al.*, 2008).

In the past decades, numerous techniques have been developed to investigate the subcellular localization of small molecule drugs. Generally, high-resolution fluorescence microsocopy has become the method-of-choice for studying molecular dynamics on a subcellular level in living cells. However, only few small molecule drugs possess intrinsic fluorescence compatible with live cell microscopy. One such example is doxorubicin (de Lange *et al.*, 1992; Lankelma *et al.*, 1999). In contrast, the majority of small molecule drugs lacks such characteristics therefore requiring conjugation to fluorophores for visualization. Alternatively, the molecular localization of unlabeled proteins, peptides and small molecules in tissues can be determined by mass spectrometry imaging (Chaurand *et al.*, 2005; Goodwin *et al.*, 2008; Signor *et al.*, 2007). The major drawback of this technique is the comparably low spatial resolution. Nevertheless, with novel ion optics systems a resolution down to approximately 4 $\mu$m is reached (Luxembourg *et al.*, 2006). IR microscopy and Raman scanning techniques provide information about the localization and molecular nature

of macromolecular assemblies, but the detection is rather unspecific for particular molecules and the spatial resolution (> 1 $\mu$m) is limited as well in comparison to high-resolution microscopy (Boskey *et al.*, 1992; Lasch and Naumann, 2006; Gotter *et al.*, 2008). Microscopic autoradiography enables high spatial resolution in the subcellular localization of drugs, but requires the fixation of cells and the synthesis and manipulation of radioactively labeled drug molecules (Kawamoto, 1990; Stumpf, 2005).

The dihydrofolate reductase inhibitor methotrexate is a prominent example, that illustrates the potential of fluorescent labeling for an analysis of cellular transport and the subcellular localization of a drug molecule (Gapski *et al.*, 1975; Remy and Michnick, 2001; Kaufman *et al.*, 1978; Miller and Cornish, 2005; Miller *et al.*, 2004; Powell *et al.*, 2006). Fluorescein and TexasRed were used as fluorophores in these previous applications. However, due to spectral characteristics that overlap with the majority of fluorescent proteins used for the tagging of proteins, fluorescein- and TexasRed-labeled compounds have only limited suitability for a highly sensitive simultaneous detection of the drug and its target. For this purpose, red-fluorescent fluorophores such as Cy5 are preferable. This fluorophore has an excitation maximum around 670 nm and is spectrally well separated from green fluorophores with excitation maxima below 550 nm, enabling the simultaneous detection with proteins fused to green fluorescent protein (GFP). Especially for the highly sensitive detection of molecular interactions by fluorescence cross-correlation spectroscopy (FCCS), avoidance of fluorescence resonance energy transfer (FRET) (Clegg, 1995) is highly preferable (Weidemann *et al.*, 2002; Földes-Papp, 2005).

FCCS is an extension of fluorescence correlation spectroscopy (FCS) (Schwille *et al.*, 1997). In FCS, information on the mobility and concentration of molecules is obtained from an analysis of fluorescence fluctuations, caused by diffusion of molecules through a subfemtoliter confocal detection volume (Rigler *et al.*, 1993). With a sensitivity in the subnanomolar range, FCS has become a highly powerful tool to address molecular dynamics in cells and subcellular compartments (Brock *et al.*, 1999; Sorscher *et al.*, 1980; Brock and Jovin, 1998; Schwille *et al.*, 1999; Hink *et al.*, 2000; Wachsmuth *et al.*, 2000; Koopman *et al.*, 2007). Binding of a low-molecular weight drug candidate to a target protein slows down diffusion. Binding equilibria can be derived from the contributions of a slow and fast moving fraction to the total autocorrelation function (Meseth *et al.*, 1999). In recent years, FCS-based high-throughput methods have gained singificant importance in drug discovery (Hintersteiner and Auer, 2008).

In FCCS, concerted fluorescence fluctuations, caused by codiffusion of two spectrally well separated fluorophores are detected. For the detection of drug-target interactions two main characteristics set this method apart from FRET: First, there is no dependence of the signal on the distance of the fluorophores. Therefore, there are no constraints on the use of linker

molecules between drug and fluorophore. Second, especially for interacting molecules that are homogeneously distributed throughout a cell and at low concentrations, FCCS has a much higher sensitivity for the detection of interactions. Also for FCCS intracellular applications have been presented (Schwille *et al.*, 1999) (Schwille *et al.*, 1999; Bacia *et al.*, 2006), including the determination of binding constants of fluorescent proteins (Shi *et al.*, 2009).

Given these powerful characteristics for the detection of molecular interactions, we here employed a combination of confocal laser scanning microscopy, FCS and FCCS to investigate the subcellular pharmacokinetics and -dynamics of Cy5-labeled anti-cancer drugs. Methotrexate (MTX), purvalanol B (Pur) and Parke-Davis compound PD173956 (PD) were selected for this purpose. Previous studies had shown that these compounds show bioactivity in the lower nanomolar range (Washtien, 1982; Gray *et al.*, 1998; Kraker *et al.*, 2000). Hydrophobicity is a major determinant for the pharmacological properties of a drug (Lipinski *et al.*, 2001). Therefore, the drugs were selected to cover a broad range of hydrophobicity. Whereas the antimetabolite methotrexate is hydrophilic, having a logarithmic octanol/water partition coefficient (logP) of -1.8, the kinase inhibitor purvalanol has a logP of 3.8 and the kinase inhibitor Parke-Davis compound PD173956 a logP of approximately 5, according to the PubChem data base (National Center for Biotechnology Information (NCBI), Bethesda, USA).

The intracellular localization of MTX-Cy5, Pur-Cy5 and PD-Cy5 was determined in living human cervical cancer HeLa cells and the human embryonic kidney cell line Hek293. The hydrophobic kinase inhibitors both accumulated in the plasma membrane and vesicular structures. For assessing molecular interactions in the cytosol, this accumulation could be overcome by import of molecules via electroporation (Knight and Scrutton, 1986; Gehl, 2003; Melvik *et al.*, 1986). For cells expressing GFP-tagged target proteins of MTX and PD, FCS and FCCS were employed for detecting interactions of these two molecules inside the cell. Whereas FCCS specifically detected interactions with GFP-tagged target proteins, FCS yielded information on the total fraction of bound molecules. PD-Cy5 showed a much stronger off-target binding to intracellular structures than MTX-Cy5. The different characteristics of these drugs also confirmed that the Cy5 label did not impart the analysis of subcellular pharmacology. In summary, our results reveal major differences in intracellular off-target binding for different drug molecules and demonstrate that a combination of FCS, FCCS and confocal microscopy is a powerful combination to address such differences.
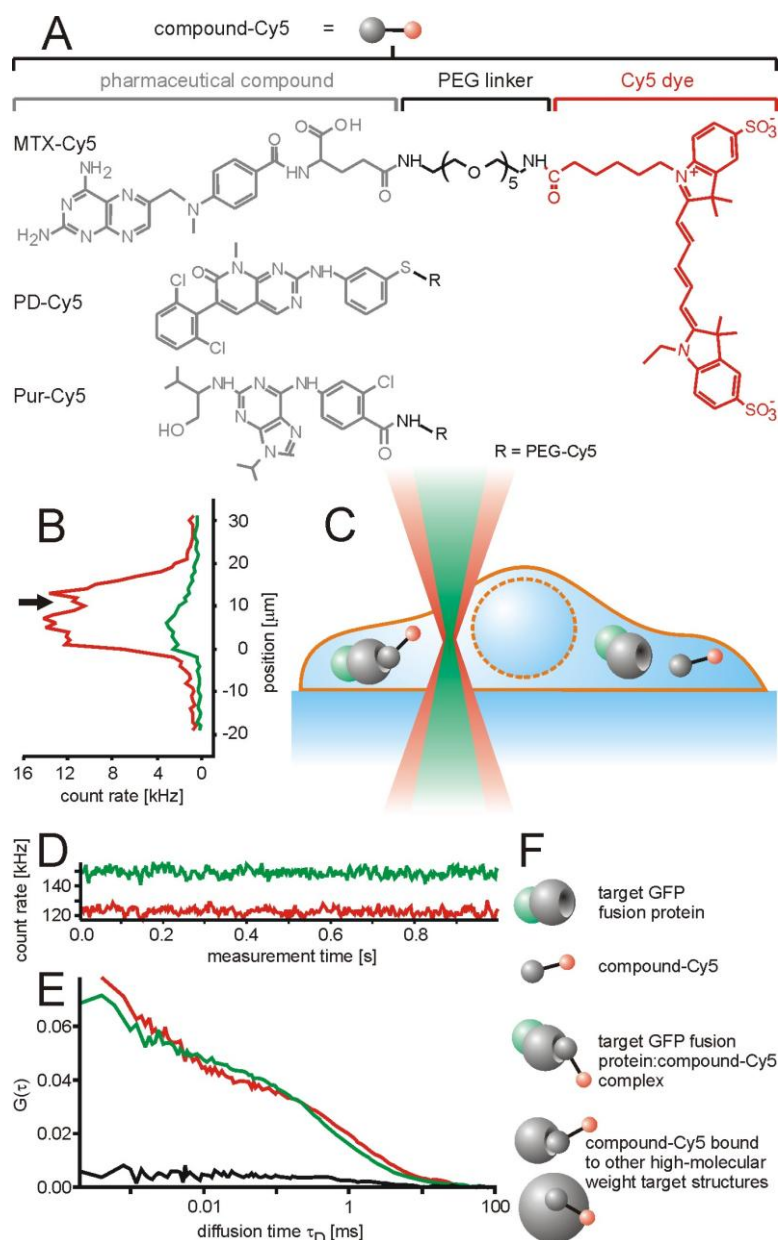
**Scheme 6.1.** Determination of the intracellular pharmacological properties of small molecule drugs by a combination of FCS and FCCS measurements in living cells. (A) The drug molecules were conjugated to the fluorescent dye Cy5 via a PEG linker. (B) Cells expressing GFP-tagged target proteins were loaded with the Cy5-labeled compounds and observed by confocal laser scanning microscopy. Subsequently, the laser beam was displaced vertically in order to identify a measurement position of the detection volume inside the cytoplasm along the optical axis (z-position). Alternatively, the z-position was identified from a confocal section in x-z-position. Measurements of interactions inside the cell (C) resulted in (D) a fluorescent count trace over time from which (E) autocorrelation functions $G(\tau)$ for both channels (red and green) and a cross-correlation function $G(\tau)$ (black) were calculated. (F) From the auto- and cross-correlation functions, concentrations of the various fluorescent species could be derived such as free GFP-tagged target protein, unbound compound-Cy5, compound-Cy5:target protein-GFP complexes and compound-Cy5 bound to high-molecular weight structures.

## 6.3. Experimental procedures

## 6.3.1. Cells and Reagents

The human cervical carcinoma cell line HeLa was obtained from the American Type Culture Collection (ATCC) (Manassas, VA, USA). T-Rex-293 cells, the T-Rex vector pcDNA4/TO, Zeocin , Blasticidin and TetraSpeck microspheres were purchased from Invitrogen (Carlsbad, USA). Effectene Transfection Reagent and QIAquick PCR Purification Kits were obtained from QIAGEN (Hagen, Germany). The Phusion DNA Polymerase Kit supplied by Finnzymes (Woburn, USA). PAGE- and HPLC-purified RhG- and Cy5-labeled primers were obtained from Thermo Electron GmbH (Ulm, Germany). Tissue culture media and fetal calf serum (FCS) were purchased from PAN biotech (Aidenbach, Germany), the Cy5 monofunctional reactive dye from GE Healthcare (Little Chalfont, UK). The electroporation kits Cell Line Nucleofector Kit V and Cell Line Nucleofector Kit R were obtained from Lonza Cologne (Cologne, Germany). The dye S0387 was purchased from FEW Chemicals (Bitterfeld-Wolfen, Germany), the dye sodium fluorescein was obtained from Fluka (Deisenhofen, Germany).

## 6.3.2. Generation of the doubly-labeled FCCS standard

In order to determine the exact spectral overlap of the detection volumes of both channels a doubly-labeled FCCS standard of 109 bp (≈37 nm) was generated by means of PCR. The *Src homology 2 domain containing adaptor protein B* (SHB) was employed as template DNA. The forward primer was labeled with the fluorescent dye Cy5 (5´-Cy5-`ATA TGG TAT CAC GGA GCC ATC AG`-3´), the reverse primer was labeled with Rhodamine Green (RhG) (5´-RhG-`TAG TCA TGC TTG CTG GTC TGG`-3´). For the amplification a Phusion DNA Polymerase Kit was used according to the supplier's manual. The PCR reaction was conducted in a GeneAmp PCR System 9700 (PE Applied Biosystems Weiterstadt, Germany) (Scheme 6.2.). Subsequently, the FCCS standard was purified by a QIAquick PCR Purification Kit according to the supplier's manual, analyzed by gel electrophoresis, diluted 20-fold in PBS buffer and finally stored in glass vials at -20°C. Additionally, un- and mono-labeled standards were generated to characterize the spectral properties of the standard.
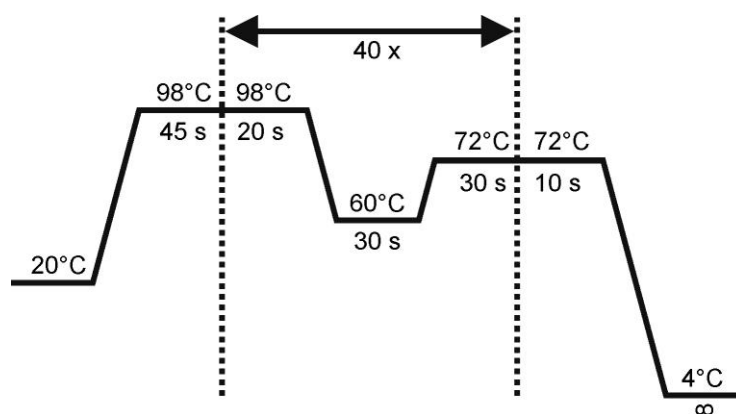
**Scheme 6.2.** Settings of the PCR system.

## 6.3.3. Synthesis of labeled compounds

Compounds carrying a 5-PEG linker with a terminal amino group were synthesized at GPC Biotech. 500 nmol of these conjugates were dissolved in 100 $\mu$L dimethyl sulfoxide and 0.7 $\mu$L N,N-diisopropylethylamine. The solution was added to one aliquot of Cy5 monofunctional reactive dye and incubated in the dark at RT for 20 h. Subsequently, purification was performed by preparative RP-HPLC (Gilson, Middleton, USA) using a linear gradient of water (0.1 % trifluoroacetic acid) - acetonitrile (0.1 % trifluoroacetic acid). The identity of the Cy5-labeled compounds was confirmed by mass spectrometry.

## 6.3.4. Tissue culture

Hek293 and HeLa wild type cell lines were grown in RPMI1640 medium containing 5% fetal calf serum at 37°C and 5% $CO_2$. The cell lines T-Rex-293 and HeLa-T-Rex stably transfected with the vector pcDNA4/TO were grown in RPMI1640 medium containing 10% fetal calf serum and the selection factors 100 $\mu$g/ml Zeocin and 5 $\mu$g/ml Blasticidin at 37°C and 5% $CO_2$.

## 6.3.5. Generation of stable T-Rex-293 and HeLa-T-Rex cell lines expressing ABL1-GFP and DHFR-GFP

$5 \times 10^6$ T-Rex-293 cells and $2 \times 10^6$ HeLa cells were transfected with 2 µg of the respective plasmids encoding GFP-tagged target proteins and a Zeocin resistance cassette using Effectene Transfection Reagent. Transfected cells were selected using Zeocin at a concentration of 0.1 mg/ml over a period of several weeks, eliminating all cells that did not express the Zeocin resistance gene at sufficient amounts. The polyclonal T-Rex-293 and HeLa-T-Rex strains were kept under selective pressure of 100 µg/ml Zeocin and 5 µg/ml Blasticidin throughout the experiment.

## 6.3.6. Cellular import of drug molecules

T-Rex-293 cells expressing low amounts of ABL1-GFP were detached by Trypsin/EDTA and washed in medium. Subsequently, different concentrations of PD-Cy5 were electroporated into the cells (single pulse, 130 V, 500 µF, Fischer Electroporator, Heidelberg, Germany). For analysis of the direct uptake of PD-Cy5 without electroporation, T-Rex-293 cells expressing ABL1-GFP were grown in 8-well chambered coverglass slides (Nunc, Rochester, USA) and incubated with different concentrations of PD-Cy5 for 3h at 37°C.

For analysing the interaction of MTX-Cy5 with DHFR-GFP, T-Rex-293 cells stably transfected with DHFR-GFP were detached by Trypsin/EDTA, washed in medium and resuspended in 100 µL Nucleofector Solution R containing 4 µM MTX-Cy5. MTX-Cy5 was imported by electroporation (Nucleofector, Lonza Cologne) using the electroporation method I-013 according to the recommendations of the manufacturer. Subsequently, 500 µL RPMI medium were added carefully and the cells were incubated for 10 min at 37°C. Subsequently, the cell suspension was washed in medium twice by centrifugation. The cells were seeded in 8-well chambered coverglass slides (Nunc, Rochester, USA).

HeLa-T-Rex cells expressing low amounts of DHFR-GFP were detached by Trypsin/EDTA and washed in medium. Cells were electroporated in a solution of 1 µM MTX-Cy5 in RPMI medium (single pulse, 130 V, 500 µF, Fischer Electroporator). The cells were washed three times with medium and finally seeded in a 8-well chambered coverglass slide.

## 6.3.7. Intracellular FCCS measurements

FCCS measurements were performed with a TCS SP5 confocal microscope/dual channel fluorescence correlation spectroscopy unit equipped with an HCX PL APO 63x N.A. 1.2 water immersion lens (Leica Microsystems, Mannheim, Germany) and with a ConfoCor2 fluorescence correlation spectroscopy unit connected to an Axiovert 100M equipped with a C-Apochromat 40x N.A. 1.2 water immersion lens (Carl Zeiss, Jena, Germany). In case of the TCS SP5, fluorescence was split by a BS 625 beam splitter. Fluorescence in the green channel was detected using a BP 500-550 band pass filter, fluorescence in the red channel with a BP 647-703 band pass filter. For the ConfoCor2, fluorescence was split by an NFT 610 beam splitter, green fluorescence was detected with a BP 500-550 IR band pass filter, red fluorescence with an LP 650 long pass filter. The GFP fusion proteins were excited with the 488 nm laser line of an argon-ion laser, Cy5 with a 633 helium-neon laser. In order to avoid high background signals resulting from autofluorescence and minimize bleaching, the power of both lasers was adjusted to a low intensity. The argon-ion laser was adjusted to 20 $\mu$W and 11 $\mu$W for the TCS SP5 and the ConfoCor2, respectively, the helium-neon laser to 19 $\mu$W and 8 $\mu$W, measured with an X1-1 laser power meter equipped with an LSM-9901 Luminous Flux detector head (Gigahetz-Optik, Puchheim, Germany) at the exit aperture of the lens.

For each setup these parameters led to comparable molecular brightness (fluorescence per molecule – fpm) in both channels. Solution measurements were carried out with a sample volume of 20 $\mu$L in a 384-well plate (175 $\mu$m, low-base design, MMI, Eching, Germany). The short wavelength channel was calibrated with a 10 nM sodium fluorescein solution. For measurements of GFP fusion proteins, the structure parameter corresponding to the ratio of the radii of the detection volume along the optical axis and in the focal plane $S = z_0/\omega_0$ was fixed to the value determined by fitting the autocorrelation function for this measurement. The structure parameter S for the long-wavelength channel was determined by an autocorrelation measurement of a 10 nM S0387 solution. This indocyanine dye has spectral properties comparable to Cy5 (Mader *et al.*, 2004). The spectral overlap of the detection volumes was determined by a cross-correlation measurement of a doubly-labeled FCCS standard, terminally labeled with Rhodamine Green (RhG) and Cy5, similar to a standard described previously (Baudendistel *et al.*, 2005). Cells with low expression of GFP fusion proteins were selected by confocal imaging. The detection volume for the FCCS measurements was placed inside the cytosol near to the nucleus. The signal of immobile molecules was removed by a pre-bleaching pulse of a few seconds at the same laser power employed for the subsequent measurements, followed by recording of either 5 to 60 autocorrelation

functions of 1 s each for the ConfoCor2 or 5 to 10 measurements of 5 s each for the TCS SP5. Autocorrelation functions not affected by strong fluctuations of fluorescence as caused by diffusion of vesicles were averaged for each cell for further analysis.

Autocorrelation functions of Cy5-labeled compounds were fitted with a 3D Gaussian algorithm containing two diffusing components and a triplet term. Either the diffusional autocorrelation times $\tau_D$ and fractions of both components were variable or the $\tau_D$ of the fast component was fixed to the value determined for the respective Cy5-labeled compound in solution multiplied by a factor of four in order to account for the higher viscosity of the cytoplasm (Ellis, 2001; Berland *et al.*, 1995).

For the analysis of cross-correlation functions, the structure parameters S in both channels were fixed to the values determined by measurements of fluorescein and S0387, respectively. The triplet times of GFP and Cy5 were fixed to values derived from measurements in solution. For the cross-correlation curve no triplet term was included in the fitting algorithm.

The autocorrelation amplitudes of the GFP channel $G_{green}(0)$ and the Cy5 channel $G_{red}(0)$ and the cross-correlation amplitude $G_{CC}(0)$ were determined. The ratio CC(measured) between $G_{green}(0)$ and $G_{CC}(0)$ represented the fraction of the Cy5-labeled compounds that formed a complex with GFP fusion proteins (Schwille *et al.*, 1997). The results were normalized by the value CC(max) determined for the doubly-labeled FCCS standard in the same experiment. Here, the device-dependent values were between 41 and 45 %. Due to the wavelength dependence of diffraction this value can maximally amount to 54 % in a perfectly adjusted microscope (Weidemann *et al.*, 2002). The fraction of the Cy5-labeled compound bound to the GFP-tagged target protein CC(corr.) was corrected by

$$CC(corr.) = \frac{CC(measured) \cdot 100\%}{CC(\max)}$$

(6.1)

The particle number N derived from the autocorrelation functions was corrected for non-correlating autofluorescence background (Koppel, 1974),

$$N_{corrected} = N_{measured} \cdot \left(1 - \frac{I_{background}}{I_{total}}\right)^2$$

(6.2)

as was the fluorescence per molecule (fpm).

$$fpm = \frac{I_{total} - I_{background}}{N_{corrected}}$$

(6.3)

Deviations of the fpm from values measured in solution indicated the presence of fluorescence energy transfer (FRET) and quenching (Weidemann *et al.*, 2002; Földes-Papp, 2005) or poor overlap of the detection volume with the cell.

The number of Cy5-labeled drug molecules bound to their respective GFP-target proteins $N_{red\text{-}bound}$ was calculated according to

$$N_{red\text{-}bound} = N_{corrected} \cdot CC(corr.) \tag{6.4}$$

With knowledge of the size of the detection volumes, which were approximately 0.3 fl for the detection volume of the green and 0.6 fl for the detection volume of the red channel, the concentrations of Cy5-labeled compounds and GFP-tagged target protein could be calculated. The determination of detection volumes was based on experimentally determined point spread functions using TetraSpeck microspheres of 0.1 $\mu$m.

Assuming thermodynamic equilibrium for the interaction of compound and target

$$C_{compound\text{-}Cy5,\,free} + C_{Protein\text{-}GFP,\,free} \leftrightarrows C_{complex} \tag{6.5}$$

the dissociation constant Kd could be determined by

$$Kd = C_{compound\text{-}Cy5,\,free} \cdot C_{Protein\text{-}GFP,\,free} \cdot C_{complex}^{-1} \tag{6.6}$$

Here, the concentration of unbound compound-Cy5 ($C_{compound\text{-}Cy5,\,free}$) was deduced from the fraction of free molecules obtained from two-component fits of the autocorrelation functions. The concentration of the compound-Cy5:target protein-GFP complex ($C_{complex}$) was determined by cross-correlation measurements and the concentration of unbound GFP fusion protein ($C_{protein\text{-}GFP,\,free}$) was calculated by the substraction of $C_{complex}$ from the total concentration of the GFP fusion protein.

## 6.4. Results

## 6.4.1. Characterization of the doubly-labeled FCCS standard

Solutions of the doubly-labeled FCCS standards were analyzed by agarose gel electrophoresis. According to a DNA-based molecular weight standard the detected DNA fragments had a size of about 100 bp. Larger DNA fragments such as template strands or other impurities could not be detected (Fig 6.1.A). Furthermore, FCCS measurements were conducted. Optical effects such as spectral cross-talk and FRET were quantified by mono-labeled DNA standards. At laser powers of 10.7 $\mu$W for the 488 nm line of an argon-ion laser and 7.6 $\mu$W for the helium-neon laser at 633 nm comparable molecular brightnesses were obtained in both channels. A weak cross-talk of the RhG emission spectrum (mono-labeled RhG-standard) into the red detection channel of 3.5 % could detected. Furthermore the argon-ion laser excited the mono-labeled Cy5-standard leading to an intensity of 1.7 % relative to the Cy5 signal upon excitation with the helium-neon laser. In summary, cross-talk effects and cross-excitation contributed 5.2 %. The doubly-labeled standard also showed 5.2 % cross-talk and cross-excitation upon excitation with the argon-ion laser only. This clearly indicated that no FRET was detectable. Moreover, an unlabeled standard did not show detectable autofluorescence. Upon excitation with both lasers the doubly-labeled FCCS standard showed cross-correlation amplitudes between 44 and 48 % (Fig 6.1.B). Due to dependence of the detection volume on the excitation and emission wavelengths the maximal spatial overlap of the detection volumes and thus also the theoretical maximum of the cross-correlation amplitude is 54 %.
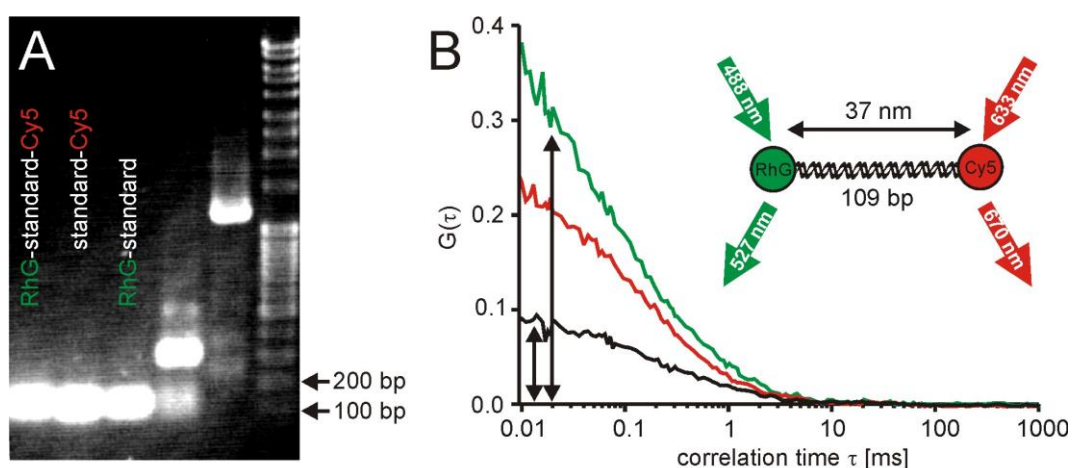


**Fig. 6.1.** Properties of the doubly-labeled FCCS standard. (A) The purity of the FCCS standard was controlled by gel electrophoresis. (B) The standard was measured by FCCS. The height of the cross-correlation amplitude (black curve, small arrow) was referred to the height of the autocorrelation amplitude of the RhG channel (green curve, large arrow).

## 6.4.2. Synthesis of Cy5-labeled drug molecules

The pentamethine indocyanine dye Cy5 was selected as a fluorophore for the labeling of the drug molecules. With an emission maximum of around 670 nm, the fluorescence of this molecule shows very little spectral overlap with the emission of the green fluorescent protein (Southwick *et al.*, 1990). For the conjugation to drug molecules, functional groups had to be selected that are not part of the pharmacophore. Methotrexate was labeled at the free carboxyl group of the glutamate residue as described before (Gapski *et al.*, 1975). For the compounds PD173956 and purvalanol B the position for labeling was based on preceding SAR studies, that verified that the conjugated compounds maintained their specific activity (Becker *et al.*, 2004; Caligiuri *et al.*, 2005).

In order to further minimize interference of the fluorophore with the binding of the compounds and to prevent FRET, the fluorophore was coupled via a polyethylene glycol (PEG) spacer. Due to its hydrophilicity, the PEG spacer should promote the solubility of the compounds and minimize hydrophobic interactions with membranes and proteins. Cy5 was employed as a commercially available, preactivated succinimidyl active ester (Scheme 1.A).

## 6.4.3. Intracellular distribution of the Cy5-labeled compounds

First, we were interested to explore the intracellular distribution of the compounds. When using fluorescently labeled analogs, an influence of the fluorophore on the distribution of the molecule of interest is an important concern. HeLa and Hek293 wild type cells were incubated with 5 $\mu$M of the respected compounds for 90 min. In comparison to previous studies the incubation time with methotrexate was rather short (Kaufman *et al.*, 1978). This short incubation time was mainly chosen to prevent unintended effects on cell viability.

The hydrophobic compounds PD-Cy5 and Pur-Cy5 were taken up efficiently into HeLa and Hek293 cells. Both conjugates were primarily localized in membranes and vesicular structures. In contrast, the uptake efficiency of the hydrophilic drug MTX-Cy5 was lower and its localization was more diffuse (Fig. 6.2).

While these results do not fully exclude an influence of the fluorophore on the characteristics of the compounds, they clearly show that the compound is decisive for the subcellular pharmacokinetics of the conjugates. As we had stable cell lines expressing GFP-tagged DHFR and the Abl1 kinase domain under the control of a tetracyclin-inducible promoter in our hands, the labeled compounds MTX-Cy5 and PD-Cy5 were selected for further experiments to address intracellular interactions by FCS and FCCS.
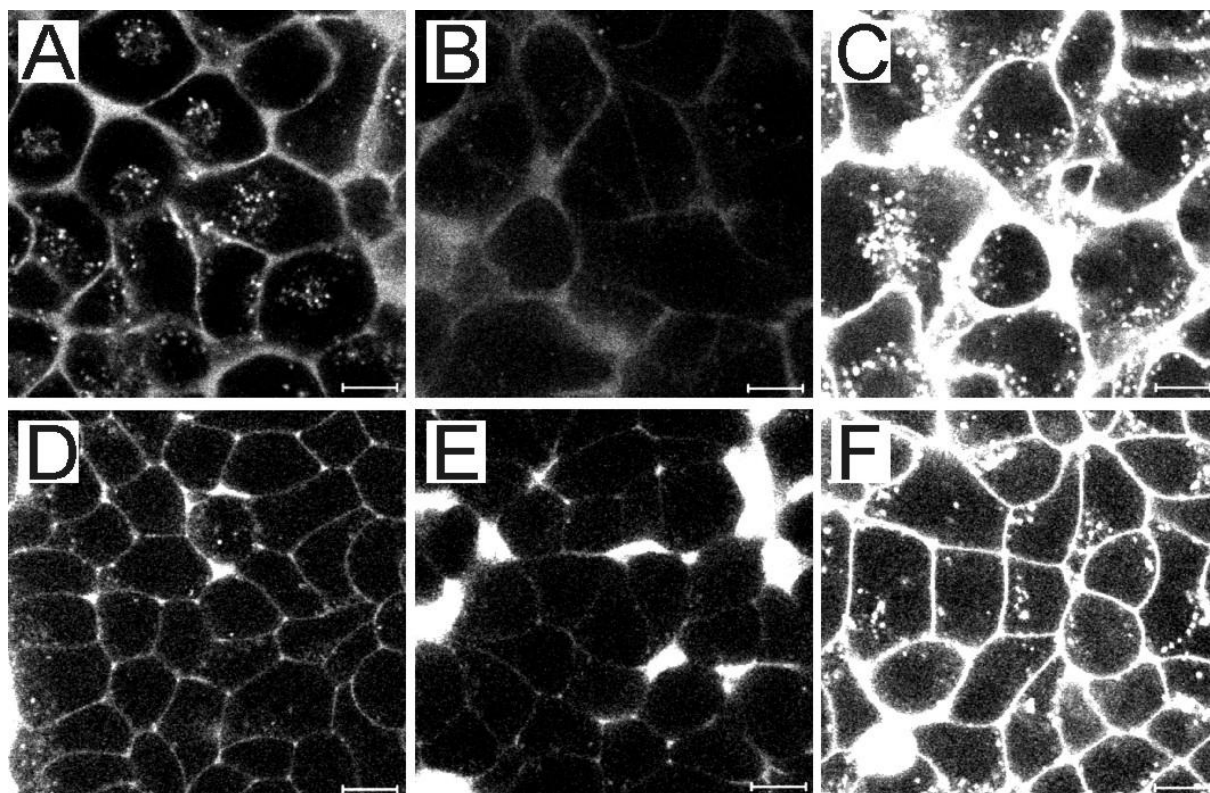
**Fig. 6.2.** Intracellular localization of three Cy5-labeled representative anti-cancer drugs. (A-C) HeLa cells and (D-F) Hek293 cells were treated with each 5 μM of (A and D) PD-Cy5, (B and E) MTX-Cy5 and (C and F) Pur-Cy5 for 90 min at 37°C. The scale bars denote 20 μm.

## 6.4.4. Intracellular interactions of MTX-Cy5 in DHFR-GFP-expressing HeLa cells

Confocal microscopy is very instructive to study the subcellular distribution of molecules (Pygall *et al.*, 2007). However, the method provides little information on the possible association of compounds with homogenously distributed intracellular structures. Moreover, information on concentrations is very difficult to obtain. Fluorescence recovery after photobleaching (FRAP) (Meyvis *et al.*, 1999), a method frequently used to study association and mobility of molecules inside cells does not provide sufficient temporal resolution to analyze the mobility of small molecules and/or very low concentrations of fluorescent molecules (Lippincott-Schwartz *et al.*, 2001). Therefore, for the analysis of the association of small molecules with subcellular structures at low concentrations, FCS and FCCS are the methods-of-choice.

When using low micromolar concentrations of Cy5-MTX for 90 min, we failed to acquire intracellular autocorrelation functions. It has been shown previously, that the cellular uptake

of fluorescein-labeled MTX is slow, requiring several hours before reaching equilibrium (Kaufman *et al.*, 1978). In order to avoid potential negative pharmacologic effects of the antimetabolite methotrexate on viability, the cells were not incubated with MTX-Cy5 for such a long period of time. Instead, we explored the use of electroporation for the cytoplasmic import of the conjugate. Electroporation achieves a cytoplasmic import of solutes by application of short high-voltage pulses that induce transient pore formation in the plasma membrane (Gehl, 2003).
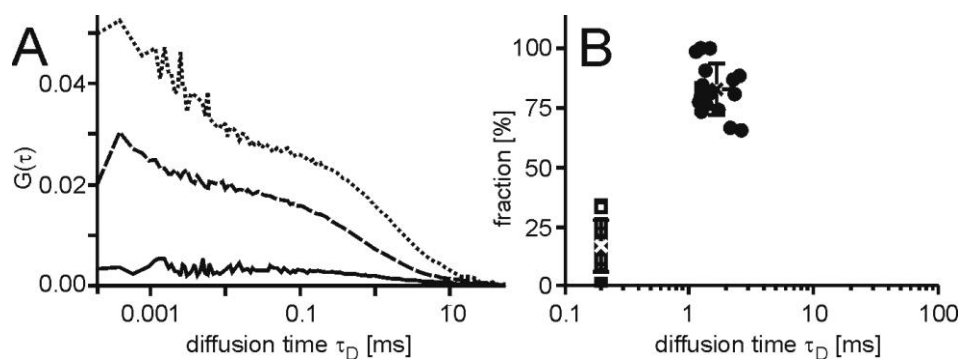


**Fig. 6.3.** Interaction of MTX-Cy5 in HeLa-TREx cells expressing DHFR-GFP. (A) Characteristic autocorrelation functions for DHFR-GFP (dashed line) and MTX-Cy5 (dotted line) and the cross-correlation function for the DHFR-GFP:MTX-Cy5 complex (solid line). (B) Scatter plots of relative contributions to the autocorrelation function versus diffusional autocorrelation times derived from fits to the autocorrelation functions with an algorithm comprising two diffusing components in which the diffusion time $\tau$D of the low-molecular weight fraction was fixed to 200 $\mu$s. Averages (cross) and standard deviations are indicated.

Subsequently, FCCS measurements were performed with a combined FCCS/confocal microscope while the cells were still not entirely flattened and attached to the bottom. Confocal imaging enabled a precise placement of the confocal measurement volume for FCCS measurements in three dimensions (Scheme 1B-F). In the slightly rounded cells the confocal volume could be placed inside the cytosol more easily than in entirely attached cells.

HeLa-T-Rex cells expressing low concentrations of DHFR-GFP in the absence of tetracycline were electroporated with the compound. In the absence of tetracycline the DHFR-GFP concentration was in the range of 313 ±187 nM, indicating a considerable leakiness of the promotor. Still, the use of an inducible promoter was by far superior to the use of a constitutive promoter, which typically yields too high expression levels for FCS measurements. A 1 $\mu$M solution of MTX-Cy5 was electroporated into the cells, yielding typical intracellular MTX-Cy5 concentrations of approximately 40-70 nM, thus, in a

concentration range in which standard microscopy techniques fail to provide suitable results. The concentrations were derived from the amplitudes of the autocorrelation functions. In FCS, the amplitude is inversely correlated to the average number of molecules in the detection volume. Using experimentally determined detection volumes for both channels, these molecule numbers were converted into concentrations.

Dividing the fluorescence by the number of molecules yields the fluorescence-per-molecule (fpm). For cellular FCS measurements large variations of this value between individual measurements indicate inhomogeneities in the sample or cell movement. Moreover, the fpm may vary in dependence of the molecular environment of a fluorophore.

The molecular brightness fpm of GFP was highly constant within the samples and was approximately 4.0 ± 1.2 kHz. The intracellular molecular brightness (fpm) of MTX-Cy5 was slightly lower than the extracellular fpm indicating that in the cytosol no significant quenching occurred.

In most cases, the first two measurements of a consecutive series of measurements in a single cell were affected by bleaching of immobilized MTX-Cy5 and therefore were omitted from the further analysis. The autocorrelation functions for MTX-Cy5 were fitted with two diffusing components and a triplett term (Fig. 6.3.A). The diffusional autocorrelation time $\tau_D$ reflects the average time that a fluorophore needs to diffuse through the detection volume. This time is directly correlated with the radius of the molecule. Therefore, the larger the molecule the bigger $\tau_D$. The ability to describe the autocorrelation functions with two components does not imply that MTX-Cy5 was only present in two molecular forms, as for example free drug molecule and in a molecular complex of a defined molecular weight. Given the fact that the molecular radius correlates with the cubic root of the molecular weight of a molecule, which means that it is rather little depends on the molecular weight, especially the high molecular weight form may represent multiple different complexes.

The $\tau_D$ of the fast component was fixed to 200 µs. This value was based on the $\tau_D$ of MTX-Cy5 in PBS buffer of approximately 50 µs, in comparison to 35 µs of the free dye, considering that the viscosity of the cytoplasm is about 4-fold higher in comparison to an aqueous buffer. In order to represent the variation between individual measurements, a graphical presentation according to (Brock *et al.*, 1999) was chosen (Fig. 6.3.B). Here, for each fraction, the relative contribution to the autocorrelation amplitude is plotted versus the diffusional autocorrelation time $\tau_D$.

The bound MTX-Cy5 fraction accounted for approximately 83 ± 11 % and had an average diffusional autocorrelation time $\tau_D$ of 1.7 ± 0.5 ms. The diffusional autocorrelation time $\tau_D$ of the DHFR-GFP was 1.3 ± 0.6 ms. Assuming identical mobilities for the DHFR-GFP and the MTX-Cy5, the MTX-Cy5 should have a diffusional autocorrelation time of about 2.2 ms. This

estimate is based on the larger dimensions of the detection volume due to the wavelength dependence of diffraction (Weidemann *et al.*, 2002) and the proportionality of $\tau_D \sim \omega_x\omega_y$, where $\omega_x$ and $\omega_y$ represent the lateral extensions of the detection volume (Schwille *et al.*, 1997). The exact dimensions of the latter were determined by measuring the point spread function of the objective using sub-resolution fluorescent microspheres.

In addition to the autocorrelation functions of MTX-Cy5 and DHFR-GFP, the cross-correlation functions were calculated. For the HeLa-T-Rex cells cross-correlation amplitudes of 19.0 ± 6.4 % in comparison to the autocorrelation amplitude of the DHFR-GFP channel were obtained. By relating this value to the maximum attainable cross-correlation amplitude of 45 % if all molecules were in a complex, these data showed that on average approximately 42 % of the MTX-Cy5 was bound to the specific target protein DHFR-GFP. This in turn means that on average about 51 % of the MTX-Cy5 molecules that were bound to high-molecular targets were in complex with DHFR-GFP. Based on these numbers, the dissociation constant Kd for the interaction of MTX-Cy5 with DHFR-GFP was calculated. The dissociation constant of MTX-Cy5:DHFR-GFP determined in 10 HeLa-T-Rex cells was 125 ± 54 nM.

## 6.4.5. Intracellular interactions of MTX-Cy5 in DHFR-GFP-expressing HEK293 cells

In order to investigate to which degree this interaction pattern was a characteristic of the specific cell type, we next performed a corresponding set of measurements in HEK293 cells, expressing the DHFR-GFP fusion protein under control of the tetracycline promotor.

In the absence of tetracycline, an intracellular DHFR-GFP concentration of 27 ± 14 nM was obtained. The concentrations were considerably lower than in HeLa-T-Rex cells, indicating that the tetracycline repressor was less leaky in HEK293 cells.

Due to a lower electroporation efficiency, in this case the cells were electroporated with a solution containing 4 $\mu$M MTX-Cy5. This led to typical cytosolic concentrations in the range of 20-50 nM as determined by FCS.

Again, the molecular brightness of GFP was highly constant within the samples and was approximately 2.3 ± 0.4 kHz. The fpm of the MTX-Cy5 varied between independent measurements. This variation was likely due to the interactions of the compound with high-molecular weight structures that partially perturbed the autocorrelation measurements. The differences in fpm between HeLa and Hek cells most likely reflect the fact that both cell types were measured with different instruments.

For the analysis of the autocorrelation functions (Fig. 6.4.A), first the $\tau_D$ of the fast component was fixed again to 200 $\mu$s. In this case, the fast fraction accounted for 62 % of the autocorrelation amplitude; the slow component accounted for 38 % of MTX-Cy5 with a $\tau_D$ of 5.8 ± 2.6 ms (Fig. 6.4.B). The $\tau_D$ of the slow component had a much stronger variation than for the HeLa cells. Therefore, the autocorrelation functions were also fitted with both diffusional autocorrelation times $\tau_D$ kept variable. In that case, the fast fraction had an average $\tau_D$ of 437 $\mu$s representing 65 ± 20 % of the total amount of MTX-Cy5, the slow-diffusing fraction a $\tau_D$ of 132 ms (35 % of the total amount) (Fig. 6.4.C). The comparability of results obtained with both fitting procedures strongly indicates that the rapidly diffusing component corresponds to free compound and that in this case, more than half of the molecules diffused freely in the cytoplasm.

The diffusional autocorrelation time $\tau_D$ of the DHFR-GFP was 972 ± 294 $\mu$s and thus slightly shorter than the one measured for HeLa cells. Thus, DHFR-GFP-bound MTX-Cy5 should have a diffusional autocorrelation time of about 1.6 ms. However, the bound compound showed a clearly higher diffusion time than expected for MTX-Cy5 bound to its 48 kDa target protein DHFR-GFP.

The cross-correlation functions had amplitudes in the range of 7.2 ± 1.9 % of the one of the DHFR-GFP channel. These data indicated that on average a fraction of approximately 16 % of the MTX-Cy5 molecules were bound to the specific target protein DHFR-GFP. Given the total fraction of bound molecules of 38 % this result showed that on average only about 42 % of the MTX-Cy5 molecules bound to high-molecular targets was bound to DHFR-GFP, considerably less than for the HeLa cells. The average dissociation constant determined from measurements in 18 cells was 86 ± 45 nM. The Kd value as determined in the above experiments was measured in the presence of intrinsic dihydrofolate which competes with MTX-Cy5 for the binding sites on DHFR-GFP; thus the calculated binding constants are regarded as apparent Kd-values, that may differ from values determined in biochemical assays.
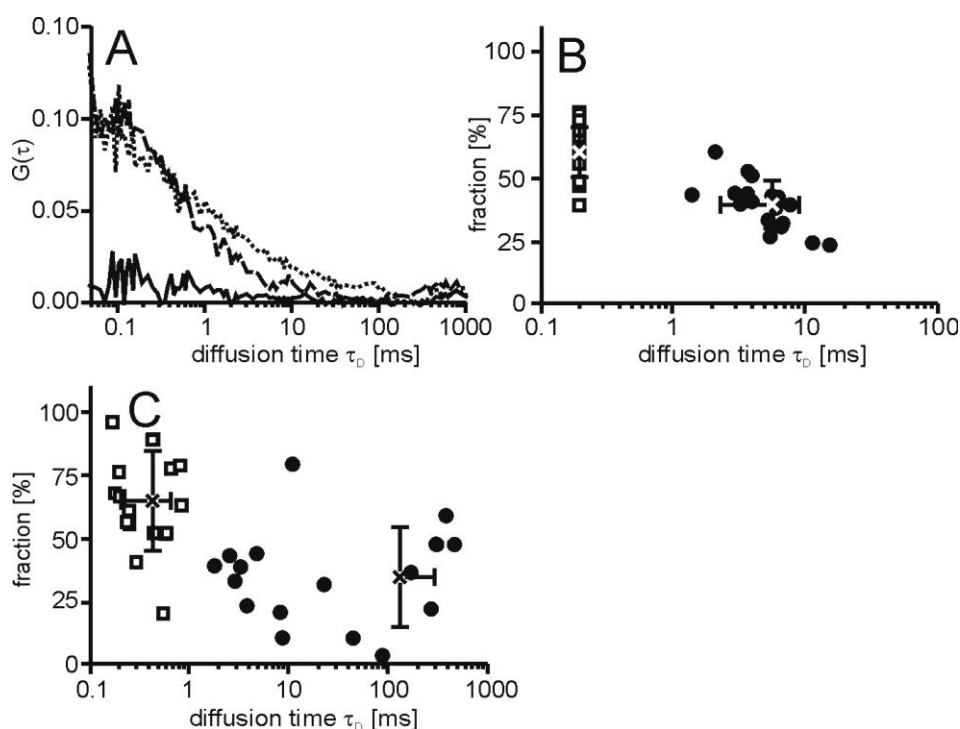
**Fig. 6.4.** Interactions of MTX-Cy5 in T-Rex-293 cells expressing DHFR-GFP. (A) Characteristic autocorrelation functions for DHFR-GFP (dashed line), MTX-C5 (dotted line) and the respective cross-correlation function (solid line). (B,C) Dot plots of the relative fractions of each component versus the diffusional autocorrelation $\tau_D$ of MTX-Cy5 derived from two-component fits with averages (cross) and standard deviations, in which the fast component was fixed to 200 $\mu$s (B) or both diffusional autocorrelation times were allowed to vary (C).

## 6.4.6. Intracellular binding of PD-Cy5 to high-molecular target structures in T-Rex-293 cells

Finally, we were interested to investigate the intracellular interaction pattern for the hydrophobic compound PD-Cy5. T-Rex-293 cells expressed low amounts of ABL1-GFP in the range of 50-130 nM. The cells were electroporated with 0.2 $\mu$M Parke-Davis compound. This led to PD-Cy5 concentrations of 320 ± 165 nM. These concentrations were significantly higher than the concentrations determined for MTX-Cy5. Also in measurements in which cells were directly incubated with the compound, much higher intracellular concentrations were reached. These results indicate that PD-Cy5 enters cells much more efficiently than MTX-Cy5 and that also during the electroporation procedure, for this hydrophobic compound, a direct crossing of the plasma membrane greatly contributed to cell entry.

Again, the autocorrelation functions were analyzed with two-component fits in which the diffusion time $\tau_D$ of the low-molecular weight component was fixed to 200 $\mu$s. The determined

diffusion time $\tau_D$ of the high-molecular weight fraction was high, mostly >10 ms, indicating an interaction between the compound and cellular structures that were significantly larger in molecular weight than the 60 kDa ABL1-GFP molecule. The diffusion time $\tau_D$ of the ABL1-GFP was 541 ± 112 µs, and therefore shorter than the one for the DHFR-GFP. The high-molecular fraction accounted for 70 ± 10 % of the total PD-Cy5 fraction. Additionally, a large fraction PD-Cy5 was bleached within the first seconds of the measurements indicating complete immobilization or trapping in vesicular structures. This strong bleaching of immobile fluorescence is therefore consistent with the distribution of fluorescence seen by confocal microscopy.
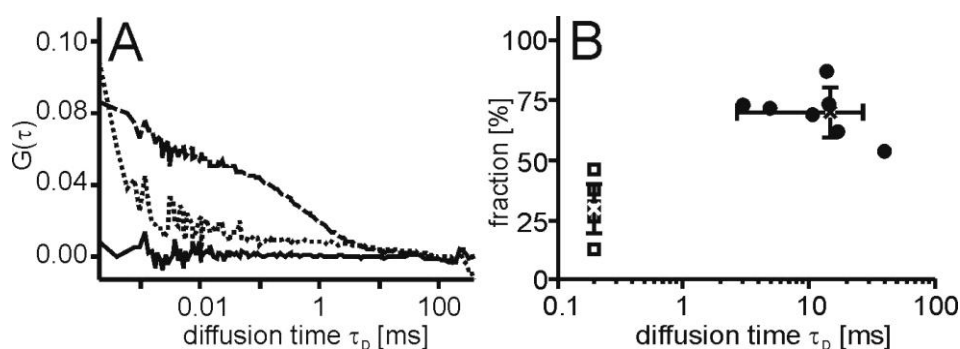


**Fig. 6.5.** Interaction of PD-Cy5 in cells. (A,B) T-Rex-293 cells expressing ABL1-GFP were electroporated with PD-Cy5. (A) Characteristic autocorrelation functions for ABL1-GFP (dashed line) and PD-Cy5 (dotted line) and the cross-correlation function (solid line). (B) Dot plot of the relative contribution to the autocorrelation amplitude versus diffusional autocorrelation time $\tau_D$ for PD-Cy5 with the fast component fixed to 200 µs with averages (cross) and standard deviations.

Interestingly, no cross-correlation could be observed in the cells, although previous experiments had shown a high affinity of binding in cell lysate with Kd values in the lower nanomolar range. Varying of the concentrations of the PD-Cy5 used for electroporation did not improve the result. The measurements with MTX-Cy5 had demonstrated the possibility to determine dissociation constants inside cells at a similar total degree of drug binding, as determined by FCS. Apparently, the fraction of molecules binding to their target was below the detection limit. We therefore conclude that off-target binding to other proteins and/or membranes inside the cell plays a much stronger role for PD-Cy5 than for MTX-Cy5.

## 6.5. Conclusions

At present, detailed molecular analyses of the biological activity of drugs and drug candidates are restricted to *in vitro* tests. Cellular assays typically report on the activity of a compound in a very complex molecular context. Molecular interactions with the drug target and off-target binding are not addressed explicitly. In this work, we achieved such an analysis for small molecule anti-cancer drugs using laser scanning microscopy and a combination of fluorescence correlation spectroscopy (FCS) and fluorescence cross-correlation spectroscopy (FCCS). For this purpose, Cy5-labeled molecules were synthesized. To our knowledge Cy5 has not been used for the labeling of small molecule drugs and their application in intracellular studies before.

Confocal microscopy revealed that Pur-Cy5 and PD-Cy5 were taken up into HeLa and Hek293 cells efficiently, but localized in vesicular structures, whereas MTX-Cy5 entered the cells poorly, but showed a homogenous intracellular distribution. The localization and poor uptake for such short incubation times were consistent with results reported for Fluorescein-MTX before (Kaufman *et al.*, 1978). The subcellular distribution of PD and Pur demonstrated that sequestration in membranes and vesicular structures should be a limiting factor for the intracellular bioavailability of these compounds. Indeed, FCS revealed that a considerable fraction of the compound PD-Cy5 was bound to high-molecular weight structures. Cross-correlations, reflecting an interaction of PD-Cy5 with with the ABL1-GFP target molecule could not be detected. If such particles were present their fraction in comparison to the non-interacting molecules was too low to give rise to a cross-correlation amplitude. A too high number of non-interacting molecules limits the detectability of molecular interactions in FCCS as these lead to a decrease in the amplitude of the cross-correlation function. The ability of PD-Cy5 to interact with the target was confirmed in lysates of cells strongly overexpressing the fusion protein. However, in these cell lysates, a significant fraction of membranes had been removed by centrifugation prior to the FCCS measurements.

In contrast to PD-Cy5, the interaction of the hydrophilic drug methotrexate MTX-Cy5 with its specific molecular target DHFR could be detected in living cells. The Kd values determined in the T-Rex-293 and HeLa-T-Rex cells were highly comparable, even though expression levels of the target protein varied by one order of magnitude and the overall interaction pattern was also different. In T-Rex cells, more than one third of the molecules were freely diffusive, in contrast to only 17 % in HeLa cells. Moreover, in T-Rex-293 cells, a lower fraction of MTX-Cy5 specifically bound to DHFR-GFP. This reduced binding was accompanied by increased off-target binding to high molecular weight intracellular structures, as indicated by the longer and more heterogeneous $\tau_D$ values.

It is a particular strength of FCCS to directly provide information on all molecular species in equilibrium. Therefore, a dissociation constant can be derived from one single measurement. In this case, in which off-target binding also occurred, the combination of FCS and FCCS proved to be highly powerful. Both measurement modalities provided complementary information on the fraction of bound molecules. With FCS, total binding of the compound was determined. FCCS selectively reported on those MTX-Cy5 molecules specifically bound to DHFR-GFP.

The dissociation constants were about two orders of magnitude higher than the values determined in vitro for purified DHFR (Rajagopalan *et al.*, 2002; Mayer *et al.*, 1986; Remy and Michnick, 2001). A major reason for this difference will be the presence of endogenous dihydrofolate (DHF). Whereas in resting cells the intracellular DHF concentration is in the lower nanomolar range, it can increase over several orders of magnitudes in proliferating cells (Assaraf, 2007). Both, Hek293 and HeLa cells are highly proliferating cell lines, so it is reasonable to assume a rather high DHF concentration.

Next to the fusion protein, endogenous DHFR is also present inside the cells. However, since the binding of MTX-Cy5 to DHFR-GFP was measured in equilibrium, this endogenous protein will not affect the apparent Kd values measured for DHFR-GFP:MTX-Cy5 by FCCS. Instead, we may assume that endogenous DHFR may account at least for a fraction of the off-target binding, determined by the differences of bound fraction determined with FCS and FCCS.

In summary, this study demonstrates the potential of a combination of FCS and FCCS to define target and off-target binding profiles of drugs inside cells. Exploitation of the leakiness of inducible promoters turned out as an important technical detail to reliably achieve low expression levels of fusion proteins also in only transiently transfected cells.

# 7. Appendix

## 7.1. Macro for the quantification of cellular fluorescence

The macro was set up on *ImageJ 1.41* based on *Java 1.6.0_10*. The threshold (8th row from the top) was adjusted according to each experiment independently.

```
close();
run("Duplicate...", "title=1");
run("Smooth");
run("Duplicate...", "title=2");
run("Set Scale...", "distance=0 known=1 pixel=1 unit=cm global");
setAutoThreshold();
//run("Threshold...");
setThreshold(6, 255);
run("Analyze Particles...", "size=3000-infinity circularity=0.00-1.00 show=Masks");
run("Watershed");
run("Analyze Particles...", "size=3000-infinity circularity=0.00-1.00 show=Masks
add");
selectWindow("1");
setOption("Show All",true);
run("Set Measurements...", "area mean standard min circularity median redirect=None
decimal=3");
roiManager("Measure");
saveAs("Measurements", "C:\\Documents and
Settings\\z718203\\Desktop\\Results.xls");
```
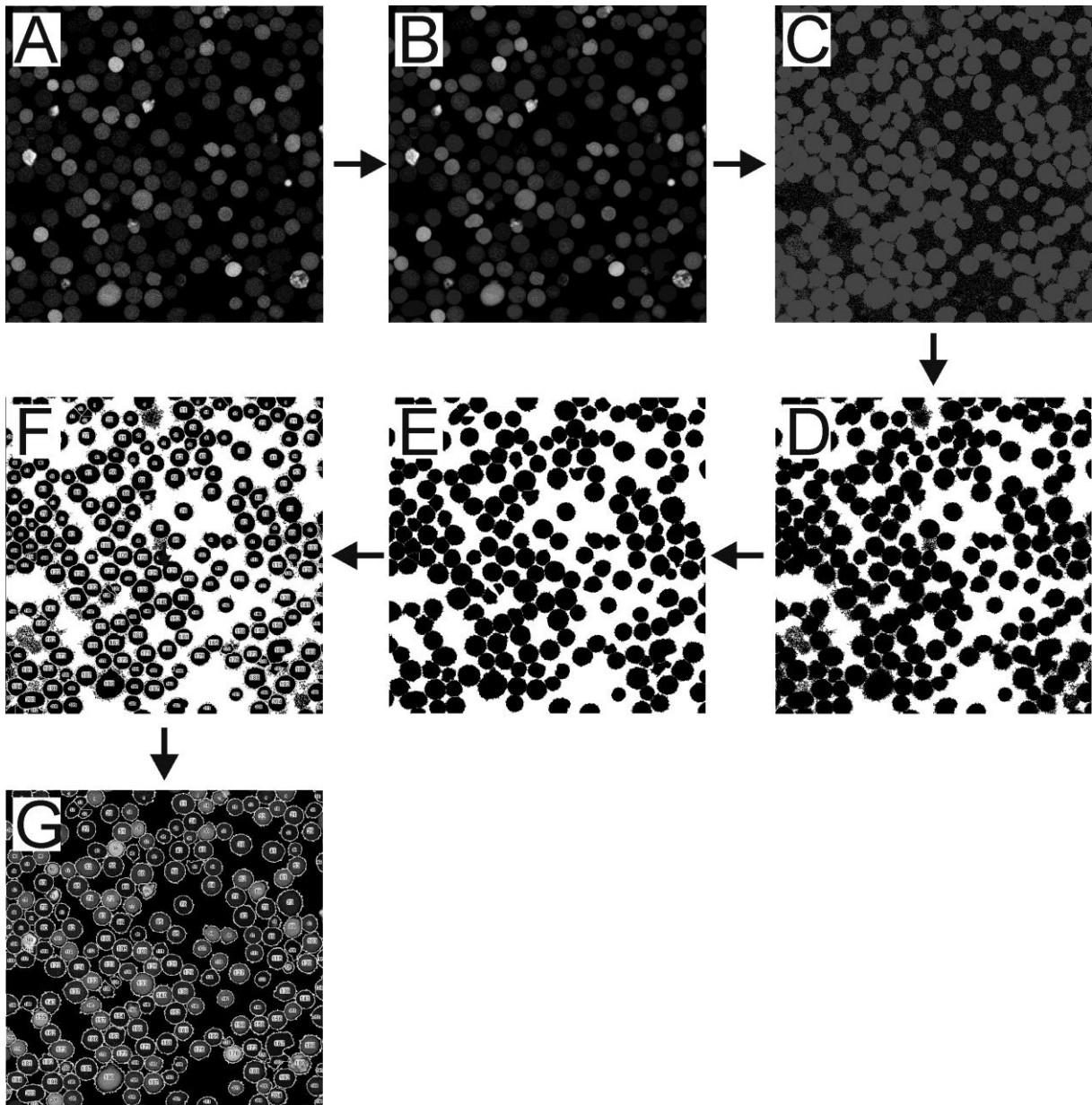
**Fig 7.1**. Automatized image analysis procedure. The (A) raw image is smoothed (B). A threshold is set in order to distinguish between cells and background (C). From these data a binary mask is generated (D) and a minimal size threshold is set in order to exclude single bright pixels from being detected as cells. The conduction of a watershed fit enables to distinguish between adjacent cells (E). The cells are identified as single objects in the binary mask (F). Finally, the mask is applied on the smoothed original image (G) and the cellular brightness of the particles is determined.

# 8. References

1. Almela, M. J., Torres, P. A., Lozano, S. und Herreros, E. (2009). Characterization of the phospholipidogenic potential of 4(1H)-pyridone antimalarial derivatives. *Toxicol.In Vitro.*

2. Amyere, M., Mettlen, M., Van Der, S. P., Platek, A., Payrastre, B., Veithen, A. und Courtoy, P. J. (2002). Origin, originality, functions, subversions and molecular signalling of macropinocytosis. *Int.J.Med.Microbiol.,* **291**, 487-494.

3. Anderson, B. F., Baker, H. M., Norris, G. E., Rumball, S. V. und Baker, E. N. (1990). Apolactoferrin structure demonstrates ligand-induced conformational change in transferrins. *Nature,* **344**, 784-787.

4. Assaraf, Y. G. (2007). Molecular basis of antifolate resistance. *Cancer Metastasis Rev.,* **26**, 153-181.

5. Augustinus (398). *Confessiones,* **Liber XI. caput 24**.

6. Bacia, K., Kim, S. A. und Schwille, P. (2006). Fluorescence cross-correlation spectroscopy in living cells. *Nat.Methods,* **3**, 83-89.

7. Bantscheff, M., Eberhard, D., Abraham, Y., Bastuck, S., Boesche, M., Hobson, S., Mathieson, T., Perrin, J., Raida, M., Rau, C., Reader, V., Sweetman, G., Bauer, A., Bouwmeester, T., Hopf, C., Kruse, U., Neubauer, G., Ramsden, N., Rick, J., Kuster, B. und Drewes, G. (2007). Quantitative chemical proteomics reveals mechanisms of action of clinical ABL kinase inhibitors. *Nat.Biotechnol.*.

8. Bareford, L. M. und Swaan, P. W. (2007). Endocytic mechanisms for targeted drug delivery. *Adv.Drug Deliv.Rev.,* **59**, 748-758.

9. Barr, A. J., Ugochukwu, E., Lee, W. H., King, O. N., Filippakopoulos, P., Alfano, I., Savitsky, P., Burgess-Brown, N. A., Muller, S. und Knapp, S. (2009). Large-scale structural analysis of the classical human protein tyrosine phosphatome. *Cell,* **136**, 352-363.

10. Baudendistel, N., Muller, G., Waldeck, W., Angel, P. und Langowski, J. (2005). Two-hybrid fluorescence cross-correlation spectroscopy detects protein-protein interactions in vivo. *Chemphyschem.,* **6**, 984-990.

11. Becker, F., Murthi, K., Smith, C., Come, J., Costa-Roldan, N., Kaufmann, C., Hanke, U., Degenhart, C., Baumann, S., Wallner, W., Huber, A., Dedier, S., Dill, S., Kinsman, D., Hediger, M., Bockovich, N., Meier-Ewert, S., Kluge, A. F. und Kley, N. (2004). A three-hybrid approach to scanning the proteome for targets of small molecule kinase inhibitors. *Chem.Biol.,* **11**, 211-223.

12. Bellamy, W., Takase, M., Yamauchi, K., Wakabayashi, H., Kawase, K. und Tomita, M. (1992). Identification of the bactericidal domain of lactoferrin. *Biochim.Biophys.Acta,* **1121**, 130-136.

13. Berg, T. (2008). Small-molecule inhibitors of protein-protein interactions. *Curr.Opin.Drug Discov.Devel.,* **11**, 666-674.

14. Berland, K. M., So, P. T. und Gratton, E. (1995). Two-photon fluorescence correlation spectroscopy: method and application to the intracellular environment. *Biophys.J.,* **68**, 694-701.

15. Boskey, A. L., Camacho, N. P., Mendelsohn, R., Doty, S. B. und Binderman, I. (1992). FT-IR microscopic mappings of early mineralization in chick limb bud mesenchymal cell cultures. *Calcif.Tissue Int.,* **51**, 443-448.

16. Bracci, L., Falciani, C., Lelli, B., Lozzi, L., Runci, Y., Pini, A., De Montis, M. G., Tagliamonte, A. und Neri, P. (2003). Synthetic peptides in the form of dendrimers become resistant to protease activity. *J Biol.Chem.,* **278**, 46590-46595.

17. Brandner, G., Mueller, N., Graessmann, A., Graessmann, M., Niebel, J. und Hoffmann, H. (1974). Inhibition by interferon of SV40 tumor antigen formation in cells injected with SV40 cRNA transcribed in vitro. *FEBS Lett.,* **39**, 249-251.

18. Bray, B. L. (2003). Large-scale manufacture of peptide therapeutics by chemical synthesis. *Nat.Rev.Drug Discov.,* **2**, 587-593.

19. Brinckerhoff, L. H., Kalashnikov, V. V., Thompson, L. W., Yamshchikov, G. V., Pierce, R. A., Galavotti, H. S., Engelhard, V. H. und Slingluff, C. L., Jr. (1999). Terminal modifications inhibit proteolytic degradation of an immunogenic MART-1(27-35) peptide: implications for peptide vaccines. *Int.J Cancer,* **83**, 326-334.

20. Brock, Fischer, Fotin-Mleczek and Hufnagel. (2007) *"Peptides Useful as Cell-Penetrating Peptides".* **European Patent** [EP1966240]

21. Brock, R., Hink, M. A. und Jovin, T. M. (1998). Fluorescence correlation microscopy of cells in the presence of autofluorescence. *Biophys.J.,* **75**, 2547-2557.

22. Brock, R. und Jovin, T. M. (1998). Fluorescence correlation microscopy (FCM)-fluorescence correlation spectroscopy (FCS) taken into the cell. *Cell Mol.Biol.(Noisy.-le-grand),* **44**, 847-856.

23. Brock, R., Vamosi, G., Vereb, G. und Jovin, T. M. (1999). Rapid characterization of green fluorescent protein fusion proteins on the molecular and cellular level by fluorescence correlation microscopy. *Proc.Natl.Acad.Sci U.S.A,* **96**, 10123-10128.

24. Buffy, J. J., Waring, A. J., Lehrer, R. I. und Hong, M. (2003). Immobilization and aggregation of the antimicrobial peptide protegrin-1 in lipid bilayers investigated by solid-state NMR. *Biochemistry,* **42**, 13725-13734.

25. Buschmann, Kramer, Koberling, Macdonald and Ruttinger. (2007) *"Quantitative FCS: Determination of the Confocal Volume by FCS and Bead Scanning with the MicroTime 200"*. **PicoQuant, AppNote Quantitative FCS** , 1-8

26. Butt, A. J., Caldon, C. E., McNeil, C. M., Swarbrick, A., Musgrove, E. A. und Sutherland, R. L. (2008). Cell cycle machinery: links with genesis and treatment of breast cancer. *Adv.Exp.Med.Biol.,* **630**, 189-205.

27. Caligiuri, M., Becker, F., Murthi, K., Kaplan, F., Dedier, S., Kaufmann, C., Machl, A., Zybarth, G., Richard, J., Bockovich, N., Kluge, A. und Kley, N. (2005). A proteome-wide CDK/CRK-specific kinase inhibitor promotes tumor cell death in the absence of cell cycle progression. *Chem.Biol.,* **12**, 1103-1115.

28. Capdeville, R., Buchdunger, E., Zimmermann, J. und Matter, A. (2002). Glivec (STI571, imatinib), a rationally developed, targeted anticancer drug. *Nat.Rev.Drug Discov.,* **1**, 493-502.

29. Casnellie, J. E. (1991). Assay of protein kinases using peptides with basic residues for phosphocellulose binding. *Methods Enzymol.,* **200**, 115-120.

30. Celis, J. E. (1984). Microinjection of somatic cells with micropipettes: comparison with other transfer techniques. *Biochem.J.,* **223**, 281-291.

31. Chang, M., Chou, J. C. und Lee, H. J. (2005). Cellular internalization of fluorescent proteins via arginine-rich intracellular delivery peptide in plant cells. *Plant Cell Physiol,* **46**, 482-488.

32. Chapman, E. und Wong, C. H. (2002). A pH sensitive colorometric assay for the high-throughput screening of enzyme inhibitors and substrates: a case study using kinases. *Bioorg.Med.Chem,* **10**, 551-555.

33. Chauhan, S. S., Liang, X. J., Su, A. W., Pai-Panandiker, A., Shen, D. W., Hanover, J. A. und Gottesman, M. M. (2003). Reduced endocytosis and altered lysosome function in cisplatin-resistant cell lines. *Br.J.Cancer,* **88**, 1327-1334.

34. Chaurand, P., Schwartz, S. A., Reyzer, M. L. und Caprioli, R. M. (2005). Imaging mass spectrometry: principles and potentials. *Toxicol.Pathol.,* **33**, 92-101.

35. Chen, R. F. und Knutson, J. R. (1988). Mechanism of fluorescence concentration quenching of carboxyfluorescein in liposomes: energy transfer to nonfluorescent dimers. *Anal.Biochem.,* **172**, 61-77.

36. Cheng, Y. und Prusoff, W. H. (1973). Relationship between the inhibition constant (K1) and the concentration of inhibitor which causes 50 per cent inhibition (I50) of an enzymatic reaction. *Biochem.Pharmacol.,* **22**, 3099-3108.

37. Choi, M., Rolle, S., Wellner, M., Cardoso, M. C., Scheidereit, C., Luft, F. C. und Kettritz, R. (2003). Inhibition of NF-kappaB by a TAT-NEMO-binding domain peptide accelerates constitutive apoptosis and abrogates LPS-delayed neutrophil apoptosis. *Blood,* **102**, 2259-2267.

38. Chorev, M., Shavitz, R., Goodman, M., Minick, S. und Guillemin, R. (1979). Partially modified retro-inverso-enkephalinamides: topochemical long-acting analogs in vitro and in vivo. *Science,* **204**, 1210-1212.

39. Chrisman, T. D., Sobo, G. E. und Exton, J. H. (1984). The Mg2+ requirements of nonactivated and activated rat liver phosphorylase kinase. Inhibition of the activated form by free Mg2+. *FEBS Lett.,* **167**, 295-300.

40. Chugh, A. und Eudes, F. (2007). Translocation and nuclear accumulation of monomer and dimer of HIV-1 Tat basic domain in triticale mesophyll protoplasts. *Biochim.Biophys.Acta,* **1768**, 419-426.

41. Chugh, A. und Eudes, F. (2008). Cellular uptake of cell-penetrating peptides pVEC and transportan in plants. *J.Pept.Sci.,* **14**, 477-481.

42. Clegg, R. M. (1995). Fluorescence resonance energy transfer. *Curr.Opin.Biotechnol.,* **6**, 103-110.

43. Conner, S. D. und Schmid, S. L. (2003). Regulated portals of entry into the cell. *Nature,* **422**, 37-44.

44. Cooper, M. A. (2002). Optical biosensors in drug discovery. *Nat.Rev.Drug Discov.,* **1**, 515-528.

45. Cooper, W. J. und Waters, M. L. (2005). Molecular recognition with designed peptides and proteins. *Curr.Opin.Chem.Biol.,* **9**, 627-631.

46. Cory, S., Huang, D. C. und Adams, J. M. (2003). The Bcl-2 family: roles in cell survival and oncogenesis. *Oncogene,* **22**, 8590-8607.

47. Davies, S. P., Reddy, H., Caivano, M. und Cohen, P. (2000). Specificity and mechanism of action of some commonly used protein kinase inhibitors. *Biochem.J.,* **351**, 95-105.

48. Dawson, P. E., Muir, T. W., Clark-Lewis, I. und Kent, S. B. (1994). Synthesis of proteins by native chemical ligation. *Science,* **266**, 776-779.

49. de Lange, J. H., Schipper, N. W., Schuurhuis, G. J., ten Kate, T. K., van Heijningen, T. H., Pinedo, H. M., Lankelma, J. und Baak, J. P. (1992). Quantification by laser scan microscopy of intracellular doxorubicin distribution. *Cytometry,* **13**, 571-576.

50. De, S. K. und Contreras, R. (2005). Human antimicrobial peptides: defensins, cathelicidins and histatins. *Biotechnol.Lett.,* **27**, 1337-1347.

51. Derossi, D., Joliot, A. H., Chassaing, G. und Prochiantz, A. (1994). The third helix of the Antennapedia homeodomain translocates through biological membranes. *J Biol.Chem,* **269**, 10444-10450.

52. Digman, M. A., Wiseman, P. W., Horwitz, A. R. und Gratton, E. (2009). Detecting protein complexes in living cells from laser scanning confocal image sequences by the cross correlation raster image spectroscopy method. *Biophys.J.,* **96**, 707-716.

53. Ding, H., Prodinger, W. M. und Kopecek, J. (2006). Identification of CD21-binding peptides with phage display and investigation of binding properties of HPMA copolymer-peptide conjugates. *Bioconjug.Chem.,* **17**, 514-523.

54. Doherty, T., Waring, A. J. und Hong, M. (2008). Dynamic structure of disulfide-removed linear analogs of tachyplesin-I in the lipid bilayer from solid-state NMR. *Biochemistry,* **47**, 1105-1116.

55. Donovan, M. D., Flynn, G. L. und Amidon, G. L. (1990a). Absorption of polyethylene glycols 600 through 2000: the molecular weight dependence of gastrointestinal and nasal absorption. *Pharm.Res.,* **7**, 863-868.

56. Donovan, M. D., Flynn, G. L. und Amidon, G. L. (1990b). The molecular weight dependence of nasal absorption: the effect of absorption enhancers. *Pharm.Res.,* **7**, 808-815.

57. Drews, J. (2000). Drug discovery: a historical perspective. *Science,* **287**, 1960-1964.

58. Drews, J. und Ryser, S. (1997). The role of innovation in drug development. *Nat.Biotechnol.,* **15**, 1318-1319.

59. Drummond, D. C., Meyer, O., Hong, K., Kirpotin, D. B. und Papahadjopoulos, D. (1999). Optimizing liposomes for delivery of chemotherapeutic agents to solid tumors. *Pharmacol.Rev.,* **51**, 691-743.

60. Du, C., Fang, M., Li, Y., Li, L. und Wang, X. (2000). Smac, a mitochondrial protein that promotes cytochrome c-dependent caspase activation by eliminating IAP inhibition. *Cell,* **102**, 33-42.

61. Duchardt, F., Fotin-Mleczek, M., Schwarz, H., Fischer, R. und Brock, R. (2007). A comprehensive model for the cellular uptake of cationic cell-penetrating peptides. *Traffic.,* **8**, 848-866.

62. Duncan, R. (2003). The dawning era of polymer therapeutics. *Nat.Rev Drug Discov.,* **2**, 347-360.

63. Duncan, R., Coatsworth, J. K. und Burtles, S. (1998). Preclinical toxicology of a novel polymeric antitumour agent: HPMA copolymer-doxorubicin (PK1). *Hum.Exp.Toxicol.,* **17**, 93-104.

64. Dupont, E., Prochiantz, A. und Joliot, A. (2007). Identification of a signal peptide for unconventional secretion. *Journal of Biological Chemistry,* **282**, 8994-9000.

65. El-Andaloussi, S., Johansson, H. J., Lundberg, P. und Langel, U. (2006). Induction of splice correction by cell-penetrating peptide nucleic acids. *J.Gene Med., **8***, 1262-1273.

66. Elass-Rochard, E., Roseanu, A., Legrand, D., Trif, M., Salmon, V., Motas, C., Montreuil, J. und Spik, G. (1995). Lactoferrin-lipopolysaccharide interaction: involvement of the 28-34 loop region of human lactoferrin in the high-affinity binding to Escherichia coli 055B5 lipopolysaccharide. *Biochem.J., **312 ( Pt 3)***, 839-845.

67. Ellis, R. J. (2001). Macromolecular crowding: obvious but underappreciated. *Trends Biochem.Sci., **26***, 597-604.

68. Elson, E. L. und Webb, W. W. (1975). Concentration correlation spectroscopy: a new biophysical probe based on occupation number fluctuations. *Annu.Rev Biophys.Bioeng., **4***, 311-334.

69. Ertl, P., Rohde, B. und Selzer, P. (2000). Fast calculation of molecular polar surface area as a sum of fragment-based contributions and its application to the prediction of drug transport properties. *J.Med.Chem., **43***, 3714-3717.

70. Esposito, P., Barbero, L., Caccia, P., Caliceti, P., D'Antonio, M., Piquet, G. und Veronese, F. M. (2003). PEGylation of growth hormone-releasing hormone (GRF) analogues. *Adv.Drug Deliv.Rev., **55***, 1279-1291.

71. Fasano, A. und Uzzau, S. (1997). Modulation of intestinal tight junctions by Zonula occludens toxin permits enteral administration of insulin and other macromolecules in an animal model. *J.Clin.Invest, **99***, 1158-1164.

72. Fawell, S., Seery, J., Daikh, Y., Moore, C., Chen, L. L., Pepinsky, B. und Barsoum, J. (1994). Tat-mediated delivery of heterologous proteins into cells. *Proc.Natl.Acad.Sci.U.S.A, **91***, 664-668.

73. Fischer, P. M., Krausz, E. und Lane, D. P. (2001). Cellular delivery of impermeable effector molecules in the form of conjugates with peptides capable of mediating membrane translocation. *Bioconjug.Chem., **12***, 825-841.

74. Fischer, R., Fotin-Mleczek, M., Hufnagel, H. und Brock, R. (2005). Break on through to the other side-biophysics and cell biology shed light on cell-penetrating peptides. *Chembiochem., **6***, 2126-2142.

75. Fischer, R., Kohler, K., Fotin-Mleczek, M. und Brock, R. (2004). A stepwise dissection of the intracellular fate of cationic cell-penetrating peptides. *Journal of Biological Chemistry, **279***, 12625-12635.

76. Fischer, R., Mader, O., Jung, G. und Brock, R. (2003). Extending the applicability of carboxyfluorescein in solid-phase synthesis. *Bioconjug.Chem., **14***, 653-660.

77. Fischer, R., Waizenegger, T., Kohler, K. und Brock, R. (2002). A quantitative validation of fluorophore-labelled cell-permeable peptide conjugates: fluorophore and cargo dependence of import. *Biochim.Biophys.Acta, **1564***, 365-374.

78. Flanagan, M. T. und Pantell, R. H. (1984). Surface plasmon resonance and immunosensors. *Electron Lett.,* 968-970.

79. Foerg, C. und Merkle, H. P. (2008). On the biomedical promise of cell penetrating peptides: limits versus prospects. *J Pharm.Sci.,* **97**, 144-162.

80. Földes-Papp, Z. (2005). How the Molecule Number Is Corectly Quantified in Two-Color Fluorescence Cross-Correlating Spectroscopy: Corrections for Cross-Talk and Quenching in Experiments. *Curr.Pharmaceutical Biotechnology,* **6**, 437-444.

81. Fotin-Mleczek, M., Fischer, R. und Brock, R. (2005a). Endocytosis and cationic cell-penetrating peptides--a merger of concepts and methods. *Curr.Pharm.Des,* **11**, 3613-3628.

82. Fotin-Mleczek, M., Welte, S., Mader, O., Duchardt, F., Fischer, R., Hufnagel, H., Scheurich, P. und Brock, R. (2005b). Cationic cell-penetrating peptides interfere with TNF signalling by induction of TNF receptor internalization. *J Cell Sci,* **118**, 3339-3351.

83. Frackenpohl, J., Arvidsson, P. I., Schreiber, J. V. und Seebach, D. (2001). The outstanding biological stability of beta- and gamma-peptides toward proteolytic enzymes: an in vitro investigation with fifteen peptidases. *Chembiochem.,* **2**, 445-455.

84. Fuchs, S. M. und Raines, R. T. (2004). Pathway for polyarginine entry into mammalian cells. *Biochemistry,* **43**, 2438-2444.

85. Fulda, S., Wick, W., Weller, M. und Debatin, K. M. (2002a). Smac agonists sensitize for Apo2L/T. *Nat.Med.,* **8**, 808-815.

86. Fulda, S., Wick, W., Weller, M. und Debatin, K. M. (2002b). Smac agonists sensitize for Apo2L/Trail- or anticancer drug-induced apoptosis and induce regression of malignant glioma in vivo. *Nat.Med.,* **8**, 808-815.

87. Gapski, G. R., Whiteley, J. M., Rader, J. I., Cramer, P. L., Henderson, G. B., Neef, V. und Huennekens, F. M. (1975). Synthesis of a fluorescent derivative of amethopterin. *J.Med.Chem.,* **18**, 526-528.

88. Gehl, J. (2003). Electroporation: theory and methods, perspectives for drug delivery, gene therapy and research. *Acta Physiol Scand.,* **177**, 437-447.

89. Ghose, A. K., Viswanadhan, V. N. und Wendoloski, J. J. (1999). A knowledge-based approach in designing combinatorial or medicinal chemistry libraries for drug discovery. 1. A qualitative and quantitative characterization of known drug databases. *J.Comb.Chem.,* **1**, 55-68.

90. Gifford, J. L., Hunter, H. N. und Vogel, H. J. (2005). Lactoferricin: a lactoferrin-derived peptide with antimicrobial, antiviral, antitumor and immunological properties. *Cell Mol.Life Sci.,* **62**, 2588-2598.

91. Gohlke, H. und Klebe, G. (2002). Approaches to the description and prediction of the binding affinity of small-molecule ligands to macromolecular receptors. *Angew.Chem.Int.Ed Engl.,* **41**, 2644-2676.

92. Goldberg, M. und Gomez-Orellana, I. (2003). Challenges for the oral delivery of macromolecules. *Nat.Rev.Drug Discov.,* **2**, 289-295.

93. Goldsmith, K. C., Liu, X., Dam, V., Morgan, B. T., Shabbout, M., Cnaan, A., Letai, A., Korsmeyer, S. J. und Hogarty, M. D. (2006). BH3 peptidomimetics potently activate apoptosis and demonstrate single agent efficacy in neuroblastoma. *Oncogene,* **25**, 4525-4533.

94. Goodwin, R. J., Pennington, S. R. und Pitt, A. R. (2008). Protein and peptides in pictures: imaging with MALDI mass spectrometry. *Proteomics.,* **8**, 3785-3800.

95. Gordon, D. J., Sciarretta, K. L. und Meredith, S. C. (2001). Inhibition of beta-amyloid(40) fibrillogenesis and disassembly of beta-amyloid(40) fibrils by short beta-amyloid congeners containing N-methyl amino acids at alternate residues. *Biochemistry,* **40**, 8237-8245.

96. Gotter, B., Faubel, W. und Neubert, R. H. (2008). Optical methods for measurements of skin penetration. *Skin Pharmacol.Physiol,* **21**, 156-165.

97. Gray, N. S., Wodicka, L., Thunnissen, A. M., Norman, T. C., Kwon, S., Espinoza, F. H., Morgan, D. O., Barnes, G., LeClerc, S., Meijer, L., Kim, S. H., Lockhart, D. J. und Schultz, P. G. (1998). Exploiting chemical libraries, structure, and genomics in the search for kinase inhibitors. *Science,* **281**, 533-538.

98. Griffith, O. W. (1986). Beta-amino acids: mammalian metabolism and utility as alpha-amino acid analogues. *Annu.Rev Biochem,* **55**, 855-878.

99. Groenink, J., Walgreen-Weterings, E., van 't, H. W., Veerman, E. C. und Nieuw Amerongen, A. V. (1999). Cationic amphipathic peptides, derived from bovine and human lactoferrins, with antimicrobial activity against oral pathogens. *FEMS Microbiol.Lett.,* **179**, 217-222.

100. Gschwendt, M., Muller, H. J., Kielbassa, K., Zang, R., Kittstein, W., Rincke, G. und Marks, F. (1994). Rottlerin, a novel protein kinase inhibitor. *Biochem.Biophys.Res Commun.,* **199**, 93-98.

101. Haag, R. und Vogtle, F. (2004). Highly branched macromolecules at the interface of chemistry, biology, physics, and medicine. *Angew.Chem Int.Ed Engl.,* **43**, 272-273.

102. Hällbrink, Kilk, Elmquist, Lundberg, Lindgren, Jiang, Pooga, Soomets and Langel. (2005) *"Prediction of cell-penetrating peptides"*. **Int.J.Pep.Res.Ther.** *11*, 249-259

103. Harris, J. M. und Chess, R. B. (2003). Effect of pegylation on pharmaceuticals. *Nat.Rev.Drug Discov.,* **2**, 214-221.

104. Herman, S., Zurgil, N. und Deutsch, M. (2005). Low dose methotrexate induces apoptosis with reactive oxygen species involvement in T lymphocytic cell lines to a greater extent than in monocytic lines. *Inflamm.Res.,* **54**, 273-280.

105. Hink, M. A., Griep, R. A., Borst, J. W., van, H. A., Eppink, M. H., Schots, A. und Visser, A. J. (2000). Structural dynamics of green fluorescent protein alone and fused with a single chain Fv protein. *Journal of Biological Chemistry,* **275**, 17556-17560.

106. Hintersteiner, M. und Auer, M. (2008). Single-bead, single-molecule, single-cell fluorescence: technologies for drug screening and target validation. *Ann.N.Y.Acad.Sci.,* **1130**, 1-11.

107. Horejsi, V., Zhang, W. und Schraven, B. (2004). Transmembrane adaptor proteins: organizers of immunoreceptor signalling. *Nat.Rev.Immunol.,* **4**, 603-616.

108. Hruby, V. J. und Balse, P. M. (2000). Conformational and topographical considerations in designing agonist peptidomimetics from peptide leads. *Curr.Med.Chem.,* **7**, 945-970.

109. Huang, W., Lee, S. L. und Yu, L. X. (2009). Mechanistic approaches to predicting oral drug absorption. *AAPS.J.,* **11**, 217-224.

110. Hunter, H. N., Demcoe, A. R., Jenssen, H., Gutteberg, T. J. und Vogel, H. J. (2005). Human lactoferricin is partially folded in aqueous solution and is better stabilized in a membrane mimetic solvent. *Antimicrob.Agents Chemother.,* **49**, 3387-3395.

111. Imming, P., Sinning, C. und Meyer, A. (2006). Drugs, their targets and the nature and number of drug targets. *Nat.Rev.Drug Discov.,* **5**, 821-834.

112. IUPAC (1984). IUPAC-IUB Joint Commission on Biochemical Nomenclature (JCBN). Nomenclature and symbolism for amino acids and peptides. Recommendations 1983. *Eur.J.Biochem.,* **138**, 9-37.

113. Jarver, P., Langel, K., El Andaloussi, S. und Langel, U. (2007). Applications of cell-penetrating peptides in regulation of gene expression. *Biochem.Soc.Trans.,* **35**, 770-774.

114. Kapp, T., Muller, S. und Gust, R. (2006). Dinuclear alkylamine platinum(II) complexes of [1,2-bis(4-fluorophenyl)ethylenediamine]platinum(II): influence of endocytosis and copper and organic cation transport systems on cellular uptake. *ChemMedChem.,* **1**, 560-564.

115. Kastrup, L., Blom, H., Eggeling, C. und Hell, S. W. (2005). Fluorescence fluctuation spectroscopy in subdiffraction focal volumes. *Phys.Rev.Lett.,* **94**, 178104.

116. Kaufman, R. J., Bertino, J. R. und Schimke, R. T. (1978). Quantitation of dihydrofolate reductase in individual parental and methotrexate-resistant murine cells. Use of a fluorescence activated cell sorter. *Journal of Biological Chemistry,* **253**, 5852-5860.

117. Kawamoto, T. (1990). Light microscopic autoradiography for study of early changes in the distribution of water-soluble materials. *J.Histochem.Cytochem.,* **38**, 1805-1814.

118. Kawamura, K. S., Sung, M., Bolewska-Pedyczak, E. und Gariepy, J. (2006). Probing the impact of valency on the routing of arginine-rich peptides into eukaryotic cells. *Biochemistry,* **45**, 1116-1127.

119. Kelly, S. M., Jess, T. J. und Price, N. C. (2005). How to study proteins by circular dichroism. *Biochim.Biophys.Acta,* **1751**, 119-139.

120. Kim, S. A., Heinze, K. G. und Schwille, P. (2007). Fluorescence correlation spectroscopy in living cells. *Nat.Methods,* **4**, 963-973.

121. Knight, D. E. und Scrutton, M. C. (1986). Gaining access to the cytosol: the technique and some applications of electropermeabilization. *Biochem.J.,* **234**, 497-506.

122. Knight, Z. A. und Shokat, K. M. (2005). Features of selective kinase inhibitors. *Chem Biol.,* **12**, 621-637.

123. Kohler, K., Ganser, A., Andre, T., Roth, G., Grosse-Hovest, L., Jung, G. und Brock, R. (2008). Stimulus dependence of the action of small-molecule inhibitors in the CD3/CD28 signalling network. *ChemMedChem.,* **3**, 1404-1411.

124. Koopman, W. J., Hink, M. A., Verkaart, S., Visch, H. J., Smeitink, J. A. und Willems, P. H. (2007). Partial complex I inhibition decreases mitochondrial motility and increases matrix protein diffusion as revealed by fluorescence correlation spectroscopy. *Biochim.Biophys.Acta,* **1767**, 940-947.

125. Kopecek, J. und Bazilova, H. (1973). Poly[N-(2-hydroxypropyl)methacrylamide] I. Radical polymerisation and copolymerisation. *Eur.Polym.,* **9**, 7-14.

126. Kopecek, J., Kopeckova, P., Minko, T. und Lu, Z.-R. (2000). HPMA copolymer-anticancer drug conjugates: design, activity, and mechanism of action. *European Journal of Pharmaceutics and Biopharmaceutics,* **50**, 61-81.

127. Koppel, D. E. (1974). Statistical accuracy in fluorescence correlation spectroscopy. *Phys.Rev.A,* **10**, 1938-1945.

128. Korn, K. und Krausz, E. (2007). Cell-based high-content screening of small-molecule libraries. *Curr.Opin.Chem.Biol.,* **11**, 503-510.

129. Kosuge, M., Takeuchi, T., Nakase, I., Jones, A. T. und Futaki, S. (2008). Cellular internalization and distribution of arginine-rich peptides as a function of extracellular Peptide concentration, serum, and plasma membrane associated proteoglycans. *Bioconjug.Chem.,* **19**, 656-664.

130. Kovar, M., Strohalm, J., Etrych, T., Ulbrich, K. und Rihova, B. (2002). Star structure of antibody-targeted HPMA copolymer-bound doxorubicin: a novel type of polymeric

conjugate for targeted drug delivery with potent antitumor effect. *Bioconjug.Chem,* **13**, 206-215.

131. Kraker, A. J., Hartl, B. G., Amar, A. M., Barvian, M. R., Showalter, H. D. und Moore, C. W. (2000). Biochemical and cellular effects of c-Src kinase-selective pyrido[2, 3-d]pyrimidine tyrosine kinase inhibitors. *Biochem.Pharmacol.,* **60**, 885-898.

132. Kroczek, R. A., Mages, H. W. und Hutloff, A. (2004). Emerging paradigms of T-cell co-stimulation. *Curr.Opin.Immunol.,* **16**, 321-327.

133. Kubinyi, H. (1994). [The key and the lock. I. The basis of drug action]. *Pharm.Unserer Zeit,* **23**, 158-168.

134. Kuwana, T., Mackey, M. R., Perkins, G., Ellisman, M. H., Latterich, M., Schneiter, R., Green, D. R. und Newmeyer, D. D. (2002). Bid, Bax, and lipids cooperate to form supramolecular openings in the outer mitochondrial membrane. *Cell,* **111**, 331-342.

135. Lang, P., Yeow, K., Nichols, A. und Scheer, A. (2006). Cellular imaging in drug discovery. *Nat.Rev.Drug Discov.,* **5**, 343-356.

136. Langel, U. 2002. *Cell Penetrating Peptides: Processes and Applications.*, Boca Raton: CRC Press.

137. Lankelma, J., Dekker, H., Luque, F. R., Luykx, S., Hoekman, K., van, d., V, van Diest, P. J. und Pinedo, H. M. (1999). Doxorubicin gradients in human breast cancer. *Clin.Cancer Res.,* **5**, 1703-1707.

138. Lasch, P. und Naumann, D. (2006). Spatial resolution in infrared microspectroscopic imaging of tissues. *Biochim.Biophys.Acta,* **1758**, 814-829.

139. Law, B., Quinti, L., Choi, Y., Weissleder, R. und Tung, C. H. (2006). A mitochondrial targeted fusion peptide exhibits remarkable cytotoxicity. *Mol.Cancer Ther.,* **5**, 1944-1949.

140. Leader, B., Baca, Q. J. und Golan, D. E. (2008). Protein therapeutics: a summary and pharmacological classification. *Nat.Rev.Drug Discov.,* **7**, 21-39.

141. Lee, K. C., Moon, S. C., Park, M. O., Lee, J. T., Na, D. H., Yoo, S. D., Lee, H. S. und DeLuca, P. P. (1999). Isolation, characterization, and stability of positional isomers of mono-PEGylated salmon calcitonins. *Pharm.Res.,* **16**, 813-818.

142. Legrand, D., Mazurier, J., Elass, A., Rochard, E., Vergoten, G., Maes, P., Montreuil, J. und Spik, G. (1992). Molecular interactions between human lactotransferrin and the phytohemagglutinin-activated human lymphocyte lactotransferrin receptor lie in two loop-containing regions of the N-terminal domain I of human lactotransferrin. *Biochemistry,* **31**, 9243-9251.

143. Legrand, D., Pierce, A., Elass, E., Carpentier, M., Mariller, C. und Mazurier, J. (2008). Lactoferrin structure and functions. *Adv.Exp.Med.Biol.,* **606**, 163-194.

144. Lehel, C., niel-Issakani, S., Brasseur, M. und Strulovici, B. (1997). A chemiluminescent microtiter plate assay for sensitive detection of protein kinase activity. *Anal.Biochem.,* **244**, 340-346.

145. Levay, P. F. und Viljoen, M. (1995). Lactoferrin: a general review. *Haematologica,* **80**, 252-267.

146. Leveugle, B., Mazurier, J., Legrand, D., Mazurier, C., Montreuil, J. und Spik, G. (1993). Lactotransferrin binding to its platelet receptor inhibits platelet aggregation. *Eur.J Biochem.,* **213**, 1205-1211.

147. Lewin, M., Carlesso, N., Tung, C. H., Tang, X. W., Cory, D., Scadden, D. T. und Weissleder, R. (2000). Tat peptide-derivatized magnetic nanoparticles allow in vivo tracking and recovery of progenitor cells. *Nat.Biotechnol.,* **18**, 410-414.

148. Li, S. S. (2005). Specificity and versatility of SH3 and other proline-recognition domains: structural basis and implications for cellular signal transduction. *Biochem.J.,* **390**, 641-653.

149. Liebecq, C. Ed. 1992. *Biochemical Nomenclature and Related Documents.*

150. Lipinski, C. A., Lombardo, F., Dominy, B. W. und Feeney, P. J. (2001). Experimental and computational approaches to estimate solubility and permeability in drug discovery and development settings. *Adv.Drug Deliv.Rev.,* **46**, 3-26.

151. Lippincott-Schwartz, J., Snapp, E. und Kenworthy, A. (2001). Studying protein dynamics in living cells. *Nat.Rev.Mol.Cell Biol.,* **2**, 444-456.

152. Liu, B. A., Jablonowski, K., Raina, M., Arce, M., Pawson, T. und Nash, P. D. (2006). The human and mouse complement of SH2 domain proteins-establishing the boundaries of phosphotyrosine signaling. *Mol.Cell,* **22**, 851-868.

153. Lobley, A., Whitmore, L. und Wallace, B. A. (2002). DICHROWEB: an interactive website for the analysis of protein secondary structure from circular dichroism spectra. *Bioinformatics.,* **18**, 211-212.

154. Lundin, P., Johansson, H., Guterstam, P., Holm, T., Hansen, M., Langel, U. und El, A. S. (2008). Distinct uptake routes of cell-penetrating peptide conjugates. *Bioconjug.Chem.,* **19**, 2535-2542.

155. Luxembourg, S. L., Vaezaddeh, A. R., Amstalden, E. R., Zimmermann-Ivol, C. G., Hochstrasser, D. F. und Heeren, R. M. (2006). The molecular scanner in microscope mode. *Rapid Commun.Mass Spectrom.,* **20**, 3435-3442.

156. Mader, O., Reiner, K., Egelhaaf, H. J., Fischer, R. und Brock, R. (2004). Structure property analysis of pentamethine indocyanine dyes: identification of a new dye for life science applications. *Bioconjug.Chem.,* **15**, 70-78.

157. Maeda, H. (2001). SMANCS and polymer-conjugated macromolecular drugs: advantages in cancer chemotherapy. *Adv.Drug Deliv.Rev.,* **46**, 169-185.

158. Magzoub, M., Kilk, K., Eriksson, L. E., Langel, U. und Graslund, A. (2001). Interaction and structure induction of cell-penetrating peptides in the presence of phospholipid vesicles. *Biochim.Biophys.Acta,* **1512**, 77-89.

159. Magzoub, M., Pramanik, A. und Graslund, A. (2005). Modeling the endosomal escape of cell-penetrating peptides: transmembrane pH gradient driven translocation across phospholipid bilayers. *Biochemistry,* **44**, 14890-14897.

160. Malkov, D., Angelo, R., Wang, H. Z., Flanders, E., Tang, H. und Gomez-Orellana, I. (2005). Oral delivery of insulin with the eligen technology: mechanistic studies. *Curr.Drug Deliv.,* **2**, 191-197.

161. Malugin, A., Kopeckova, P. und Kopecek, J. (2004). HPMA copolymer-bound doxorubicin induces apoptosis in human ovarian carcinoma cells by a Fas-independent pathway. *Mol.Pharm.,* **1**, 174-182.

162. Mammen, M., Choi, S.-K. und Whitesides, G. M. (1998). Polyvalente Wechselwirkungen in biologischen Systemen: Auswirkungen auf das Design und die Verwendung multivalenter Liganden und Inhibitoren. *Angew.Chem.,* **110**, 2908-2953.

163. Manning, G., Whyte, D. B., Martinez, R., Hunter, T. und Sudarsanam, S. (2002). The protein kinase complement of the human genome. *Science,* **298**, 1912-1934.

164. Matsuzaki, K., Yoneyama, S., Fujii, N., Miyajima, K., Yamada, K., Kirino, Y. und Anzai, K. (1997). Membrane permeabilization mechanisms of a cyclic antimicrobial peptide, tachyplesin I, and its linear analog. *Biochemistry,* **36**, 9799-9806.

165. Mayer, R. J., Chen, J. T., Taira, K., Fierke, C. A. und Benkovic, S. J. (1986). Importance of a hydrophobic residue in binding and catalysis by dihydrofolate reductase. *Proc.Natl.Acad.Sci.U.S.A,* **83**, 7718-7720.

166. Melvik, J. E., Pettersen, E. O., Gordon, P. B. und Seglen, P. O. (1986). Increase in cis-dichlorodiammineplatinum (II) cytotoxicity upon reversible electropermeabilization of the plasma membrane in cultured human NHIK 3025 cells. *Eur.J.Cancer Clin.Oncol.,* **22**, 1523-1530.

167. Meseth, U., Wohland, T., Rigler, R. und Vogel, H. (1999). Resolution of fluorescence correlation measurements. *Biophys.J.,* **76**, 1619-1631.

168. Metz-Boutigue, M. H., Jolles, J., Mazurier, J., Schoentgen, F., Legrand, D., Spik, G., Montreuil, J. und Jolles, P. (1984). Human lactotransferrin: amino acid sequence and structural comparisons with other transferrins. *Eur.J.Biochem.,* **145**, 659-676.

169. Meyvis, T. K., De Smedt, S. C., Van, O. P. und Demeester, J. (1999). Fluorescence recovery after photobleaching: a versatile tool for mobility and interaction measurements in pharmaceutical research. *Pharm.Res.,* **16**, 1153-1162.

170. Michaelis, L. und Menten, M. L. (1913). Die Kinetik der Invertinwirkung. *Biochem.Z.,* **49**, 333-369.

171. Miller, L. W. und Cornish, V. W. (2005). Selective chemical labeling of proteins in living cells. *Curr.Opin.Chem.Biol.,* **9**, 56-61.

172. Miller, L. W., Sable, J., Goelet, P., Sheetz, M. P. und Cornish, V. W. (2004). Methotrexate conjugates: a molecular in vivo protein tag. *Angew.Chem.Int.Ed Engl.,* **43**, 1672-1675.

173. Miller, M. L., Jensen, L. J., Diella, F., Jorgensen, C., Tinti, M., Li, L., Hsiung, M., Parker, S. A., Bordeaux, J., Sicheritz-Ponten, T., Olhovsky, M., Pasculescu, A., Alexander, J., Knapp, S., Blom, N., Bork, P., Li, S., Cesareni, G., Pawson, T., Turk, B. E., Yaffe, M. B., Brunak, S. und Linding, R. (2008). Linear motif atlas for phosphorylation-dependent signaling. *Sci.Signal.,* **1**, ra2.

174. Mir, L. M., Banoun, H. und Paoletti, C. (1988). Introduction of definite amounts of nonpermeant molecules into living cells after electropermeabilization: direct access to the cytosol. *Exp.Cell Res.,* **175**, 15-25.

175. Mitchell, D. J., Kim, D. T., Steinman, L., Fathman, C. G. und Rothbard, J. B. (2000). Polyarginine enters cells more efficiently than other polycationic homopolymers. *J Pept.Res.,* **56**, 318-325.

176. Mizuno, T., Miyashita, M. und Miyagawa, H. (2009). Cellular internalization of arginine-rich peptides into tobacco suspension cells: a structure-activity relationship study. *J.Pept.Sci.,* **15**, 259-263.

177. Nagahara, H., Vocero-Akbani, A. M., Snyder, E. L., Ho, A., Latham, D. G., Lissy, N. A., Becker-Hapak, M., Ezhevsky, S. A. und Dowdy, S. F. (1998). Transduction of full-length TAT fusion proteins into mammalian cells: TAT-p27Kip1 induces cell migration. *Nat.Med.,* **4**, 1449-1452.

178. Nekhotiaeva, N., Elmquist, A., Rajarao, G. K., Hallbrink, M., Langel, U. und Good, L. (2004). Cell entry and antimicrobial properties of eukaryotic cell-penetrating peptides. *FASEB J.,* **18**, 394-396.

179. Neumann, E., Schaefer-Ridder, M., Wang, Y. und Hofschneider, P. H. (1982). Gene transfer into mouse lyoma cells by electroporation in high electric fields. *EMBO J.,* **1**, 841-845.

180. Nielsen, C. U., Andersen, R., Brodin, B., Frokjaer, S., Taub, M. E. und Steffansen, B. (2001). Dipeptide model prodrugs for the intestinal oligopeptide transporter. Affinity for and transport via hPepT1 in the human intestinal Caco-2 cell line. *J.Control Release,* **76**, 129-138.

181. Nolan, G. P. (2007). What's wrong with drug screening today. *Nat.Chem.Biol.,* **3**, 187-191.

182.  Noor, F., Kinscherf, R., Bonaterra, G. A., Walczak, S., Wolfl, S. und Metzler-Nolte, N. (2009). Enhanced Cellular Uptake and Cytotoxicity Studies of Organometallic Bioconjugates of the NLS Peptide in Hep G2 Cells. *Chembiochem.,* **10**, 493-502.

183.  Nori, A., Jensen, K. D., Tijerina, M., Kopeckova, P. und Kopecek, J. (2003). Tat-conjugated synthetic macromolecules facilitate cytoplasmic drug delivery to human ovarian carcinoma cells. *Bioconjug.Chem.,* **14**, 44-50.

184.  Oehlke, J., Wallukat, G., Wolf, Y., Ehrlich, A., Wiesner, B., Berger, H. und Bienert, M. (2004). Enhancement of intracellular concentration and biological activity of PNA after conjugation with a cell-penetrating synthetic model peptide. *Eur.J.Biochem.,* **271**, 3043-3049.

185.  Oesch, F., Fabian, E., Oesch-Bartlomowicz, B., Werner, C. und Landsiedel, R. (2007). Drug-metabolizing enzymes in the skin of man, rat, and pig. *Drug Metab Rev.,* **39**, 659-698.

186.  Omelyanenko, V., Kopeckova, P., Gentry, C. und Kopecek, J. (1998). Targetable HPMA copolymer-adriamycin conjugates. Recognition, internalization, and subcellular fate. *J.Control Release,* **53**, 25-37.

187.  Pace, C. N., Vajdos, F., Fee, L., Grimsley, G. und Gray, T. (1995). How to measure and predict the molar absorption coefficient of a protein. *Protein Sci.,* **4**, 2411-2423.

188.  Pawson, T. und Nash, P. (2003). Assembly of cell regulatory systems through protein interaction domains. *Science,* **300**, 445-452.

189.  Pedersen, P. L. (2007). Transport ATPases into the year 2008: a brief overview related to types, structures, functions and roles in health and disease. *J.Bioenerg.Biomembr.,* **39**, 349-355.

190.  Pellecchia, M., Sem, D. S. und Wuthrich, K. (2002). NMR in drug discovery. *Nat.Rev.Drug Discov.,* **1**, 211-219.

191.  Perlman, Z. E., Slack, M. D., Feng, Y., Mitchison, T. J., Wu, L. F. und Altschuler, S. J. (2004). Multidimensional drug profiling by automated microscopy. *Science,* **306**, 1194-1198.

192.  Peterson, N. A., Anderson, B. F., Jameson, G. B., Tweedie, J. W. und Baker, E. N. (2000). Crystal structure and iron-binding properties of the R210K mutant of the N-lobe of human lactoferrin: implications for iron release from transferrins. *Biochemistry,* **39**, 6625-6633.

193.  Piehler, J., Brecht, A., Geckeler, K. E. und Gauglitz, G. (1996). Surface modification for direct immunoprobes. *Biosens.Bioelectron.,* **11**, 579-590.

194.  Poon, G. M. und Gariepy, J. (2007). Cell-surface proteoglycans as molecular portals for cationic peptide and polymer entry into cells. *Biochem.Soc.Trans.,* **35**, 788-793.

195. Postema, M. und Gilja, O. H. (2007). Ultrasound-directed drug delivery. *Curr.Pharm.Biotechnol.,* **8**, 355-361.

196. Powell, M. S., Barnes, N. C., Bradford, T. M., Musgrave, I. F., Wines, B. D., Cambier, J. C. und Hogarth, P. M. (2006). Alteration of the Fc gamma RIIa dimer interface affects receptor signaling but not ligand binding. *J.Immunol.,* **176**, 7489-7494.

197. Provencher, S. W. und Glockner, J. (1981). Estimation of globular protein secondary structure from circular dichroism. *Biochemistry,* **20**, 33-37.

198. Pygall, S. R., Whetstone, J., Timmins, P. und Melia, C. D. (2007). Pharmaceutical applications of confocal laser scanning microscopy: the physical characterisation of pharmaceutical systems. *Adv.Drug Deliv.Rev.,* **59**, 1434-1452.

199. Rademann, J. und Jung G (2000). Drug discovery - Integrating combinatorial synthesis and bioassays. *Science,* **287**, 1947-1948.

200. Rajagopalan, P. T., Zhang, Z., McCourt, L., Dwyer, M., Benkovic, S. J. und Hammes, G. G. (2002). Interaction of dihydrofolate reductase with methotrexate: ensemble and single-molecule kinetics. *Proc.Natl.Acad.Sci.U.S.A,* **99**, 13481-13486.

201. Ram, N., Aroui, S., Jaumain, E., Bichraoui, H., Mabrouk, K., Ronjat, M., Lortat-Jacob, H. und De, W. M. (2008). Direct peptide interaction with surface glycosaminoglycans contributes to the cell penetration of maurocalcine. *J.Biol.Chem.,* **283**, 24274-24284.

202. Ramamoorthy, A., Thennarasu, S., Tan, A., Gottipati, K., Sreekumar, S., Heyl, D. L., An, F. Y. und Shelburne, C. E. (2006). Deletion of all cysteines in tachyplesin I abolishes hemolytic activity and retains antimicrobial activity and lipopolysaccharide selective binding. *Biochemistry,* **45**, 6529-6540.

203. Rao, M. und Alving, C. R. (2000). Delivery of lipids and liposomal proteins to the cytoplasm and Golgi of antigen-presenting cells. *Adv.Drug Deliv.Rev.,* **41**, 171-188.

204. Rautio, J., Kumpulainen, H., Heimbach, T., Oliyai, R., Oh, D., Jarvinen, T. und Savolainen, J. (2008). Prodrugs: design and clinical applications. *Nat.Rev.Drug Discov.,* **7**, 255-270.

205. Reichmann, D., Rahat, O., Cohen, M., Neuvirth, H. und Schreiber, G. (2007). The molecular architecture of protein-protein binding sites. *Curr.Opin.Struct.Biol.,* **17**, 67-76.

206. Remy, I. und Michnick, S. W. (2001). Visualization of biochemical networks in living cells. *Proc.Natl.Acad.Sci.U.S.A,* **98**, 7678-7683.

207. Rigler, R., Mets, U., Widengren, J. und Kask, P. (1993). Fluorescence corelation spectroscopy with high count rate and low background: Analysis of translational diffusion. *Eur.Biophys.J.,* **22**, 169-175.

208. Robinson, J. A., Demarco, S., Gombert, F., Moehle, K. und Obrecht, D. (2008). The design, structures and therapeutic potential of protein epitope mimetics. *Drug Discov.Today,* **13**, 944-951.

209. Rohrbach, S., Muller-Werdan, U., Werdan, K., Koch, S., Gellerich, N. F. und Holtz, J. (2005). Apoptosis-modulating interaction of the neuregulin/erbB pathway with anthracyclines in regulating Bcl-xS and Bcl-xL in cardiomyocytes. *J.Mol.Cell Cardiol.,* **38**, 485-493.

210. Rojas, M., Donahue, J. P., Tan, Z. und Lin, Y. Z. (1998). Genetic engineering of proteins with cell membrane permeability. *Nat.Biotechnol.,* **16**, 370-375.

211. Roodhart, J. M., Langenberg, M. H., Witteveen, E. und Voest, E. E. (2008). The molecular basis of class side effects due to treatment with inhibitors of the VEGF/VEGFR pathway. *Curr.Clin.Pharmacol.,* **3**, 132-143.

212. Rouquayrol, M., Gaucher, B., Roche, D., Greiner, J. und Vierling, P. (2002). Transepithelial transport of prodrugs of the HIV protease inhibitors saquinavir, indinavir, and nelfinavir across Caco-2 cell monolayers. *Pharm.Res.,* **19**, 1704-1712.

213. Ruijtenbeek, R., Kruijtzer, J. A., van de, W. W., Fischer, M. J., Fluck, M., Redegeld, F. A., Liskamp, R. M. und Nijkamp, F. P. (2001). Peptoid - peptide hybrids that bind Syk SH2 domains involved in signal transduction. *Chembiochem.,* **2**, 171-179.

214. Russell-Jones, G. J., Westwood, S. W. und Habberfield, A. D. (1995). Vitamin B12 mediated oral delivery systems for granulocyte-colony stimulating factor and erythropoietin. *Bioconjug.Chem.,* **6**, 459-465.

215. Ruttekolk, I. R., Duchardt, F., Fischer, R., Wiesmuller, K. H., Rademann, J. und Brock, R. (2008). HPMA as a scaffold for the modular assembly of functional peptide polymers by native chemical ligation. *Bioconjug.Chem.,* **19**, 2081-2087.

216. Ryser, H. J. und Shen, W. C. (1978). Conjugation of methotrexate to poly(L-lysine) increases drug transport and overcomes drug resistance in cultured cells. *Proc.Natl.Acad.Sci.U.S.A,* **75**, 3867-3870.

217. Ryser, H. J., Shen, W. C. und Merk, F. B. (1978). Membrane transport of macromolecules: new carrier functions of proteins and poly(amino acids). *Life Sci.,* **22**, 1253-1260.

218. Sandanaraj, B. S., Vutukuri, D. R., Simard, J. M., Klaikherd, A., Hong, R., Rotello, V. M. und Thayumanavan, S. (2005). Noncovalent modification of chymotrypsin surface using an amphiphilic polymer scaffold: implications in modulating protein function. *J Am.Chem Soc.,* **127**, 10693-10698.

219. Santra, S., Yang, H., Holloway, P. H., Stanley, J. T. und Mericle, R. A. (2005a). Synthesis of water-dispersible fluorescent, radio-opaque, and paramagnetic CdS:Mn/ZnS quantum dots: a multifunctional probe for bioimaging. *J.Am.Chem.Soc.,* **127**, 1656-1657.

220. Santra, S., Yang, H., Stanley, J. T., Holloway, P. H., Moudgil, B. M., Walter, G. und Mericle, R. A. (2005b). Rapid and effective labeling of brain tissue using TAT-conjugated CdS:Mn/ZnS quantum dots. *Chem.Commun.(Camb.),* 3144-3146.

221. Satchi-Fainaro, R., Puder, M., Davies, J. W., Tran, H. T., Sampson, D. A., Greene, A. K., Corfas, G. und Folkman, J. (2004). Targeting angiogenesis with a conjugate of HPMA copolymer and TNP-470. *Nat.Med.,* **10**, 255-261.

222. Schmidt, M. C., Rothen-Rutishauser, B., Rist, B., Beck-Sickinger, A., Wunderli-Allenspach, H., Rubas, W., Sadee, W. und Merkle, H. P. (1998). Translocation of human calcitonin in respiratory nasal epithelium is associated with self-assembly in lipid membrane. *Biochemistry,* **37**, 16582-16590.

223. Schwarze, S. R., Ho, A., Vocero-Akbani, A. und Dowdy, S. F. (1999). In vivo protein transduction: delivery of a biologically active protein into the mouse. *Science,* **285**, 1569-1572.

224. Schwille, P., Haupts, U., Maiti, S. und Webb, W. W. (1999). Molecular dynamics in living cells observed by fluorescence correlation spectroscopy with one- and two-photon excitation. *Biophys.J,* **77**, 2251-2265.

225. Schwille, P., Meyer-Almes, F. J. und Rigler, R. (1997). Dual-color fluorescence cross-correlation spectroscopy for multicomponent diffusional analysis in solution. *Biophys.J,* **72**, 1878-1886.

226. Searle, F., Gac-Breton, S., Keane, R., Dimitrijevic, S., Brocchini, S., Sausville, E. A. und Duncan, R. (2001). N-(2-hydroxypropyl)methacrylamide copolymer-6-(3-aminopropyl)-ellipticine conjugates. Synthesis, in vitro, and preliminary in vivo evaluation. *Bioconjug.Chem,* **12**, 711-718.

227. Seethala, R. und Menzel, R. (1997). A homogeneous, fluorescence polarization assay for src-family tyrosine kinases. *Anal.Biochem.,* **253**, 210-218.

228. Selsted, M. E. (2004). Theta-defensins: cyclic antimicrobial peptides produced by binary ligation of truncated alpha-defensins. *Curr.Protein Pept.Sci.,* **5**, 365-371.

229. Seymour, L. W., Miyamoto, Y., Maeda, H., Brereton, M., Strohalm, J., Ulbrich, K. und Duncan, R. (1995). Influence of molecular weight on passive tumour accumulation of a soluble macromolecular drug carrier. *Eur.J.Cancer,* **31A**, 766-770.

230. Seymour, L. W., Ulbrich, K., Strohalm, J., Kopecek, J. und Duncan, R. (1990). The pharmacokinetics of polymer-bound adriamycin. *Biochem Pharmacol.,* **39**, 1125-1131.

231. Shen, W. C. und Ryser, H. J. (1978). Conjugation of poly-L-lysine to albumin and horseradish peroxidase: a novel method of enhancing the cellular uptake of proteins. *Proc.Natl.Acad.Sci.U.S.A,* **75**, 1872-1876.

232. Shi, X., Foo, Y. H., Sudhaharan, T., Chong, S. W., Korzh, V., Ahmed, S. und Wohland, T. (2009). Determination of dissociation constants in living zebrafish

embryos with single wavelength fluorescence cross-correlation spectroscopy. *Biophys.J.,* **97**, 678-686.

233. Signor, L., Varesio, E., Staack, R. F., Starke, V., Richter, W. F. und Hopfgartner, G. (2007). Analysis of erlotinib and its metabolites in rat tissue sections by MALDI quadrupole time-of-flight mass spectrometry. *J.Mass Spectrom.,* **42**, 900-909.

234. So, A., Hadaschik, B., Sowery, R. und Gleave, M. (2007). The role of stress proteins in prostate cancer. *Curr.Genomics,* **8**, 252-261.

235. Sonnevend, A., Knoop, F. C., Patel, M., Pal, T., Soto, A. M. und Conlon, J. M. (2004). Antimicrobial properties of the frog skin peptide, ranatuerin-1 and its [Lys-8]-substituted analog. *Peptides,* **25**, 29-36.

236. Sorscher, S. M., Bartholomew, J. C. und Klein, M. P. (1980). The use of fluorescence correlations spectroscopy to probe chromatin in the cell nucleus. *Biochim.Biophys.Acta,* **610**, 28-46.

237. Southwick, P. L., Ernst, L. A., Tauriello, E. W., Parker, S. R., Mujumdar, R. B., Mujumdar, S. R., Clever, H. A. und Waggoner, A. S. (1990). Cyanine dye labeling reagents--carboxymethylindocyanine succinimidyl esters. *Cytometry,* **11**, 418-430.

238. Spiekermann, G. M., Finn, P. W., Ward, E. S., Dumont, J., Dickinson, B. L., Blumberg, R. S. und Lencer, W. I. (2002). Receptor-mediated immunoglobulin G transport across mucosal barriers in adult life: functional expression of FcRn in the mammalian lung. *J.Exp.Med.,* **196**, 303-310.

239. Steinhilber/Schubert-Zsilavecz/Roth 2005. *Medizinische Chemie - Targets und Arzneistoffe*, Deutscher Apotheker Verlag Stuttgart.

240. Stephens, D. J. und Pepperkok, R. (2001). The many ways to cross the plasma membrane. *Proc.Natl.Acad.Sci.U.S.A,* **98**, 4295-4298.

241. Stoevesandt, O., Elbs, M., Kohler, K., Lellouch, A. C., Fischer, R., Andre, T. und Brock, R. (2005a). Peptide microarrays for the detection of molecular interactions in cellular signal transduction. *Proteomics.,* **5**, 2010-2017.

242. Stoevesandt, O., Kohler, K., Fischer, R., Johnston, I. C. und Brock, R. (2005b). One-step analysis of protein complexes in microliters of cell lysate. *Nat.Methods,* **2**, 833-835.

243. Stoevesandt, O. und Taussig, M. J. (2007). Affinity reagent resources for human proteome detection: initiatives and perspectives. *Proteomics.,* **7**, 2738-2750.

244. Strasser, A., Jost, P. J. und Nagata, S. (2009). The many roles of FAS receptor signaling in the immune system. *Immunity.,* **30**, 180-192.

245. Stumpf, W. E. (2005). Drug localization and targeting with receptor microscopic autoradiography. *J.Pharmacol.Toxicol.Methods,* **51**, 25-40.

246. Stumpf, W. E., Hayakawa, N. und Bidmon, H. J. (2008). Skin research and drug localization with receptor microscopic autoradiography. *Exp.Dermatol.,* **17**, 133-138.

247. Sun, X. L., Baker, H. M., Shewry, S. C., Jameson, G. B. und Baker, E. N. (1999). Structure of recombinant human lactoferrin expressed in Aspergillus awamori. *Acta Crystallogr.D.Biol.Crystallogr.,* **55**, 403-407.

248. Suzuki, Y. A., Lopez, V. und Lonnerdal, B. (2005). Mammalian lactoferrin receptors: structure and function. *Cell Mol.Life Sci.,* **62**, 2560-2575.

249. Swaan, P. W., Hillgren, K. M., Szoka, F. C., Jr. und Oie, S. (1997). Enhanced transepithelial transport of peptides by conjugation to cholic acid. *Bioconjug.Chem.,* **8**, 520-525.

250. Takeshima, K., Chikushi, A., Lee, K.-K., Yonehara, S. und Matsuzaki, K. (2003). Translocation of analogues of the antimicrobial peptides Magainin and Buforin across human cell membranes. *J.Biol.Chem.,* **278**, 1310-1315.

251. Tam, J. P., Xu, J. und Eom, K. D. (2001). Methods and strategies of peptide ligation. *Biopolymers,* **60**, 194-205.

252. Testa, B. (2009). Prodrugs: bridging pharmacodynamic/pharmacokinetic gaps. *Curr.Opin.Chem.Biol.*.

253. Testa, B. und Kramer, S. D. (2009). The biochemistry of drug metabolism--an introduction: part 5. Metabolism and bioactivity. *Chem.Biodivers.,* **6**, 591-684.

254. Thanou, M., Verhoef, J. C. und Junginger, H. E. (2001). Oral drug absorption enhancement by chitosan and its derivatives. *Adv.Drug Deliv.Rev.,* **52**, 117-126.

255. Tirlapur, U. K. und Konig, K. (2002). Targeted transfection by femtosecond laser. *Nature,* **418**, 290-291.

256. Toke, O. (2005). Antimicrobial peptides: new candidates in the fight against bacterial infections. *Biopolymers,* **80**, 717-735.

257. Tunnemann, G., Martin, R. M., Haupt, S., Patsch, C., Edenhofer, F. und Cardoso, M. C. (2006). Cargo-dependent mode of uptake and bioavailability of TAT-containing proteins and peptides in living cells. *FASEB J.,* **20**, 1775-1784.

258. Tunnemann, G., Ter-Avetisyan, G., Martin, R. M., Stockl, M., Herrmann, A. und Cardoso, M. C. (2008). Live-cell analysis of cell penetration ability and toxicity of oligo-arginines. *J.Pept.Sci.,* **14**, 469-476.

259. Turner, J. J., Ivanova, G. D., Verbeure, B., Williams, D., Arzumanov, A. A., Abes, S., Lebleu, B. und Gait, M. J. (2005). Cell-penetrating peptide conjugates of peptide nucleic acids (PNA) as inhibitors of HIV-1 Tat-dependent trans-activation in cells. *Nucleic Acids Res.,* **33**, 6837-6849.

260. Turner, M. und Billadeau, D. D. (2002). VAV proteins as signal integrators for multi-subunit immune-recognition receptors. *Nat.Rev.Immunol., 2*, 476-486.

261. Tyagi, M., Rusnati, M., Presta, M. und Giacca, M. (2001). Internalization of HIV-1 tat requires cell surface heparan sulfate proteoglycans. *J.Biol.Chem., 276*, 3254-3261.

262. Unnamalai, N., Kang, B. G. und Lee, W. S. (2004). Cationic oligopeptide-mediated delivery of dsRNA for post-transcriptional gene silencing in plant cells. *FEBS Lett., 566*, 307-310.

263. Valenti, P. und Antonini, G. (2005). Lactoferrin: an important host defence against microbial and viral attack. *Cell Mol.Life Sci., 62*, 2576-2587.

264. van de Ven, M., van Ginkel, G. und Levine, Y. K. (1984). Angle resolved fluorescence depolarisation of 1,6-diphenyl-1,3,5 hexatriene (DPH) in unsaturated digalactosyl diacylglycerol (DGDG) lipid bilayers. *Biochem Biophys.Res.Commun., 123*, 352-357.

265. van de Waterbeemd, H. (1998). The fundamental variables of the biopharmaceutics classification system (BCS): a commentary. *Eur.J.Pharm.Sci., 7*, 1-3.

266. van Kuppevelt, T. H., Dennissen, M. A., van Venrooij, W. J., Hoet, R. M. und Veerkamp, J. H. (1998). Generation and application of type-specific anti-heparan sulfate antibodies using phage display technology. Further evidence for heparan sulfate heterogeneity in the kidney. *J Biol.Chem., 273*, 12960-12966.

267. van, S., I, Spoelder, H. J., Bloemendal, M., van, G. R. und Groen, F. C. (1990). Estimation of protein secondary structure and error analysis from circular dichroism spectra. *Anal.Biochem., 191*, 110-118.

268. Verma, A., Uzun, O., Hu, Y., Hu, Y., Han, H. S., Watson, N., Chen, S., Irvine, D. J. und Stellacci, F. (2008). Surface-structure-regulated cell-membrane penetration by monolayer-protected nanoparticles. *Nat.Mater., 7*, 588-595.

269. Veronese, F. M. (2001). Peptide and protein PEGylation: a review of problems and solutions. *Biomaterials, 22*, 405-417.

270. Vicent, M. J. und Duncan, R. (2006). Polymer conjugates: nanosized medicines for treating cancer. *TRENDS in Biotechnology, 24*, 39-47.

271. Vives, E., Brodin, P. und Lebleu, B. (1997). A truncated HIV-1 Tat protein basic domain rapidly translocates through the plasma membrane and accumulates in the cell nucleus. *J Biol.Chem, 272*, 16010-16017.

272. Wachsmuth, M., Waldeck, W. und Langowski, J. (2000). Anomalous diffusion of fluorescent probes inside living cell nuclei investigated by spatially-resolved fluorescence correlation spectroscopy. *J.Mol.Biol., 298*, 677-689.

273. Wadhwani, P., Afonin, S., Ieronimo, M., Buerck, J. und Ulrich, A. S. (2006). Optimized protocol for synthesis of cyclic gramicidin S: starting amino acid is key to high yield. *J.Org.Chem.,* **71**, 55-61.

274. Wadia, J. S., Stan, R. V. und Dowdy, S. F. (2004). Transducible TAT-HA fusogenic peptide enhances escape of TAT-fusion proteins after lipid raft macropinocytosis. *Nat.Med.,* **10**, 310-315.

275. Wagner, G. und Laufer, S. (2006). Small molecular anti-cytokine agents. *Med.Res.Rev.,* **26**, 1-62.

276. Walensky, L. D., Pitter, K., Morash, J., Oh, K. J., Barbuto, S., Fisher, J., Smith, E., Verdine, G. L. und Korsmeyer, S. J. (2006). A stapled BID BH3 helix directly binds and activates BAX. *Mol.Cell,* **24**, 199-210.

277. Ward, P. P. und Conneely, O. M. (2004). Lactoferrin: role in iron homeostasis and host defense against microbial infection. *Biometals,* **17**, 203-208.

278. Washtien, W. L. (1982). Thymidylate synthetase levels as a factor in 5-fluorodeoxyuridine and methotrexate cytotoxicity in gastrointestinal tumor cells. *Mol.Pharmacol.,* **21**, 723-728.

279. Weidemann, T., Wachsmuth, M., Tewes, M., Rippe, K. und Langowski, J. (2002). Analysis of Ligand Binding by Two-Colour Fluorescence Cross-Corelation Spectroscopy. *Single Mol.,* **1**, 49-61.

280. Wender, P. A., Mitchell, D. J., Pattabiraman, K., Pelkey, E. T., Steinman, L. und Rothbard, J. B. (2000). The design, synthesis, and evaluation of molecules that enable or enhance cellular uptake: peptoid molecular transporters. *Proc.Natl.Acad.Sci U.S.A,* **97**, 13003-13008.

281. Westphal, V. und Hell, S. W. (2005). Nanoscale resolution in the focal plane of an optical microscope. *Phys.Rev.Lett.,* **94**, 143903.

282. Whitmore, L. und Wallace, B. A. (2004). DICHROWEB, an online server for protein secondary structure analyses from circular dichroism spectroscopic data. *Nucleic Acids Res.,* **32**, W668-W673.

283. Willis, S. N. und Adams, J. M. (2005). Life in the balance: how BH3-only proteins induce apoptosis. *Curr.Opin.Cell Biol.,* **17**, 617-625.

284. Witt, J. J. und Roskoski, R., Jr. (1975). Rapid protein kinase assay using phosphocellulose-paper absorption. *Anal.Biochem.,* **66**, 253-258.

285. Wolf, Y., Pritz, S., Abes, S., Bienert, M., Lebleu, B. und Oehlke, J. (2006). Structural requirements for cellular uptake and antisense activity of peptide nucleic acids conjugated with various peptides. *Biochemistry,* **45**, 14944-14954.

286. Wu, G., Chai, J., Suber, T. L., Wu, J. W., Du, C., Wang, X. und Shi, Y. (2000). Structural basis of IAP recognition by Smac/DIABLO. *Nature,* **408**, 1008-1012.

287. Wu, M. und Hancock, R. E. (1999). Interaction of the cyclic antimicrobial cationic peptide bactenecin with the outer and cytoplasmic membrane. *Journal of Biological Chemistry,* **274**, 29-35.

288. Yaffe, M. B. (2002). Phosphotyrosine-binding domains in signal transduction. *Nat.Rev.Mol.Cell Biol.,* **3**, 177-186.

289. Yamamoto, A., Tatsumi, H., Maruyama, M., Uchiyama, T., Okada, N. und Fujita, T. (2001). Modulation of intestinal permeability by nitric oxide donors: implications in intestinal delivery of poorly absorbable drugs. *J.Pharmacol.Exp.Ther.,* **296**, 84-90.

290. Yaroslavov, A. A., Sitnikova, T. A., Rakhnyanskaya, A. A., Yaroslavova, E. G., Davydov, D. A., Burova, T. V., Grinberg, V. Y., Shi, L. und Menger, F. M. (2009). Biomembrane Sensitivity to Structural Changes in Bound Polymers. *J.Am.Chem.Soc..*

291. Yen, W. C. und Lee, V. H. (1995). Role of Na+ in the asymmetric paracellular transport of 4-phenylazobenzyloxycarbonyl-L-Pro-L-Leu-Gly-L-Pro-D-Arg across rabbit colonic segments and Caco-2 cell monolayers. *J.Pharmacol.Exp.Ther.,* **275**, 114-119.

292. Zhang, W. und Smith, S. O. (2005). Mechanism of penetration of Antp(43-58) into membrane bilayers. *Biochemistry,* **44**, 10110-10118.

293. Zhang, Y. und Yu, L. C. (2008). Microinjection as a tool of mechanical delivery. *Curr.Opin.Biotechnol.,* **19**, 506-510.

# 9. Academic teachers

K. Albert, E.O. Bayer, C.F. Bardele, H. Bisswanger, K.W. Bock, P. Bohley, U. Breyer-Pfaff, R. Brock, A. Buchmann, M. Duszenko, H.-J. Egelhaaf, K. Eisele, G. Gaugliz, G. Häfelinger, B. Hamprecht, H. Kalbacher, C. Köhle, S. Laufer, E. Lindner, F. Madeo, W. Maier, P.A. Münzel, H. Ninnemann, H. Oberhammer, H. Pommer, K. Reutter, H. Schott, M. Schwarz, G. Steinbrück, R. Süssmuth, J. Strähle, S. Verleysdonk, J. Werringloer, U. Weser, K.-H. Wiesmüller, K.-P. Zeller

# 10.1. LEBENSLAUF (DEUTSCH)

IVO ROBERT RUTTEKOLK, GEBOREN AM 14. JULI 1980 IN SOLINGEN

## PROMOTIONSTÄTIGKEIT

| | |
|---|---|
| August 2007 - November 2009 | Fortsetzung der Arbeit in Nijmegen (Niederlande) *"Untersuchung zur Zellulären Pharmakologie von peptidischen und nichtpeptidischen Wirkstoffmolekülen"*, betreut durch Prof. Dr. R. Brock, *Nijmegen Centre of Molecular Life Sciences* (*NCMLS*), und Prof. Dr. S. Laufer, *Institut für Pharmazeutische Chemie*, Tübingen |
| August 2007 | Umzug der Arbeitsgruppe in die Niederlande |
| April 2006 - Juli 2007 | Beginn der Promitionstätigkeit in Tübingen |

## BIOCHEMIESTUDIUM

| | |
|---|---|
| März 2006 | Biochemiediplom (Wahlfächer: Toxikologie, Analytische Chemie) |
| Juli 2005 - März 2006 | Diplomarbeit *"Synthese, Charakterisierung und zelluläre Testung polymerkonjugierter, funktioneller Peptide"*, Prof. Dr. K.-H. Wiesmüller, *EMC microcollections GmbH* und *Institut für Organische Chemie* und Dr. R. Brock, *Institut für Zellbiologie*, Tübingen |
| April 2001 - März 2006 | Biochemiestudium in Tübingen (Vordiplom: Juli 2003) |

## SANITÄTSDIENST DER BUNDESWEHR

| | |
|---|---|
| Juli 2000 - März 2001 | sanitätsdienstliche und organisatorische Aufgaben |

## SCHULAUSBILDUNG

| | |
|---|---|
| September 1991 - Juni 2000 | Gymnasium *August-Dicke-Schule*, Solingen, Abschluss: Abitur |

## INDUSTRIEERFAHRUNG

| | |
|---|---|
| Januar - April 2008 | dreimonatiger Laboraufenthalt bei *EVONIK Industries* (Industriepark Marl) |
| Mai 2007 - September 2009 | Zusammenarbeit mit *EVONIK Industries* (Marl/Darmstadt)*,* |
| April 2006 - September 2009 | enge Zusammenarbeit mit den deutschen Biotechnologieunternehmen *gpc-biotech* (München) und *Intana Bioscience* (München), |
| Mai - Juli 2008 | Kooperation mit dem Technologieunternehmen *Lonza (Köln)*, |

# 10.2. CURRICULUM VITAE (ENGLISH)

IVO R. RUTTEKOLK, BORN ON JULY 14TH, 1980 IN SOLINGEN

## PHD THESIS

| | |
|---|---|
| August 2007 - November 2009 | Completion of the PhD thesis in Nijmegen (The Netherlands) *"Investigation of the Cellular Pharmacology of Peptidic and Non-Peptidic Compounds"*, supervised by Prof. Dr. R. Brock, *Nijmegen Centre of Molecular Life Sciences* (*NCMLS*), and Prof. Dr. S. Laufer, *Institute for Pharmaceutical Chemistry*, Tübingen |
| since August 2007 | Move of the workgroup to The Netherlands |
| April 2006 - July 2007 | Start of the PhD thesis in Tübingen |

## STUDIES OF BIOCHEMISTRY

| | |
|---|---|
| March 2006 | Diploma in biochemistry (specialization: toxicology, analytical chemistry) |
| July 2005 - March 2006 | Diploma thesis *"Synthesis, Characterization and Cellular Testing of Polymer-Conjugated, Functional Peptides"*, supervised by Prof. Dr. K.-H. Wiesmüller, *EMC microcollections GmbH* and *Institute for Organic Chemistry* and Dr. R. Brock, *Institute for Cell Biology*, Tübingen |
| April 2001 - March 2006 | Studies in Biochemistry, Tübingen (July 2003: prediploma) |

## MILITARY DUTY IN THE MEDICAL SERVICE

| | |
|---|---|
| July 2000 - March 2001 | Medical and organisational practice |

## EDUCATION

| | |
|---|---|
| September 1991 - June 2000 | Gymnasium August-Dicke-Schule, Solingen, graduation: Abitur |

## INDUSTRIAL EXPERIENCE

| | |
|---|---|
| January - April 2008 | Full-time internship with *EVONIK Industries* (Industrial Centre Marl), |
| May 2007 - September 2009 | Cooperation with *EVONIK Industries* (Marl/Darmstadt): |
| April 2006 - September 2009 | Tight cooperation with the German biotechnological company *gpc biotech* (Munich) and *Intana Bioscience* (Munich) |
| May - September 2008 | Conjoint project with the technological company *Lonza* (Cologne) |